AD-A186 086 A WEIGHTING SEQUENCE APPROACH TO THE ANALYSIS AND 1/3
DESIGN OF MULTIVARIABLE CONTROL SYSTEMS(U) AIR FORCE
INST OF TECH WRIGHT-PATTERSON AFB OH D J CLOUD 1987
UNCLASSIFIED AFIT/CI/NR-87-131D F/G 12/4 NL

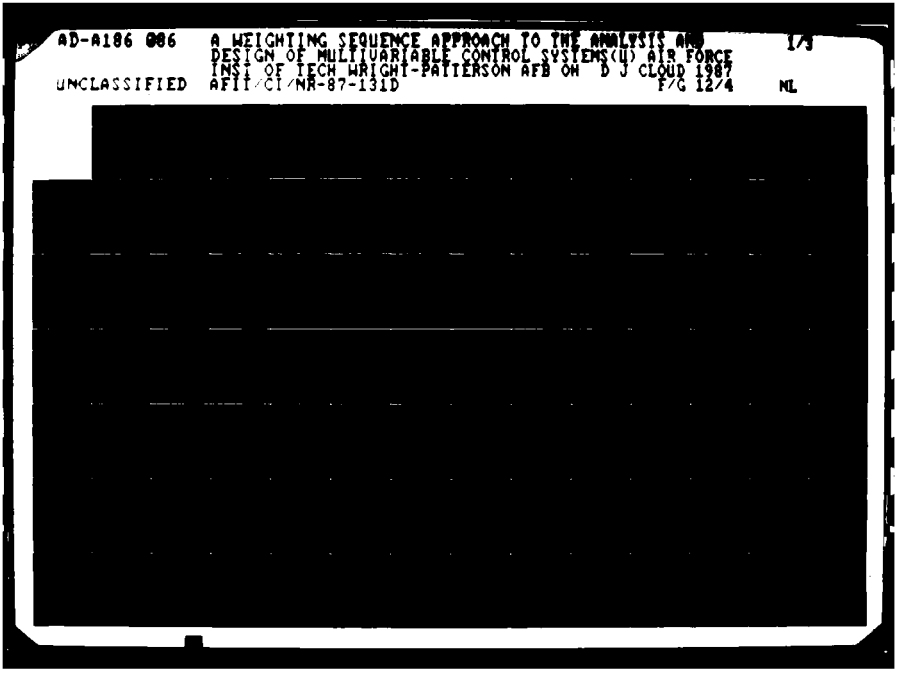

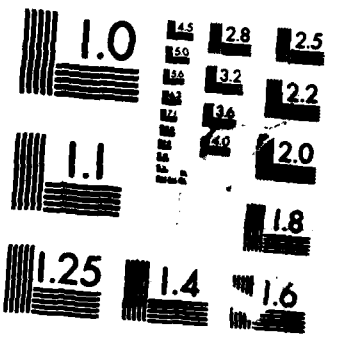

MICROCOPY RESOLUTION TEST CHART
NATIONAL BUREAU OF STANDARDS-1963-A

AD-A186 086

UNCLASSIFIED
SECURITY CLASSIFICATION OF THIS PAGE (When Data Entered)

REPORT DOCUMENTATION PAGE

READ INSTRUCTIONS BEFORE COMPLETING FORM

1. REPORT NUMBER: AFIT/CI/NR 87-131D
2. GOVT ACCESSION NO.: ADA186-086
3. RECIPIENT'S CATALOG NUMBER: DTIC FILE COPY

4. TITLE (and Subtitle): A Weightings Sequence Approach To The Analysis And Design Of Multivariable Control Systems
5. TYPE OF REPORT & PERIOD COVERED: ~~THESIS~~/DISSERTATION
6. PERFORMING ORG. REPORT NUMBER

7. AUTHOR(s): David J. Cloud
8. CONTRACT OR GRANT NUMBER(s)

9. PERFORMING ORGANIZATION NAME AND ADDRESS: AFIT STUDENT AT: Merton College, University of Oxford
10. PROGRAM ELEMENT, PROJECT, TASK AREA & WORK UNIT NUMBERS

11. CONTROLLING OFFICE NAME AND ADDRESS: AFIT/NR, WPAFB OH 45433-6583
12. REPORT DATE: 1987
13. NUMBER OF PAGES: 249

14. MONITORING AGENCY NAME & ADDRESS (if different from Controlling Office)
15. SECURITY CLASS. (of this report): UNCLASSIFIED
15a. DECLASSIFICATION/DOWNGRADING SCHEDULE

16. DISTRIBUTION STATEMENT (of this Report)

APPROVED FOR PUBLIC RELEASE; DISTRIBUTION UNLIMITED

DTIC ELECTE S NOV 23 1987 D

17. DISTRIBUTION STATEMENT (of the abstract entered in Block 20, if different from Report)

18. SUPPLEMENTARY NOTES

APPROVED FOR PUBLIC RELEASE: IAW AFR 190-1

LYNN E. WOLAVER 26 Oct 87
Dean for Research and Professional Development
AFIT/NR

19. KEY WORDS (Continue on reverse side if necessary and identify by block number)

20. ABSTRACT (Continue on reverse side if necessary and identify by block number)

ATTACHED

DD FORM 1 JAN 73 1473 EDITION OF 1 NOV 65 IS OBSOLETE

SECURITY CLASSIFICATION OF THIS PAGE (When Data Entered)

87 11 10 091

A WEIGHTING SEQUENCE APPROACH TO THE ANALYSIS AND DESIGN OF MULTIVARIABLE CONTROL SYSTEMS

David J. Cloud

Merton College

This thesis is submitted in partial fulfilment of the requirements for the degree of Doctor of Philosophy at the University of Oxford, Trinity Term 1987.

87 11 10 091

To My Family

ABSTRACT

A WEIGHTING SEQUENCE APPROACH TO THE ANALYSIS AND DESIGN OF MULTIVARIABLE CONTROL SYSTEMS

David J. Cloud

Merton College

Submitted for the Degree of Doctor of Philosophy; Trinity Term, 1987.

Over the past decade, considerable effort has been devoted to the analysis and design of feedback controllers for systems characterized by uncertain dynamic descriptions, and both frequency-domain and time-domain techniques have been produced by these studies. In this ~~thesis~~, additional aspects of the analysis and design problems are investigated. Techniques are derived to enhance the frequency-domain analysis of perturbed systems and to generalize the time-domain concept of self-tuning control to multivariable systems.

The first part of ~~the thesis~~ addresses the problem of generating an accurate description of frequency response uncertainty for systems whose models are generated via system identification. Finite weighting sequence models are found to be particularly useful for this purpose. Techniques are derived to quantify the variability of the frequency response estimates associated with the given model, to identify the optimal truncation level for the specified identification test, and to assess the impact of the bias introduced by truncation. These results are used to establish precise element-by-element frequency response uncertainty bounds which can, for example, be used to produce characteristic locus inclusion bands for the analysis of perturbed system stability and performance.

The second part ~~of the~~ thesis considers the use of multivariable weighting sequences in the development of on-line computer-implemented control algorithms. "Characteristic subsystem" decompositions are derived for multivariable systems to establish system descriptions that are amenable to the development of real-time computer algorithms which achieve the desired control objectives in a true generalized-Nyquist sense. This "characteristic subsystem" formulation is shown to produce a much more accurate means of implementing conventional characteristic locus designs. More importantly, it is used to derive a multivariable, generalized-Nyquist extension of standard single-input/single-output self-tuning algorithms for the control of uncertain multivariable systems.

Accesion For
NTIS CRA&I
DTIC TAB
Unannounced
Justification
By
Distribution /
Availability Codes
Dist | Avail and / or Special
A-1

DTIC COPY INSPECTED

ACKNOWLEDGEMENTS

I am pleased to take this opportunity to thank my supervisor, Dr B. Kouvaritakis, for his guidance and assistance during the course of my research. His enthusiasm, inspiration, and dedication have proven to be a constant source of encouragement to me over the past three years.

I have also benefited greatly from my association with many colleagues in the Department of Engineering Science. Among these, I would especially like to thank Dr Haniph Latchman, Dr Rob Harrison, and Dr Coorous Mohtadi-Haghighi for many interesting and informative discussions. I also gratefully acknowledge the financial support provided by the U.S. Air Force throughout the course of this research.

Finally, I would like to express my most sincere gratitude to my wife, Barb. Her love, understanding, and support have made these last three years one of the most enjoyable experiences of my life.

TABLE OF CONTENTS

CHAPTER ONE

INTRODUCTION

1.1 Historical Background

By the beginning of the twentieth century, the basic analytical concepts of automatic control were well established in terms of "time-domain" formulations involving ordinary differential equations and their related characteristic algebraic equations. However, in-depth studies of automatic control did not begin to flourish until the early 1930s, with advances in the area of long-range communication. Spurred by the development of feedback amplifiers and, more specifically, the peculiar relationship between changes in loop gain and system stability, H. Nyquist introduced the powerful tools of complex variable theory to the analysis of feedback system behaviour and produced his now-celebrated "Nyquist stability criterion" to explain the observed phenomena.

Interest in a frequency response approach to feedback control became even more intense with H.W. Bode's development of rules for the optimum shaping of the loop-gain frequency function for feedback amplifiers and with the introduction of gain/phase vs frequency diagrams (Bode plots) and the concepts of gain and phase margins. The recognized flexibility of these frequency response methods soon led to the spread of frequency response concepts into other fields (such as mechanical and aeronautical engineering) as well. Indeed, the tremendous research efforts spawned by the Second World War soon produced a unified and coherent theory for single-loop feedback systems based on these frequency response concepts. By the 1950s, frequency response techniques (such as Nyquist diagrams, Bode plots, and Evans' root locus approach) were used routinely for the analysis and design of feedback control systems.

In the late 1950s however, interest began to shift away from the use of frequency response methods in automatic control due mainly to the emergence of the digital computer as a reliable and widely-available engineering tool

and to a simultaneous growing interest in space exploration. With the increasing availability of tremendous computing power and speed, it was now becoming possible to address much more difficult control problems (such as the simultaneous control of several interacting variables) and to consider different controller objectives for which the now-classical frequency response theory was inappropriate. Furthermore, the primary technical problems of interest at the time (those posed by the space program) were particularly amenable to formulations based on very accurate mathematical models and on performance objectives which could be conveniently stated in terms of "economic" conditions (e.g. minimum fuel or minimum time). For these reasons, attention was refocused on the ordinary differential equation approach to control system design, and the development of a "state-space" description for dynamical systems was soon combined with advances in optimal control theory to produce an effective means of addressing the multivariable control problem. Indeed, investigations of the linear optimal control problem with a quadratic performance index using a state-space framework produced the well-known Linear Quadratic (LQ) state feedback theory; a theory which established a powerful synthesis tool for the solution of multivariable control problems. In addition, a precise duality between the control problem and the filtering (or state estimation) problem was soon recognized and used to derive state-space techniques for extracting state estimates from corrupted measurements. Ultimately, this led to the Linear Quadratic Gaussian (LQG) optimal control methodology which became the foundation for the state-space treatment of multivariable control problems.

While state-space and optimal control techniques proved to be particularly useful in aerospace applications, it was soon recognized that these same techniques were inappropriate for many industrial applications. For instance, the mathematically-precise system models available for aerospace systems were not generally available for many industrial systems. In addition, the specification of control objectives in terms of precise

performance indices was much less obvious, particularly to control engineers who were well-versed in the classical frequency response approach to control. Furthermore, the dynamical complexity of the LQG controller was, in many cases, not appropriate for the simple control tasks to be performed. For these reasons, interest in multivariable extensions of classical frequency response methods arose.

Initial attempts to achieve these extensions focused on the task of selecting a cascaded compensator to diagonalize the system transfer function matrix. Once this was achieved, controller design could be completed using standard single-loop techniques. But, it was soon recognized that the identification of a "diagonalizing" compensator was complicated and, more importantly, was unreliable and unnecessary. Indeed, Rosenbrock, with the development of his inverse Nyquist array (INA) design methodology [ROS1], used the concept of diagonal dominance to demonstrate that cascaded compensators need only be introduced to reduce multivariable interaction to an acceptable level, thereby permitting the successful application of single-loop techniques. However, because the INA approach produced only sufficient conditions for system stability, an element of conservatism was introduced in the resulting design process, and this conservatism generated a tendency to overdesign the closed-loop system. In addition, the selection of compensators to achieve diagonal dominance was still found to be an ad hoc and, in many instances, daunting task, which (though vital to the INA method) was not necessary for good system performance.

The motivation for the INA approach to multivariable control design was the eventual deployment of classical single-input/single-output (SISO) frequency response techniques during the last stage of the design study. However, investigations soon began to focus on the multivariable system in terms of a single entity, the system transfer function matrix, rather than as a collection of distinct scalar loops and to address the task of generalizing the basic concepts of the classical single-loop approach to

this new problem. Again, a complex variable approach proved to be particularly useful and led to the development of the Characteristic Locus Method (CLM) for the analysis and design of multivariable systems ([MAC1], [MAC2], [MAC3]). In essence, the characteristic locus technique reduced the open-loop multivariable system to a set of SISO "subsystems" using frequency-dependent eigenvalue/eigenvector decompositions. This procedure established a necessary and sufficient condition (the generalized Nyquist criterion) for the assessment of multivariable system stability. Furthermore, the analyticity of the eigenvalue representations at almost all points in the complex plane was shown to guarantee a one-to-one correspondence between the distance of the characteristic loci from the (-1,0) point and the location of the system's closed-loop poles. As such, the direct manipulation of the characteristic loci using classical SISO frequency response methods was found to produce effective compensation, and so multivariable feedback compensators could be designed without resorting to ad hoc attempts to diagonalize the plant. In effect, the CLM provided a firm theoretical foundation for the direct application of classical frequency response techniques to the much more difficult multivariable control problem.

1.2 Recent Developments

Over the past decade, control research has shifted its attention from the development of analysis and design techniques for accurately-known systems to the more realistic situation where there is an element of uncertainty (e.g. unmodelled dynamics, parameter variations, etc) associated with the system. Under these more realistic conditions, examples have been generated to demonstrate that, in certain cases, commonly-used design techniques (e.g. LQG, INA and CLM) may lead to unreliable closed-loop designs. These examples have clearly pointed out a need for the systematic treatment of model uncertainties in the development of analysis techniques to assess the robust stability and performance characteristics of feedback

control systems and in the development of design techniques to produce adequate and robust closed-loop behaviour. Recent investigations have, in fact, produced important results in each of these areas.

For analysis purposes, a number of studies have focused on frequency-domain concepts to address the problem of model uncertainty. From these efforts, two particularly important methods have emerged: (1) the use of frequency-dependent singular value bounds to assess uncertainty tolerance via the small gains theorem, and (2) the development of characteristic locus inclusion bands to produce a direct extension of the generalized Nyquist diagram for uncertain systems. Initial investigations by Doyle and Stein [DOY1] examined the situation where system uncertainty is modelled as norm-bounded (but otherwise unconstrained) perturbations to a nominal model in the frequency domain, and they derived a necessary and sufficient singular value condition for perturbed system stability. This condition yields a quick assessment of stability tolerances via an upper bound on the size of allowable perturbations, but it does not take explicit account of the phase information required to assess robust performance using a generalized-Nyquist approach. In an attempt to retain this phase information, a number of efforts have focused on the development of eigenvalue inclusion bands for the same class of unstructured perturbations [DAN1], [DAN2]. These efforts have led to the "E-contour" method proposed by Daniel and Kouvaritakis [DAN3] which produces exact inclusion regions for the characteristic loci of the perturbed system and, hence, establishes a necessary and sufficient stability condition via the generalized Nyquist criterion while simultaneously providing both gain and phase information on the perturbed system.

The desire to extend these analysis results to the more likely situation where structural information on the perturbation is available has also yielded a number of useful results. For example, Safonov [SAF1] has examined the class of diagonal perturbations for the purpose of stipulating robust stability margins, while Doyle [DOY2] has examined the same problem

for the more general class of block-structured perturbations. In both cases, the use of similarity scaling techniques to exploit uncertainty structure was found to yield results superior to those obtained using an unstructured uncertainty approach. Indeed, the stability results derived by Doyle are known to be necessary and sufficient for the case of up to three blocks in the perturbation matrix, and hence provide an exact assessment of perturbed system stability for these situations. The block-structured results can also be applied to the case where a known upper bound on the magnitude of the frequency response uncertainty associated with each element of the transfer function matrix is available. However, the complexity of the algorithm used to compute the stability bound and the potential conservatism in the resulting stability assessment have prompted other researchers to investigate this element-by-element structured uncertainty problem in more detail. Results derived by Kantor and Andres [KAN1], Lunze [LUN1], and Owens and Chotai [OWE1] each yield an explicit and easy-to-compute stability condition for this problem. But because these conditions rely on spectral radius results, the stability assessment may be very conservative. Kouvaritakis and Latchman have also examined this problem in detail ([KOU4], [KOU5]), and they have demonstrated that optimal nonsimilarity scaling can be used to produce an exact stability assessment for the element-by-element problem. Moreover, these results have been extended to the more general block-structured perturbation problem [KOU7], [DAN4]. In addition, although these results rely on singular value conditions, they have also been used to extend the E-contour results to the case of structured perturbations [KOU4], [KOU6]. Hence, both singular value and eigenvalue inclusion techniques are now available to assess system robustness for the much more realistic problem of structured uncertainties.

Frequency-domain techniques have also proven to be popular for the development of robust design procedures. Indeed, using frequency response uncertainty bounds to characterize performance and stability limitations,

Doyle and Stein have proposed an extension of the state-space LQG design approach for systems with model uncertainties [DOY1], a procedure which has come to be known as the Linear Quadratic Gaussian with Loop Transfer Recovery (LQG/LTR) design method. But by combining state-space and frequency-domain concepts, this methodology tends to rely on engineering insight rather than a closed-form synthesis procedure to develop the appropriate compensator. In search of a closed-form solution to the robust design problem, research has focused instead on the H^∞ approach to feedback design proposed originally by Zames [ZAM1]. In general, the H^∞ methods that have been developed to date rely on a unique formulation (the "Youla parametrization") for the set of all stabilizing controllers, Q(s), to obtain the particular controller which minimizes the H^∞ norm of an appropriately weighted combination of the sensitivity and complementary sensitivity functions for the given system. [Note that, for a system with transfer function matrix G(s), the H^∞ norm is given by $\sup_\omega \bar{\sigma}\{G(j\omega)\}$.] This H^∞ optimization produces a closed-form solution for the specified control problem which is guaranteed to be stable and simultaneouly satisfies the robust design requirements that have been implicitly incorporated into the problem by the selection of appropriate frequency-dependent weighting. Indeed, this H^∞ approach addresses the robust design problem in much the same way as the state-space/optimal control approach addresses the conventional multivariable control problem. As such, the same concerns arise. For example, the selection of suitable weighting functions for use in the performance index is not obvious and the effects of changing these functions is not apparent. In addition, the optimal H^∞ controller tends to be very complex. It might, therefore, be argued that alternative design procedures may be required for a wide variety of systems where the complexity of the H^∞ design approach is not justified. In light of this, the development of design techniques which parallel the classical frequency response methods but which also cater for the robustness aspects of the

problem may offer an effective alternative. Some preliminary efforts in this area have been generated by Daniel and Kouvaritakis [DAN2], though a great deal of additional research is still required. With the analysis tools that are now available, it seems reasonable to anticipate that significant progress in this area can be achieved provided accurate frequency response uncertainty information can be included in the analysis.

Although the development of robust control design methodologies has tended to rely on frequency-domain techniques, the past decade has also been witness to the development of an alternate, time-domain approach to control design which caters for system uncertainty. This approach, commonly referred to as self-tuning control, combines an on-line computer-implemented control algorithm with an on-line model identification algorithm to update the system description based on observed changes in the input/output data of the plant. In effect, the self-tuning approach to control design accounts for system uncertainty by adjusting the feedback control algorithm in real-time based on available observations. Initiated by the key paper of Astrom and Wittenmark [AST1], research in this area has generated a number of successful SISO algorithms including methods based on the concepts of 'Generalized Minimum Variance' ([CLA1], [CLA2]), pole placement ([WEL1], [AST2]), and long-range predictive control ([CUT1], [CLA3], [CLA4]). This success has also prompted attempts by a number of researchers (including Borisson [BOR1]; Goodwin et al [GOO2], Koivo [KOI1], and Dugard et al [DUG1]) to extend these SISO self-tuning algorithms to multivariable systems. However, like initial attempts to extend classical frequency-domain techniques to the multivariable problem, these multivariable efforts have focused primarily on producing designs which completely decouple the dynamics of the open-loop plant so that SISO techniques can be applied directly to the diagonal elements of the noninteractive system. As such, they fail to account for the true multivariable characteristics of the system and, as a result, have met with only limited success in solving the

self-tuning problem for multivariable systems.

1.3 Description of the Thesis

1.3.1 Objectives

From the discussion above, it is clear that significant progress has been made towards the goal of establishing analysis and design techniques which address the practical problem of robust control system design in a systematic manner. But, it is also apparent that considerable effort is still required to complete the task. From a frequency-domain perspective, the ability to accurately quantify frequency response uncertainty is a particularly pressing issue. Indeed, each of the frequency-domain techniques highlighted above relies, to a large extent, on an accurate description of frequency response uncertainty. Without this information, the robust stability criteria provide only an indication of the size of assumed perturbations that can be tolerated before stability problems arise. No information on the robust performance characteristics of the system can be produced. Hence, in the absence of this uncertainty information, these analysis tools can provide only part of the assessment required for the design of robust control systems. For the LQG/LTR and H^{∞} design methods meanwhile, the lack of accurate frequency response uncertainty information leaves the design engineer at a loss when attempting to specify precise control design objectives. So, instead of producing a design tailored to the uncertainty characteristics of the system, these methodologies may yield arbitrary designs based on the specification of inappropriate design objectives.

Unfortunately, while the development of frequency-domain analysis and design tools has flourished, the task of generating the required uncertainty information has been virtually ignored. For the large class of practical systems whose models are generated via system identification procedures, it is, however, possible to generate an accurate statistical description of

frequency response uncertainty. Indeed, some recent developments (e.g. [LJU1], [LJU2], [EDM2], [LOH1]) have yielded limited results by producing various procedures for generating statistical information on the frequency response estimates at specified individual frequencies. The statistical nature of the uncertainty, however, suggests that the uncertainty description at any one frequency is dependent upon information at other frequencies. Thus, an uncertainty description that will be useful within the framework of available analysis and design methodologies (a framework which requires this information over a large range of frequencies) must quantify both the statistical uncertainty at individual frequencies and the interfrequency relationships associated with this information.

In the first part of the thesis, an investigation of this problem is conducted with the goal of developing procedures to generate a complete statistical description of frequency response uncertainty. As a parametric approach to model identification is adopted, the development addresses both the problem of quantifying the variability of the frequency response estimates associated with the estimated model and the problem of describing the bias introduced by the selection of a given model structure. In addition, the problem of characterizing the interfrequency dependence of the uncertainty information will be solved by producing an algorithm which yields accurate statistical information simultaneously over the entire frequency range of interest. The results derived yield not only an accurate description of frequency response uncertainty, but also a description that can be tailored to the specific frequency response characteristics of the system. In addition, the information will be produced in a format that is appropriate for use in existing robust analysis and design methodologies.

Following these developments, attention shifts to the problem of control design and, more specifically, to the problem of developing a multivariable algorithm that is suitable for on-line computer implementations. As highlighted previously, several such algorithms have

already been proposed for multivariable self-tuning applications. For the most part however, these results have met with limited success because, like the first attempts to extend classical frequency response techniques to the multivariable problem, they have focused on attempts to decouple the plant dynamics so that SISO techniques can be applied directly. As suggested by the frequency-domain developments of the generalized-Nyquist approach, what is clearly required to address this time-domain multivariable problem in a direct manner is the ability to embed existing SISO algorithms within a characteristic locus framework. In the second part of the thesis, the task of developing this capability is undertaken with the goal of producing an on-line multivariable control algorithm that can be used with conventional frequency-domain designs to yield much more accurate control implementations than those currently available and, in addition, is suitable for self-tuning implementations to handle the control problems associated with uncertain multivariable systems. Weighting sequence models, which proved useful for the frequency response uncertainty developments in the first part of the thesis, also provide a direct link from the frequency domain to the time domain. This link is used to develop a "characteristic subsystem" decomposition for multivariable systems within which existing SISO algorithms can be applied. For conventional designs, this decomposition is used to generate an "exactly" commutative controller which permits the direct modification of the open-loop characteristic loci simultaneously over all frequencies. For self-tuning applications, the result is an on-line algorithm which handles the multivariable characteristics of the system explicitly within a generalized-Nyquist framework.

1.3.2 Structure

The material presented in this thesis is organized into nine chapters according to the following general structure:

Chapter 1 : Introduction

Chapter 2 : Summary of Multivariable Frequency Response Methods

Chapters 3-6: Identification of Frequency Response Uncertainty Information

Chapters 7-8: On-Line Multivariable Control Design

Chapter 9 : Conclusion

Chapter 2 summarizes the predominant frequency-domain methods for the analysis of "certain" and "uncertain" multivariable systems. For "certain" systems, the generalized-Nyquist/characteristic-locus approach is described, and its implications for the assessment of closed-loop stability and performance are discussed. For "uncertain" systems, several important analysis techniques are described including results based on both singular value bounds and eigenvalue inclusion regions. The results for the case of element-by-element structured uncertainty are of particular interest and are described in some detail. These frequency-domain concepts provide the foundation and motivation for most of the subsequent developments.

The problem of defining a precise class of allowable element-by-element perturbations for systems whose dynamic descriptions are produced via system identification techniques is addressed in Chapters 3 through 6, and accurate statistical descriptions of frequency response uncertainty are derived for both scalar and multivariable systems. The development begins in Chapter 3 with an investigation of the variability of the frequency response estimates produced by the identification process [CL01]. A parametric approach to the model identification problem is adopted and, by first quantifying uncertainty in the parameter space and then transforming this information into the frequency domain, an accurate frequency response uncertainty description (in terms of confidence regions for the true system frequency response) is derived at each individual frequency. At the same time, the interfrequency dependence of this uncertainty information is quantified by producing a description that is valid simultaneously over all frequencies.

Finite weighting sequence models are found to be particularly useful for this purpose because they define exact linear transformations from the parameter space to the frequency domain. The introduction of these models,

however, necessarily implies the need for truncation to identify the appropriate model. This requirement also introduces a second element of uncertainty: the bias introduced by truncation. Although a number of order selection criteria have been proposed to solve the model selection problem by establishing an optimal trade-off between estimate variability and bias, these criteria are ineffective for weighting sequence truncation. Furthermore, they fail to account for the frequency response characteristics of the system; characteristics which are particularly important for the application proposed here. For these reasons, the truncation selection problem is examined in Chapters 4 and 5, and two new selection criteria are proposed.

The first criterion is presented in Chapter 4. Using geometric interpretations of the standard "parameter-space" problem, the truncation selection problem is reformulated in terms of the system frequency response characteristics at a preselected frequency [CL02]. An easy-to-implement criterion is derived to handle bias implicitly by selecting the truncation which establishes an optimal trade-off between estimate-variability and bias in the frequency domain. This criterion establishes the correct dependence of truncation level on frequency and, because an optimal trade-off between bias and variability has been achieved, the frequency response confidence bounds (derived in Chapter 3) will be accurate at the specified frequency. However, the identified truncation is frequency-specific. As such, accurate uncertainty information will only be available over a limited range of frequencies. So, the ability to quantify the interfrequency dependence of this information will be severely restricted.

To retain information on the interdependence of the uncertainty descriptions at individual frequencies [CL03], an alternative criterion is derived in Chapter 5. First, a statistical definition of the optimal model order (based on maximum likelihood arguments) is presented. Theoretically, this optimal model order can be identified using Akaike's Information

Theoretic Criterion [AKA1]. However, practical implementations of this criterion are found to require "correction factors" to ensure that the proper model is selected. For weighting sequence truncation, appropriate corrections are identified and used to establish an alternative, implementable criterion. This criterion not only identifies the optimal truncation, it also quantifies the bias associated with this truncation. Thus, by establishing appropriate frequency-domain extensions, this criterion is shown to produce explicit bounds on the frequency response bias introduced by truncation at each and every frequency.

In Chapter 6, the results of Chapters 3 and 5 are consolidated and used to produce a complete description of frequency response uncertainty (including the effects of both estimate-variability and bias). Techniques are also developed to optimize this uncertainty description based on the frequency response characteristics of the system. Furthermore, it is shown that the procedures derived for SISO systems can be readily extended to multivariable systems to establish an accurate element-by-element description of frequency response uncertainty. Finally, this element-by-element uncertainty description is combined with the structured uncertainty analysis techniques summarized in Chapter 2 to generate bounds for the characteristic loci of the perturbed system, and the implications of the resulting uncertainty description are discussed.

An investigation of the multivariable control design problem begins in Chapter 7 with the derivation of a system description which transforms the fundamental concepts of the frequency-domain, characteristic-locus design philosophy into a time-domain format and which permits the development of on-line control algorithms in a true generalized-Nyquist sense [CL04]. Again, weighting sequence models are found to be particularly useful in establishing the required link between the frequency domain and the time domain. More specifically, it is shown that the 'characteristic sequences' method [KOU2] generates a time-domain (weighting sequence) description for

the eigenstructure of a multivariable system. This sequence representation is used to establish an alternative z-domain "characteristic subsystem" description for the system, and the properties of this subsystem description are investigated. Although it is found that, in some instances, this z-domain description may not be suitable for control design purposes, conditions which guarantee the utility of the representation are identified and techniques to ensure the availability of suitable representations are proposed. The utility of the computer implementations based on this "characteristic subsystem" methodology is then demonstrated using a conventional characteristic-locus/commutative-controller design technique, and it is shown that these new implementations produce much more accurate results than those currently in use.

In Chapter 8, a multivariable self-tuning algorithm is proposed, which incorporates existing SISO self-tuning algorithms into the now-available "characteristic subsystem" framework [CL05]. The SISO Generalized Predictive Control algorithm proposed by Clarke et al [CLA3] is found to be particularly useful for this purpose because it explicitly uses a finite number of weighting sequence elements to derive the desired control law. As such, it can be readily generalized to the multivariable problem using the sequence representations developed previously. Several implementation considerations (unique to the multivariable problem) are also highlighted, and the resulting algorithm is shown (via simulation) to produce effective control. Finally, the problem of on-line identification is considered, and two algorithms are proposed for the identification of the "characteristic subsystem" descriptions directly from input/output data. It is suggested that, using these algorithms, both the output prediction and control calculation tasks can be performed entirely as scalar operations, thereby reducing the computational complexity of the overall self-tuning algorithm.

The thesis concludes in Chapter 9 with a brief summary and proposals for further research.

1.3.3 Notation

The following notational conventions will be used throughout this thesis unless explicitly redefined elsewhere:

SISO :	Single-Input/Single-Output	MIMO :	Multi-Input/Multi-Output
min :	minimum	sup :	supremum
max :	maximum	inf :	infimum

R : the field of real numbers

R^n : the n-dimensional vector space defined over R

R_+ : the set of non-negative numbers

C : the field of complex numbers

C^{nxm} : the set of matrices with n rows and m columns with elements in C

$|x|$: absolute value of the scalar x

$\arg(x)$: argument of the complex scalar x

x^t : the transpose of the vector x

e_i : the i^{th} standard basis vector (i.e. the i^{th} column of the identity matrix)

$\overline{XY}$: the vector defined from point X to point Y

$||x||$: the two-norm of the vector x, defined by $\sqrt{x^t x}$

A^T : the transpose of the matrix A

$\lambda(A)$: an eigenvalue of the matrix A

$\rho(A)$: the spectral radius of the matrix A, defined by $\max_i |\lambda_i(A)|$

$\sigma(A)$: a singular value of the matrix A

$\bar{\sigma}(A)$: the maximum singular value of the matrix A

$\underline{\sigma}(A)$: the minimum singular value of the matrix A

tr [A] : the trace of the matrix A

det [A], |A| : the determinant of the matrix A

A^+ : a matrix with all elements replaced by their absolute values

T : the sample interval for a discrete-time system

$y(kT) = y(k)$: the time-domain quantity y, defined at sample time kT

${}^{s}g$: a sequence of quantities defined at discrete points in time (e.g. ${}^{s}g = [g(0), g(1), \cdots]$)

α : a specified level of confidence (between 0 and 1)

$P\{S\}$: the probability associated with the occurrence of the event S

$E\{x\}$: the expected value of the random variable x

σ_x^2 : the variance of the scalar random variable x

Additional notation will be defined as required.

CHAPTER TWO

FREQUENCY DOMAIN ANALYSIS OF MULTIVARIABLE SYSTEMS

As highlighted in the introduction, the implementation of frequency response methods for the analysis and design of multivariable feedback control systems has staged a dramatic comeback over the past two decades. This chapter summarizes relevant aspects of the most important developments associated with the frequency-domain analysis of both "certain" (unperturbed) and "uncertain" (perturbed) multivariable systems.

2.1 Analysis of Unperturbed Systems: The Characteristic Locus Method

The generalized-Nyquist/characteristic-locus method proposed by MacFarlane and Belletrutti [MAC1], MacFarlane and Postlethwaite [MAC2] and MacFarlane and Kouvaritakis [MAC3] is a particularly useful tool for the analysis and design of unperturbed systems. Among the most important reasons for this are the following:

(i) It establishes necessary and sufficient conditions for the stability of the closed-loop system.

(ii) It reduces the multivariable design problem to a set of SISO problems on which classical frequency response analysis and design concepts can be applied.

The foundation for this frequency-domain method is the theory of algebraic functions [BLI1] which makes it possible to relate a scalar algebraic function, $g(s)$, to an $m \times m$ matrix-valued function of a complex variable, $G(s)$, whose elements are rational functions in s. More specifically, this theory can be used to define a set of characteristic gain functions, $g_j(s)$, which satisfy the characteristic equation:

$$\Delta(s,g) = \det\{g(s)I - G(s)\} = \prod_{j=1}^{k} \Delta_j(s,g) = 0 \qquad \ldots.(2.1)$$

where each $\Delta_j(s,g)$ is a polynomial in $g(s)$ of order z_j (with coefficients $\{\alpha_{ji}(s);\ i=0,\cdots,z_j\}$) which is irreducible over the field of rational

functions and each one of the functions $g_j(s)$ is associated with a single $\Delta_j(s,g)$. Although eqn 2.1 defines the most general expression for the characteristic equation, for most practical systems the polynomial $\Delta(s,g) = \det\{g(s)I - G(s)\}$ is itself irreducible. So for simplicity in the following presentation, it will be assumed that there is a single characteristic gain function, g(s), defined by the solution of:

$$\Delta(s,g) = \det\{g(s)I - G(s)\} = a_m(s)\, g^m + \cdots + a_0(s) = 0, \quad \ldots.(2.2)$$

Since $\Delta(s,g)$ is irreducible, the characteristic gain will be multi-valued over the field of complex numbers, C. Hence, closed curves in the complex s-plane may not map to closed curves in the g(s)-plane. To overcome this difficulty, g(s) must be defined on an m-sheeted Riemann surface consisting of m copies of the complex plane appropriately joined together so that g(s) is single-valued in this domain [MAC2]. The generalization of the SISO frequency response plot follows immediately by mapping m copies of the Nyquist D-contour (one on each of the m copies of the complex plane described above) under the characteristic gain function, g(s).

A practical alternative to the Riemann surface development summarized above is provided by the fact that, almost everywhere on the complex plane, the m roots of eqn 2.2 (i.e. the eigenvalues of G(s)) form a set of locally-distinct analytic branches $\{g_i(s);\ i=1,\cdots,m\}$ which will be referred to as the eigenfunctions of G(s). The generalized frequency response plot can, therefore, be generated as the composite plot of the set of loci traced out by the eigenvalues of G(s) as s traverses a single copy of the Nyquist contour. The loci generated in this manner are called the characteristic loci of the system and, for practical systems, the characteristic loci (possibly after appropriate pairing of positive and negative frequencies) will form closed curves so that it is convenient to think of them as m distinct plots. Furthermore, to each eigenfunction, $g_i(s)$, of G(s), there correspond two vector-valued functions of s, $w_i(s)$ and $v_i^t(s)$, which satisfy the standard eigenvalue/eigenvector relationships for G(s); namely,

$$G(s)\, w_i(s) = g_i(s)\, w_i(s) \qquad v_i^t(s)\, G(s) = g_i(s)\, v_i^t(s)$$

$$v_i^t(s)\, w_i(s) = 1\ , \quad \forall\, i \qquad\qquad v_i^t(s)\, w_k(s) = 0\ , \quad \forall\, i,k \quad i \neq k$$

These vector-valued functions will be referred to as the characteristic directions (or eigenvectors) and the dual characteristic directions (or dual eigenvectors) of G(s), respectively.

Using the definitions above, G(s) may be rewritten in terms of the eigenfunctions, eigenvectors, and dual eigenvectors as:

$$G(s) = W(s)\, \Lambda(s)\, V(s) = \sum_{i=1}^{m} g_i(s)\, w_i(s)\, v_i^t(s) \qquad ....(2.3)$$

In addition, the closed-loop transfer function $R(s) = \{[I + G(s)]^{-1}\, G(s)\}$ can be related to the open-loop eigenfunctions and characteristic directions in the following way:

$$R(s) = W(s)\, \{[I + \Lambda(s)]^{-1}\, \Lambda(s)\}\, V(s) = \sum_{i=1}^{m} \frac{g_i(s)}{1 + g_i(s)}\, w_i(s)\, v_i^t(s) \qquad ....(2.4)$$

Eqn 2.4 clearly highlights two particularly noteworthy characteristics. First, the eigenvector structures of the open-loop and closed-loop systems are identical. Second, the open-loop and closed-loop eigenfunctions maintain the classical open- to closed-loop relationship typically associated with SISO systems. These properties can, in fact, be used to relate the frequency response characteristics of the open-loop eigenfunctions and characteristic directions to the stability and performance characteristics of the closed-loop system as described below.

2.1.1 Stability Assessment

For SISO systems, the return difference operator, $f(s) = 1 + g(s)$, is related to the closed-loop poles of the system by:

$$f(s) = 1 + g(s) = \frac{p_c(s)}{p_o(s)} \qquad ....(2.5)$$

where $p_c(s)$ and $p_o(s)$ are the closed-loop and open-loop pole polynomials of the system respectively. This relationship, when used in conjunction

with the principle of the argument, leads to the well-known Nyquist stability criterion for SISO systems.

A relationship similar to eqn 2.5 can also be established for multivariable systems. For proper systems, this relationship is:

$$\det\{F(s)\} = \det\{I + G(s)\} = \gamma \frac{p_c(s)}{p_o(s)} \qquad \ldots.(2.6)$$

where F(s) is the multivariable counterpart of f(s) and γ is a constant. Indeed, eqn 2.6 may be used with the principle of the argument to establish the closed-loop stability of multivariable systems. Unfortunately, no convenient relationships between det{F(s)} and det{G(s)} exist, so this result cannot be used to generate the same simple relationship between open-loop frequency response and closed-loop stability that is available for SISO systems. However, eqn 2.6 may be reduced to a more recognizable form using the eigenfunctions of F(s) and G(s). In particular, noting that the eigenfunctions, $f_i(s)$, of F(s) can be defined in the same manner as the eigenfunctions of G(s), a standard result from matrix algebra can be used to rewrite eqn 2.6 as:

$$\det\{F(s)\} = \prod_{i=1}^{m} f_i(s) = \prod_{i=1}^{m} [1 + g_i(s)] = \gamma \frac{p_c(s)}{p_o(s)} \qquad \ldots.(2.7)$$

Eqn 2.7 is now in a form which enables the application of a generalized principle of the argument to establish the generalized Nyquist criterion. A rigorous derivation of this criterion is given in [MAC2]. It suffices here, however, to note that the characteristic loci of F(s) form a set of closed curves on the complex plane which can be used to investigate closed-loop stability. In addition, the characteristic loci of G(s) may be related to those of F(s) (for purposes of this stability investigation) by shifting attention from the origin to the critical point, [-1,0], in the complex plane. Hence, the characteristic loci of G(s) emerge as the appropriate medium for defining the generalized Nyquist criterion which may be stated as follows:

The multivariable system defined by G(s) (with no unstable modes which are uncontrollable and/or unobservable) will be stable under unity feedback if, and only if, the net sum of counterclockwise encirclements of the critical point [-1,0] by the characteristic loci of G(s) is equal to the number of open-loop unstable poles of G(s).

2.1.2 Performance Evaluation

The relationships identified above can be used not only to establish the multivariable generalization of the Nyquist stability criterion, but also (because of the analytic nature of the eigenfunctions, $g_i(s)$) to assess the closed-loop performance of the system. In particular, the same one-to-one relationship between the proximity of $g(j\omega)$ to the [-1,0] point and the location of the closed-loop poles that holds for SISO systems also applies directly to the characteristic loci of multivariable systems. As a result, the classical frequency-domain concepts of bandwidth and gain/phase margins can be applied to the open-loop characteristic loci to assess the transient response characteristics (i.e. rise time, settling time, percent overshoot, etc.) of the closed-loop system. Because of the additional multidimensional aspects of the problem however, there are other considerations which must also be addressed.

As shown in [MAC3], these additional topics can be highlighted by considering the response of the closed-loop system to a reference input vector sinusoid represented by means of the input phasor vector $r(j\omega)$. From eqn 2.4, closed-loop system output for this specific input is given by:

$$y(j\omega) = \sum_{i=1}^{m} \frac{g_i(j\omega)}{1 + g_i(j\omega)} \{v_i^t(j\omega) \cdot r(j\omega)\} \, w_i(j\omega) \qquad \ldots.(2.8)$$

Eqn 2.8 clearly demonstrates that system output can be expressed as the sum of m components, each of which lies along a characteristic direction, $w_i(j\omega)$, and is modulated by the corresponding frequency-dependent eigenfunction of the closed-loop system, $g_i(j\omega)/\{1+g_i(j\omega)\}$. As such, closed-loop accuracy and multivariable interaction may be analyzed in terms

of the eigenfunctions and characteristic directions of the system. In particular, when the moduli of all the frequency-dependent eigenfunctions, $g_i(j\omega)$, are sufficiently large, $g_i(j\omega)/\{1+g_i(j\omega)\} \simeq 1$ and eqn 2.8 reduces to:

$$y(j\omega) \simeq \sum_{i=1}^{m} \{w_i(j\omega)\, v_i^t(j\omega)\}\, r(j\omega) = r(j\omega)$$

So, large moduli lead to good accuracy. This relationship also suggests that the response of the j^{th} output to the i^{th} input (for $j \neq i$) is negligible. Hence, large moduli will also act to suppress interaction. Alternatively, when large gains cannot be achieved (due to stability considerations or power limitations, for example), low interaction can be achieved by aligning the characteristic directions to the standard basis vectors. When this is accomplished, an input in the direction of the i^{th} standard basis vector, e_i, produces an output which is itself in the direction of e_i (as demonstrated by eqn 2.8). Hence, interaction is again suppressed and an appropriate level of accuracy can be achieved by manipulation of the appropriate $g_i(j\omega)$.

The observations above can be used to identify the following set of conditions which must be satisfied to ensure satisfactory closed-loop performance in terms of stability and low interaction:

(i) The set of characteristic loci, $\{g_i(j\omega),\ j=1,\ldots,m\}$, must satisfy the generalized Nyquist stability criterion.

(ii) The characteristic loci must all have sufficiently high gain over a desired operating bandwidth to provide the required accuracy for the tracking of a reference input vector by the output vector.

(iii) The high frequency alignment of the characteristic directions of G(s) to the standard basis direction set should be sufficiently good to keep high frequency interaction within acceptable limits.

Once these conditions have been satisfied, the eigenvalue, $g_i(j\omega)$ associated with the eigenvector, $w_i(j\omega)$, which aligns best with the j^{th} standard basis

vector, e_j, can be regarded as a good practical approximation to the transference between the j^{th} input and j^{th} output at the specified frequency. Thus, an assessment of loop-by-loop performance (i.e. the closed-loop response of the j^{th} output to the j^{th} input) can be based on an inspection of the appropriate characteristic locus and classical frequency response concepts may be applied to ascertain the dynamic performance characteristics of each individual loop. Finally, control designs based on the manipulation of the characteristic loci can be used to achieve the desired response.

2.2 Analysis of Perturbed Systems

For practical situations, the errors inherent in describing any physical system by a finite-dimensional linear model introduce uncertainties which cannot be handled explicitly in the design process. Yet adequate control designs must incorporate features that allow the closed-loop system to function properly despite these uncertainties. Although common multivariable design algorithms (including the characteristic locus method) work exceptionally well in the absence of uncertainty, examples have been generated to demonstrate the sensitivity of these methods to changes in the nominal plant. Due to this sensitivity, designs based on a specific nominal plant model may not produce reliable closed-loop behaviour in the presence of uncertainty.

To investigate the adequacy of any control system design, it is therefore necessary to assess not only the nominal behaviour of the plant but also the robustness characteristics associated with this behaviour. As mentioned previously, interest in this aspect of feedback control has prompted a great deal of research over the past several years (e.g. [ILM1], [ISR1]), and many interesting and useful results have been produced. A necessary first step in developing analysis techniques to assess system robustness is the development of a mathematical formulation of the

perturbation problem. Two widely-used uncertainty descriptions for this purpose are given by additive and multiplicative perturbations to a nominal transfer function matrix, G, as shown here:

$$G_p(s) = G(s) + \Delta(s) \qquad G_p(s) = [I + D(s)]\, G(s) \quad ....(2.9a,b)$$

Since the developments for both representations are similar, only additive perturbations will be considered further here. Simple extensions of the following results to the case of multiplicative perturbations can be obtained by making appropriate substitutions in the development.

Given the additive perturbation representation above, the use of frequency response characteristics to assess the robust stability properties of multivariable systems has proven to be particularly effective. Under the assumption that the number of unstable open-loop poles of $G_p(s)$ and $G(s)$ are identical, an extension of the generalized Nyquist criterion to the analysis of perturbed systems clearly suggests that the closed-loop system will remain stable if, and only if, the nominal characteristic loci of the system satisfy the generalized Nyquist criterion and none of the nominal characteristic loci can be deformed so as to pass through the [-1,0] point as G is warped continuously toward G_p. This condition, in turn, is satisfied if, and only if,

$$|I + G + \Delta| \neq 0; \qquad \forall\, \Delta \qquad ....(2.10)$$

But condition 2.10 can be rewritten as:

$$|I + G + \Delta| = |I + G|\, |I + (I + G)^{-1} \Delta| \neq 0$$

and, since $|I + G| \neq 0$, this result implies the following spectral radius condition:

$$\max_i |\lambda_i[(I+G)^{-1} \Delta]| = \rho[(I+G)^{-1} \Delta] < 1; \qquad \forall\, \Delta \quad ....(2.11)$$

Conditions 2.10 and 2.11 provide necessary and sufficient conditions for the guaranteed stability of the perturbed closed-loop system and form the basis for many of the robust stability criteria that have been proposed to date.

Effective criteria, however, require more than the simple uncertainty formulations defined by eqns 2.9a,b. An accurate, more-detailed

mathematical description of the class of allowable perturbations is also required; a description that must be sufficiently simple to yield useful analytical results, yet complex enough to restrict the class to only those perturbations that can actually occur. Several such descriptions are presented below, and the robustness criteria arising from these descriptions are summarized.

2.2.1 The Case of Unstructured Perturbations

A large number of studies have focused on the relatively simple case where the only available information on $\Delta(s)$ is an upper bound on its maximum singular value at each frequency. This class of "unstructured" perturbations can be described by:

$$D_U = \{\Delta(s): \bar{\sigma}[\Delta(s)] \leq \delta(s) \in R_+; \ \forall s = j\omega\} \qquad \ldots.(2.12)$$

Using a singular value analysis, Doyle and Stein [DOY1] have shown that, when the nominal system is closed-loop stable and the number of unstable poles of G and G_p are identical, the perturbed system will remain stable for all allowable perturbations if, and only if,

$$\underline{\sigma}[I + G(s)] > \bar{\sigma}[\Delta(s)] \qquad \forall s = j\omega \qquad \ldots.(2.13)$$

This result follows directly from inequality 2.11 since

$$\rho[(I+G)^{-1}\Delta] \leq \bar{\sigma}[(I+G)^{-1}\Delta] \leq \bar{\sigma}[(I+G)^{-1}]\,\bar{\sigma}[\Delta] \qquad \ldots.(2.14)$$

and it can be shown that there exists at least one $\Delta \in D_U$ such that the equalities in eqn 2.14 hold. Hence, a necessary and sufficient condition for perturbed system stability is:

$$\bar{\sigma}[(I+G)^{-1}]\,\bar{\sigma}[\Delta] < 1$$

and condition 2.13 follows immediately. Other singular value criteria (based on an inverse Nyquist test) have been proposed for the less likely situation where the number of unstable open-loop poles of G and G_p are not the same and when information on the size of the perturbation associated with the inverse plant is available [POS1], but these criteria will not be discussed in detail here.

Singular value criteria such as the one identified by condition 2.13 provide an immediate assessment of the magnitude of uncertainty that can be tolerated while maintaining closed-loop stability. However, these criteria focus on system gain information while failing to account directly for any available phase information. Yet, as suggested by the characteristic locus method, the eigenvalues of the perturbed system may also be used to assess the robust performance of the system provided appropriate phase information can be generated. Towards this goal, several results ([DAN1]-[DAN3],[HAR1]) have been produced to establish characteristic locus inclusion bands based on the assumption of unstructured uncertainties.

A useful starting point for the development of characteristic locus bounds is the Bauer-Fike eigenvalue perturbation result [WIL1] given by:

$$|\lambda(G_p) - \lambda(G)| \leq c\,\delta \qquad \ldots.(2.15)$$

where c is the condition number of the nominal eigenvector matrix W defined by $\bar{\sigma}(W)/\underline{\sigma}(W)$. This result can be used to construct circular regions in the complex plane which contain the perturbed system characteristic loci. However, in situations where the eigenvectors of G are skew, these regions may be excessively large and may also be extremely sensitive to small changes in the nominal. To overcome these problems, Daniel and Kouvaritakis ([DAN1],[DAN2]) have suggested the use of normal approximations to the nominal plant and have demonstrated the improvements in both size and sensitivity that can be achieved using this approach. Furthermore, the normal approximation bounds can be refined still further by combining them with information on the numerical range of G [DAN2] and by implementing similarity scaling techniques [HAR1] to produce eigenvalue inclusion regions which are easy to compute and insensitive to changes in the nominal. The resulting characteristic locus description for the perturbed system paves the way, as highlighted in [DAN2], for a systematic design methodology based on the manipulation of the characteristic locus bands in a robust manner. Unfortunately, the design procedure may, in this case, generate conservative

results due to the fact that the inclusion bands are not tight (i.e. boundary points of the given eigenvalue inclusion regions may not be attainable for any Δ in the specified class).

In search of non-conservative results, it should be recognized that the eigenvalues of $G + \Delta$ are given by the solutions, z, of:

$$|G + \Delta - zI| = 0 \quad \text{or equivalently} \quad \underline{\sigma}(G - zI + \Delta) = 0$$

Using the singular value inequality [GAN1],

$$\underline{\sigma}(G + \Delta - zI) \geq \underline{\sigma}(G - zI) - \bar{\sigma}(\Delta), \qquad \ldots.(2.16)$$

the following theorem may be stated:

Theorem 2.1: [DAN3] Let $z \in C$ and $\Delta \in D_U$, then

(i) if $\underline{\sigma}(G-zI) > \delta$, z is not an eigenvalue of $G + \Delta$ for any $\Delta \in D_U$;

(ii) if $\underline{\sigma}(G-zI) \leq \delta$, there exists a $\Delta \in D_U$ such that z is an eigenvalue of $G + \Delta$.

This result leads directly to the construction of exact characteristic locus inclusion regions (referred to as E-contours). If $z = \lambda_i + \rho(\theta)\, e^{j\theta}$ where λ_i represents an eigenvalue of the nominal system at a given frequency, $0 \leq \theta < 2\pi$ and $\rho(\theta) \in R_+$, then the first solution, z, of $\underline{\sigma}(G - zI) = \delta$ as $\rho(\theta)$ increases identifies a point on the boundary of the region at the specified frequency. It has been shown [DAN3] that the E-contours formed in this manner generate simply-connected closed curves, the union of which contains the characteristic loci of the perturbed system. Once these bounds are established, robust stability can be assessed using the generalized Nyquist criterion and, since the characteristic loci of G_p will lie on the boundary for some $\Delta \in D_U$, the resulting stability criterion is necessary and sufficient (providing an alternative to the Doyle/Stein criterion identified by condition 2.13). Indeed, the equivalence of these criteria can be established by setting $z = -1$ in Theorem 2.1. The key additional feature of the E-contour result, however, is the addition of phase information to the uncertainty description; an addition which preserves the classical Nyquist

attributes of the frequency-domain description of the system and permits the assessment of both robust stability and robust performance.

2.2.2 The Case of Structured Perturbations

Although the assumption of unstructured perturbations produces a particularly convenient mathematical description of uncertainty for analysis purposes, this description cannot accommodate information on individual elements or blocks of the perturbation. In most practical situations however, any non-arbitrary estimate for the upper bound on $\bar{\sigma}(\Delta)$ generally implies that this extra information is available. Under these circumstances, a robustness analysis based on unstructured uncertainty may be unduly conservative due to the fact that this additional information has been ignored and, hence, that the true class of allowable perturbations has not been precisely defined. To reduce this conservatism, the description of the class of perturbations under investigation must be refined and appropriate analysis tools to accommodate these refinements must be developed. Several particularly useful descriptions of uncertainty for this purpose have been identified and the classes of perturbations associated with these descriptions are defined by:

(i) the class of "block-diagonal" perturbations:

$$D_D = \{\Delta \in C^{m\times m}: \ \Delta = \text{diag}\{\Delta_{ii}\} \ ; \ \bar{\sigma}(\Delta_{ii}) \leq \delta \in R_+\} \quad ....(2.17a)$$

(i.e. Δ_{ii} is an unstructured block along the diagonal of Δ);

(ii) the class of "block-structured" perturbations:

$$D_B = \{\Delta \in C^{m\times m}: \ \Delta = [[\Delta_{ij}]]; \ \bar{\sigma}(\Delta_{ij}) \leq \delta \in R_+\} \quad ....(2.17b)$$

where $\Delta = [[\Delta_{ij}]]$ indicates that the matrix Δ is composed of several arbitrarily-positioned, unstructured blocks; and

(iii) the class of element-by-element, bounded perturbations:

$$D_S = \{\Delta \in C^{m\times m}: \ |\Delta_{ij}| \leq p_{ij} \in R_+; \ \arg(\Delta_{ij}) = \theta_{ij}, \ 0 \leq \theta_{ij} < 2\pi\}$$
$$= \{\Delta \in C^{m\times m}: \ \Delta^+ \leq P \} \quad ....(2.17c)$$

To initiate investigations of the structured perturbation problem, Doyle [DOY2] defined the function μ such that:

$$\mu(M) = \begin{cases} 0 \text{ if no } \Delta \in D_D \text{ solves } |I + M\Delta| = 0 \\ [\min \bar{\sigma}(\Delta): |I + M\Delta| = 0]^{-1}; \quad \Delta \in D_D \end{cases} \quad \ldots.(2.18)$$

where $M = (I + G)^{-1}$. Using this definition, a necessary and sufficient condition for robust stability is:

$$\mu(M)\ \delta < 1 \quad \ldots.(2.19)$$

In effect, condition 2.19 reiterates the spectral radius condition defined by condition 2.11 except that now $\mu(M)$ (and any upper bounds generated for it) must explicitly account for the structure of the assumed perturbations.

One means of accomplishing this task is the use of eigenvalue-preserving scaling techniques. As shown in [DOY2] and [SAF1], similarity scaling with a positive, diagonal scaling matrix S may be used to attack the problem of diagonal perturbations. In particular,

$$\sup_{\Delta \in D_D} \rho(M\Delta) = \sup_{\Delta \in D_D} \rho(S M \Delta S^{-1}) = \delta \sup_{U} \rho(SMS^{-1}U) = \delta \sup_{U} \rho(\tilde{M} U)$$

where U is a unitary matrix containing the phase information associated with $\Delta \in D_D$. Under these circumstances, μ takes the form:

$$\mu = \sup_{U} \rho(\tilde{M} U) \leq \inf_{S} \{\bar{\sigma}(SMS^{-1})\} \quad \ldots.(2.20)$$

Thus, an upper bound on μ (which incorporates structural information) can be identified by selecting S to minimize $\bar{\sigma}(SMS^{-1})$. This similarity-scaling approach also applies to the more general block-structured problem since any block-structured matrix can be rearranged into block-diagonal form using appropriate eigenvalue-preserving transformations [DOY2]. Doyle has also shown that equality in eqn 2.20 holds for up to three distinct blocks and, hence, a stability criterion based on $\inf_{S} \{\bar{\sigma}(SMS^{-1})\}$ is necessary and sufficient for at least this set of structured perturbation problems.

The block-structured/similarity-scaling approach can, of course, be applied directly to element-by-element, bounded perturbations as well. In this case however, the dimension of the optimization problem increases from

$m-1$ to m^2-1, and the complexity of the optimization problem increases commensurately. As a result, additional research has focused on generating alternative criteria for this problem. Early efforts ([KAN1], [LUN1], [OWE1]) used positive matrix results based on the spectral radius relationship:

$$\rho(M\Delta) \leq \rho(M^{+}P)$$

to generate stability criteria which can be easily computed. However, because these criteria ignore available phase information on M, the resulting analysis tends to be unnecessarily conservative. Kouvaritakis and Latchman have shown that such conservatism can be reduced using scaling techniques [KOU4]. Because of the element-by-element nature of the problem, it is possible, as demonstrated below, to introduce all of the flexibility required by using $2m-1$ "non-similarity" scaling parameters instead of the m^2-1 similarity scaling parameters discussed above.

Returning to condition 2.11, a necessary and sufficient condition for robust stability is given by $\rho(M\Delta) < 1$. But,

$$\begin{aligned}\rho(M\Delta) = \rho(R^{-1}M\Delta R) = \rho(R^{-1}ML^{-1}L\Delta R) &\leq \bar{\sigma}(R^{-1}ML^{-1}L\Delta R) \\ &\leq \bar{\sigma}(R^{-1}ML^{-1})\ \bar{\sigma}(L\Delta R) \qquad \ldots.(2.21)\end{aligned}$$

where L and R are positive, diagonal matrices. Hence, selecting L and R to minimize the "cross-condition number" defined by:

$$k\{P,M^{-1}\} = \bar{\sigma}(LPR) \,/\, \underline{\sigma}(LM^{-1}R) \qquad \ldots.(2.22)$$

will significantly reduce the calculated upper bound on $\rho(M\Delta)$ and the corresponding stability criterion can be made less conservative. In fact, condition 2.21 suggests that (after implementing non-similarity scaling) the only remaining conservatism arises from either of the two inequalities:

$$\rho(R^{-1}ML^{-1}L\Delta R) \leq \bar{\sigma}(R^{-1}ML^{-1}L\Delta R) \quad \text{or} \quad \bar{\sigma}(R^{-1}ML^{-1}L\Delta R) \leq \bar{\sigma}(R^{-1}ML^{-1})\ \bar{\sigma}(L\Delta R)$$

So, the conservatism in the resulting stability condition will be completely eliminated if the equalities in both these relationships hold simultaneously. As shown in [KOU5], this goal is attained when certain relationships between $\tilde{M} = R^{-1}ML^{-1}$ and the "worst-case" $\tilde{\Delta} = L\Delta R$ exist. In

particular, if the major input and output principal directions of a matrix A ($\bar{y}_A$ and $\bar{x}_A$, respectively) are defined as the eigenvectors associated with the maximum singular value of A in the following manner:

$$A^*A\,\bar{y} = \bar{\sigma}^2\,\bar{y} \qquad\qquad A\,A^*\,\bar{x} = \bar{\sigma}^2\,\bar{x}$$

it is possible to establish the following result:

THE MAJOR PRINCIPAL DIRECTION ALIGNMENT (MPDA) PRINCIPLE: [KOU5]

$\rho(\tilde{M}\tilde{\Delta}) = \bar{\sigma}(\tilde{M})\,\bar{\sigma}(\tilde{\Delta})$ if, and only if, $\underset{\sim}{\bar{x}}_M = e^{j\psi}\,\underset{\sim}{\bar{y}}_\Delta$ and $\underset{\sim}{\bar{y}}_M = e^{j\phi}\,\underset{\sim}{\bar{x}}_\Delta$ (i.e. the major principal directions of $\tilde{M}$ and $\tilde{\Delta}$ are 'aligned').

Based on this result, a singular value analysis of robust stability will yield necessary and sufficient conditions if, and only if, MPDA holds for $\tilde{M}$ and the "worst-case" $\tilde{\Delta}$. It is interesting to note here that, for the case of unstructured uncertainty, MPDA is always satisfied without scaling due to the phase flexibility in the prescribed perturbation class. However, the structural properties associated with the class of perturbations defined by D_S necessarily constrains the principal directions of Δ and so scaling must be used to precondition the problem with a view towards achieving MPDA In fact, it has been shown [KOU5] that, for independent element-by-element perturbations, the scaling matrices (L and R) which minimize the cross-condition number defined by eqn 2.22 also equalize the moduli of the elements of $(\underset{\sim}{\bar{x}}_M, \underset{\sim}{\bar{y}}_\Delta)$ and $(\underset{\sim}{\bar{x}}_\Delta, \underset{\sim}{\bar{y}}_M)$ simultaneously provided that either $\tilde{M}$ is 2 x 2 or the maximum singular value of $R^{-1}ML^{-1}$ has a stationary point. Furthermore, because the phases of the elements of Δ can be adjusted independently, it is always possible to select a perturbation $\Delta \in D_S$ which aligns the principal directions for the given scaling. When combined, these results produce:

The Cross-Condition Number Criterion: [KOU5],[LAT1] For all s on the Nyquist D-contour,

(i) Let G(s) denote the nominal open-loop transfer function matrix of a linear, time-invariant multivariable system which is stable under unity feedback;

(ii) let $\Delta(s)$ be a stable transfer function matrix such that $\Delta(s)$ exists in D_s; and

(iii) assume that G(s) is 2 x 2 or that the cross-condition number (eqn 2.22) has a stationary point.

Then the perturbed system, $G(s) + \Delta(s)$, is guaranteed to be stable if and only if the optimal cross-condition number defined by:

$$k_o\{P,M^{-1}\} = \inf_{L(s),\ R(s)} \{\bar{\sigma}(LPR) \ / \ \underline{\sigma}(LM^{-1}R)\} \qquad ....(2.23)$$

is less than unity for all s.

Although developed originally for independent element-by-element bounded perturbations, this result has also been extended to the more general block-structured problem. For independent block-structured perturbations, diagonal similarity scaling provides enough degrees of freedom to achieve MPDA. However, non-diagonal scaling is required when dependent perturbations exist and, when the cross-condition number does not have a stationary point, a general principal direction alignment property must be combined with the eigenvalue shift property to compute the desired bound. The details of these additional developments are beyond the scope of this summary and are not directly relevant to the following discussions. For these reasons, the extensions will not be discussed further here. An in depth development of these results can, however, be found in [DAN4], [KOU6], and [KOU7].

As was true for the unstructured uncertainty analysis discussed previously, the structured perturbation criteria (eqns 2.19 and 2.23) focus strictly on system gain to produce an immediate assessment of the magnitude of uncertainty that can be tolerated while maintaining closed-loop stability. Again, phase information has been discarded and, hence, these

criteria cannot be used to extend the analysis beyond the assessment of stability. To overcome this shortcoming, an extension to the unstructured E-contour results discussed previously has been proposed based on the following result:

Theorem 2.2: [KOU4],[KOU6] Let the points on the E-contours constructed for the unstructured perturbations, $\Delta \in D_U$, be denoted by $z_b = \lambda_i + \rho_{E_i}(\theta)\, e^{j\theta}$; and let $\delta\rho_i(\theta) \in R_+$ be the smallest value such that

$$k_o\left\{ P\ ,\ [G - \{z_b - \delta\rho_i(\theta)\ \varepsilon^{j\theta}\}\ I] \right\} = 1.$$

Then, the loci of points

$$\lambda_i + \{\rho_{E_i}(\theta) - \delta\rho_i(\theta)\}\ e^{j\theta}$$

form closed curves which contain the eigenvalue inclusion regions for the structured perturbations, $\Delta \in D_S$.

By invoking MPDA, the resulting structured E-contour bounds can be shown to be nonconservative and, hence, the generalized Nyquist criterion establishes a necessary and sufficient condition for robust stability. In addition, the introduction of phase information on the perturbed system has direct implications for the assessment of robust performance. Thus, it becomes possible to extend a complete Nyquist analysis to systems with realistic perturbations (such as those defined by the class of element-by-element bounded perturbations) provided appropriate information on the size and structure of the allowable perturbations is available.

Before proceeding on, it must be pointed out that all of the frequency response techniques summarized in this chapter for continuous-time systems are equally valid for discrete-time systems with $s = j\omega$ replaced by $z = \exp(j\omega T)$. Indeed, the remaining chapters of the thesis will focus primarily on the discrete-time formulations of these methods.

CHAPTER THREE

STATISTICAL UNCERTAINTY FOR SISO SYSTEMS

A key missing element in each of the uncertainty analysis techniques described in Chapter 2 is the ability to quantify the frequency response uncertainty associated with a given system model. Yet, the practical value of these techniques in control design can only be fully realized when this information is known. For situations where system identification is used to generate system descriptions, it is possible to quantify system uncertainty in statistical terms. The question that then arises is whether or not the available statistical information can be manipulated to produce an accurate multivariable characterization of frequency response uncertainty. A logical first step towards solving this problem is the development of frequency response uncertainty descriptions for scalar systems.

Either of two widely-recognized identification approaches, spectral estimation (to estimate frequency response directly from input/output data) or parameter estimation (to generate frequency response estimates using the identified system transfer function), may be used to estimate system frequency response. However, the additional requirement to quantify the uncertainty associated with the frequency response estimates implies that any proposed methodology must not only be able to generate accurate frequency response estimates, it must also be able to guarantee the accuracy of the uncertainty description at individual frequencies and to characterize the interfrequency dependence of the uncertainty that arises from the use of finite data sets. Furthermore, the resulting description for scalar systems should be compatible with the desired goal of quantifying multivariable uncertainty for use in a generalized-Nyquist analysis of perturbed multivariable systems as described in Chapter 2.

Research has recently begun to address the problem of characterizing frequency response uncertainty, and some interesting results have already been produced. Using spectral estimation, Loh et al [LOH1] have generated

confidence bounds for the magnitude and phase of system frequency response at selected individual frequencies. However, due to the low signal-to-noise ratios that are inherently present at high frequencies, the resulting uncertainty bounds will be unnecessarily large at these frequencies. In addition, these results fail to address the topic of interfrequency dependence. So the bounds generated at any one frequency are valid only in isolation; a significant problem when one is concerned about uncertainty at several frequencies simultaneously for stability and gain/phase margin assessments. Finally, it should be noted that this procedure establishes distinct gain and phase bounds which lead to a characterization of uncertainty that is not particularly well suited to generalized-Nyquist extensions for multivariable systems.

The problems highlighted above are generally applicable to methods which utilize spectral estimation. For this reason, it appears that parameter estimation techniques may well be better suited to the problem at hand. Some results in this area are also available. Ljung and Yuan [LJU1] and Ljung [LJU2] have produced asymptotic variance expressions for the frequency response estimates at specified individual frequencies which can be used to generate confidence bounds at these frequencies, while Edmunds [EDM2] has proposed a procedure to generate confidence bounds at individual frequencies by transforming parameter estimate statistics into corresponding frequency response statistics. As with spectral estimation however, these developments are valid only at individually specified frequencies and, hence, fail to account for interfrequency dependence. In addition, Edmunds' procedure relies on a single-term Taylor series approximation to establish the required transformation and, thus, produces only an approximate result. Janiszowski [JAN1] has also addressed the frequency response uncertainty problem and has produced distinct gain and phase bounds that are valid simultaneously over all frequencies. But, these bounds are not exact and, because the gain and phase bounds are separate, this uncertainty description

is not well suited for extensions to a generalized-Nyquist analysis of perturbed multivariable systems. Thus, existing techniques fail to produce the desired results.

This chapter also addresses the problem of characterizing frequency response uncertainty from a parameter estimation perspective. A technique is developed to establish statistically-derived bounds on system frequency response from corresponding bounds on the parameters of the selected model. These bounds are valid simultaneously over all frequencies; thus accounting for the interfrequency dependence of the estimates. Furthermore, this characterization defines confidence regions in the complex Nyquist plane rather than separate bounds on gain and phase, so it can be readily adapted to multivariable systems. The development begins with a review of the parameter identification problem and a discussion of model selection considerations in Section 3.1. Confidence limits on the parameters of the selected system model are developed in Section 3.2 using statistical information on the parameter estimates. These confidence bounds are then transformed into frequency response bounds using results derived in Section 3.3. Methods to modify and improve the resulting frequency response bounds are discussed in Section 3.4, and the chapter concludes with a simulation example to demonstrate the procedure.

3.1 Model Parameter Identification

3.1.1 Least-Squares Estimation and Related Statistical Results

For applications where parametric models are to be generated from available data, scalar discrete-time dynamical systems may be described by the input/output relationship:

$$y(kT) = d^t(kT)\ \theta^o + \varepsilon(kT) \qquad \ldots.(3.1)$$

where θ^o is a $(q_o \times 1)$ vector of true model parameters,

$d^t(kT)$ is a $(1 \times q_o)$ vector of past inputs and outputs,

$\varepsilon(kT)$ is an unknown, random error,

and T is the specified sample time for the system.

When a set of N output observations is available, eqn 3.1 can be used to generate a vector equation of the form:

$$y = D\,\theta^{o} + \varepsilon \qquad \ldots.(3.2)$$

where y is a $(N \times 1)$ vector of outputs, $y(T),\cdots,y(NT)$

D is a $(N \times q_o)$ data matrix containing $d^t(kT)$, $k=1,\cdots,N$

and ε is a $(N \times 1)$ vector of random errors, $\varepsilon(kT)$, $k=1,\cdots,N$.

For this formulation of the problem, several distinct parameter estimation techniques exist [SCH1]. Among these, the most widely-used method is the least-squares algorithm which derives parameter estimates to minimize the sum of the squares of the differences between measured and estimated system outputs. Using this procedure, the parameter estimates are given by:

$$\hat{\theta} = (D^T D)^{-1} D^T y \qquad \ldots.(3.3)$$

[Note: From this point on, vector transposition will be denoted by the superscript 't' and matrix transposition will be denoted by the superscript 'T'.] Errors in the observations ensure that $\hat{\theta}$ is a random vector and, under the assumptions that the elements of D are deterministic and ε is Gaussian white measurement noise with zero mean and covariance $\sigma_\varepsilon^2 I$, it can be shown (e.g. [FRA1]) that $\hat{\theta}$ is Gaussian with mean and covariance given by:

$$E\{\hat{\theta}\} = \theta^{o} \qquad \ldots.(3.4a)$$

$$V = E\{(\hat{\theta} - \theta^{o})\,(\hat{\theta} - \theta^{o})^t\} = \sigma_\varepsilon^2\,(D^T D)^{-1} \qquad \ldots.(3.4b)$$

3.1.2 Model Structures

Least-squares parameter estimates can be obtained for any model structure which defines an input/output relationship of the form shown in eqn 3.1. However, the accuracy of the statistical information associated with these estimates depends on the validity of the assumptions highlighted above. To establish an accurate description of system uncertainty, a model structure which satisfies these assumptions must be selected.

One commonly used model structure is the difference equation model defined by:

$$y(kT) = \frac{b(z^{-1})}{a(z^{-1})} u(kT) \qquad ....(3.5)$$

where $b(z^{-1})$ and $a(z^{-1})$ are polynomials in the delay operator, z^{-1}, whose coefficients define the model parameters. For the case of white measurement noise however, this model fails to produce accurate statistical information on $\hat{\theta}$ because the noise associated with the model is not white. Furthermore, the data matrix D contains past values of the observed (noisy) output so that D is correlated with the measurement noise. Indeed, this second problem persists even if the model noise is white. As a result, the expectation arguments used to derive the mean and covariance of $\hat{\theta}$ are only valid asymptotically. Despite these statistical problems, the difference equation model is often used for applications requiring accurate output prediction because of the relatively small number of parameters required to describe the system.

To generate accurate statistical information from a finite number of measurements, other model structures must be considered. A particularly useful model structure for this purpose is the weighting sequence model whose parameters are related to system output via the convolution summation:

$$y(kT) = \sum_{i=-\infty}^{\infty} g_i \, u([k-i]T) + \varepsilon(kT) \qquad ....(3.6)$$

Under the assumptions that the system is stable, strictly causal (i.e. the system does not respond to inputs which have yet to be applied, nor does it respond instantaneously to a current input) and initially at rest, the infinite convolution summation above can be accurately approximated by the truncated summation [CAD1]:

$$y(kT) = \sum_{i=1}^{q} g_i \, u([k-i]T) + \varepsilon(kT) \qquad ....(3.7)$$

where q represents the number of significant elements in the model. The use of this finite-dimensional weighting sequence model avoids the problems

mentioned previously, as the measurement noise associated with the model remains white and the data matrix D does not contain past noisy measurements. Thus, the assumptions required to develop the estimate statistics in eqns 3.4a,b are satisfied.

One additional feature of the weighting sequence model is its linear relationship to system frequency response. The z-domain transfer function for this model is given by:

$$g(z) = g_1 z^{-1} + g_2 z^{-2} + \cdots + g_q z^{-q}$$

$$= h^t(z^{-1})\ \theta \qquad \ldots.(3.8)$$

where $h^t(z^{-1}) = [z^{-1} \quad z^{-2} \cdots \quad z^{-q}]$ and $\theta = [g_1 \quad g_2 \cdots \quad g_q]^t$. System frequency response can then be identified using the expression

$$z = \exp(j\omega T) = \cos(\omega T) + j \sin(\omega T)$$

for all frequencies $\omega T \leq \pi$. Because $\exp(j\omega T)$ is generally complex, $g\{\exp(j\omega T)\}$ can be rewritten as the following two-dimensional vector:

$$g\{\exp(j\omega T)\} = \begin{bmatrix} g_{real} \\ g_{imag} \end{bmatrix} = \begin{bmatrix} \cos(\omega T) & \cos(2\omega T) & \cdots & \cos(q\omega T) \\ -\sin(\omega T) & -\sin(2\omega T) & \cdots & -\sin(q\omega T) \end{bmatrix} \theta$$

$$g = H^T \theta \qquad \ldots.(3.9)$$

The linear relationship defined by eqn 3.9 is an especially important tool for transforming statistical information on the model parameters into corresponding frequency response uncertainty information. This development will be discussed at length in Section 3.3. However, it is important to note here that weighting sequence models produce this linear relationship directly, whereas similar relationships for difference equation models can only be established using single-term Taylor-series approximations (as shown in [EDM2]). This difference provides further justification for the selection of weighting sequence models to generate accurate statistical descriptions of frequency response uncertainty.

3.2 Model Parameter Confidence Regions

3.2.1 Bounds Based on the Chi-Square Distribution

The least-squares parameter estimates for a weighting sequence model, as mentioned earlier, are normally-distributed random variables. Thus, they can be used to construct confidence regions for the true parameters. Rather than generate bounds for each individual parameter as done by Janiszowski [JAN1], it will be useful for further frequency response developments to establish bounds on a scalar quadratic function of the error between the true and estimated parameters instead. Lemma 3.1 identifies the desired function and its probability distribution.

Lemma 3.1: [DEU1] For the parameter estimates and associated statistics in eqns 3.3 and 3.4a,b, let $\Delta\theta = \hat{\theta} - \theta^o$. Then $\Delta\theta$ is normally distributed with zero mean and covariance $V = \sigma_\varepsilon^2 (D^T D)^{-1}$, and

$$Q = \Delta\theta^t V^{-1} \Delta\theta \qquad \ldots.(3.10)$$

is a chi-square random variable with q degrees of freedom (where q is the number of estimated parameters).

Proof: The distribution and statistics of $\Delta\theta$ follow immediately from its definition and eqns 3.4a,b. The distribution of Q can be established in the following way. Since $V = \sigma_\varepsilon^2 (D^T D)^{-1}$, its eigenvalues are all positive and it can be rewritten in eigenvalue/eigenvector form as

$$V = U \Sigma^2 U^T \quad \text{with} \quad U^T U = I \qquad \ldots.(3.11)$$

Now, let

$$\tilde{\Delta\theta} = \Sigma^{-1} U^T \Delta\theta \qquad \ldots.(3.12)$$

Then, $E\{\tilde{\Delta\theta}\} = 0$ and $E\{\tilde{\Delta\theta}\ \tilde{\Delta\theta}^t\} = \Sigma^{-1} U^T E\{\Delta\theta\ \Delta\theta^t\}\ U\ \Sigma^{-1} = I$. Hence, the elements of $\tilde{\Delta\theta}$ are standard normal variables and, since Q is simply the sum of the squares of these elements, it has, by definition, a chi-square distribution with q degrees of freedom.

....QED

As Q is a chi-square random variable, confidence bounds can be established using the cumulative chi-square distribution. For a given confidence level α, the probability statement associated with Q is:

$$P\{Q \leq Q_{\alpha,q}\} = \alpha \times 100\%$$

where $Q_{\alpha,q}$ is a known constant obtained from cumulative chi-square distribution tables or calculated using a normal approximation as described in Section 3.2.3. The corresponding α x 100% confidence bound is defined by:

$$Q = \Delta\theta^t V^{-1} \Delta\theta = Q_{\alpha,q} \qquad \ldots.(3.13)$$

Since V is positive definite and Q is quadratic in $\Delta\theta$, the region $Q \leq Q_{\alpha,q}$ defines an ellipsoid in the q-dimensional parameter space centred at $\hat{\theta}$ and containing the true model parameters with α x 100% confidence.

3.2.2 Bounds Based on the F Distribution

A difficulty in producing the chi-square confidence ellipsoid above stems from the assumption that the noise variance σ_ε^2 is known; an assumption required to establish Q as a chi-square random variable. In practice, this variance is not known and can, at best, be estimated from the available parameter estimates and data measurements. For this situation, the results of Section 3.2.1 can be extended as shown below.

To begin, the following lemma identifies an estimate for the noise variance and the probability distribution associated with this estimate.

Lemma 3.2: [KEN1] For the parameter estimates defined by eqn 3.3,

$$s^2 = \{(y - D\hat{\theta})^t (y - D\hat{\theta})\} / \{N - q\} \qquad \ldots.(3.14)$$

is an unbiased estimate of σ_ε^2. Furthermore, the quantity $(N - q)\, s^2/\sigma_\varepsilon^2$ is a chi-square random variable with (N - q) degrees of freedom.

Lemma 3.2 is simply an extension of standard results when N observations and q estimated parameters are used to obtain the variance estimate.

Using the results of Lemmas 3.1 and 3.2, it is possible to verify the following theorem:

Theorem 3.1: Let $\Delta\theta = \hat{\theta} - \theta^o$ and let s^2 represent the estimated variance

of the noise (defined by eqn 3.14). Then, the quantity

$$F = \{ \Delta\theta^t \hat{V}^{-1} \Delta\theta \} / q \quad \text{with} \quad \hat{V} = s^2 (D^T D)^{-1} \quad \ldots.(3.15)$$

has an F distribution with q numerator degrees of freedom and N - q denominator degrees of freedom.

Proof: An F-distributed variable is defined as the ratio of two chi-square variables (Q_1, Q_2) in the following way:

$$F = \{Q_1/n_1\} / \{Q_2/n_2\}$$

where Q_1 and Q_2 have n_1 and n_2 degrees of freedom respectively [GIB1]. From Lemma 3.1, $Q = \Delta\theta^t V^{-1} \Delta\theta$ is chi-square distributed with q degrees of freedom, and Lemma 3.2 demonstrates that $(N-q)s^2/\sigma_\varepsilon^2$ has a chi-square distribution with N - q degrees of freedom. Now,

$$\frac{\Delta\theta^t \hat{V}^{-1} \Delta\theta}{q} = \frac{\Delta\theta^t (D^T D) \Delta\theta}{q\, s^2} = \frac{\{\Delta\theta^t (D^T D) \Delta\theta\}/q\sigma_\varepsilon^2}{\{(N-q)\, s^2/\sigma_\varepsilon^2\}/(N-q)} = \frac{Q_1 / q}{Q_2 / (N-q)}$$

where $Q_1 = Q$ (as per eqn 3.10) nd $Q_2 = (N-q)\, s^2/\sigma_\varepsilon^2$ (as per Lemma 3.2). By definition, this quantity is F-distributed with q numerator degrees of freedom and N - q denominator degrees of freedom.

....QED

Using Theorem 3.1, new ellipsoidal confidence regions can be generated using the cumulative F-distribution. The probability statement and corresponding confidence bound are given respectively by:

$$P\{F \leq F_{\alpha,q,N-q}\} = \alpha \times 100\% \quad \ldots.(3.16a)$$

$$\Delta\theta^t \hat{V}^{-1} \Delta\theta = q\, F_{\alpha,q,N-q} \quad \ldots.(3.16b)$$

where $F_{\alpha,q,N-q}$ is a known constant obtained from cumulative F-distribution tables or calculated using a normal approximation as described in Appendix 3.1.

Remark: Theorem 3.1 extends the development of parameter confidence regions to the more practical situation where the noise variance is estimated from available data. In many situations however, the difference

between chi-square and F statistics is negligible. As the number of measurements increases, s^2 approaches σ_ε^2 and the chi-square and F bounds become identical (see the last column of Table 3.1 and note that the square root is used to give a measure of the maximum distance from the centre of the uncertainty region to its boundary). Hence, chi-square assumptions may be used with an estimate of σ_ε^2 to establish the desired parameter bounds provided the number of available measurements is sufficiently large. In situations where this condition is not satisfied, the desired bounds must be developed using the appropriate F statistic.

3.2.3 Normal Approximations for Chi-Square and F Statistics

To generate the confidence bounds defined by eqns 3.13 and 3.16b, statistical limits ($Q_{\alpha,q}$ and $F_{\alpha,q,N-q}$) must be obtained from the appropriate cumulative distribution. Although tables do exist, the confidence levels in these tables are typically restricted to a small number of commonly-used values and linear interpolation between values is inaccurate. To overcome this problem, normal approximations for both chi-square and F statistics have been developed. These approximations can be used with the standard

	Confidence Level, α	Number of measurements	$Q_{\alpha,q}$	$qF_{\alpha,q,N-q}$	$\sqrt{[qF/Q]}$
q=20		200		29.23	1.015
	0.90	500	28.40	28.72	1.006
		1000		28.56	1.003
		200		32.58	1.019
	0.95	500	31.40	31.85	1.007
		1000		31.62	1.003
q=40		200		54.00	1.021
	0.90	500	51.80	52.56	1.007
		1000		52.16	1.003
		200		58.80	1.027
	0.95	500	55.75	56.84	1.010
		1000		56.28	1.005

Table 3.1: Comparison of Statistical Limits

normal distribution to generate accurate confidence limits for variables with chi-square and F distributions. The Wilson-Hilferty approximation for chi-square variables is given by:

Lemma 3.3: [WIL2] If Q is a chi-square random variable with q degrees of freedom, then $\{Q/q\}^{1/3}$ is approximately normal with mean and variance

$$\mu = 1 - \frac{2}{9q} \qquad \sigma^2 = \frac{2}{9q} \qquad \ldots.(3.17a,b)$$

This approximation leads to the following confidence limits for Q:

Theorem 3.2: An α x 100% confidence bound for Q is given by

$$Q = q\{\mu + \sigma Z_\alpha\}^3 \qquad \ldots.(3.18)$$

where Z_α is a known constant obtained from the cumulative standard normal distribution.

Proof: From Lemma 3.3, $\{Q/q\}^{1/3}$ is approximately normal with mean and variance given by eqns 3.17a,b. The probability statement and corresponding confidence bound for this variable are, therefore, given by:

$$P\left\{\frac{(Q/q)^{1/3} - \mu}{\sigma} \leq Z_\alpha\right\} = \alpha \text{ x } 100\% \quad \text{and} \quad (Q/q)^{1/3} = \mu + \sigma Z_\alpha$$

Solving the second expression for Q produces the desired result.

....QED

Similar confidence bounds for F-distributed variables can be obtained using the Peizer-Pratt approximation [PEI1] summarized in Appendix 3.1.

3.3 Frequency Response Confidence Regions

For any specified level of confidence, the ellipsoidal regions described by eqns 3.13 or 3.16b define the complete set of parametric models for the given system. These regions must, therefore, also contain the information required to completely quantify system frequency response uncertainty. Using the linear relationship defined by eqn 3.9, this additional uncertainty information may be developed by transforming the

given parameter bounds into frequency response confidence limits which are valid simultaneously over all frequencies from 0 to π/T. The following theorem describes this transformation:

Theorem 3.3: Let $\Delta\theta = \hat{\theta} - \theta^o$ and let $\Delta\theta^t\, V^{-1}\, \Delta\theta = b$ define an ellipsoidal boundary in the parameter space. If $\Delta g = H^T\Delta\theta = \hat{g} - g^o$ is the image of $\Delta\theta$ in the complex plane at any specified frequency ωT, then

(i) every Δg on the frequency response ellipse described by

$$\Delta g^t (H^T V H)^{-1} \Delta g = b \qquad \ldots.(3.19)$$

has at least one pre-image $\Delta\theta$ which lies on the given parameter boundary;

(ii) no point $\Delta\theta$ on or inside the ellipsoid boundary maps outside this frequency response ellipse.

Proof: (i) Consider a point $\Delta\theta$ on the boundary defined by $\Delta\theta^t\, V^{-1}\, \Delta\theta = b$, and let $\Delta g = H^T\Delta\theta$ represent the image of $\Delta\theta$ in the complex plane at some frequency ωT. Now suppose the matrix S defines an arbitrary ellipse in the complex plane such that $\Delta g^t\, S\, \Delta g = b$. For both $\Delta\theta$ and its image Δg to lie on their respective boundaries simultaneously, the following condition must be satisfied:

$$\Delta\theta^t\, V^{-1}\, \Delta\theta = \Delta g^t\, S\, \Delta g = \Delta\theta^t\, HSH^T\, \Delta\theta.$$

This equation can be rewritten in the following form:

$$\Delta\theta^t \{V^{-1} - HSH^T\}\, \Delta\theta = 0 \qquad \ldots.(3.20)$$

Clearly, when $\Delta\theta$ is selected to satisfy $\{V^{-1} - HSH^T\}\, \Delta\theta = 0$, eqn 3.20 will be satisfied and both $\Delta\theta$ and Δg will lie on their specified boundaries. This condition implies that $\Delta\theta$ must satisfy the following relationship:

$$\Delta\theta = V\, H\, S\, H^T\, \Delta\theta \qquad \ldots.(3.21)$$

But $\Delta g = H^T\Delta\theta$, so premultiplying eqn 3.21 by H^T and rearranging the result yields:

$$\{I - H^T VHS\}\, \Delta g = 0 \qquad \ldots.(3.22)$$

If S is selected to make $\{I - H^T VHS\}$ rank deficient (by one degree), eqn 3.22 will be satisfied for a single Δg. However if $S = (H^T VH)^{-1}$, the condition is satisfied for all Δg (and $\Delta\theta$). Hence, all points on the frequency response ellipse $\Delta g^t (H^T VH)^{-1} \Delta g = b$ are images of points on the parameter space ellipsoid $\Delta\theta^t V^{-1} \Delta\theta = b$.

(ii) Consider the quantity

$$\delta = \Delta\theta^t V^{-1}\Delta\theta - \Delta g^t\{H^T VH\}^{-1}\Delta g \qquad \ldots.(3.23)$$

Using the transformation defined by eqn 3.12, the following expressions can be developed:

$$\Delta\theta^t V^{-1}\Delta\theta = \Delta\tilde{\theta}^t \Delta\tilde{\theta} \qquad \Delta g = H^T\Delta\theta = \tilde{H}^T \Delta\tilde{\theta}$$

with $\tilde{H}^T = H^T U \Sigma$. Thus, eqn 3.23 can be rewritten as:

$$\delta = \Delta\theta^t V^{-1}\Delta\theta - \Delta g^t\{H^T VH\}^{-1}\Delta g = \Delta\tilde{\theta}^t \Delta\tilde{\theta} - \Delta\tilde{\theta}^t \tilde{H}(\tilde{H}^T\tilde{H})^{-1}\tilde{H}^T \Delta\tilde{\theta}$$
$$= \Delta\tilde{\theta}^t\{I - \tilde{H}(\tilde{H}^T\tilde{H})^{-1}\tilde{H}^T\} \Delta\tilde{\theta} \qquad \ldots.(3.24)$$

If $\tilde{M}$ is defined to be the matrix representation of the kernel of $\tilde{H}^T$ (i.e. $\tilde{H}^T \tilde{M} = 0$), a matrix identity (established in Appendix 3.2) can be used to rewrite eqn 3.24 in the following form:

$$\delta = \Delta\theta^t V^{-1} \Delta\theta - \Delta g^t \{H^T VH\}^{-1} \Delta g = \Delta\tilde{\theta}^t \tilde{M}(\tilde{M}^T\tilde{M})^{-1}\tilde{M}^T \Delta\tilde{\theta} \qquad \ldots.(3.25)$$

But the nonzero eigenvalues of $\tilde{M}(\tilde{M}^T\tilde{M})^{-1}\tilde{M}^T$ are equal to the eigenvalues of $(\tilde{M}^T\tilde{M})^{-1} \tilde{M}^T\tilde{M} = I$, so $\tilde{M}(\tilde{M}^T\tilde{M})^{-1}\tilde{M}^T$ is positive semidefinite. Thus, the difference δ must be greater than or equal to zero for all values of $\Delta\tilde{\theta} = \Sigma^{-1}U^T\Delta\theta$, and so

$$\Delta\theta^t V^{-1} \Delta\theta \geq \Delta g^t \{H^T VH\}^{-1} \Delta g$$

for all $\Delta\theta$. This result clearly demonstrates that no point on the given parameter space ellipsoid maps outside the corresponding frequency response ellipse. It also prohibits points inside the given parameter boundary from mapping to points on or outside the given frequency response ellipse since such points must necessarily lie on a smaller ellipsoid and, hence, must map to points on or inside a corresponding smaller ellipse.

....QED

Theorem 3.3 is an extension of set-theoretic results identified by

Schweppe [SCH1] to the problem of generating confidence bounds on system frequency response. It clearly demonstrates that the ellipsoidal confidence region containing the true weighting sequence parameters maps completely to a set of uncertainty regions in the complex plane which contain the true system frequency response over all frequencies from 0 to π/T. The boundaries of these frequency response regions are described by eqn 3.19 where the constant b is now defined by the assumed distribution of the parameter estimates (i.e. $b = Q_{\alpha,q}$ or $b = q\, F_{\alpha,q,N-q}$). In addition, the maximum distance from the centre of the region to its boundary at any given frequency ωT is given by:

$$|\Delta g|_{max} = \sqrt{[b \times \lambda_{max}(H^T V H)]} \qquad \ldots.(3.26)$$

The key characteristic of the uncertainty description developed here is its ability to quantify the interfrequency dependence of the resulting confidence bounds. When finite data sets are used to estimate system frequency response, the uncertainty information at any one frequency necessarily depends upon uncertainty information at other frequencies. A complete description of frequency response uncertainty must account for this interdependence. Since the description derived in Theorem 3.3 is generated from a single confidence bound on the model parameters, the bounds defined by eqn 3.19 are valid simultaneously over all frequencies. Hence, these bounds quantify both the estimate uncertainty at individual frequencies and the interdependence between frequencies.

Theorem 3.3 does not preclude points which lie outside the specified parameter ellipsoid from mapping into these frequency response regions. To investigate the existence of such points, consider first a single frequency $\omega_1 T$ and select a point $\tilde{\Delta\theta}^* = \Sigma^{-1} U^T \Delta\theta$ on the ellipsoid boundary defined by $\tilde{\Delta\theta}^t \tilde{\Delta\theta} = b$ that has a component in the kernel of $\tilde{H}^T$ at $\omega_1 T$. $\tilde{\Delta\theta}^*$ can be written in terms of $\Delta g^* = \tilde{H}^T \tilde{\Delta\theta}^*$ as:

$$\tilde{\Delta\theta}^* = \tilde{H}(\tilde{H}^T\tilde{H})^{-1}\Delta g^* + \tilde{M}\, x$$

where x is a nonzero vector that identifies the component of $\Delta\tilde{\theta}^*$ in the kernel. Using this expression for $\Delta\tilde{\theta}^*$, the following relationship can be developed:

$$\Delta\tilde{\theta}^{*t}\ \Delta\tilde{\theta}^* = \Delta g^{*t}\ (\tilde{H}^T\tilde{H})^{-1}\ \Delta g^* + x^T\ \tilde{M}^T\tilde{M}\ x = b \qquad \ldots.(3.27)$$

But $\tilde{M}^T\tilde{M}$ is positive definite, so eqn 3.27 implies that $\Delta g^{*t}\ (\tilde{H}^T\tilde{H})^{-1}\ \Delta g^* < b$. In other words, the map of $\Delta\tilde{\theta}^*$ in the complex plane at $\omega_1 T$ lies inside the given frequency response ellipse. On the basis of this observation, it is possible to identify points which lie outside the parameter ellipsoid but which map inside or onto the frequency response ellipse at $\omega_1 T$. More specifically, any $\Delta\tilde{\theta} = c\ \Delta\tilde{\theta}^*$, where c is a constant in the range

$$1 < c^2 \leq b\ /\ \{b - x^t\ \tilde{M}^T\tilde{M}\ x\}, \qquad \ldots.(3.28)$$

will satisfy this condition. Furthermore, if $\Delta\tilde{\theta}^*$ is completely in the kernel of $\tilde{H}^T$, an upper bound on the modulus of these points does not exist.

Upon extending this argument over all frequencies from 0 to π/T, it becomes clear that the only points outside the parameter ellipsoid which map into the frequency response regions at each and every frequency correspond to points on the ellipsoid boundary which have a component in the kernel of $\tilde{H}^T$ at every frequency. Such points do, in fact, exist. However, it can be shown that there is no direction in the parameter space that lies entirely within the kernel of $\tilde{H}^T$ at all frequencies. As a result, the problem points outside the ellipsoid are necessarily bounded in modulus as shown in eqn 3.28. In addition, the correct upper bound on the points in each direction must be calculated at the frequency where $x^t\ \tilde{M}^T\tilde{M}\ x$ is a minimum. Hence, these points comprise only small portions of the parameter space outside the specified ellipsoid.

The existence of this small set of additional points suggests that the α x 100% confidence associated with the parameter ellipsoid is a lower bound on the confidence associated with the frequency response regions established in Theorem 3.3. However, it must be noted that every point on each

frequency response ellipse has a pre-image on the given parameter ellipsoid. As a result, the bounds defined by eqn 3.19 over all frequencies from 0 to π/T represent attainable maximum bounds on system frequency response for the prescribed set of possible models. Hence, these regions provide the best possible multifrequency description of frequency response uncertainty for the specified problem.

3.4 Confidence Bound Adjustment Techniques

The results presented in the previous sections establish the methodology for generating statistical bounds on system frequency response for any given set of input/output data. Of course, the ultimate goal of the identification process is to produce the most accurate information possible. Within this context, the statistical nature of these uncertainty descriptions provides special opportunities to modify and improve the frequency response confidence bounds at specific frequencies of interest. Two particularly important techniques to accomplish this task are discussed below, and their effects on frequency response uncertainty will be demonstrated by example in Section 3.5.

3.4.1 Test Input Selection

Although some situations may dictate certain restrictions, the user is generally free to select the test conditions (e.g. system inputs, sampling rates, number of samples, etc.) for any given identification test. It is widely recognized that this extra freedom can be used to improve the accuracy of the resulting system description. For open-loop identification, the selection of test inputs plays a particularly important role in this area, and a great deal of research has focused on the design of inputs which are optimal in some "estimate accuracy" sense. Historically, the goal of time-domain identification has been parameter estimation. Hence, optimal input design research has focused almost exclusively on generating accurate parameter estimates, and comprehensive results in this area have been

presented by Goodwin and Payne [GOO1] and Mehra [MEH1]. In fact, when input power is constrained and the criterion to be minimized is defined by:

$$J = - \log \{\det V^{-1}\}$$

where V is the parameter estimate covariance matrix (eqn 3.4b), it has been shown that the optimal input for identifying the parameters of the weighting sequence model in eqn 3.7 is a white noise sequence.

Clearly however, the primary goal of the identification process for applications such as those described in Chapter 2 is accurate frequency response information, not accurate parameter estimates. It seems reasonable, therefore, to anticipate that the optimal input design to meet this goal may differ from that discussed above. Indeed, recent work by Yuan and Ljung [YUA1] relies on an alternative frequency-domain optimization criterion to produce results which demonstrate the importance of using frequency-dependent inputs to improve frequency response accuracy. Although the details of their work are beyond the scope of this section, their results suggest that even relatively simple input designs (such as filtered random inputs) can be used to improve the accuracy of the frequency response information over specified frequency regions. These results are particularly useful when the critical frequencies of the system are known to the user, as it may then be possible to design inputs which generate a more accurate evaluation of system performance in terms of gain and phase margins.

It should be noted however that, under common test constraints (such as limitations on input power), improvements in accuracy at certain frequencies are necessarily offset by degradations at other frequencies. Furthermore, as shown in the example in Section 3.5, both the size and shape of the resulting confidence bounds are influenced by the inputs used. These conditions suggest that it may still be practical to consider the use of white noise inputs (such as pseudorandom binary or normally-distributed sequences). In fact, the use of this type of input produces interesting effects of its own, as demonstrated by the following result:

Theorem 3.4: If $V = \sigma^2 I$, then

$$\frac{\lambda_{max}(H^T V H)}{\lambda_{min}(H^T V H)} = \frac{(1 + \beta/q)}{(1 - \beta/q)} \qquad \ldots.(3.29)$$

where $\beta = \dfrac{(1 - \cos(2q\phi))}{(1 - \cos(2\phi))}$ and $\phi = \omega T$

Proof: If $V = \sigma^2 I$, then $H^T V H = \sigma^2 (H^T H)$ and eqn 3.29 is simply the ratio of the eigenvalues of $H^T H$. If U is defined as:

$$U = 1/\sqrt{2} \begin{bmatrix} 1 & -j \\ 1 & j \end{bmatrix}$$

then $U U^* = I$ and the eigenvalues of $UH^T HU^*$ and $H^T H$ are identical. Using the expression for H^T in eqn 3.9 and recognizing that

$$\sum_{k=1}^{q} \exp\{j2k\phi\} = \exp\{j2\phi\} \left\{ \frac{1 - \exp\{j2q\phi\}}{1 - \exp\{j2\phi\}} \right\},$$

the following expression for $UH^T HU^*$ can be developed:

$$UH^T HU^* = (1/2) \begin{bmatrix} q & \exp(j2\phi) \dfrac{1 - \exp\{j2q\phi\}}{1 - \exp\{j2\phi\}} \\ \exp(-j2\phi) \dfrac{1 - \exp\{-j2q\phi\}}{1 - \exp\{-j2\phi\}} & q \end{bmatrix}$$

The eigenvalues of this matrix are solutions of the equation:

$$\lambda^2 - q\lambda + (1/4) \left\{ q^2 - \frac{1 - \exp\{-j2q\phi\}}{1 - \exp\{-j2\phi\}} \frac{1 - \exp\{j2q\phi\}}{1 - \exp\{j2\phi\}} \right\} = 0$$

which can be rewritten as:

$$\lambda^2 - q\lambda + (1/4) \left\{ q^2 - \frac{1 - \cos\{2q\phi\}}{1 - \cos\{2\phi\}} \right\} = 0$$

Letting $\beta^2 = (1 - \cos\{2q\phi\})/(1 - \cos\{2\phi\})$ and solving for λ yields:

$$\lambda_{max} = q/2 + \beta/2 \qquad \lambda_{min} = q/2 - \beta/2$$

Hence, the ratio $\lambda_{max}/\lambda_{min}$ is given by eqn 3.29.

....QED

For weighting sequence models, the least-squares data matrix D contains only system inputs. As a result, white noise inputs with variance σ_u^2 will produce a matrix $(D^T D)$ which tends to $N\sigma_u^2 I$ as the number of measurements

increases. So, the parameter estimate covariance matrix will be a constant diagonal matrix. By Theorem 3.4 then, the resulting frequency response boundaries will be circular at frequencies corresponding to nonzero integer multiples of π/qT. Furthermore, the deviation of these bounds away from circles at other frequencies can be predicted. For any angle $\Delta\phi$ between $k\pi/q$ and $(k+1)\pi/q$, $\lambda_{max}/\lambda_{min}$ can be calculated using the following expression for β:

$$\beta = \frac{1 - \cos(2q\ \Delta\phi)}{\sqrt{[1 - a\cos(2\ \Delta\phi) + b\sin(2\ \Delta\phi)\ ]}}$$

$$a = \cos(2\pi k/q) \qquad b = \sin(2\pi k/q)$$

The ratio of the length of the semimajor axis to that of the semiminor axis is then simply the square root of $(1 + \beta/q)/(1 - \beta/q)$. For a 40-parameter model, this quantity ranges from 1.025 to 1.25 for $4.5^o \leq \omega T \leq 175.5^o$ [CL01] and suggests that the use of random zero-mean inputs will, indeed, produce nearly circular bounds over a wide range of frequencies. This characteristic is particularly important when the description of frequency response uncertainty is extended to multivariable systems as will be discussed in Chapter 6.

3.4.2 Parameter Weighting

A second approach to reducing the size and altering the shape of the desired frequency response bounds arises from the fact that the parameter estimate ellipsoid is simply an intermediate step from input/output data to frequency response uncertainty. Parameter alterations may, therefore, be used to generate improvements in the frequency response bounds provided the confidence associated with the modified parameter-space ellipsoid remains unchanged. One technique to accomplish this task involves weighting of the model parameters as described below.

If $Q = \Delta\theta^t\ V^{-1}\Delta\theta$ is a chi-square random variable, it is possible to generate confidence bounds for the quantity:

$$Q_w = (\Delta\theta^t U \Sigma^{-1}) W^{-1} (\Sigma^{-1} U^T \Delta\theta) = \Delta\tilde{\theta}^t W^{-1} \Delta\tilde{\theta} \quad \ldots.(3.30)$$

where W^{-1} is a positive diagonal matrix and V has been rewritten in eigenvalue/eigenvector form as shown in eqn 3.11. The cumulative distribution for any given Q_w is a function of the number of parameters and the specified weights. Although this distribution can be identified and tables of confidence limits can be generated [JOH1, JOH2, SOL1], it is generally not practical to develop exact limits for all possible situations. To overcome this problem, Jensen and Solomon [JEN1] have identified a function of the variable Q_w that can be accurately approximated by a normal random variable; thus permitting the use of the cumulative standard normal distribution to derive appropriate confidence limits. The function and its statistics are described in the following lemma:

Lemma 3.4: [JEN1] The quantity $\{Q_w/(\text{tr } W^{-1})\}^{h_0}$ where

$$h_0 = 1 - \frac{2(\text{tr } W^{-1})(\text{tr } W^{-3})}{3(\text{tr } W^{-2})^2} \quad \ldots.(3.31)$$

is approximately normal with mean and variance given by:

$$\mu = 1 + \frac{h_0(h_0 - 1)(\text{tr } W)}{(\text{tr } W^{-1})^2} \qquad \sigma^2 = \frac{2h_0^2(\text{tr } W^{-2})}{(\text{tr } W^{-1})^2} \quad \ldots.(3.32)$$

Using Lemma 3.4, confidence bounds can be established as demonstrated in the following theorem:

Theorem 3.5: An α x 100% confidence boundary for Q_w is given by

$$Q_w \leq Q_{w_{\alpha,q}} = (\text{tr } W^{-1}) \{\mu + \sigma Z_\alpha\}^{1/h_0} \quad \ldots.(3.33)$$

where Z_α is a known constant obtained from the cumulative standard normal distribution.

Proof: See Theorem 3.2.

The approximate limits in eqn 3.33 have been compared to exact limits for up to 5 parameters [JEN1]. For the 5 parameter case with weights ranging from 2.5 to 0.4, this comparison indicated errors of less than 0.6% for $\alpha > 0.9$. It also suggested that, in general, the approximation improves as confidence levels increase and variations among the weighting elements decrease. As no comparisons are available for situations involving more than 5 parameters, Monte-Carlo simulations were conducted using the example in Section 3.5 to verify the approximation for larger numbers of parameters. The results of these simulations are presented and discussed in detail in Appendix 3.3, but, to summarize here, these results suggest that the approximation is, indeed, accurate for much larger numbers of parameters.

Using Theorem 3.5 to establish appropriate confidence limits, parameter weighting may be applied to alter the shape of the parameter space ellipsoid while maintaining the same level of confidence. The new boundary is described by:

$$\Delta\tilde{\theta}^t \, W^{-1} \, \Delta\tilde{\theta} = Q_{W_{\alpha,q}} \qquad \ldots.(3.34)$$

From Theorem 3.3, the frequency response bounds corresponding to this new parameter space bound are given by:

$$\Delta g^t \, (\tilde{H}^T W \, \tilde{H})^{-1} \, \Delta g = Q_{W_{\alpha,q}} \quad \text{where} \quad \tilde{H}^T = H^T U \, \Sigma \qquad \ldots.(3.35)$$

Thus, parameter weighting also affects the resulting frequency response bounds, and this result may be used to generate tighter bounds over specified frequency ranges. One particularly useful approach to accomplish this task is to select the elements of W so that the maximum distance from the center of the ellipse to its boundary, defined by:

$$|\Delta g|_{max} = \sqrt{[Q_{W_{\alpha,q}} \times \lambda_{max}(\tilde{H}^T W \, \tilde{H})]} \, , \qquad \ldots.(3.36)$$

is minimized at a particular frequency. Because $|\Delta g|_{max}$ is a nonlinear function of the elements of W, it is not possible to obtain an analytic solution to this problem. However, a numerical solution can be readily identified using common multivariable optimization algorithms.

It must be noted that the parameter weights generated using the procedure outlined above are optimal only at the single frequency specified during the optimization. However, as suggested by the example in Section 3.5, the effects of this weighting can be expected to generate reduced bounds over a range of frequencies surrounding the specified frequency. These simulation results also demonstrate that the optimal weighting tends to produce circular bounds over the same range of frequencies. Finally, unlike the design of modified test inputs, prior knowledge of the critical frequency range is not required as parameter weighting may be applied after the identification test to any set of parameter estimates. Hence, the unweighted parameter estimates can be used to identify the critical frequency range, and new tighter bounds can then be generated using parameter weighting to produce a more effective assessment of system stability margins.

3.5 Simulation Example

Input/output simulations were used to demonstrate the concepts presented in this chapter. The system model selected for the example was an exact 40-element weighting sequence whose coefficients are given by the first 40 terms in the impulse response of the transfer function:

$$g(z) = \frac{.721\ z^3 - .941\ z^2 + .255\ z + .0283}{z\ (z^3 - 2.071\ z^2 + 1.351\ z - .267)}$$

The true coefficients are displayed in Figure 3.1 (where a solid line has been used to connect the terms). Two sets of data (consisting of 220 samples each) were generated using white measurement noise with a standard deviation of 0.05. Test inputs for Simulation 1 were generated as a zero-mean pseudo-random Gaussian sequence with a standard deviation of 0.45, while inputs for Simulation 2 were generated as a pseudo-random Gaussian sequence with the same statistics but modified by a high pass filter described by the transfer function $f(z) = (z-1)/(z-0.6)$.

The input/output information generated for each test was used in an off-line least-squares algorithm to estimate the 40 coefficients in the assumed model. These estimates are superimposed on the true weighting sequence in Figure 3.1. Then, using the procedures described in this chapter, 90% confidence bounds on system frequency response were identified using the following relationships:

$$\text{Chi-square:} \qquad \Delta g^t \, (H^T V H)^{-1} \, \Delta g \leq 51.80$$

$$\text{F:} \qquad \Delta g^t \, (H^T \hat{V} H)^{-1} \, \Delta g \leq 53.76$$

The chi-square bounds are displayed in Figure 3.2 for seven frequencies between $\omega T = 1^o$ and $\omega T = 179^o$. Bounds for the F-distribution limit differ only slightly in size (larger by 1.9%) and are not displayed. In addition, Table 3.2 lists the maximum distance from the centre of the uncertainty region to its boundary (i.e. the length of the semimajor axis of the ellipse) at each frequency.

The results presented in Figure 3.2 and Table 3.2 clearly demonstrate

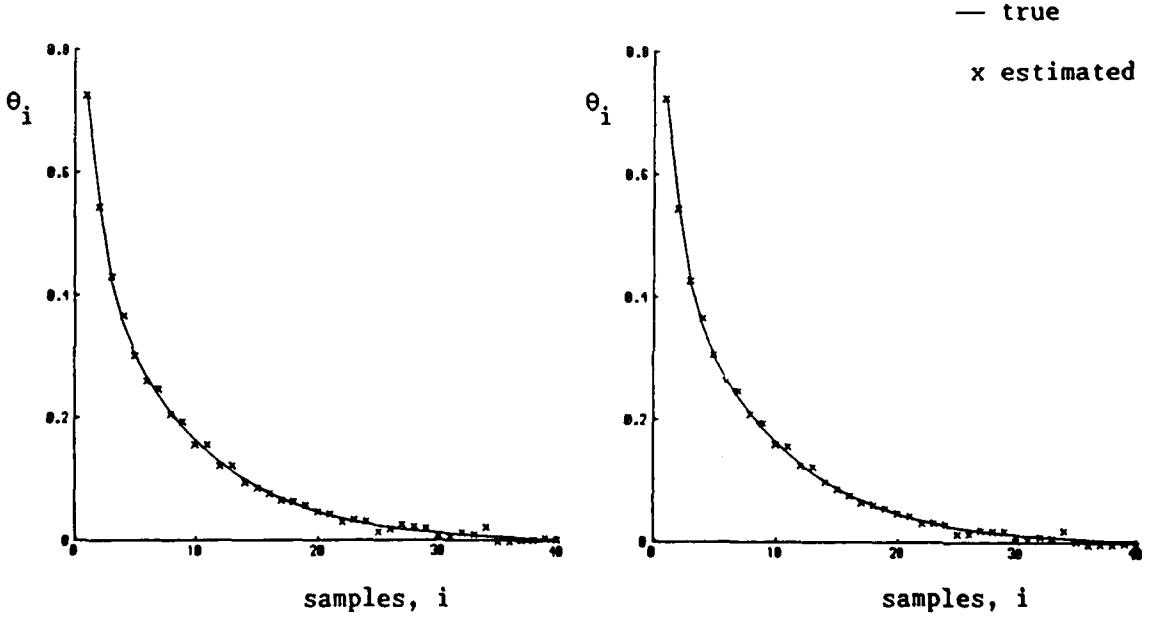

a) Random Input b) Filtered Random Input

Figure 3.1: System Weighting Sequence Parameters

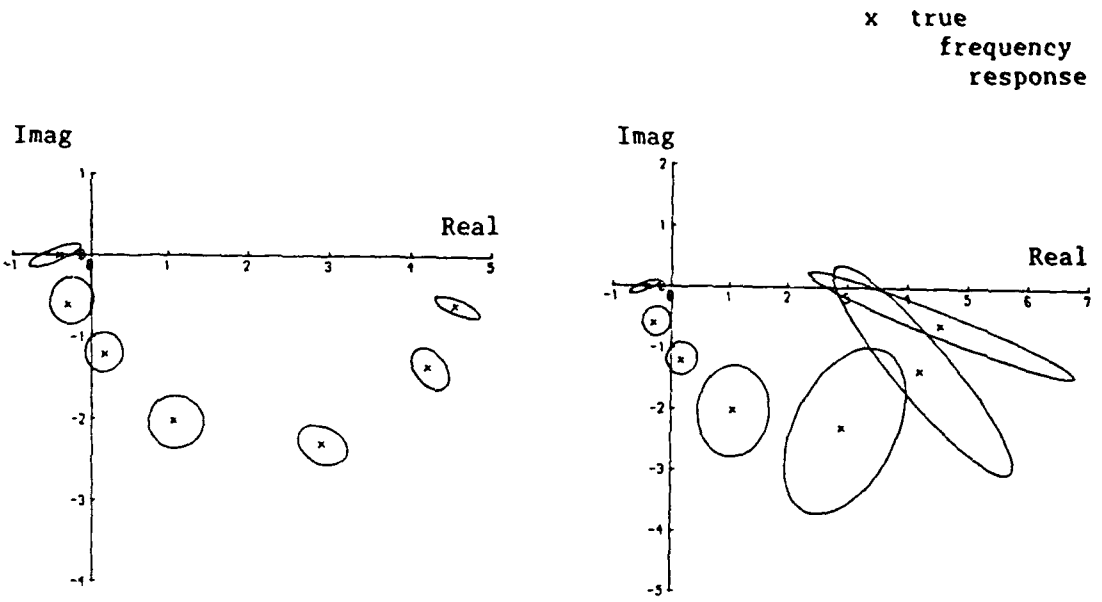

a) Random Input b) Filtered Random Input

Figure 3.2: System Frequency Response Confidence Bounds

Frequency (deg)	Random input	Filtered random input	Filtered random input with parameter weighting
1.00	0.307	2.387	1.245
2.37	0.282	2.225	1.157
5.64	0.318	1.478	0.780
13.38	0.355	0.750	0.571
31.76	0.243	0.268	0.287
75.40	0.286	0.241	0.260
179.0	0.353	0.283	0.305

Table 3.2: Maximum Frequency Response Error Bounds

the ability of the procedure developed in this chapter to characterize and quantify the statistical uncertainty associated with the given frequency response estimates. As predicted, the use of random inputs produced near-circular frequency response bounds over most frequencies, while the use of frequency-modified inputs improved these bounds over a selected range of frequencies. Indeed for this example, the use of high-pass-filtered random inputs reduced the size of the uncertainty regions by from 16% to 20% for frequencies above $\omega T = 75^{o}$. As these frequencies represent the critical frequencies of the system, this result demonstrates the importance of input selection in generating tight uncertainty bounds and, ultimately, in producing a more effective assessment of system behaviour. However, it should be noted that the boundary reductions at high frequency were achieved at the expense of significantly larger and more elliptical bounds over a range of low frequencies. Although these low frequency changes do not affect the evaluation of gain and phase margins in this example, they do suggest that the indiscriminate application of frequency-modified inputs can lead to erroneous assessments of system performance based on bounds at critical frequencies which are generated in conjunction with unacceptably large bounds at other frequencies.

In addition to demonstrating the effects of test input selection, the results from Simulation 2 (the test using high-pass-filtered inputs) were also used to examine the effects of parameter weighting on the size and shape of the frequency response bounds. In this case, parameter weights were generated to minimize the maximum error bound at $\omega T = 5.64^{o}$ using the procedure described in Section 3.4.2. The set of frequency response bounds produced after implementing the optimal weighting are displayed in Fig. 3.3 along with a comparison of the before- and after-weighting bounds at $\omega T = 5.64^{o}$. In addition, the new maximum error bound at each frequency is listed in Table 3.2. The effects of parameter weighting in this example are dramatic. Over frequencies from $\omega T = 1^{o}$ to $\omega T = 15^{o}$, the maximum error

bounds have been reduced significantly (by as much as 40% for frequencies less than $\omega T = 6^{o}$) at the expense of only minimal increases at frequencies much larger than $\omega T = 5.64^{o}$. Indeed, much of the high frequency boundary reduction initially achieved by using frequency-modified inputs has been preserved despite the application of parameter weighting at a significantly lower frequency. Furthermore, the elliptical bound at $\omega T = 5.64^{o}$ is now circular. It should, however, be noted that $\omega T = 5.64^{o}$ was selected primarily to demonstrate the effects of parameter weighting. Because the critical frequencies for this system are significantly larger than $\omega T = 5.64^{o}$, practical applications of parameter weighting may, perhaps, have been focused instead on achieving larger improvements in the intermediate frequency range from 25^{o} to 60^{o} at the expense of such dramatic improvements at low frequencies. Nevertheless, the simulation results presented here clearly demonstrate the usefulness of parameter weighting in reducing boundary size and altering boundary shape at specific frequencies. Potential improvements in the assessment of system behaviour are apparent.

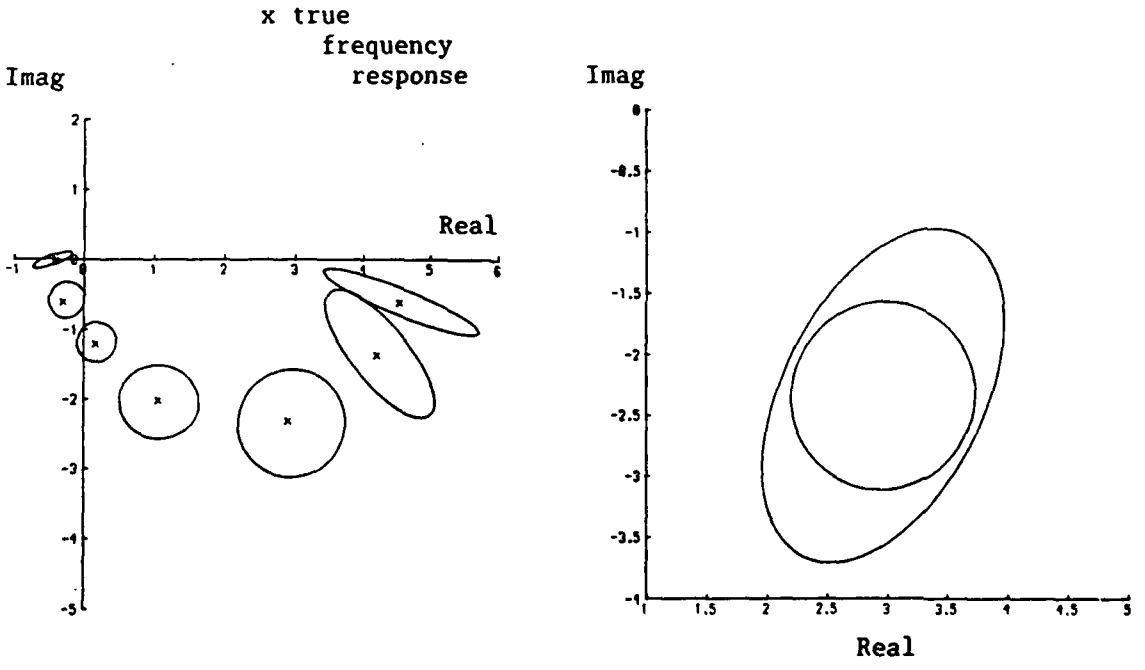

Figure 3.3: Frequency Response Confidence Bounds after Parameter Weighting

Appendix 3.1: The Peizer-Pratt Approximation for F Statistics [PEI1]

Let F denote an F-distributed random variable with k numerator degrees of freedom and m denominator degrees of freedom, and let $F_{k,m}$ denote a known upper bound on F. Then $P\{F \leq F_{k,m}\} = \alpha \times 100\%$, and the confidence level, α, can be identified using the following procedure:

Define:

$$S = 1/2\ \{m-1\} \quad ; \quad n = 1/2\ \{k+m\} - 1 \quad ; \quad p = \frac{m}{kF_{k,m} + m}$$

$$T = 1/2\ \{k-1\} \quad ; \quad q = 1 - p$$

Then compute:

$$d_1 = S + (1/6) - (n + [1/3])p$$

$$d_2 = d_1 + 0.02 \left\{ \frac{q}{(S + 0.5)} - \frac{p}{(T = 0.5)} + \frac{(q - 0.5)}{(n + 1)} \right\}$$

$$Z = d_2 \left\{ \frac{1 + q\ f\{S/np\} + p\ f\{T/nq\}}{(n + [1/6]\ p\ q} \right\}^{1/2}$$

where $f\{x\} = \dfrac{1 - x^2 + (2x)\ \ln\ (x)}{(1 - x)^2}$ and Z denotes the standard normal confidence limit that defines α for the given bound, $F_{k,m}$.

Appendix 3.2: A Matrix Identity

Given a full-rank matrix H^T [2 x q], it is always possible to find a full-rank matrix M [q x (q-2)] such that $H^TM = 0$. Furthermore, the inverse of the partitioned matrix $A = \begin{bmatrix} H^T \\ \hline M^T \end{bmatrix}$ is given by $A^{-1} = [H(H^TH)^{-1} \mid M(M^TM)^{-1}]$.

This can be verified as follows:

$$\begin{bmatrix} H^T \\ \hline M^T \end{bmatrix} [H(H^TH)^{-1} \mid M(M^TM)^{-1}] = \left[\begin{array}{cc|cc} (H^TH) & & (H^TH)^{-1} & \\ & 0 & & \\ \hline & 0 & (M^TM) & \\ & & & (M^TM)^{-1} \end{array}\right] = I,$$

Since $AA^{-1} = I = A^{-1}A$, the following relationship can also be established:

$$[H(H^TH)^{-1} \mid M(M^TM)^{-1}] \begin{bmatrix} H^T \\ \hline M^T \end{bmatrix} = H(H^TH)^{-1}H^T + M(M^TM)^{-1}M^T = I.$$

Rearranging this result yields: $M(M^TM)^{-1}M^T = I - H(H^TH)^{-1}H^T$.

Appendix 3.3: Verification of Weighted-Parameter Confidence Bounds

As described in Section 3.5, simulations were produced using a 40-parameter weighting sequence to generate system input/output data. An off-line least-squares algorithm was used to estimate the model parameters, and the parameter estimates and associated covariance matrix were used to produce frequency response confidence regions. Using this same information, parameter weights may be identified to minimize the maximum frequency response uncertainty bound at any specified frequency as described in Section 3.4.2. For a given set of optimal weights, an approximate α x 100% confidence region for Q_W (eqn 3.30) is given by:

$$Q_W = \Delta\tilde{\theta}^t W_{opt}^{-1} \Delta\tilde{\theta} \leq Q_{W_{\alpha,q}} \quad \ldots.(A3.1)$$

where $Q_{W_{\alpha,q}}$ is defined by eqn 3.33.

By definition, the elements of $\Delta\tilde{\theta}$ are standard normal random variables. Hence, eqn A3.1 can be used to verify the accuracy of $Q_{W_{\alpha,q}}$ using Monte Carlo simulations. To accomplish this task, optimal parameter weights were identified at three different frequencies ($\omega T = 5.64^o$, 75.4^o, and 179.0^o) using the information from Simulation 2 in Section 3.5. For these optimal weights, 100 trials were generated at each frequency to investigate the accuracy of $Q_{W_{\alpha,q}}$ for $\alpha = 0.974$. Each individual trial consisted of 6000 distinct test samples in which the 40 elements of $\Delta\tilde{\theta}$ were generated (using a random number generator) as independent normal random variables with zero mean and unit variance and the quantity $\Delta\tilde{\theta}^t W_{opt}^{-1} \Delta\tilde{\theta}$ was calculated and compared to $Q_{W_{.974,40}}$. A test sample was judged to be a success if $\Delta\tilde{\theta}^t W_{opt}^{-1} \Delta\tilde{\theta} \leq Q_{W_{.974,40}}$ and a failure if $\Delta\tilde{\theta}^t W_{opt}^{-1} \Delta\tilde{\theta} > Q_{W_{.974,40}}$, and the total number of successes (out of 6000 samples) for each trial was recorded.

A statistical summary of the results of the Monte Carlo simulations described above is presented in Table A3.1. For $\alpha = 0.974$, the anticipated number of successes for any one trial (6000 test samples) is 5844. As shown

in the table, this value compares quite favourably with the average number of successes recorded for the 100 trials at each frequency. Indeed, the difference between the average success rate from the simulations and the desired rate of 0.974 ranged from 0.08% to 0.28% for the three frequencies examined. These differences agree closely with similar results produced by Jensen and Solomon [JEN1] for much smaller numbers of parameters and suggest that the normal approximation used to generate the parameter-weighted confidence bound, $Q_{w_{\alpha,q}}$, is accurate for much larger parameter sets.

Frequency for Parameter Optimization (deg)	Boundary Failures Per Trial		Average Success Rate
	Mean	Standard Deviation	$\left\{\frac{6000 - \text{Mean}}{6000}\right\}$
5.64	5860.3	11.3	0.9767
75.40	5848.8	12.2	0.9748
179.0	5859.0	11.9	0.9765

Table A3.1: Monte-Carlo Simulation Results

CHAPTER FOUR

A GEOMETRIC FREQUENCY RESPONSE-BASED TRUNCATION CRITERION

The results in Chapter 3 establish a statistical description of the uncertainty associated with the estimated frequency response for any given system. This description is obtained using a parametric approach to the system identification problem, and a key ingredient in the development is the selection of finite weighting sequence models to describe system dynamics. Since most systems are more realistically described by infinite weighting sequences, any practical implementation of the procedure to accurately quantify frequency response uncertainty must necessarily rely on an effective truncation of the true weighting sequence.

The truncation problem described here is, in essence, a special case of the general model order selection problem (a problem that has received wide attention in the literature). It seems reasonable, therefore, to expect that any of the most widely-used criteria can be introduced to solve this special problem. However now, the primary goal of the identification process is to obtain accurate frequency response information. Since the selected model serves only as a vehicle for generating this information, an appropriate truncation criterion should concentrate on frequency response considerations. Unfortunately, the available order selection criteria focus solely on the problem of generating accurate parametric (time-domain) descriptions of the system. Hence, they are not well suited to this frequency-domain problem.

Existing results do, however, offer valuable insights into the development of an appropriate frequency response-based criterion. In this chapter, a geometric interpretation of the time-domain order selection problem is used to highlight important concepts for the development of an alternative frequency-dependent criterion. The geometric relationships developed from this analysis are extended to the complex Nyquist plane to produce the desired frequency response-based criterion. The resulting

criterion is easy to implement and, as demonstrated by Monte Carlo simulations, identifies the correct dependence of truncation level on frequency. Thus, for specified individual frequencies, the criterion identifies the proper finite-length model required to produce accurate statistical bounds on system frequency response.

4.1 The Time-Domain Order Selection Problem: A Geometric Perspective

A common goal of model order selection is to establish an appropriate trade-off between variability in the parameter estimates and quality of fit to the observed output data. Indeed, many order selection criteria have been proposed to achieve this goal through the use of statistical information on the parameter estimates [FRE1]. However, using geometrical interpretations of Akaike's AIC criterion [AKA1], it is possible to establish an alternative criterion which achieves the same goal and yet is amenable to extension for frequency response purposes.

Under the assumption that the "best" model is smaller in dimension than the true model, system output (as defined by eqn 3.2) can be rewritten in the following way:

$$y = y^o + \varepsilon = D\,\theta^o + \varepsilon = D_q\,\theta_q + \tilde{D}_q\,\tilde{\theta}_q + \varepsilon \qquad ....(4.1)$$

where $y^o = D\,\theta^o \in R^N$ is the true output; $\theta^o \in R^{q_o}$ is the set of true parameters; θ_q denotes the first q elements of θ^o; $\tilde{\theta}_q$ denotes the elements of θ^o not included in θ_q; and D_q and $\tilde{D}_q$ are matrices defined by partitioning D appropriately. For any given q, y^o can be estimated by $\hat{y} = D_q\,\hat{\theta}_q$ where $\hat{\theta}_q$ represents the least-squares estimate defined by eqn 3.3. Given this relationship between system output and model parameters, it seems reasonable to suggest that the order selection process should focus on identifying the model which most closely matches the estimated output, $\hat{y}$, to the true output, y^o; a goal achieved by selecting the order which minimizes $J_y = ||y^o - \hat{y}||^2$. Since $\hat{y}$ is random, a practical alternative cost function

is given by:

$$E\{J_y\} = E\{||y^o - \hat{y}||^2\} = ||y^o - y^*||^2 + E\{||y^* - \hat{y}||^2\} \quad ....(4.2)$$

where $y^* = P_q\, y^o = D_q\, \theta_q^*$ is the orthogonal projection of y^o onto the q-dimensional subspace of R^N spanned by the columns of D_q, $P_q = D_q(D_q^T D_q)^{-1} D_q^T$ is the orthogonal projection operator onto the range space of D_q, and $\theta_q^* = E\{\hat{\theta}_q\}$. Indeed, this formulation of the problem not only ensures that the selected model will, on average, minimize $||y^o - \hat{y}||^2$, but it also implicitly establishes a trade-off between variability (as measured by $E\{||y^* - \hat{y}||^2\}$) and bias ($||y^o - y^*||^2$).

A solution to the problem posed above clearly relies on the ability to identify the bias and variability terms associated with each model order. To visualize the development of appropriate estimates for these quantities, consider the simplified case when N = 3 and q = 2 as displayed in Figure 4.1 (where the directed line segments $\overline{BA}$, $\overline{DB}$, and $\overline{AC}$ denote the vectors $(y_o - y^*)$, $(y^* - \hat{y})$, and the true noise ε, respectively). [Note: Although the following discussion makes reference to this diagram, the results derived are valid for arbitrary N and q.] When ε is Gaussian white noise, $E\{\varepsilon^t\varepsilon\} = ||\overline{AC}||^2 = N\sigma_\varepsilon^2$. Since $(\hat{y} - y^*) = \overline{BD}$ is the orthogonal projection of ε onto the specified q-dimensional subspace, it can, therefore, be shown that $E\{||y^* - \hat{y}||^2\} = q\sigma_\varepsilon^2$. The bias, however, is more difficult to estimate because both θ^o and θ_q^* are unknown. An accurate estimate can be generated in the following way. By adding and subtracting y, $||y^o - y^*||$ can be written as:

$$||y^o - y^*||^2 = ||y^o - y||^2 + 2\,(y^o - y)^t(y - y^*) + ||y - y^*||^2 \quad ....(4.3)$$

Note that eqn 4.3 is obtained by rewriting the vector $\overline{BA}$ in Figure 4.1 as the sum of $\overline{BC}$ and $\overline{CA}$. By definition, $||y^o - y||^2 = ||\overline{CA}||^2 = \varepsilon^t\varepsilon$ and the two remaining terms in eqn 4.3 can be rewritten in the following form:

$$2\,(y^o - y)^t(y - y^*) = -2\,\varepsilon^t(I-P_q)\tilde{D}_q\,\tilde{\theta}_q - 2\varepsilon^t\varepsilon \qquad \ldots.(4.4a)$$

$$||y - y^*||^2 = ||y - \hat{y}||^2 + 2\,(y - \hat{y})^t(\hat{y} - y^*) + ||\hat{y} - y^*||^2 \quad \ldots.(4.4b)$$

where eqn 4.4a is derived from the definitions of y, y^o, and y^*, and eqn 4.4b is generated by replacing $\overline{BC}$ in Figure 4.1 by the vector sum of $\overline{BD}$ and $\overline{DC}$. Since $E\{\varepsilon\} = E\{\hat{y} - y^*\} = 0$, $-2\varepsilon^t(I-P_q)\tilde{D}_q\tilde{\theta}_q$ and $2(y - \hat{y})^t(\hat{y} - y^*)$ will, on average, be zero and, hence, these terms can be neglected. As discussed earlier, $E\{||\hat{y} - y^*||^2\} = ||\overline{BD}||^2 = q\sigma_\varepsilon^2$. So for any given test, the best available estimate of $||\hat{y} - y^*||^2$ is qs^2 where s^2 is defined by Lemma 3.2 (eqn 3.14). In addition, $||y - \hat{y}||^2 = ||\overline{DC}||^2 = \hat{\varepsilon}^t\hat{\varepsilon}$ is simply the sum of the squares of the residuals of the given data fit. Finally, since $\varepsilon^t\varepsilon = ||\overline{AC}||^2$ is independent of model order, it is constant for all specified models. Thus, $||y^o - y^*||^2$ may be accurately estimated by $\hat{\varepsilon}^t\hat{\varepsilon} + qs^2$ + constant.

Rewriting eqn 4.2 in terms of the expressions derived above yields:

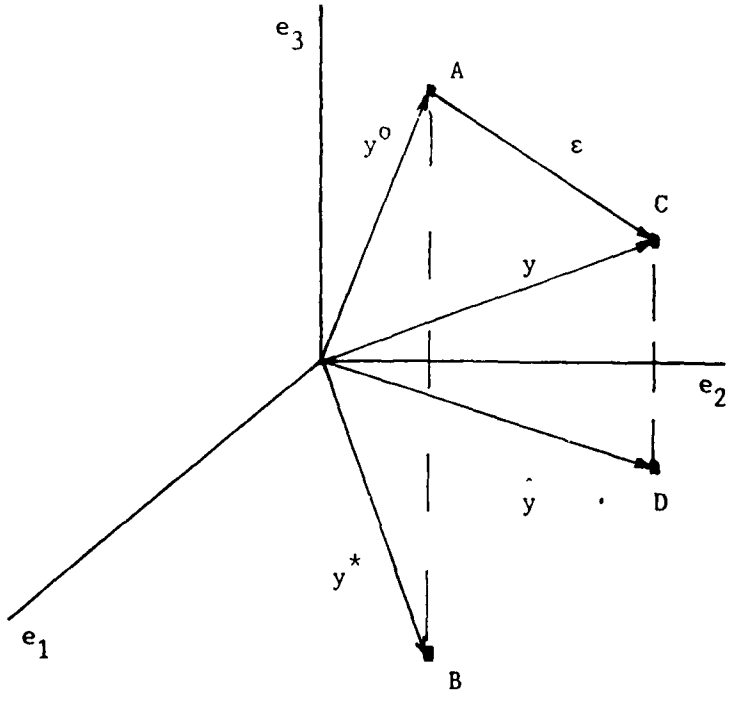

Figure 4.1: A Three-Dimensional Perspective

$$E\{J_y\} \simeq \hat{\varepsilon}^t\hat{\varepsilon} + 2qs^2 + \text{constant},$$

and the correct model order can be selected using the following criterion:

Criterion 4.1: Select the model order q which minimizes

$$J = \hat{\varepsilon}^t\hat{\varepsilon} + 2qs^2 \qquad \ldots.(4.5)$$

over all model orders, where $\hat{\varepsilon} = (y - D_q \hat{\theta}_q)$ is the vector of residuals for the given parameter estimates.

It is interesting to note that, for $q << N$, this criterion can be shown (on the basis of expressions developed in Chapter 5) to yield the same result as practical implementations of Akaike's AIC criterion.

4.2 Adaptations for Frequency Response Applications

When frequency response estimation is the goal, the output relationships described above are no longer relevant. Instead, a more realistic objective is to minimize the distance between the estimated frequency response, $\hat{g}$, and the true frequency response, g^o, at some specified frequency, ωT. Since $\hat{g}$ is random, an appropriate measure of this distance is given by:

$$J_g = E\{||g^o - \hat{g}||^2\} = ||g^o - g^*||^2 + E\{||g^* - \hat{g}||^2\} \qquad \ldots.(4.6)$$

where $g^* = E\{\hat{g}\}$. This formulation again highlights the bias/variability tradeoff; a tradeoff that has been discussed in general frequency response terms by Ljung and Yuan [LJU1]. To establish an appropriate order selection criterion however, one needs accurate estimates of both quantities.

For weighting sequence models, appropriate estimates may be obtained using an approach analogous to that of the previous section. A key ingredient in this development is the linear relationship between the model parameters and system frequency response described by eqn 3.9. First, consider $E\{||g^* - \hat{g}||^2\}$. Since $\hat{g} = H_q^T \hat{\theta}_q$ and $g^* = H_q^T \theta_q^*$, this quantity can be written as:

$$E\{||g^* - \hat{g}||^2\} = \text{tr}\,[H_q^T\, E\{(\theta_q^* - \hat{\theta}_q)(\theta_q^* - \hat{\theta}_q)^t\}\, H_q]$$

By definition, $\hat{\theta}_q - \theta_q^* = (D_q^T D_q)^{-1} D_q^T \varepsilon$. So, $E\{(\theta_q^* - \hat{\theta}_q)(\theta_q^* - \hat{\theta}_q)^t\} = \sigma_\varepsilon^2 (D_q^T D_q)^{-1}$ and the expression above reduces to:

$$E\{||g^* - \hat{g}||^2\} = \sigma_\varepsilon^2\, \text{tr}\,[H_q^T (D_q^T D_q)^{-1} H_q] \qquad \ldots.(4.7)$$

Next, consider $||g^o - g^*||^2$. To estimate this quantity, define

$$g_m = H_o^T\, D^L\, y \qquad \ldots.(4.8)$$

where $D^L = (D^T D)^{-1} D^T$ is the left inverse of D and the dimensions of D and H_o^T are $(N \times q_o)$ and $(2 \times q_o)$ respectively. The bias can then be written as:

$$||g^o - g^*||^2 = ||g^o - g_m||^2 + 2\,(g^o - g_m)^t (g_m - g^*) + ||g_m - g^*||^2 \qquad \ldots.(4.9)$$

Using the relationships for y and g_m given by eqns 4.1 and 4.8, the three terms above can be rewritten as:

$$||g^o - g_m||^2 = ||H_o^T\, D^L\, \varepsilon||^2$$

$$2\,(g^o - g_m)^t (g_m - g^*) = -2\,\varepsilon^t (D^L)^T\, H_o \{H_o^T\, \theta_o - H_q^T\, \theta_q^*\} - 2\,||H_o^T\, D^L\, \varepsilon||^2$$

$$||g_m - g^*||^2 = ||g_m - \hat{g}||^2 + 2(g_m - \hat{g})^t (\hat{g} - g^*) + ||\hat{g} - g^*||^2$$

Since $E\{\varepsilon\} = E\{\hat{g} - g^*\} = 0$, $-2\varepsilon^t (D^L)^T H_o \{H_o^T\, \theta_o - H_q^T\, \theta_q^*\}$ and $(g_m - \hat{g})^t (\hat{g} - g^*)$ will, on average, be zero and, hence, these terms can be neglected. With these simplifications, substitution of the above expressions (together with eqn 4.7) into eqn 4.9 yields the following result:

$$||g^o - g^*||^2 = ||g_m - \hat{g}||^2 + s^2\, \text{tr}\, H_q^T (D_q^T D_q)^{-1} H_q - ||H_o^T\, D^L\, \varepsilon||^2 \qquad \ldots.(4.10)$$

Now, combining eqns 4.6, 4.7 and 4.10 and recognizing that $||H_o^T\, D^L\, \varepsilon||^2$ is constant for all q produces:

$$J_g \simeq ||g_m - \hat{g}||^2 + 2s^2\, \text{tr}\, H_q^T (D_q^T D_q)^{-1} H_q + \text{constant}$$

Hence, the correct order can be selected using the following criterion:

Criterion 4.2: Select the model order q which minimizes

$$J_g = ||g_m - \hat{g}||^2 + 2s^2\, \text{tr}[H_q^T (D_q^T D_q)^{-1} H_q] \qquad \ldots.(4.11)$$

over all model orders, where H_q is calculated at the specified frequency of interest.

To identify J_g in eqn 4.11, g_m must be calculated using the relationship defined by eqn 4.8. This implies that q_o must be known. But for weighting sequences, q_o is theoretically infinite. In practice, one can choose an appropriately large finite value to obtain accurate results. Indeed, the simulation results in the next section demonstrate that the chosen truncation level is insensitive to this specification provided q_o is sufficiently large.

4.3 Monte Carlo Simulation Results

Input/output simulations were performed using two systems described by the transfer functions:

$$g_{S1}(z) = \frac{.75}{z - .85} \qquad g_{S2}(z) = \frac{.5\ (z + .7)}{z^2 - 1.65z + .68}$$

For each simulation, random inputs with unit variance were used to generate N = 1000 output samples, each corrupted by Gaussian noise with variance $\sigma_\varepsilon^2 = 0.0625$. Criterion 4.2 was implemented using various values for q_o, and the resulting frequency-dependent truncation levels (along with the truncation which minimized the true value of $||g^o - \hat{g}||^2$) were observed.

The procedure above was repeated 100 times for each system to produce a representative sample, and the resulting sample statistics are presented in Table 4.1. The results obtained using Criterion 4.2 (denoted by J_g in the table) can be seen to give good agreement with the true optimal truncation levels (denoted by $J = ||g^o - \hat{g}||^2$ in the table). Furthermore, the results suggest that the level of truncation selected is insensitive to the value of q_o used, provided q_o is chosen to be sufficiently large. More importantly, unlike standard order selection criteria [FRE1], Criterion 4.2 does not identify a single best order, but rather, in agreement with the true results, establishes the correct dependence of truncation level on frequency. For comparison, the commonly-used interpretation (defined by the cost function $J_A = N \ln(\hat{\varepsilon}^t\hat{\varepsilon}) + 2q$) of Akaike's AIC criterion as well as

Bhansali and Downham's modified AIC criterion (defined by the cost function $J_B = N \ln(\hat{\varepsilon}^t\hat{\varepsilon}) + 4q$) were applied to the same test data, and the following results (average truncation level ± 1 standard deviation) were obtained:

	q_{opt} for J_A	q_{opt} for J_B
S1:	27.4 ± 2.6	24.4 ± 1.8
S2:	32.7 ± 4.5	28.3 ± 1.7

A comparison of these values with the true results in Table 4.1 demonstrates that the single truncation levels obtained using these "parameter space" criteria do not accurately reflect the true optimal trade-off between bias and variability of the frequency response estimates; yielding results which do not properly account for bias at low frequencies and which produce unnecessarily conservative confidence bounds at high frequency. For frequency response applications therefore, Criterion 4.2 can be seen to produce results which are superior to those of other commonly-used order selection criteria.

	ωT (deg)	q_{ot} for $J=\|\|g^o - \hat{g}\|\|^2$	q_{opt} for J_g (q_o=100)	q_{opt} for J_g (q_o=125)	q_{opt} for J_g (q_o=150)
	0	35.9 ± 6.7	32.3 ± 7.1	32.7 ± 7.5	32.1 ± 8.4
S1:	15	33.2 ± 7.5	28.5 ± 6.3	28.6 ± 7.2	28.7 ± 7.3
	45	23.5 ± 3.7	19.0 ± 3.0	18.3 ± 3.5	17.4 ± 3.7
	0	39.8 ± 7.4	35.7 ± 7.5	35.0 ± 7.6	34.6 ± 8.3
S2:	15	36.5 ± 7.3	32.6 ± 6.7	31.8 ± 6.7	30.3 ± 7.2
	45	25.6 ± 3.4	21.3 ± 3.8	20.8 ± 4.0	18.9 ± 3.8

Table 4.1: Statistical Summary of Selected Truncations from Simulation (Average Value ± 1 Standard Deviation)

CHAPTER FIVE

OPTIMAL TRUNCATION WITH BIAS IDENTIFICATION

As discussed previously, the use of finite weighting sequences to describe system dynamics imposes a practical requirement to establish an appropriate level of truncation. Furthermore, our desire to accurately characterize frequency response uncertainty suggests that any criterion used to establish the truncation should incorporate both the available statistical information from the identification process and appropriate frequency response information. The geometric criterion proposed in Chapter 4 offers one means of accomplishing this task. This criterion leads to an easy-to-implement procedure that incorporates frequency response information at a single specified frequency (via the linear transformation defined by eqn 3.9) to generate appropriate frequency-dependent truncation levels. It is, however, frequency-specific. As such, the resulting truncation (when used to develop the statistical description of uncertainty described in Chapter 3) yields an accurate description of frequency response uncertainty over only a small range of frequencies in the vicinity of the selected frequency. Indeed, because the criterion does not account for bias at other frequencies, the statistical bounds derived from the selected model at these other frequencies may either be unnecessarily conservative or may actually fail to include the true frequency response of the system. As a result, though the uncertainty results at the specified frequency are valid and accurate, it may not be possible to generate accurate bounds at other frequencies. Hence, it may not be possible to describe accurately the interdependence of the frequency response estimates.

To retain the characterization of interfrequency dependence that is inherent in the statistical bounds established by Theorem 3.3 and to ensure that these bounds produce an accurate description of uncertainty, other methods of identifying the proper truncation must be investigated. Again, commonly-used parameter-space criteria provide a useful starting point for

this investigation. Practical implementations of these criteria, as suggested in the previous chapter, are not generally well suited to this specific problem for a number of reasons including their failure to include frequency response information and their inability to quantify the bias introduced by the selected model. However, the theoretical foundations of these criteria do provide valuable insights into the solution of the problem. More specifically, the statistical characteristics associated with Akaike's information theoretic criterion [AKA1], when combined with certain unique characteristics of weighting sequence models, establish a framework for the development of a new truncation criterion to accomplish the desired tasks.

The goal of this chapter is to develop an alternative criterion (using the framework mentioned above) which combines information on the variability of the estimates and the bias introduced by truncation to establish an optimal level of truncation. It will be shown that this criterion not only identifies the truncation which produces an optimal statistical trade-off between variability and bias, but that it also establishes an explicit upper bound on the bias introduced by this truncation. Furthermore, this bias bound can be generated in either the parameter space or the frequency domain to quantify either "parameter" bias or frequency response bias. The chapter begins by developing the proposed criterion in the parameter space and then extends the results to establish an appropriate frequency-domain alternative which provides the remaining information needed to completely quantify frequency response uncertainty.

5.1 Optimal Truncation: Preliminary Developments

5.1.1 Akaike's Criterion and Associated Implementation Problems

For systems described by the input-output relationship in eqn 3.1, the development of an appropriate system description relies not only on one's ability to generate parameter estimates (for a given model) which provide

the best fit to the observed data, but also on one's ability to select the proper model from a specified class of models. One widely-used criterion to achieve this second objective is the information theoretic criterion proposed by Akaike [AKA1]. Using this statistical criterion, the "best" model for the system can be defined by:

Definition 5.1: For the system described by eqn 3.1 and any specified set of input/output data, the "best" model for the system is the model identified by minimizing:

AIC = -2 ln{maximum likelihood} + 2 {number of free parameters}

or, for Gaussian white noise,

$$AIC = N \ln \{\hat{\sigma}_\varepsilon^2\} + 2q \qquad \ldots.(5.1)$$

where N is the number of output measurements, q is the number of parameters in the assumed model (i.e. the dimension of the model), and $\hat{\sigma}_\varepsilon^2$ represents the maximum likelihood estimate of σ_ε^2 obtained from the residuals of the data fit.

A key element in the development of minimum AIC as an appropriate criterion for model selection is the assumption that the class of models from which the "best" model is to be selected does not contain the true model, but instead contains only models of lower order which are "sufficiently close" to it [AKA1]. This assumption necessarily implies that the residuals obtained for any estimated model in the class include a non-random component resulting from the difference in order between the true and estimated models. This non-random element poses a problem for practical implementations of the minimum AIC criterion.

For any model in the specified class, the true maximum likelihood estimate of σ_ε^2 is given by:

$$\hat{\sigma}_\varepsilon^2 = \{\hat{\varepsilon} - \mu\}^t \{\hat{\varepsilon} - \mu\} / N$$

where $\hat{\varepsilon}$ denotes the residuals generated by the estimated model and μ represents the non-random component. Using this relationship, AIC can be

rewritten as:

$$AIC = N \ln\{[\hat{\varepsilon} - \mu]^t[\hat{\varepsilon} - \mu]/N\} + 2q = N \ln\{[\hat{\varepsilon} - \mu]^t[\hat{\varepsilon} - \mu]\} - N \ln N + 2q$$

Since $N \ln N$ is constant for any given set of data, it can be ignored when minimizing AIC, and an alternative form of the criterion is given by:

$$AIC = N \ln\{[\hat{\varepsilon} - \mu]^t[\hat{\varepsilon} - \mu]\} + 2q \quad ....(5.2)$$

But μ is unknown and, hence, implementation of the criterion originally proposed by Akaike cannot be accomplished in practice.

For practical purposes however, an effective criterion can still be established provided a reliable estimate of AIC is available. One commonly-used estimate is obtained by neglecting the non-random element to produce:

$$\hat{AIC} = N \ln\{\hat{\varepsilon}^t \hat{\varepsilon}\} + 2q \quad ....(5.3)$$

Indeed, the assumption that all models in the specified class are "sufficiently close" to the true model appears to justify the further assumption that μ can be neglected. However when the statistical perspective originally taken by Akaike is considered, this assumption is not justified. When several models are sufficiently close to the true one, the best model (from a statistical "distribution-matching" point of view) is the one for which the estimated variance obtained from the residuals most closely matches the true variance of the noise present in the data. Minimum AIC (using the true maximum likelihood estimate of σ_ε^2) accomplishes this task. On the other hand, $\hat{AIC}$ introduces additional terms associated with the neglected element which can corrupt the desired information and lead to an incorrect selection of model order. Indeed, Monte Carlo simulations presented in [BHA1] and [FRE1] clearly demonstrate the inadequacy of minimum $\hat{AIC}$ as an effective criterion for model selection.

5.1.2 Incremental Adjustments to Improve Order Selection Accuracy

As suggested above, $\hat{AIC}$ is not accurate enough to be used in place of AIC to establish the correct model order. It is, however, possible to

identify the inaccuracies more clearly by examining the incremental differences between AIC and $\hat{AIC}$ as shown below. The results of this comparison can be used to suggest adjustments which, when included in $\hat{AIC}$, will reproduce the true value of AIC. These adjustments prove to be particularly helpful when weighting sequence truncation is investigated.

Consider a system described by the standard input/output relationship in eqn 3.2. As shown in Section 4.1, this relationship can be rewritten in the following way:

$$y = D_q \theta_q + \tilde{D}_q \tilde{\theta}_q + \varepsilon = D_q \theta_q + \varepsilon_q$$

where $\varepsilon_q = \tilde{D}_q \tilde{\theta}_q + \varepsilon$. Now, the least-squares solution for θ_q is:

$$\hat{\theta}_q = (D_q^T D_q)^{-1} D_q^T y \qquad ....(5.4)$$

and the residuals of the fit can be calculated by:

$$\hat{\varepsilon}_q = y - D_q \hat{\theta}_q = y - D_q (D_q^T D_q)^{-1} D_q^T y$$
$$= (D_q \theta_q + \tilde{D}_q \tilde{\theta}_q + \varepsilon) - (D_q \hat{\theta}_q + P_q \tilde{D}_q \tilde{\theta}_q - P_q \varepsilon)$$

$$\hat{\varepsilon}_q = (I - P_q)(\tilde{D}_q \tilde{\theta}_q + \varepsilon) \qquad ....(5.5)$$

where $P_q = D_q (D_q^T D_q)^{-1} D_q^T$ is the orthogonal projection operator defined in the previous chapter. Thus, the mean value of $\hat{\varepsilon}_q$ is:

$$\mu_q = E\{\hat{\varepsilon}_q\} = (I - P_q) \tilde{D}_q \tilde{\theta}_q \qquad ....(5.6)$$

Furthermore,

$$E\{[\hat{\varepsilon}_q - \mu_q]^t [\hat{\varepsilon}_q - \mu_q]\} = E\{\varepsilon^t (I - P_q) \varepsilon\} = (N - q) \sigma_\varepsilon^2 \qquad ....(5.7)$$

and so subtracting $\mu = \mu_q$ from $\hat{\varepsilon}_q$ produces an effective estimate of the true noise variance.

For a model of order q, AIC_q can now be rewritten in terms of $\hat{AIC}_q$, $\hat{\varepsilon}_q$, and $\tilde{\theta}_q$ by combining eqns 5.2, 5.3 and 5.6 to produce:

$$AIC_q = N \ln (\hat{\varepsilon}_q^t \hat{\varepsilon}_q) + N \ln (1 - \beta_q) + 2q = \hat{AIC}_q + N \ln (1 - \beta_q) \qquad ....(5.8)$$

where $$\beta_q = \frac{2 \hat{\varepsilon}_q^t (I - P_q) \tilde{D}_q \tilde{\theta}_q - \tilde{\theta}_q^t \tilde{D}_q^T (I - P_q) \tilde{D}_q \tilde{\theta}_q}{\hat{\varepsilon}_q^t \hat{\varepsilon}_q} \qquad ....(5.9a)$$

or, as a consequence of eqn 5.5,

$$\beta_q = \frac{2\,\varepsilon^t\,(I - P_q)\,\tilde{D}_q\,\tilde{\theta}_q + \tilde{\theta}_q^t\,\tilde{D}_q^T\,(I - P_q)\,\tilde{D}_q\,\tilde{\theta}_q}{\hat{\varepsilon}_q^t\,\hat{\varepsilon}_q} \qquad \ldots.(5.9b)$$

Before continuing, the following assumption will also be made:

Assumption 5.1: Let Θ denote the class of models within which the "best" model exists and let $\tilde{\theta}_q$ denote the vector of elements of the true system model not included in a model of dimension q within Θ. Then, it will be assumed that Θ contains only those models for which the elements of $\tilde{\theta}_q$ are small enough to ensure that β_q (eqn 5.9b) is much less than unity. The dimension of the model of lowest dimension within Θ will be denoted by q_0.

Assumption 5.1 simply implies the obvious; namely, that the order of the "best" model cannot be arbitrarily small since this would lead to unacceptably large errors in data fit. It also reiterates and, in effect, quantifies Akaike's premise that the only models being considered are those "sufficiently close" to the true model. Using this assumption, $\ln(1-\beta_q)$ can be accurately approximated by the first term in its Taylor series expansion (i.e. $\ln(1-\beta_q) \simeq -\beta_q$), and the following incremental relationship between AIC and $\hat{\text{AIC}}$ for model orders of q and q+1 can be established:

$$\begin{aligned}\Delta AIC_q &= AIC_{q+1} - AIC_q = \hat{AIC}_{q+1} - \hat{AIC}_q - N\,(\beta_{q+1} - \beta_q) \\ &= \Delta\hat{AIC}_q - N\,(\beta_{q+1} - \beta_q) \qquad \ldots.(5.10)\end{aligned}$$

A more detailed investigation of the error term, $N\,(\beta_{q+1} - \beta_q)$, leads to the following result:

Result 5.1: Consider the class of models Θ established by Assumption 5.1. Let $\theta(q+1)$ represent the (q+1) parameter of the true system model, $\tilde{\theta}_{q+1}$ represent the vector of true parameters which are neglected when a (q+1)-dimensional model within Θ is used, and $\tilde{d}_1(q)$ denote the first column of $\tilde{D}_q$. Then, to within the accuracy of the Taylor series approximation for $\ln(1-\beta_q)$, ΔAIC_q may be replaced by:

$$\Delta AIC_q^{(1)} = \Delta\hat{AIC}_q + E_q \qquad \ldots.(5.11)$$

where $E_q = \frac{N}{\hat{\varepsilon}_q^t \hat{\varepsilon}_q} \Big\{\theta^2(q+1)\, \tilde{d}_1^t(q)\, [I - P_q]\, \tilde{d}_1(q)$ $\ldots.(5.12)$

$$+ \{2\,\theta(q+1) + \delta\}\, \tilde{d}_1^t(q)\, [I - P_q]\, \tilde{D}_{q+1}\, \tilde{\theta}_{q+1}$$
$$+ 2\,\varepsilon^t\, [I - P_q]\, \tilde{d}_1(q)\, \{\theta(q+1) + \delta\}\Big\},$$

$\delta = \tilde{d}_1^t(q)\, [I - P_q]\, \tilde{D}_{q+1}\, \tilde{\theta}_{q+1} / \gamma$ and $\gamma = \tilde{d}_1^t(q)\, [I - P_q]\, \tilde{d}_1(q)$

Proof: A comparison of eqns 5.10 and 5.11 indicates that $E_q = -N\,(\beta_{q+1} - \beta_q)$ where β_q is given by eqn 5.9b and β_{q+1} is given by:

$$\beta_{q+1} = \frac{1}{\hat{\varepsilon}_{q+1}^t \hat{\varepsilon}_{q+1}} \Big\{2\varepsilon^t (I - P_{q+1})\, \tilde{D}_{q+1}\, \tilde{\theta}_{q+1} + \tilde{\theta}_{q+1}^t\, \tilde{D}_{q+1}^T (I - P_{q+1})\, \tilde{D}_{q+1}\, \tilde{\theta}_{q+1}\Big\}$$

But, it can be shown that

$$E\{\hat{\varepsilon}_{q+1}^t \hat{\varepsilon}_{q+1}\} = E\{\hat{\varepsilon}_q^t \hat{\varepsilon}_q\} + \mu_{q+1}^t \mu_{q+1} - \mu_q^t \mu_q - \sigma_\varepsilon^2$$

$$= E\{\hat{\varepsilon}_q^t \hat{\varepsilon}_q\} \left\{ 1 + \frac{\mu_{q+1}^t \mu_{q+1} - \mu_q^t \mu_q - \sigma_\varepsilon^2}{E\{\hat{\varepsilon}_q^t \hat{\varepsilon}_q\}} \right\}$$

For models within $\boldsymbol{\theta}$, the second term in brackets on the right hand side of this expression produces second order effects in β_{q+1} which can be neglected and, hence, β_{q+1} can be accurately approximated by:

$$\beta_{q+1} \simeq \frac{1}{\hat{\varepsilon}_q^t \hat{\varepsilon}_q} \Big\{2\varepsilon^t (I - P_{q+1})\, \tilde{D}_{q+1}\, \tilde{\theta}_{q+1} + \tilde{\theta}_{q+1}^t\, \tilde{D}_{q+1}^T (I - P_{q+1})\, \tilde{D}_{q+1}\, \tilde{\theta}_{q+1}\Big\}$$

Now, by partitioning $\tilde{D}_q$ and D_{q+1} as shown here

$$\tilde{D}_q = [\tilde{d}_1(q) \mid \tilde{D}_{q+1}] \qquad D_{q+1} = [D_q \mid \tilde{d}_1(q)],$$

the following relationships can also be established:

$$2\varepsilon^t [I - P_q]\, \tilde{D}_q\, \tilde{\theta}_q = 2\varepsilon^t [I - P_q]\, [\tilde{d}_1(q) \mid \tilde{D}_{q+1}] \begin{bmatrix} \theta(q+1) \\ \tilde{\theta}_{q+1} \end{bmatrix}$$

$$= 2\varepsilon^t [I - P_q]\, \tilde{d}_1(q)\, \theta(q+1) + 2\varepsilon^t [I - P_q]\, \tilde{D}_{q+1} \tilde{\theta}_{q+1} \qquad \ldots.(5.13)$$

$$\tilde{\theta}_q^t \tilde{D}_q^T [I-P_q] \tilde{D}_q \tilde{\theta}_q = [\theta(q+1) \mid \hat{\theta}_{q+1}^t] \begin{bmatrix} \tilde{d}_1^t(q) \\ \tilde{D}_{q+1}^T \end{bmatrix} [I-P_q] [\tilde{d}_1(q) \mid \tilde{D}_{q+1}] \begin{bmatrix} \underline{\theta}(q+1) \\ \tilde{\theta}_{q+1} \end{bmatrix}$$

$$= \theta^2(q+1)\, \tilde{d}_1^t(q)\, [I-P_q]\, \tilde{d}_1(q) + 2\, \theta(q+1)\, \tilde{d}_1^t(q)\, [I-P_q]\, \tilde{D}_{q+1}\, \tilde{\theta}_{q+1} + \tilde{\theta}_{q+1}^t\, \tilde{D}_{q+1}^T [I-P_q]\, \tilde{D}_{q+1}\, \tilde{\theta}_{q+1} \quad \ldots.(5.14)$$

$$P_{q+1} = P_q + (P_q\, \tilde{d}_1\, \tilde{d}_1^t\, P_q - \tilde{d}_1\, \tilde{d}_1^t\, P_q - P_q\, \tilde{d}_1\, \tilde{d}_1^t + \tilde{d}_1\, \tilde{d}_1^t) / \gamma \quad \ldots.(5.15)$$

where eqn 5.15 is derived using the relationship between $(D_{q+1}^T\, D_{q+1})^{-1}$ and $(D_q^T\, D_q)^{-1}$ presented in many system identification texts (e.g. [EYK1], [STR1]). Eqn 5.12 can now be generated by substituting eqns 5.13, 5.14, and 5.15 into the appropriate expressions for β_q and β_{q+1} and performing the algebra required to compute $E_q = -N\,(\beta_{q+1} - \beta_q)$.

....QED

Result 5.1 establishes the fact that $\hat{AIC}$, the most practicable form of AIC, should be corrected by including additional terms (defined by E_q in eqn 5.12) to bring it in line with the assumptions made by Akaike in the development of the AIC criterion. It should be noted here that a number of proposed, "AIC-type" criteria do include some form of correction. For example, empirical results produced by Bhansali and Downham [BHA1] and based on modifications of Akaike's Final Prediction Error criterion lead to a criterion of the form:

$$AIC_\alpha = N \ln(\hat{\varepsilon}^t\, \hat{\varepsilon}) + \alpha\, q$$

For $\alpha > 2$, this modification corresponds to the addition of an extra constant, $(\alpha - 2)$, to $\Delta\hat{AIC}$ at each increment. Indeed, Bhansali and Downham obtained best results with $\alpha = 4$, and further work by Edmunds [EDM3] suggests that larger values of α can be used to eliminate the possibility of overparameterizing the model. As shown in [SCH2] and [HAN1], other proposed criteria suggest additions to $\Delta\hat{AIC}$ which are a function of the number of available data samples so that, in general [DAV1], the desired criterion

takes the form:

$$N \ln(\hat{\varepsilon}^t\hat{\varepsilon}) + q\ f(N)$$

The "AIC-type" criteria identified above do not, however, account explicitly for model structure as required by Result 5.1. In many instances, this indirect approach can be justified. For autoregressive (AR) and mixed autoregressive/moving average (ARMA) models, the error terms $\theta(q+1)$ and $\tilde{\theta}_{q+1}$ cannot be systematically identified. So it is not generally possible to identify the proper, model-dependent corrections. In these situations, the criteria mentioned above offer implementable alternatives by generating appropriate approximations for the required corrections. But, when the goal of model selection is weighting sequence truncation, additional characteristics of the model class can and, in fact, must be considered to identify the "best" model. For this problem, the use of either arbitrary incremental corrections or corrections based solely on the number of data points produces arbitrary truncations; as the size of the incremental correction increases, the number of terms in the model necessarily decreases. Hence, criteria which use a correction constant, α, or a correction function, f(N), tend to generate truncation levels that depend almost entirely on an apriori choice of the correction. Instead, as shown in the following section, it is possible to systematically generate precise incremental corrections for $\hat{AIC}$ using special weighting sequence characteristics. The result is a new criterion which effectively balances the improvements in data fit achieved by increasing model order with the increased variability of the resulting parameter estimates to identify the desired truncation. At the same time, this criterion generates additional information on the errors introduced by truncation.

5.2 Optimal Truncation: An Alternative Parameter-Space Criterion

Result 5.1 establishes an accurate relationship between ΔAIC and $\Delta\hat{AIC}$. Unfortunately, this relationship is a function of several unknown

quantities. For weighting sequences however, these unknown variables can be accurately identified. As a result, an alternative realizeable criterion which identifies precisely the same truncated model as the true minimum AIC criterion can be generated. The development of this criterion begins with Result 5.2 which establishes an equivalent expression for AIC in terms of $\hat{AIC}$ and the incremental corrections defined by eqn 5.12. The discussion then focuses specifically on weighting sequence truncation. First, Result 5.3 refines the class of weighting sequence models within which the "best" model exists, and then Result 5.4 highlights additional adjustments to the criterion of Result 5.2 that are unique to weighting sequence models. From the insights obtained in Result 5.4, a new truncation criterion is proposed in Result 5.5, and this criterion is shown to possess the same properties as the minimum AIC criterion. Finally, Result 5.6 establishes the conditions required to produce an implementable procedure for the identification of the "best" truncation using this new criterion.

To begin, the minimum AIC criterion can be reformulated using Result 5.1 to produce:

Result 5.2: Consider the class of models Θ which satisfy Assumption 5.1, and let q represent the dimension of any specified model in the class. For E_q defined by eqn 5.12, define $AIC_q^{(1)}$ as follows:

$$AIC_{q_0}^{(1)} = \hat{AIC}_{q_0} \qquad \ldots.(5.16a)$$

$$AIC_q^{(1)} = \hat{AIC}_q + \sum_{i=q_0}^{q-1} E_i \qquad \text{for } q > q_0 \qquad \ldots.(5.16b)$$

Then the "best" model within Θ can be identified by minimizing $AIC_q^{(1)}$ over all $q \geq q_0$.

Proof: Consider the model of dimension q_0 within Θ. Using eqns 5.2 and 5.3, AIC_{q_0} and $\hat{AIC}_{q_0}$ can be related by:

$$AIC_{q_0} = \hat{AIC}_{q_0} + c_0 \qquad \text{....(5.17a)}$$

where $$c_0 = N \ln \left\{ 1 - \frac{2\hat{\varepsilon}^t_{q_0} \mu_{q_0}}{\hat{\varepsilon}^t_{q_0} \hat{\varepsilon}_{q_0}} + \frac{\mu^t_{q_0} \mu_{q_0}}{\hat{\varepsilon}^t_{q_0} \hat{\varepsilon}_{q_0}} \right\} = \text{constant},$$

Result 5.1 demonstrates that ΔAIC and $\Delta AIC^{(1)}$ are equivalent for models within Θ and, hence, AIC_{q_0+1} is equivalent to

$$AIC^{(1)}_{q_0+1} = AIC_{q_0} + \Delta AIC^{(1)}_{q_0} = \hat{AIC}_{q_0} + c_0 + \Delta\hat{AIC}_{q_0} + E_{q_0}$$

$$= \hat{AIC}_{q_0+1} + c_0 + E_{q_0}$$

This procedure can be repeated for each incremental change in dimension to establish the value of $AIC^{(1)}_q$ for any $q > q_0$ as:

$$AIC^{(1)}_q = \hat{AIC}_q + c_0 + \sum_{i=q_0}^{q-1} E_i \qquad \text{....(5.17b)}$$

By Definition 5.1, the "best" model within Θ is obtained by minimizing AIC_q over all models in the class. Since $\Delta AIC^{(1)}$ is equivalent to ΔAIC for all $q > q_0$, $AIC^{(1)}_q$ (as defined by eqns 5.17a,b) is equivalent to AIC_q for each $q \geq q_0$. Hence, minimizing $AIC^{(1)}_q$ also identifies the "best" model in the class. Furthermore, since the location of the minimum is unaffected by the addition of a constant, $AIC^{(1)}_q$ can be simplified by removing the constant c_0 to produce the cost function described by eqns 5.16a,b.

....QED

The order selection criterion defined by Result 5.2 still depends on several unknown quantities. For weighting sequences, important relationships between these quantities exist and can be used to transform the results above into a realizeable truncation criterion. Consider the correction to $\hat{AIC}_q$ defined by eqn 5.12. When weighting sequence models are used, the terms $\tilde{d}_1(q)$, P_q, and $\tilde{D}_{q+1}$ are simply functions of the inputs used during

the identification test, while $\theta(q+1)$ and $\tilde{\theta}_{q+1}$ behave in a predictable manner that can be identified and used to accurately estimate these quantities (as will be shown later). However, ε (the true noise in the output data) is random and cannot be identified. Since ε is uncorrelated with the true system parameters and test inputs, the average value of $2\varepsilon^t[I-P_q]\,\tilde{d}_1(q)\,\{\theta(q+1) + \delta\}$ is zero and, at first glance, it would seem reasonable to assume that this term can be neglected when calculating the desired correction, E_q. But for any given identification test, this term is not identically zero. Furthermore, because the elements of the true weighting sequence grow smaller, this term may become a significant component of E_q for many models in $\boldsymbol{\Theta}$. In these cases, the failure to account for this random effect could produce an arbitrary and erroneous selection of the "best" model order. To avoid this problem, the class of weighting sequence models established by Assumption 5.1 can be restricted as follows:

Result 5.3: Let $\boldsymbol{\Theta}_{WS}$ represent the class of weighting sequence models (obtained using a least-squares procedure) within which the "best" model exists. Then, $\boldsymbol{\Theta}_{WS}$ is a subset of $\boldsymbol{\Theta}$, and this subset contains only models which satisfy the following condition:

$$\theta^2(q+1)\,\tilde{d}_1^t(q)\,[I-P_q]\,\tilde{d}_1(q) + (2\,\theta(q+1) + \delta)\,\tilde{d}_1^t(q)\,[I - P_q]\,\tilde{D}_{q+1}\tilde{\theta}_{q+1} \gg 2\,\varepsilon^t[I-P_q]\,\tilde{d}_1(q)\,\{\theta(q+1) + \delta\} \qquad \ldots.(5.18)$$

The dimension of the model of largest dimension within $\boldsymbol{\Theta}_{WS}$ will be denoted by q_f.

Proof: Since ε is uncorrelated with the true system parameters and test inputs, $2\varepsilon^t[I-P_q]\,\tilde{d}_1(q)\,\{\theta(q+1) + \delta\}$ represents only random non-zero effects introduced by the use of finite data sets. Attempts to estimate parameters for which this quantity is significant will, therefore, be dominated by unknown random errors and the resulting parameter estimates will necessarily include large random components. Clearly, the "best"

system model cannot contain parameters for which accurate estimates are unavailable, yet these are the only models in Θ which are excluded from Θ_{WS} by condition 5.18. Hence, the "best" model must be an element of Θ_{WS}.

....QED

It is important to emphasize that Result 5.3 does not imply a direct relationship between the absolute size of the parameters that can be estimated and the size of the noise present in the data (as measured by its variance). Indeed, user-specified test conditions (e.g. sample size and system inputs) can be selected so that weighting sequence elements which are significantly smaller than the variance of the noise can still be accurately estimated. Thus, Result 5.3 simply refines the description of the model class for a given set of input/output data (as mentioned previously) so that an appropriate truncation criterion will not be affected by random, and possibly harmful, effects.

For models which satisfy Result 5.3, $2\varepsilon^t[I-P_q]\,\tilde{d}_1(q)\,\{\theta(q+1) + \delta\}$ can be neglected and the identification of ε is unnecessary. As a result, the corrections to $\hat{AIC}$ identified by eqn 5.12 for any given model are now simply functions of the known inputs and the unknown terms $\theta(q+1)$ and $\tilde{\theta}_{q+1}$. But for weighting sequences, $\theta(q+1)$ and $\tilde{\theta}_{q+1}$ can be related to the parameters of the q-dimensional model in the following way:

Definition 5.2: Let $\theta(q)$ denote the q^{th} element of the infinite weighting sequence for a stable system. Then, there exists an element $\theta(q_b)$ in the sequence such that, for all $q > q_b$, $\theta(q+k)$ can be bounded in size by a single exponential decay

$$|\theta(q+k)| \leq \rho_q^k\,|\theta^*(q)| \qquad \forall\, k > 0 \qquad \text{....(5.19)}$$

where $\theta^*(q)$ lies on the boundary of the exponential decay and ρ_q is a constant which describes the rate of decay and is defined by $\theta^*(q+1)/\theta^*(q))$. Eqn 5.19 defines the exponential bounding property for

infinite weighting sequence descriptions of stable systems.

The use of open-loop identification techniques implies that the system under investigation is stable, and so the elements of its weighting sequence will be exponentially bounded. In addition, any accurate finite weighting sequence model must necessarily exclude only elements which can be bounded by this decay. Hence, all models in Θ_{WS} will contain elements that can be exponentially bounded. As a result, the exponential decay property can be used to modify the order selection criterion established by Result 5.2 as shown here:

Result 5.4: Consider a system whose weighting sequence elements, $\theta(i)$, are sign definite for $q_0 \leq i \leq q_f$. Then for any specified set of input/output data (where the inputs are generated as an uncorrelated zero-mean sequence and $N >> q_f$), the "best" model order can be identified by minimizing $AIC_q^{(2)}$ over all q in the range $q_0 \leq q \leq q_f$, where $AIC_q^{(2)}$ is defined by:

$$AIC_{q_0}^{(2)} = \hat{AIC}_{q_0} \qquad \ldots.(5.20a)$$

$$AIC_q^{(2)} = \hat{AIC}_q + \sum_{i=q_0}^{q-1} \left\{ \frac{N}{\hat{\varepsilon}_i^t \hat{\varepsilon}_i} [\rho_i^2 \theta^{*2}(i) \tilde{d}_1^t(i) \tilde{d}_1(i)] \right\}; \quad q > q_0 \quad \ldots.(5.20b)$$

and $\theta^*(q)$ and ρ_q are defined by Definition 5.2.

Proof: Since all models in Θ_{WS} satisfy Assumption 5.1, Result 5.2 is valid and the "best" model order can be identified by selecting the model which minimizes $AIC_q^{(1)}$ (eqn 5.16) over all q in the range $q_0 \leq q \leq q_f$. Now Result 5.3 implies that $2\varepsilon^t[I-P_q]\,\tilde{d}_1(q)\,\{\theta(q+1) + \delta\}$ is negligible for all model orders $q_0 \leq q \leq q_f$. Furthermore, when $N >> q_f$, the use of uncorrelated inputs implies that the quantities $\tilde{d}_1^t(q)\,\tilde{D}_{q+1}$, $\tilde{d}_1^t(q)\,P_q\,\tilde{D}_{q+1}$, and $\tilde{d}_1^t(q)\,P_q\,\tilde{d}_1(q)$ are also negligible. Hence under the assumed conditions, E_q (eqn 5.12) can be accurately replaced by $\theta^2(q+1)\,\tilde{d}_1^t(q)\,\tilde{d}_1(q)$, and $AIC_1^{(1)}$ is equivalent to

$$AIC_{q_0}^{(2)} = \hat{AIC}_{q_0}$$

$$AIC_q^{(2)} = \hat{AIC}_q + \sum_{i=q_0}^{q-1} \left\{ \frac{N}{\hat{\varepsilon}_i^t \hat{\varepsilon}_i} [\theta^2(i+1)\, \tilde{d}_1^T(i)\, \tilde{d}_1(i)] \right\}; \quad q > q_0$$

over the desired range of q. Since $\theta(q)$ is sign definite over the same range, Definition 5.2 implies that $\theta(q+1)$ may be replaced by $\rho_q \theta^*(q)$ and $AIC_q^{(2)}$ can be rewritten as:

$$AIC_q^{(2)} = \hat{AIC}_q + \sum_{i=q_0}^{q-1} \left\{ \frac{N}{\hat{\varepsilon}_i^t \hat{\varepsilon}_i} [\rho_i^2\, \theta^{*2}(i)\, \tilde{d}_1^t(i)\, \tilde{d}_1(i)] \right\}$$

Since $AIC_q^{(2)}$ and $AIC_q^{(1)}$ are equivalent for all $q_0 \leq q \leq q_f$, minimizing $AIC_q^{(2)}$ produces the same result as minimizing $AIC_q^{(1)}$. Thus, by Result 5.2, minimizing $AIC_q^{(2)}$ must identify the "best" model within Θ_{WS}.

....QED

Result 5.4 demonstrates that minimizing $AIC_q^{(2)}$ over all q in the range $q_0 \leq q \leq q_f$ identifies the truncation level which is "best" in the statistical context of the AIC criterion initially proposed by Akaike (Definition 5.1). It should be noted that the criterion is still not implementable since, for example, apriori information on q_0 and q_f is required. However, Result 5.4 does simplify the criterion considerably and provides important insights for its implementation. These insights can be used to establish an alternative criterion which, though similar to $AIC^{(2)}$, is implementable.

Before proceeding to this development, two additional points concerning Result 5.4 should also be highlighted. First, the assumption of uncorrelated zero-mean inputs was introduced primarily to simplify the following analysis. In fact, the use of this test input guarantees equivalence between $AIC^{(2)}$ and $AIC^{(1)}$ (and hence AIC) since the quantity $\{2\theta(q+1)+\delta\}\, \tilde{d}_1^t(q)[I-P_q]\tilde{D}_{q+1}\tilde{\theta}_{q+1}$ is negligible in this situation and $\theta(q+1)$ is equal to $\rho_q\, \theta^*(q)$. When other inputs are used, Result 5.4 may be extended simply by including this additional term and using $\rho_q^k\, \theta^*(q)$ as an

upper bound on the k^{th} truncation term in the vector $\tilde{\theta}_{q+1}$. In this situation, $AIC_q^{(2)}$ establishes an accurate upper bound for $AIC_q^{(1)}$ and, in the absence of any additional information, it generates the best available estimate of AIC. Second, the assumption that the system weighting sequence elements are sign definite for $q_0 \leq q \leq q_f$ is valid for all systems except those with dominant complex poles. So the equivalence between $AIC_q^{(2)}$ and $AIC_q^{(1)}$ will hold. When the weighting sequence elements are oscillatory however, $\theta(q+1)$ is not equal to $\rho_q\ \theta^*(q)$, but instead $|\theta(q+1)| \leq \rho_q\ |\theta^*(q)|$. As a result, the correction terms used to transform $\hat{AIC}_q$ to $AIC_q^{(2)}$ are upper bounds on the true corrections required to maintain the equivalence between $AIC_q^{(2)}$ and $AIC_q^{(1)}$. It must be kept in mind, however, that the value of $AIC_q^{(2)}$ for any given q will be compared with all other values of $AIC^{(2)}$ to establish the "best" model order. Hence, the correction terms must not only provide an accurate description of parameter size, but they must also produce a description which is relevant for comparative purposes. When this perspective is taken, it is easy to see that the use of $\rho_q^2\ \theta^{*2}(q)$ in place of $\theta^2(q+1)$ for oscillatory weighting sequences accomplishes both objectives. Thus, using $AIC^{(2)}$ to identify the "best" truncation should also work effectively for oscillatory systems.

As mentioned previously, a closer examination of eqns 5.24a,b provides valuable insights into the implementation of the criterion. The term $\tilde{d}_1(q)$ is known for any q, while $\theta^*(q)$ is a function of the weighting sequence elements. For systems with a dominant [illegible] best estimate of $\theta^*(q)$ is simply the last parameter in the [illegible] of dimension q; while for systems with dominant [illegible] estimated on the basis of the dominant [illegible] several parameter estimates. Since R[illegible]

AD-A186 086 A WEIGHTING SEQUENCE APPROACH TO THE ANALYSIS AND DESIGN OF MULTIVARIABLE CONTROL SYSTEMS(U) AIR FORCE INST OF TECH WRIGHT-PATTERSON AFB OH D J CLOUD 1987 2/3

UNCLASSIFIED AFIT/CI/NR-87-131D F/G 12/4 NL

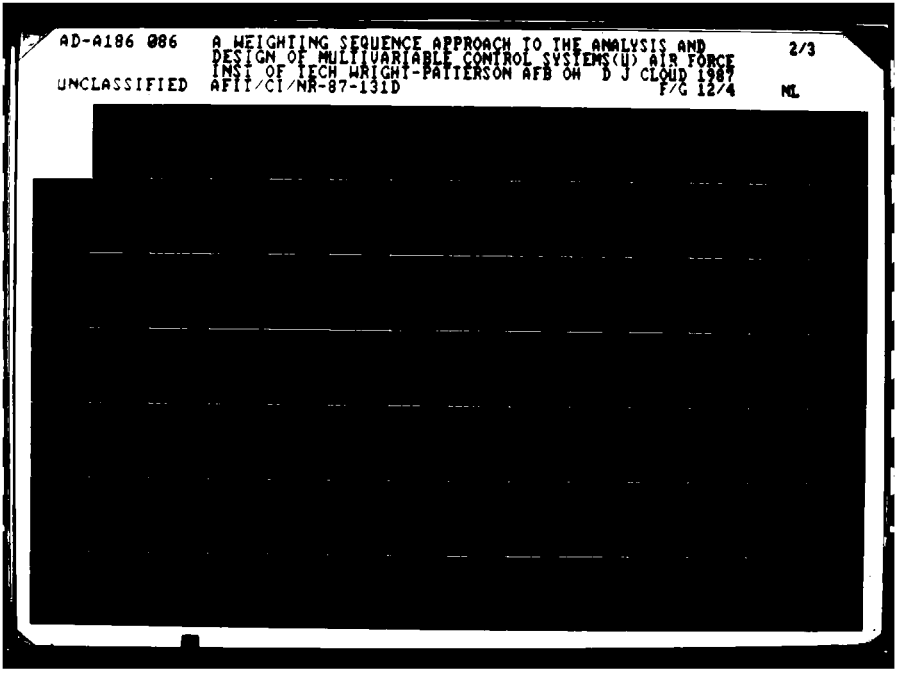

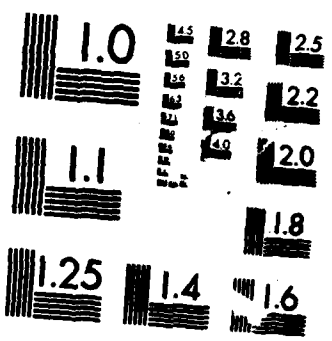

MICROCOPY RESOLUTION TEST CHART
NATIONAL BUREAU OF STANDARDS-1963-A

within Θ_{WS}, the model parameter estimates are necessarily reliable representations of the true parameters, and so they can indeed be used to identify $\theta^*(q)$ accurately. The only remaining unknown in $AIC_q^{(2)}$ is the decay constant ρ_q. At first glance, it may seem strange to introduce this parameter into the criterion. Since $\theta^2(q+1) = \rho_q^2\ \theta^{*2}(q)$, Result 5.4 implies that the appropriate correction term for $\hat{AIC}_q$ only requires knowledge of $\theta^2(i)$ for $i = q_0, \cdots, q_f$ and, for models within Θ_{WS}, accurate estimates of these quantities are available. Thus, it would appear that these estimates may be used to establish $AIC_q^{(2)}$. However as noted above, q_0 and q_f are unknown. So, the model class Θ_{WS} is not known apriori. If models outside Θ_{WS} are included in the investigation, the correction terms associated with these models will be incorrect. As a result, $AIC_q^{(2)}$ will not be an accurate representation of AIC_q, and the truncation which minimizes $AIC^{(2)}$ will not necessarily correspond to the "best" truncation. In many cases therefore, the indiscriminate use of parameter estimates alone to calculate $AIC_q^{(2)}$ will lead to erroneous truncations.

The introduction of the decay constant ρ, however, offers an alternative view of the required corrections. In particular, each ρ_i may be interpreted as a "scale factor" for the specified correction. When this perspective is taken, a new truncation criterion which avoids the problem described above can be generated. For any specified model in Θ_{WS}, the exponential decay associated with this model can be directly related to the "parameter" bias of the model defined by $\sqrt{(\tilde{\theta}_q^t\ \tilde{\theta}_q)}$ (i.e. the size of the error introduced by truncation). More specifically,

$$\tilde{\theta}_q^t\ \tilde{\theta}_q \leq \rho_q^2\ \theta^{*2}(q) / (1 - \rho_q^2) = B_q^2 \qquad \ldots.(5.21)$$

Hence, ρ_q quantifies an upper bound on "parameter" bias for the specified model. Eqn 5.21 defines an interesting relationship between ρ_q, $\theta^*(q)$, and B_q. Clearly, if $\theta^*(q)$ and ρ_q are known, B_q can be calculated. However, the

roles of B_q and ρ_q may also be interpreted in reverse. If $\theta^*(q)$ is known and B_q is specified, ρ_q can be calculated to ensure that the equality in eqn 5.21 is satisfied. This role reversal leads to the following alternative truncation criterion:

Result 5.5: Let q_{best} denote the (as yet unknown) order of the model within Θ_{WS} which minimizes $AIC_q^{(2)}$, and let $B^2_{(q_{best}-1)}$ represent the upper bound on the "parameter" bias (eqn 5.21) associated with the model of order $q_{best}-1$; namely, let

$$B^2_{(q_{best}-1)} = \rho^2_{(q_{best}-1)} \; \theta^{*2}(q_{best}-1) \; / \; (1 - \rho^2_{(q_{best}-1)})$$

Furthermore, for any given q, define the scale factor $\tilde{\rho}_q$ such that

$$\tilde{\rho}_q^2 \; \theta^{*2}(q) \; / \; (1 - \tilde{\rho}_q^2) \; = \; B^2_{(q_{best}-1)}$$

Then, the quantity T_q defined by:

$$T_{q_0} = \hat{AIC}_{q_0} \qquad \ldots.(5.22a)$$

$$T_q = \hat{AIC}_q + \sum_{i=q_0}^{q-1} \left\{ \frac{N}{\hat{\varepsilon}_i^t \hat{\varepsilon}_i} [\tilde{\rho}_i^2 \; \theta^{*2}(i) \; \tilde{d}_1^t(i) \; \tilde{d}_1(i)] \right\}; \quad q > q_0 \quad \ldots.(5.22b)$$

will possess a unique minimum for all q in the range $q_0 \leq q \leq q_f$, and this minimum will occur at q_{best}.

Proof: First, consider models of order q within Θ_{WS} where $q > q_{best}$. For these models, $AIC_q^{(2)}$ can be related to $AIC_{q_{best}}^{(2)}$ by:

$$AIC_q^{(2)} - AIC_{q_{best}}^{(2)} = \hat{AIC}_q - \hat{AIC}_{q_{best}} + \sum_{i=q_{best}}^{q-1} \left\{ \frac{N}{\hat{\varepsilon}_i^t \hat{\varepsilon}_i} [\rho_i^2 \; \theta^{*2}(i) \; \tilde{d}_1^t(i) \; \tilde{d}_1(i)] \right\}$$

By definition, $AIC_{q_{best}}^{(2)}$ is a minimum. So, $AIC_q^{(2)} - AIC_{q_{best}}^{(2)}$ is greater than zero. As a result,

$$\hat{AIC}_q - \hat{AIC}_{q_{best}} > - \sum_{i=q_{best}}^{q-1} \left\{ \frac{N}{\hat{\varepsilon}_i^t \hat{\varepsilon}_i} [\rho_i^2 \; \theta^{*2}(i) \; \tilde{d}_1^t(i) \; \tilde{d}_1(i)] \right\} \quad \ldots.(5.23)$$

Using eqn 5.22, T_q and $T_{q_{best}}$ can be related by:

$$T_q - T_{q_{best}} = \hat{AIC}_q - \hat{AIC}_{q_{best}} + \sum_{i=q_{best}}^{q-1} \left\{ \frac{N}{\hat{\varepsilon}_i^t \hat{\varepsilon}_i} [\tilde{\rho}_i^2 \theta^{*2}(i) \tilde{d}_1^t(i) \tilde{d}_1(i)] \right\}$$

But substituting the inequality 5.23 into this expression yields:

$$T_q - T_{q_{best}} > \sum_{i=q_{best}}^{q-1} \left\{ \frac{N}{\hat{\varepsilon}_i^T \hat{\varepsilon}_i} [(\tilde{\rho}_i^2 - \rho_i^2) \theta^{*2}(i) \tilde{d}_1^T(i) \tilde{d}_1(i)] \right\}$$

Since $B^2_{(q_{best}-1)} \geq B_q^2$ for all $q \geq q_{best}$, $\tilde{\rho}_q^2 \geq \rho_q^2$. Hence, $T_q > T_{q_{best}}$ for all $q > q_{best}$.

A similar approach can be used to develop the following relationship between T_q and $T_{q_{best}}$ for any q in the range $q_0 \leq q \leq q_{best}$:

$$T_q - T_{q_{best}} > \sum_{i=q}^{q_{best}-1} \left\{ \frac{N}{\hat{\varepsilon}_i^t \hat{\varepsilon}_i} [(\rho_i^2 - \tilde{\rho}_i^2) \theta^{*2}(i) \tilde{d}_1^t(i) \tilde{d}_1(i)] \right\}$$

Since $B^2_{(q_{best}-1)} \leq B_q^2$ for all $q < q_{best}$, $\rho_q^2 \geq \tilde{\rho}_q^2$. Hence, $T_q > T_{q_{best}}$ for all q in the range $q_0 \leq q \leq q_{best}$. Combining this result with the result for $q > q_{best}$ establishes $T_{q_{best}}$ as the minimum value of T_q for all models in Θ_{WS}.

....QED

Result 5.5 produces an alternative criterion which is equivalent to the minimum $AIC^{(2)}$ criterion of Result 5.4 and, hence, this new criterion must also identify the truncation level which is "best" in the statistical sense associated with Akaike's criterion. More importantly, this alternative criterion can be implemented using data from the parameter estimation process even though q_0 and q_f are unknown. So, it will avoid the problems which can produce an erroneous identification of the "best" truncation using the minimum $AIC^{(2)}$ criterion.

An appropriate procedure for truncation level identification based on the cost function T_q (eqn 5.22) depends on several subtle implications of Result 5.5 which must be highlighted. First, the proof that T_q achieves a minimum at q_{best} relies only on differences between T_q and $T_{q_{best}}$ for q in

the range $q_0 \leq q \leq q_f$ which suggests that the relationship between T_q and $T_{q_{best}}$ (over this range) is independent of the truncation level at which T_q is initialized provided this initial truncation level is less than or equal to q_0. As suggested previously, any accurate weighting sequence model must necessarily include elements which can be exponentially bounded. Hence, by Assumption 5.1, q_0 must be greater than q_b (where q_b is defined by Definition 5.2). So, q_b provides an appropriate and, indeed, easily identifiable truncation level at which to initialize T_q. In essence, this observation implies that T_q may be recomputed using eqns 5.22a,b with q_0 replaced by q_b. For these redefined values of T_q, Result 5.5 remains valid over the interval $q_0 \leq q \leq q_f$ and T_q will reach a unique minimum at q_{best}. Thus, an implementable procedure based on Result 5.5 need not rely on knowledge of q_0 to initialize the criterion.

A second implication of Result 5.5 is the following. If $q_{\hat{AIC}}$ is the order of the weighting sequence model which minimizes $\hat{AIC}_q$, then $\hat{AIC}_q$ is, by definition, greater than $\hat{AIC}_{q_{\hat{AIC}}}$ for all $q > q_{\hat{AIC}}$. Furthermore, since T_q in eqn 5.22 is formed by adding a non-decreasing function to $\hat{AIC}_q$, it is now obvious that T_q will be greater than $T_{q_{\hat{AIC}}}$ for all $q > q_{\hat{AIC}}$. Hence, T_q must be a minimum for some $q \leq q_{\hat{AIC}}$, and so $q_{\hat{AIC}}$ establishes an easy-to-calculate upper bound for q_{best}.

Together, the observations above demonstrate that q_{best} must necessarily lie in the range $q_b < q \leq q_{\hat{AIC}}$. [Indeed, additional refinements (using $\hat{AIC}$) to reduce the number of candidates for q_{best} still further can be established as shown in Appendix 5.1. Though not essential to the development of an implementable algorithm for truncation selection, these additional refinements can be used to reduce the computational complexity of the resulting algorithm.] Once the set of potential candidates for q_{best} has been identified, the only remaining problem is to select the "best"

model from among the members of this set. A procedure to accomplish this task is suggested by the following result:

Result 5.6: Let Q define the known set of weighting sequence model orders which contains q_{best} and let q_k denote the k^{th} element in Q. In addition, define the quantity $\hat{T}_q$ to be:

$$\hat{T}_q = \hat{AIC}_q + \sum_{i=q_b}^{q-1} \left\{ \frac{N}{\hat{\varepsilon}_i^t \hat{\varepsilon}_i} [\tilde{\rho}_i^2 \hat{\theta}^{*2}(i) \tilde{d}_1^t(i) \tilde{d}_1(i)] \right\} \quad ....(5.24)$$

where $\tilde{\rho}_i$ is a scale factor computed using the relationship

$$\tilde{\rho}_i^2 \hat{\theta}^{*2}(i) / (1 - \tilde{\rho}_i^2) = \hat{B}^2 ,$$

$\hat{\theta}^*(i)$ represents the value of $\theta^*(i)$ obtained from the estimated model of dimension i, and $\hat{B}^2$ is non-negative.

Then for each q_k, examine the set of values $\hat{T}_q$ (calculated using eqn 5.24) over the range $q_b < q \leq q_k$ and let $\hat{B}^2_{max}(q_k)$ denote the maximum value of $\hat{B}^2$ for which $\hat{T}_q$ remains a minimum at q_k. The "best" model order can now be identified by selecting the largest value of q_k for which $\hat{B}^2_{max}(q_k)$ is a valid upper bound for $B^2_{(q_k-1)}$.

Proof: For weighting sequence models, increasing the model order from q to q+1 automatically improves the model fit to the observed output data. If the last estimated parameter in the model of order q+1 is an accurate estimate of the corresponding true parameter, this improvement in fit has clearly been attained by improving the weighting sequence description of the system, not by simply fitting to the noise in the data. Hence, the "best" truncation must necessarily correspond to the largest model order for which the last estimated parameter is an accurate estimate of the corresponding true parameter. Thus by Result 5.3, $q_{best} = q_f$.

Now if $q_k = q_{best}$, then $\hat{\theta}^*(q_k)$ is, by definition, an accurate

estimate of $\theta^*(q_k)$. In addition, the set of values $\hat{T}_q$ (for $q_b < q \leq q_k$) will be identical to the set of values T_q defined by eqn 5.22 when $\hat{B}^2 = B^2_{q_k-1}$. Hence, $\hat{T}_q$ (calculated using $\hat{B}^2 = B^2_{q_k-1}$) must be a minimum at q_k. But by assumption, $\hat{T}_q$ is a minimum at q_k when $\hat{B}^2 = \hat{B}^2_{max}(q_k)$, and this implies that $\hat{B}^2_{max}(q_k)$ is greater than or equal to $B^2_{q_k-1}$. Thus, if $\hat{B}^2_{max}(q_k)$ is not a valid upper bound for $B^2_{q_k-1}$, $q_k \neq q_{best}$. Furthermore from above, $q_{best} = q_f$. So, this result also implies that q_{best} must necessarily correspond to the largest model order in the set Q for which $\hat{B}^2_{max}(q_k)$ is a valid upper bound for $B^2_{q_k-1}$.

....QED

As demonstrated by Result 5.6, the problem of optimal weighting sequence truncation using the T_q criterion of Result 5.5 reduces to a problem of verifying the accuracy of the maximum bias bound established for each model order in Q. A complete procedure for identifying q_{best} via bias bound verification is presented and discussed in Appendix 5.2. The results of several Monte Carlo simulations are presented in Section 5.4 to demonstrate the validity of this procedure.

The truncation criterion established by Results 5.5 and 5.6 possesses two particularly noteworthy features which must be stressed. First, it guarantees that the specified truncation point is established in a manner consistent with the level of noise present in the data rather than an arbitrary specification of the size of the individual parameters. Second, it simultaneously generates an accurate estimate of the "parameter" bias introduced. Thus, this new criterion not only establishes a statistically optimal truncation for the system, but it also quantifies the affects of this truncation. Although the truncation effects are currently quantified in terms of "parameter" bias, it is possible to extend the

criterion to generate frequency response bias information as demonstrated in the following section.

5.3 Optimal Truncation: Frequency Domain Extensions

5.3.1 A Modified Criterion to Identify Frequency Response Bias

For infinite weighting sequence models, the effects of truncation on system frequency response can be related to the parameters of the given model using relationships defined in the previous sections. In particular, the error introduced by truncation at any specified z is given by:

$$g_E(z) = \sum_{i=q+1}^{\infty} g_i \, z^{-i} \, . \qquad \ldots.(5.25)$$

So, the magnitude of $g_E(z)$ can be bounded for all $|z| = 1$ in the following way:

Result 5.7: Consider a stable system described by the z-domain transfer function

$$g(z) = \sum_{i=1}^{\infty} \theta(i) \, z^{-i}$$

where $\theta(i)$ now represents the i^{th} element of the infinite weighting sequence. Let q represent the dimension of the truncated model such that $q > q_b$ (where q_b is defined by Definition 5.2). Then, the magnitude of the frequency response bias introduced by this truncation is bounded over all frequencies from 0 to π/T by:

$$|g_E(z)|^2 \leq \rho_q^2 \, \theta^{*2}(q) \, / \, (1 - \rho_q)^2 = B_{FR}^2(q) \qquad \ldots.(5.26)$$

Proof: $$|g_E(z)| = \left| \sum_{i=q+1}^{\infty} \theta(i) \, z^{-i} \right| \leq \sum_{i=q+1}^{\infty} |\theta(i)| \, |z^{-i}|$$

But for $z = exp(j\omega T)$, $|z^{-i}| = 1$ and so

$$|g_E(z)| \leq \sum_{i=q+1}^{\infty} |\theta(i)|$$

Since the weighting sequence elements are exponentially bounded,

$$|g_E(z)| \leq \rho_q |\theta^*(q)| [1 + \rho_q + \rho_q^2 + \cdots] = \rho_q |\theta^*(q)| / (1 - \rho_q)$$

and eqn 5.26 follows immediately.

....QED

Result 5.7 establishes a single upper bound on the frequency response bias introduced by truncation in terms of the bounding exponential decay constant, ρ, and the parameters of the specified finite weighting sequence model. But this is precisely the same information required to define the "parameter" bias bound used to derive Result 5.5. Indeed, a comparison of eqns 5.21 and 5.26 indicates that B_q^2 and $B_{FR}^2(q)$ are related by:

$$B_{FR}^2(q) = B_q^2 (1 + \rho_q) / (1 - \rho_q), \qquad ....(5.27)$$

and this relationship suggests that the optimal truncation criterion can be redefined using $B_{FR}^2(q)$ as shown here:

Result 5.8: Let q_{best} denote the (as yet unknown) order of the model within Θ_{WS} which minimizes $AIC_q^{(2)}$, and let $B_{FR}^2(q_{best}-1)$ denote the upper bound on frequency response bias (defined by eqn 5.26) associated with the model of order $q_{best}-1$. In addition, define the scale factor $\tilde{\rho}_{FR}(q)$ (for any given q) such that

$$\tilde{\rho}_{FR}^2(q)\, \theta^{*2}(q) / [1 - \tilde{\rho}_{FR}(q)]^2 = B_{FR}^2(q_{best}-1)$$

Then, the quantity $T_{FR}(q)$ defined (for $q > q_b$) by:

$$T_{FR}(q) = \hat{AIC}_q + \sum_{i=q_b}^{q-1} \left[\frac{N}{\hat{\varepsilon}_i^t \hat{\varepsilon}_i} \tilde{\rho}_{FR}^2(i)\, \theta^{*2}(i)\, \tilde{d}_1^t(i)\, \tilde{d}_1(i) \right] \qquad ....(5.28)$$

will possess a unique minimum for all q in the range $q_0 \leq q \leq q_f$, and this minimum will occur at q_{best}.

Proof: Since $B_{FR}^2(q)$ and B_q^2 are related by eqn 5.27, the relationships used to prove Result 5.5 are also valid for $T_{FR}(q)$. Thus, the proof here is identical to that of Result 5.5.

....QED

The similarities between Results 5.5 and 5.8 can also be used to extend Result 5.6 to the frequency domain as shown here:

Result 5.9: Let Q define the known set of weighting sequence model orders which contains q_{best} and let q_k denote the k^{th} element in Q. In addition, define the quantity $\hat{T}_{FR}(q)$ to be:

$$\hat{T}_{FR}(q) = \hat{AIC}_q + \sum_{i=q_b}^{q-1} \left\{ \frac{N}{\hat{\varepsilon}_i^t \hat{\varepsilon}_i} [\tilde{\rho}_{FR}^2(i)\ \hat{\theta}^{*2}(i)\ \tilde{d}_1^t(i)\ \tilde{d}_1(i)] \right\} \quad ....(5.29)$$

where $\tilde{\rho}_{FR}(i)$ is a scale factor computed using the relationship

$$\tilde{\rho}_{FR}^2(i)\ \hat{\theta}^{*2}(i) \ / \ [1 - \tilde{\rho}_{FR}(i)]^2 \ = \ \hat{B}_{FR}^2 \ ,$$

$\hat{\theta}^*(i)$ represents the value of $\theta^*(i)$ obtained from the estimated model of dimension i, and $\hat{B}_{FR}^2$ is non-negative.

Then for each q_k, examine the set of values $\hat{T}_{FR}(q)$ (calculated using eqn 5.29) over the range $q_b < q \leq q_k$ and let $\hat{B}_{FR_{max}}^2(q_k)$ denote the maximum value of $\hat{B}_{FR}^2$ for which $\hat{T}_{FR}(q)$ remains a minimum at q_k. The "best" model order can now be identified by selecting the largest value of q_k for which $\hat{B}_{FR_{max}}^2(q_k)$ is a valid upper bound for $B_{FR}^2(q_k\text{-}1)$.

Proof: With appropriate substitutions, the proof is identical to that of Result 5.6. ....QED

It should be noted that, since $B_{FR}^2(q)$ is proportional to B_q^2, the truncation established by the modified criterion of Results 5.8 and 5.9 must necessarily be identical to the truncation established using Results 5.5 and 5.6. The only difference between these two criteria is the interpretation given to the maximum bias bounds generated by the procedures. When the frequency response criterion is used, $B_{FR_{max}}^2(q_{best})$ is a valid upper bound for $B_{FR}^2(q_{best}\text{-}1)$ and, by Result 5.7, it is also a valid upper bound on the

magnitude of the frequency response bias introduced by truncation for all frequencies from 0 to π/T. Monte Carlo simulations were used to demonstrate this frequency-response-based criterion, and the results presented in Section 5.4 for these simulations clearly demonstrate the validity of this modified procedure.

5.3.2 Additional Refinements for Selected Individual Frequencies

For many systems, the use of a single quantity (such as $B_{FR}^2(q)$ in Result 5.7) to bound frequency response bias produces an unnecessarily conservative description of bias over a wide range of frequencies. In these situations, further frequency response modifications can be introduced to refine the bias description by establishing frequency-dependent bias bounds which produce a more representative description at specified individual frequencies.

Consider a first-order system. For this system, the error term introduced by truncation is given exactly by

$$g_E(z) = g_{q+1}\, z^{-(q+1)}\, [1 + \rho z^{-1} + \rho^2 z^{-2} + \cdots] = g_{q+1}\, z^{-q} / (z-\rho)$$

and the frequency response bias introduced by truncation can be evaluated at any individual frequency, ωT, simply by substituting $z = \exp(j\omega T)$ into this expression. Thus, a distinct bias bound can be established at each individual frequency using the relationship:

$$|\rho\, g_q\, z^{-q}|^2 / |z-\rho|^2 = \rho^2\, g_q^2 / |z-\rho|^2 = B_{FR}^2(z;q) \quad ....(5.30)$$

In fact, eqn 5.30 provides a valid and much improved bias bound for any system whose truncated weighting sequence elements are described by a single dominant exponential decay.

Equation 5.30 also provides a second alternative relationship between the exponential decay constant, ρ, and truncation bias which can be used to redefine the criterion in Results 5.5 and 5.6 as follows:

Result 5.10: Consider the class of systems whose weighting sequence elements, $\theta(i)$, are accurately described by a single exponential decay for all $i > q_0$. Let q_{best} denote the (as yet unknown) order of the model within this class which minimizes $AIC_q^{(2)}$, and let $B_{FR}^2(z;q_{best}-1)$ represent the upper bound on frequency response bias (defined by eqn 5.30) at $z = \exp(j\omega T)$ associated with the model of order $q_{best}-1$. For any given q, define the scale factor $\tilde{\rho}_{FR}(z;q)$ so that

$$\tilde{\rho}_{FR}^2(z;q)\ \theta^{*2}(q) \ /\ |z - \tilde{\rho}_{FR}(z;q)|^2 \ = \ B_{FR}^2(z;q_{best}-1)$$

Then, the quantity $T_{FR}(z;q)$ defined (for $q > q_b$) by:

$$T_{FR}(z;q) = \hat{AIC}_q + \sum_{i=q_b}^{q-1} \left\{ \frac{N}{\hat{\varepsilon}_i^t\ \hat{\varepsilon}_i} \tilde{\rho}_{FR}^2(z;i)\ \theta^{*2}(i)\ \tilde{d}_1^t(i)\ \tilde{d}_1(i) \right\} \quad ....(5.31)$$

will possess a unique minimum for all q in the range $q_0 \leq q \leq q_f$, and this minimum will occur at q_{best}.

Proof: For systems in the specified class, $B_{FR}^2(z;q)$ is proportional to B_q^2 (eqn 5.21). As a result, the relationships used to prove Result 5.5 are also valid for $T_{FR}(z;q)$. Thus, the proof here is identical to that of Result 5.5.

....QED

Again, similarities between Results 5.5 and 5.10 can be used to extend Result 5.6 to this new situation in the following manner:

Result 5.11: Let Q define the known set of weighting sequence model orders which contains q_{best} and let q_k denote the k^{th} element in Q. For a specified $z = \exp(j\omega T)$, define the quantity $\hat{T}_{FR}(z;q)$ to be:

$$\hat{T}_{FR}(z;q) = \hat{AIC}_q + \sum_{i=q_b}^{q-1} \left\{ \frac{N}{\hat{\varepsilon}_i^t\ \hat{\varepsilon}_i} |\tilde{\rho}_{FR}^2(z;i)\ \hat{\theta}^{*2}(i)\ \tilde{d}_1^t(i)\ \tilde{d}_1(i)| \right\} \quad ....(5.32)$$

where $\tilde{\rho}_{FR}(z;i)$ is a scale factor computed using the relationship

$$\tilde{\rho}_{FR}^2(z;i)\ \hat{\theta}^{*2}(i) \ /\ |z - \tilde{\rho}_{FR}(z;i)|^2 \ = \ \hat{B}_{FR}^2(z) \ ,$$

$\hat{\theta}^*(i)$ represents the value of $\theta^*(i)$ obtained from the estimated model of dimension i, and $\hat{B}^2_{FR}(z)$ is non-negative.

Then for each q_k, examine the set of values $\hat{T}_{FR}(z;q)$ (calculated using eqn 5.32) over the range $q_b < q \leq q_k$ and let $\hat{B}^2_{FR_{max}}(z;q_k)$ denote the maximum value of $\hat{B}^2_{FR}(z)$ for which $\hat{T}_{FR}(z;q)$ remains a minimum at q_k. The "best" model order can now be identified by selecting the largest value of q_k for which $\hat{B}^2_{FR_{max}}(z;q_k)$ is a valid upper bound for $B^2_{FR}(z;q_k-1)$.

Proof: With appropriate substitutions, the proof is identical to that of Result 5.6. ....QED

The proportional relationship between $\hat{B}^2_{FR}(z;q)$ and B^2_q also implies that the truncation established by Results 5.10 and 5.11 will be identical to the optimal truncation established using Results 5.5 and 5.6. However when Results 5.10 and 5.11 are implemented for a particular value of $z = \exp(j\omega T)$, the maximum bias bound, $\hat{B}^2_{FR_{max}}(z;q_{best})$, may be interpreted as a valid upper bound on the frequency response bias at the specified frequency, ωT. In general, this quantity will represent a tighter bias bound at ωT than the one established by Results 5.8 and 5.9. Furthermore, $\hat{B}^2_{FR_{max}}(z;q_{best})$ can be used as an upper bound on the frequency response bias at all higher frequencies as demonstrated by the following result:

Result 5.12: Consider the class of systems identified in Result 5.10. Let $B^2_{FR}(z_0;q)$ denote the frequency response bias introduced by truncation for a specified frequency, $\omega T = \omega_0 T$; namely let

$$|g_E[\exp(j\omega_0 T)]|^2 = \rho^2 g_q^2 / |z_0 - \rho|^2 = B^2_{FR}(z_0;q)$$

Then for any frequency $\omega T \geq \omega_0 T$,

$$|g_E[\exp(j\omega T)]|^2 \leq B^2_{FR}(z_0;q) \qquad ....(5.33)$$

Proof: For systems in the specified class, the error term introduced by truncation can be written as:

$$g_E(z) = \rho\, g_q\, z^{-q} / (z - \rho)$$

After substituting $z = \exp(j\omega T)$ into this expression, the following result can be obtained:

$$|g_E[\exp(j\omega T)]|^2 = \rho^2\, g_q^2 / (1 - 2\rho\cos(\omega T) + \rho^2) = B_{FR}^2(z;q)$$

For $\omega T \geq \omega_0 T$, $\cos(\omega T) \leq \cos(\omega_0 T)$ and so,

$$|g_E[\exp(j\omega T)]|^2 \leq \rho^2\, g_q^2 / (1 - 2\rho\cos(\omega_0 T) + \rho^2) = B_{FR}^2(z_0;q)$$

....QED

Based on the set of results established above, the conservatism in the single frequency response bias bound of Section 5.3.1 may now be reduced at individually specified frequencies and, in many cases, the resulting improvements can be significant. In addition, the frequency-dependent procedure suggested by Result 5.11 need not be repeated at all frequencies since the bound established at any given frequency establishes an upper bound on the bias at all higher frequencies as well. Finally, although this frequency-dependent extension is strictly valid only for systems with a single dominant real pole, the results will, in practice, generate accurate bias bounds for a much wider range of systems.

To verify this assertion, consider the system described by the transfer function

$$g(z) = K/a^2\, \{1 + (\rho \ln\rho)\,(z-1)/(z-\rho)^2 - (z-1)/(z-\rho)\}$$

where $\rho = \exp(-aT)$. [This transfer function is the zero-order-hold equivalent of $g(s) = K/(s+a)^2$.] Expanding $g(z)$ in powers of z^{-1} and isolating the terms from (q+1) to infinity yields;

$$g_E(z) = (K/a^2)\, z^{-1}[(1-\rho) \sum_{i=q}^{\infty} \rho^i z^{-i} + (\rho \ln\rho) \sum_{i=q}^{\infty} \{(i+1)\rho^i z^{-i} - i\rho^{i-1} z^{-i}\}]$$

Alternatively, the infinite summations can be eliminated to produce:

$$g_E(z) = \frac{\theta_{q+1}\, z^{-q}}{(z - \rho)} \left\{ 1 + \frac{1}{z - \rho} \frac{\rho^2}{\rho_b\,(q - \gamma)} \right\}$$

where $\theta_{q+1} = (K/a^2)\,[(1-\rho)\,\rho^q + (\rho \ln \rho)\,\{(q+1)\,\rho^q - q\,\rho^{q-1}\}]$

$$\gamma = (1 \,/\, 1-\rho) + (1 \,/\, \ln \rho)$$

and ρ_b is the bounding exponential decay constant for the specified truncation defined by:

$$\rho_b = \rho\,\{1 + [1 \,/\, (q-\gamma)]\}$$

Using ρ_b, the exponential bounding function for $g_E(z)$ is given by;

$$g_b(z) = \theta_{q+1}\, z^{-q} \,/\, (z - \rho_b)$$

and the ratio of g_b to g_E can be reduced to:

$$\frac{g_b}{g_E} = \frac{(z - \rho)^2}{(z - \rho_b)\,[z - \rho\,\{(q-\gamma)/(q-\gamma+1)\}]} \qquad \ldots.(5.34)$$

Eqn 5.34 can now be used to investigate the inaccuracies introduced by the assumption of a single exponential decay at any specified frequency.

In particular, when $|g_b/g_E|$ is less than unity, the bias bound defined by eqn 5.30 will not represent an upper bound on the true frequency response bias. Unfortunately, $|g_b/g_E|$ is a function of the number of parameters in the model (q) and the decay constant (ρ) as well as frequency. As a result, the inaccuracies introduced by the single decay assumption for each given system and set of input/output data will be different and, so, it is not possible to quantify these inaccuracies precisely. General characteristics can, however, be highlighted by examining $|g_b/g_E|$ for selected values of q and ρ. A closer examination of eqn 5.34 indicates that, for any given frequency and specified value of ρ, $|g_b/g_E|$ is minimized when the dimension of the truncated model is just large enough to ensure that $\rho_b < 1$. Furthermore, as q increases, the minimum value of $|g_b/g_E|$ at each frequency also increases. These relationships are clearly demonstrated by the results in Table 5.1. For each value of ρ in this table, the first row displays information for the model of lowest order whose last element can be

exponentially bounded, while the second row summarizes the same information for a larger, more realistic model order. These results clearly indicate that, in the most pessimistic situation where q is just large enough to establish an exponential bound, the single decay assumption leads to bias bound errors of less than 15% over the entire frequency range and even these errors occur only over limited ranges. More importantly however, the errors introduced by the single decay assumption are negligible for more representative model sizes. A similar analysis has also been performed for systems described by a single pair of complex conjugate poles. Although the details of the analysis are not presented here, the results indicate that the use of a single bounding exponential decay will still generate accurate frequency response bias bounds for frequencies sufficiently far from the resonant frequency.

The information presented above suggests that, although Results 5.10 and 5.11 were derived for the case of a single dominant real pole, they can be applied to a much wider class of systems to establish valid and much improved frequency-dependent bias bounds. A particularly important

ρ	q	$\lvert g_b/g_E \rvert_{min}$	$(\omega T)_{min}$ [deg]	frequencies (ωT) between which $\lvert g_b/g_E \rvert$ is less than unity		
.75	4	.917	40	(9,10.5)	(30,49)	(176,180)
	10	.987	41		(38,44)	(178,180)
.85	7	.946	30	(5,9)	(22,38)	(178,180)
	15	.988	31		(28,35)	(179,180)
.95	20	.846	1.5	(1,5)	(10,23)	(179,180)
	30	.986	2.5	(2,3)	(14,22)	(179.5,180)

Table 5.1: Worst-Case and Representative Bounds for $\lvert g_b/g_E \rvert$

characteristic of the resulting criterion is the simplicity with which these improved bias bounds can be generated. If, however, one is concerned with generating tighter bias bounds near a resonant frequency, it should be possible to identify (much more complex) bias relationships which can be employed in a criterion similar to that established by Results 5.10 and 5.11 to accomplish this task.

5.4 Monte Carlo Simulation Results

A Monte Carlo investigation of the truncation algorithm derived from Results 5.5 and 5.6 and presented in Appendix 5.2 (and its frequency-domain extensions) was conducted to examine the validity of the procedure. The following four systems were used in the investigation:

System 1: $$g(z) = \frac{.75}{(z - .85)}$$

System 2: $$g(z) = \frac{.06\ (z + .89)}{z^2 - 1.7z + .7225} = \frac{.06\ (z + .89)}{(z - .85)^2}$$

System 3: $$g(z) = \frac{.5\ (z - .7)}{z^2 - 1.65z + .68} = \frac{.5\ (z - .7)}{(z - .85)\ (z - .8)}$$

System 4: $$g(z) = \frac{.29\ (z^3 - .105z^2 - .658z - .003)}{z^4 - 2.0707z^3 + 1.3508z^2 + .2665z}$$

$$= \frac{.29\ (z + .0046)\ (z + .758)\ (z - .867)}{z\ (z - .368)\ (z - .825)\ (z - .877)}$$

For each system, tests were conducted using three separate input signal-to-noise ratios to produce a total of 12 test combinations. For each of the 12 test combinations, 50 independent data runs were produced using the following procedure for each run:

1. Generate uncorrelated zero-mean normlly-distributed input and measurement noise sequences with specified variances.
2. Generate system output data (1000 samples) using the difference equation implied by the given g(z) and the input and noise sequences identified in (1).

3. Use a parameter-recursive least-squares procedure to estimate the parameters of each weighting sequence model up to the model of order $q_{\hat{AIC}}$.
4. Implement the refinement procedure described in Appendix 5.1 to refine the set of candidate models.
5. Implement the 6-step truncation algorithm in Appendix 5.2 to establish the optimal truncation and corresponding bias bounds.

Upon completing each data run, the following information was recorded: the optimal truncation level (q_{best}) identified by the procedure, the percentage difference between the estimated residuals ($\hat{\varepsilon}_q^t \hat{\varepsilon}_q$) and the true residuals ($\varepsilon^t[I-P_q]\ \varepsilon$) for $q = q_{best}$, and the estimated values of "parameter" bias (eqn 5.21) and frequency response bias (at $\omega T = 0^o$ and $\omega T = 70^o$) together with the corresponding true biases for $q = q_{best}$. This information is presented in Tables 5.2 through 5.6 and summarized below.

Table 5.2 identifies the 50-run average value of q_{best} for each of the 12 test combinations. As mentioned previously, test conditions can be selected to accurately identify any number of weighting sequence elements. Indeed for fixed N, increasing the input signal-to-noise ratio should increase the number of elements that can be accurately estimated. The results in Table 5.2 clearly indicate that this does happen when using the proposed algorithm.

Table 5.3 displays the average difference between the estimated and true residuals for the specified truncation. This difference indicates the size of β_q for the given truncation and, as required to validate Assumption 5.1, these values must be significantly less than 1. As shown in the table, the average value of β_q was less than 0.075 for each test combination; a result which clearly demonstrates that the optimal truncation specified using the proposed algorithm was established at a point where Assumption 5.1 is valid.

Tables 5.4 through 5.6 present the bias information generated by the procedure. Table 5.4 presents the "parameter" bias information for each test combination, while Tables 5.5 and 5.6 present the frequency response bias information at $\omega T = 0^{o}$ and $\omega T = 70^{o}$ respectively. In each case, the information presented includes:

1. the average difference between the estimated bias bound and the true bias for $q = q_{best}$;
2. the standard deviation of the difference in (1) for the 50 runs collected;
3. the average relative difference between the estimated bias bound and the true bias measured with respect to the true bias; and
4. the average relative difference between the estimated bias bound and the true bias measured with respect to either the actual size of the true weighting sequence (for "parameter" bias) or the actual size of the true frequency response (for frequency response bias).

The results in these tables clearly demonstrate the accuracy of the bias bounds generated by the algorithm. The average difference between the estimated and true frequency response biases at $\omega T = 0^{o}$ never exceeded 1.5% of the true DC gain and, in most instances, was less than 0.5%. Furthermore at $\omega T = 70^{o}$, the estimated biases established tight upper bounds on the true bias even for systems with closely spaced real poles or double poles; thus demonstrating that valid and significant improvements can be achieved using the frequency-dependent criterion of Results 5.10 and 5.11. Indeed, from the set of Monte Carlo results presented here, it is clear that the proposed truncation criteria and corresponding algorithms can be used not only to identify the optimal truncation, but also to accurately describe the associated bias.

Table 5.2: Average Model Order of Optimal Truncation

System		$\sigma_u^2/\sigma_\varepsilon^2$ = 8	16	64
1	Average Order	17.7	20.2	24.0
	Std Deviation	1.9	2.2	1.8
2	Average Order	26.6	29.5	34.1
	Std Deviation	1.9	2.5	1.8
3	Average Order	20.5	22.6	27.5
	Std Deviation	2.1	1.9	1.7
4	Average Order	17.7	19.7	23.8
	Std Deviation	1.7	1.6	1.7

Table 5.3: Residual Information for Optimal Truncation

System	$\sigma_u^2/\sigma_\varepsilon^2$ =	8	16	64
1	Average Relative Error (wrt $\varepsilon^t[I-P]\,\varepsilon$)	.053	.049	.056
	Std Deviation	.035	.035	.035
2	Average Relative Error (wrt $\varepsilon^t[I-P]\,\varepsilon$)	.065	.061	.072
	Std Deviation	.033	.031	.042
3	Average Relative Error (wrt $\varepsilon^t[I-P]\,\varepsilon$)	.056	.058	.052
	Std Deviation	.035	.050	.026
4	Average Relative Error (wrt $\varepsilon^t[I-P]\,\varepsilon$)	.048	.051	.055
	Std Deviation	.027	.025	.038

Table 5.4: "Parameter" Bias for Optimal Truncation

System	$\sigma_u^2/\sigma_\varepsilon^2$ =	8	16	64
1	Avg Absolute Error ($\hat{B}_{max} - \surd \tilde{\theta}^t \tilde{\theta}$)	.021	.012	.004
	Std Deviation	.038	.024	.010
	Avg Relative Error (wrt $\surd \tilde{\theta}^t \tilde{\theta}$)	.247	.207	.155
	Avg Relative Error (wrt $\surd \theta^t \theta$)	.0147	.0087	.0028
2	Avg Absolute Error ($\hat{B}_{max} - \surd \tilde{\theta}^t \tilde{\theta}$)	- 003	.003	.002
	Std Deviation	.030	.027	.014
	Avg Relative Error (wrt $\surd \tilde{\theta}^t \tilde{\theta}$)	-.010	.066	.075
	Avg Relative Error (wrt $\surd \theta^t \theta$)	-.0027	.0029	.0024
3	Avg Absolute Error ($\hat{B}_{max} - \surd \tilde{\theta}^t \tilde{\theta}$)	.010	-.0002	.004
	Std Deviation	.035	.018	.012
	Avg Relative Error (wrt $\surd \tilde{\theta}^t \tilde{\theta}$)	.132	-.010	.155
	Avg Relative Error (wrt $\surd \theta^t \theta$)	.0084	-.0001	.0032
4	Avg Absolute Error ($\hat{B}_{max} - \surd \tilde{\theta}^t \tilde{\theta}$)	.017	.011	.004
	Std Deviation	.033	.020	.012
	Avg Relative Error (wrt $\surd \tilde{\theta}^t \tilde{\theta}$)	.203	.195	.156
	Avg Relative Error (wrt $\surd \theta^t \theta$)	.0123	.0080	.0028

Table 5.5: Frequency Response Bias for Optimal Truncation ($\omega T = 0^o$)

System	$\sigma_u^2/\sigma_\varepsilon^2$ =	8	16	64
1	Avg Absolute Error ($\hat{B}_{max} - \lvert g_E \rvert$)	.046	.023	-.003
	Std Deviation	.193	.116	.049
	Avg Relative Error (wrt $\lvert g_E \rvert$)	.139	.084	-.005
	Avg Relative Error (wrt $\lvert g \rvert$)	.0091	.0046	-.0041
2	Avg Absolute Error ($\hat{B}_{max} - \lvert g_E \rvert$)	-.070	-.024	-.010
	Std Deviation	.161	.152	.073
	Avg Relative Error (wrt $\lvert g_E \rvert$)	-.176	-.091	-.082
	Avg Relative Error (wrt $\lvert g \rvert$)	-.0140	-.0048	-.0020
3	Avg Absolute Error ($\hat{B}_{max} - \lvert g_E \rvert$)	-.003	-.040	.0003
	Std Deviation	.178	.085	.061
	Avg Relative Error (wrt $\lvert g_E \rvert$)	-.008	-.169	.024
	Avg Relative Error (wrt $\lvert g \rvert$)	-.0007	-.0081	.0001
4	Avg Absolute Error ($\hat{B}_{max} - \lvert g_E \rvert$)	.017	.009	-.005
	Std Deviation	.157	.090	.054
	Avg Relative Error (wrt $\lvert g_E \rvert$)	.050	.054	-.019
	Avg Relative Error (wrt $\lvert g \rvert$)	.0035	.0018	-.0010

Table 5.6: Frequency Response Bias for Optimal Truncation ($\omega T = 70^{o}$)

System	$\sigma_u^2/\sigma_\varepsilon^2$ =	8	16	64
1	Avg Absolute Error $(\hat{B}_{max} - \lvert g_E \rvert)$	.014	.009	.004
	Std Deviation	.011	.007	.003
	Avg Relative Error (wrt $\lvert g_E \rvert$)	.382	.359	.305
	Avg Relative Error (wrt $\lvert g \rvert$)	.0200	.0128	.0060
2	Avg Absolute Error $(\hat{B}_{max} - \lvert g_E \rvert)$	.008	.007	.004
	Std Deviation	.009	.006	.004
	Avg Relative Error (wrt $\lvert g_E \rvert$)	.214	.291	.250
	Avg Relative Error (wrt $\lvert g \rvert$)	.0988	.0881	.0449
3	Avg Absolute Error $(\hat{B}_{max} - \lvert g_E \rvert)$	.012	.005	.004
	Std Deviation	.012	.005	.004
	Avg Relative Error (wrt $\lvert g_E \rvert$)	.330	.195	.312
	Avg Relative Error (wrt $\lvert g \rvert$)	.0028	.0118	.0089
4	Avg Absolute Error $(\hat{B}_{max} - \lvert g_E \rvert)$	.013	.009	.004
	Std Deviation	.011	.007	.003
	Avg Relative Error (wrt $\lvert g_E \rvert$)	.316	.314	.307
	Avg Relative Error (wrt $\lvert g \rvert$)	.0303	.0204	.0095

Appendix 5.1 Refinements to the Set Containing q_{best}

As indicated in Section 5.2, the optimal truncation level (q_{best}) must necessarily lie in the range $q_b < q \leq q_{\hat{AIC}}$. It is, however, possible to refine this set of candidates for q_{best} still further using the values of $\hat{AIC}_q$ (calculated per eqn 5.3). In particular, Result 5.5 demonstrates that $T_{q_{best}}$ is the minimum value of T_q for all q in the range $q_0 \leq q \leq q_f$. But T_q is related to $\hat{AIC}_q$ by eqn 5.22 and, for $q < q_{best}$, the following relationship can be established:

$$T_q - T_{q_{best}} = \hat{AIC}_q - \hat{AIC}_{q_{best}} - \sum_{i=q}^{q-1} \left\{ \frac{N}{\hat{\varepsilon}_i^t \hat{\varepsilon}_i} [\tilde{\rho}_i^2 \theta^{*2}(i) \tilde{d}_1^t(i) \tilde{d}_1(i)] \right\} > 0$$

Since the summation in the above expression is always positive, $\hat{AIC}_q$ must necessarily be greater than $\hat{AIC}_{q_{best}}$ for all $q < q_{best}$. Hence, if (for any given q_1 in the range $q_b < q_1 \leq q_{\hat{AIC}}$) $\hat{AIC}_{q_1}$ is not a minimum over the range $q_b < q \leq q_1$, then q_1 cannot be equal to q_{best} and the truncation level defined by q_1 can be dropped from further consideration. This procedure can be used for each value of q in the range $q_b < q \leq q_{\hat{AIC}}$ to reduce the number of possible candidates for q_{best}.

Appendix 5.2: A Complete Procedure for Optimal Weighting Sequence Truncation

The optimal truncation criterion defined by Results 5.5 and 5.6 relies on the ability to generate an estimate for the upper bound on bias associated with the specified truncation level as well as the ability to validate this bias bound. A complete procedure to implement the criterion is described here. To begin, a least-squares estimation algorithm that is recursive in the number of parameters [EYK1, STR1] can be used to generate the weighting sequence parameter estimates for all model orders from q_b to $q_{\hat{AIC}}$. If desired, the procedure discussed in Appendix 5.1 can then be implemented to refine the set of model orders, Q, which contains q_{best}.

After the appropriate set has been identified, the following 6-step procedure can be used to identify the optimal truncation:

Step 1: Procedure Initialization

Procedure: Arrange the elements of Q in descending order, $q_1 > q_2 > \cdots > q_n$, and let $q_{st} = q_1$.

Step 2: Bias Initialization/Identification of Candidate Model

Procedure: Initialize the "parameter" bias estimate to

$$\hat{B}^2 = \hat{\theta}^{*2}_{q_{st}}(q_{st}) \qquad \ldots.(A5.1)$$

Using this value of $\hat{B}^2$, calculate $\hat{T}_q$ (eqn 5.24) for all $q \leq q_{st}$ and identify the model order, q_{new}, which minimizes $\hat{T}_q$ over this range. If $q_{new} = q_{st}$, proceed to Step 3. If $q_{new} < q_{st}$, set q_{st} equal to the next element in Q and return to the start of Step 2.

Comment: The true bias bound for the model of order $q_{st}-1$ satisfies the relationship

$$B^2_{(q_{st}-1)} \geq \sum_{i=q_{st}}^{\infty} \theta^{*2}(i)$$

Hence, when $\hat{\theta}^*_{q_{st}}(q_{st})$ is an accurate estimate of $\theta^*(q_{st})$, $\hat{B}^2$ (defined by eqn A5.1) will necessarily be less than or equal to $B^2_{(q_{st}-1)}$. Now if $q_{new} \neq q_{st}$, then $\hat{B}^2_{max}(q_{st}) < \hat{\theta}^{*2}(q_{st})$. So, $\hat{B}^2_{max}(q_{st})$ is not a valid upper bound for $B^2_{(q_{st}-1)}$ and, by Result 5.6, q_{st} cannot be q_{best}. The search for q_{best} must, therefore, proceed to the next element of Q.

Step 3: Bias Identification for Candidate Model

Procedure: With $\hat{B}^2$ in eqn A5.1 established as a lower bound for the bias, iteratively update the bias to identify the largest value, $\hat{B}^2_{max}(q_{st})$, for which $\hat{T}_{q_{st}}$ remains a minimum. At the same time, identify the

dimension of the new model (q_{new}) which minimizes $\hat{T}_q$ for $\hat{B}^2_{max}(q_{st}) + \varepsilon$ where ε is arbitrarily small.

Comment: This step identifies the best estimate of the bias bound associated with the model of order q_{st}. The identification of q_{new} provides additional information which can be used to validate this estimate as shown in Step 5.

Step 4: Bias Verification -- Part 1

Procedure: For the estimated model of order q_{st}, calculate

$$B^2_L = \hat{\theta}^{*2}_{q_{st}}(q_{st}) / (1 - \rho^2_L) \qquad \ldots.(A5.2)$$

where ρ_L is defined by the relationship:

$$\rho^2_L \hat{\theta}^{*2}_{q_{st}}(q_{st}-1) / (1 - \rho^2_L) = \hat{\theta}^{*2}_{q_{st}}(q_{st}) \qquad \ldots.(A5.3)$$

If $\hat{B}^2_{max}(q_{st})$ is greater than B^2_L, proceed to Step 5. If not, set q_{st} equal to the next element in Q and return to Step 2.

Comment: Step 4 is simply a replay of Step 2 using a different lower bound for $B^2_{(q_{st}-1)}$. In particular, $B^2_{(q_{st}-1)}$ is defined by:

$$B^2_{(q_{st}-1)} = \theta^{*2}(q_{st}) / (1 - \rho^2_{q_{st}-1}) = \rho^2_{q_{st}-1}\, \theta^{*2}(q_{st}-1) / (1 - \rho^2_{q_{st}-1})$$

As a result, the following condition must be true for any value of ρ in the range $0 \le \rho \le \rho_{q_{st}-1}$:

$$B^2_{(q_{st}-1)} \ge \rho^2\, \theta^{*2}(q_{st}-1) / (1 - \rho^2)$$

Now if $q_{st} = q_{best}$, then $\hat{\theta}^{*2}(q_{st})$ is less than or equal to $B^2_{(q_{st}-1)}$ and calculating ρ_L (per eqn A5.3) will produce a value for ρ in the range $0 \le \rho \le \rho_{q_{st}-1}$. In this case, B^2_L (defined by eqn A5.2) will necessarily be less than or equal to $B^2_{(q_{st}-1)}$. So if $\hat{B}^2_{max}(q_{st}) < B^2_L$, then $\hat{B}^2_{max}(q_{st})$ cannot be a valid upper bound for $B^2_{(q_{st}-1)}$. Thus by Result 5.6, q_{st} cannot be q_{best} and the search for q_{best} must proceed to the next element of Q.

Step 5: Bias Verification -- Part 2

Procedure: For the estimated model of order q_{st}, calculate

$$B_L^2 = \hat{\theta}^{*2}_{q_{st}}(q_{new}+1) + \cdots + \hat{\theta}^{*2}_{q_{st}}(q_{st}) \qquad \ldots.(A5.4)$$

If $\hat{B}^2_{max}(q_{st})$ is greater than B_L^2, proceed to Step 6. If not, set q_{st} equal to the next element in Q and return to Step 2.

Comment: For any $\bar{q}$ in the range $q_0 \leq \bar{q} < q_{best}$, $\hat{T}_{\bar{q}}$ will be less than $\hat{T}_q$ for all $q < \bar{q}$ when $\hat{B}^2 = B^2_{\bar{q}-1}$. (This result is established by Result 6.3 in Chapter 6.) Since $\hat{B}^2_{max}(q_{st}) + \varepsilon$ minimizes $\hat{T}_q$ at q_{new}, $\hat{B}^2_{max}(q_{st})$ must therefore be greater than or equal to $B^2_{q_{new}}$ for q_{st} to be q_{best}. But,

$$B^2_{q_{new}} \geq \sum_{i=q_{new}+1}^{\infty} \theta^{*2}(i) \geq \sum_{i=q_{new}+1}^{q_{st}} \theta^{*2}(i)$$

So if $\hat{B}^2_{max}(q_{st}) < B_L^2$, $\hat{B}^2_{max}(q_{st})$ is not a valid upper bound for $B^2_{q_{new}}$. $\hat{B}^2_{max}(q_{st})$ must, therefore, be an erroneous estimate of bias. Hence by Result 5.6, q_{st} cannot be q_{best} and the search for q_{best} must proceed to the next element of Q.

Step 6: Final Result

Based on all available information, $\hat{B}^2_{max}(q_{st})$ is a valid upper bound for $B^2_{q_{st}-1}$. Since all elements of Q greater than q_{st} have already been eliminated, Result 5.6 implies that q_{st} is the optimal truncation level, q_{best}.

CHAPTER SIX

COMPLETE DESCRIPTIONS OF FREQUENCY RESPONSE UNCERTAINTY FOR SISO AND MIMO SYSTEMS

Results from the previous three chapters clearly suggest that generating an optimal description of frequency response uncertainty is a multifaceted problem. Indeed, an appropriately accurate description must account for both the statistical uncertainty associated with the estimates obtained from the identification process and any bias introduced by this process. Just as importantly for control system analysis and design, the resulting uncertainty description must account for the interfrequency dependence of the estimates so that it is valid simultaneously over all frequencies and, hence, can be included in an analysis based on classical frequency response techniques. Furthermore, when parametric models are employed to derive the description, other concerns such as the selection of an appropriate model structure and the identification of the "best" model within the specified class must also be addressed to achieve the desired accuracy. Finally, a truly optimal system-specific description of frequency response uncertainty can only be produced if there exists a means of tailoring the description to the specific frequency response characteristics of the system under investigation.

All of the information needed to solve this multifaceted problem for SISO systems has now been developed. Furthermore, this information has been produced in a format that can be readily extended to multivariable systems. Hence, the originally-specified problem of characterizing multivariable frequency response uncertainty can also be solved in a straightforward manner. The goal of this chapter is to consolidate the concepts established in the previous chapters into a coherent procedure for the characterization of the frequency response uncertainty associated with both SISO and MIMO systems. The development begins by combining the statistical information established in Chapter 3 with the optimal truncation results proposed in

Chapter 5 to produce a complete description of frequency response uncertainty (which includes the effects of both estimate variability and bias) for SISO systems. Further refinements, based on the frequency response characteristics of the given system, are then identified to optimize the uncertainty description for analysis purposes, and an algorithm is presented to summarize the steps in the uncertainty characterization process. Next, procedures which extend the SISO frequency response uncertainty description to MIMO systems are established. The resulting multivariable description of uncertainty is then combined with the structured uncertainty techniques described in Chapter 2 to produce a frequency response description of the perturbed multivariable system that can be readily used in a generalized-Nyquist assessment of robust stability and performance. Finally, examples are presented to demonstrate the implementation of the proposed procedures for both SISO and MIMO systems.

6.1 An Optimal Frequency Response Uncertainty Description for SISO Systems

6.1.1 Combining Statistical Uncertainty and Bias

As implied by previous discussions, the combined effects of estimate variability and truncation bias on system uncertainty can be examined in detail by rewriting the z-domain transfer function as:

$$g(z) = \sum_{i=1}^{q} g_i z^{-i} + \sum_{i=q+1}^{\infty} g_i z^{-i} = g_T[z;q] + g_E[z;q] \quad ....(6.1)$$

Eqn 6.1 conveniently separates frequency response uncertainty into two distinct parts: the uncertainty associated with the variability of the parameter estimates used to describe $g_T[z;q]$ and the unknown bias $g_E[z;q]$. This characterization suggests that a complete description of frequency response uncertainty (one that is valid simultaneously over all frequencies) can only be attained if both of these elements are identified and quantified. Using the results of Chapters 3 and 5, the task of generating this complete description can now be accomplished.

The statistical bounds identified by Theorem 3.3 provide a quantitative and nonasymptotic description of the frequency response uncertainty associated with $g_T[z;q]$. In addition, the truncation criterion described by Results 5.8 and 5.9 provides a valid upper bound on the frequency response bias introduced by truncation over all frequencies. Together, these results can be used to generate a valid set of frequency response uncertainty regions as described by the following result:

Result 6.1: Let $\hat{g}_T[z;q_{best}]$ denote the z-domain representation for the estimated weighting sequence model of order q_{best}. For any specified frequency (ωT) and confidence level (α), let $R(\omega T;\alpha;q_{best})$ denote the confidence region for $g_T[\exp(j\omega T);q_{best}]$ which is centred at $\hat{g}_T[\exp(j\omega T);q_{best}]$ and whose boundary is described by eqn 3.19. Then the true system frequency response,

$$g[\exp(j\omega T)] = g_T[\exp(j\omega T);q_{best}] + g_E[\exp(j\omega T);q_{best}] \quad ....(6.2)$$

lies in the region $R_E(\omega T;\alpha;q_{best})$ defined by extending the boundary of $R(\omega T;\alpha;q_{best})$ in all directions by $\hat{B}_{FR_{max}}(q_{best})$ (defined by Result 5.9).

Proof: From Result 5.12 (with $z_0 = 1$), it is clear that $B_{FR}(q_{best})$ (eqn 5.26) defines an upper bound for $|g_E[\exp(j\omega T);q_{best}]|$ over all frequencies $0 \leq \omega T \leq \pi$. By Result 5.9, $\hat{B}_{FR_{max}}(q_{best})$ is a valid upper bound for $B_{FR}(q_{best})$ and, hence, for $|g_E[\exp(j\omega T);q_{best}]|$. As a result, eqn 6.2 implies that the true frequency response, $g[\exp(j\omega T)]$, must lie on or inside a circle of radius $\hat{B}_{FR_{max}}(q_{best})$ centred at $g_T[\exp(j\omega T);q_{best}]$. But for the specified level of confidence, Theorem 3.3 demonstrates that $g_T[\exp(j\omega T);q_{best}]$ lies in $R(\omega T;\alpha;q_{best})$. Hence, $g[\exp(j\omega T)]$ must necessarily lie in $R_E(\omega T;\alpha;q_{best})$.

....QED

As the truncation procedure derived from Results 5.8 and 5.9 cannot generate phase information on the bias, each region established by Result 6.1 provides the best available information on the location of the true system frequency response at the specified frequency. In addition, the regions $\{R_E(\omega T;\alpha;q_{best});\ 0 \leq \omega T \leq \pi\}$ are valid simultaneously since $\hat{B}_{FR_{max}}(q_{best})$ defines an upper bound on the bias at each and every frequency. Hence, these extended regions not only quantify the effects of both estimate-variability and bias, but they also continue to account for the interfrequency dependence of the estimates.

The use of a single frequency response bias bound, however, may produce an unnecessarily conservative estimate of bias over certain frequency ranges as described in Section 5.3.2. If this occurs, the uncertainty regions defined by Result 6.1 will also be conservative. In this case, Results 5.10 and 5.11 clearly demonstrate that refined frequency-dependent bias bounds may be introduced to reduce the conservatism in the bias estimates. The resulting frequency-dependent bias bounds can then be combined with the available statistical information to generate a much sharper overall description of frequency response uncertainty as demonstrated by the following result:

Result 6.2: Let $\hat{g}_T[z;q_{best}]$ denote the z-domain representation for the estimated weighting sequence model of order q_{best}. For any specified frequency (ωT) and confidence level (α), let $R(\omega T;\alpha;q_{best})$ denote the confidence region for $g_T[\exp(j\omega T);q_{best}]$ defined in Result 6.1 and let $\hat{B}_{FR_{max}}(z;q_{best})$ represent the frequency-dependent upper bound on frequency response bias (described in Result 5.11) associated with the given model at $z = \exp(j\omega T)$. Then, the true system frequency response at ωT (eqn 6.2) lies in the region $R_{E1}(\omega T;\alpha;q_{best})$ defined by extending the boundary of $R(\omega T;\alpha;q_{best})$ in all directions by $\hat{B}_{FR_{max}}(z;q_{best})$.

Proof: By Result 5.11, $\hat{B}_{FR_{max}}(z;q_{best})$ is a valid upper bound for the frequency response bias introduced by truncation at $z = \exp(j\omega T)$. Hence, the proof of this result is identical to that of Result 6.1 with $\hat{B}_{FR_{max}}(q_{best})$ replaced by $\hat{B}_{FR_{max}}(z;q_{best})$.

....QED

One important implication of Result 6.2 is, of course, that the uncertainty bounds of Result 6.1 can be immediately reduced over a wide range of frequencies. Indeed, using the bias bounds identified by Result 5.11, significant improvements can generally be obtained over the entire frequency range ($0 \leq \omega T \leq \pi$) for non-oscillatory systems; while, for oscillatory systems, the improvements will be limited to specific frequency ranges sufficiently far from the dominant resonant frequency. It is also interesting to note that Results 6.1 and 6.2 are not restricted only to the truncation level defined by q_{best}. If valid upper bounds on frequency response bias are available for any arbitrary truncation level q, Results 6.1 and 6.2 can both be immediately extended to define valid frequency response uncertainty regions for this q-parameter weighting sequence model as well. As shown in the following section, this observation can be used to generate a more refined multifrequency description of uncertainty by redefining the optimal truncation level in terms of the frequency response characteristics of the test system.

6.1.2 Estimate Uncertainty vs Bias: An Optimal Trade-off

Returning for a moment to the developments of Chapter 5, it can be seen that the optimal truncation level, q_{best}, identified by Results 5.5 and 5.6 was selected based on Definition 5.1. This definition, in turn, relies on the AIC criterion (eqn 5.1) to define the optimal model order. But AIC was developed to establish an optimal trade-off between bias and variability in the parameter space. Thus, although q_{best} defines the optimal parametric

model for the test system, it does not necessarily correspond to the model which is optimal for frequency response applications because the criterion used to identify q_{best} fails to consider the frequency response characteristics of the system. As a result, the overall frequency response uncertainty regions described by Results 6.1 and 6.2, though valid, may not be optimal for the given system.

To establish an optimal truncation for frequency response applications, the bias/variability trade-off must necessarily be examined in the frequency domain. This suggests that both the frequency response bias and the variability of the frequency response estimates associated with various truncation levels must be quantified. Variability can, in fact, be quantified for any given truncation using the results of Chapter 3. But so far, valid bias information has only been identified for a single truncation level (that defined by q_{best}). It is, however, possible to extend the bias identification developments of Chapter 5 to other truncation levels as demonstrated here:

Result 6.3: Let $\bar{q}$ denote a specified model order in the range $q_0 \leq q \leq q_{best}$, and let $B^2_{\bar{q}-1}$ represent the upper bound on "parameter" bias associated with the model of order $\bar{q}-1$ (eqn 5.21). In addition, redefine the scale factor $\tilde{\rho}_q$ (for any given q) such that

$$\tilde{\rho}_q^2 \, \theta^{*2}(q) \; / \; (1 - \tilde{\rho}_q^2) \;=\; B^2_{\bar{q}-1}$$

Then, the quantity T_q defined by:

$$T_{q_0} = \hat{AIC}_{q_0} \qquad \ldots.(6.3a)$$

$$T_q = \hat{AIC}_q + \sum_{i=q_0}^{q-1} \left\{ \frac{N}{\hat{\varepsilon}_i^t \hat{\varepsilon}_i} [\tilde{\rho}_i^2 \, \theta^{*2}(i) \, \tilde{d}_1^t(i) \, \tilde{d}_1(i)] \right\}; \quad q > q_0 \qquad \ldots.(6.3b)$$

will possess a unique minimum for all q in the range $q_0 \leq q \leq \bar{q}$, and this minimum will occur at $\bar{q}$.

Proof: For weighting sequence models, the parameter estimates obtained for any model in the range $q_0 \leq q \leq q_{best}$ are, by definition, accurate estimates for the true model parameters. Hence, any increase in model order within this range will improve the fit to the observed data and simultaneously improve the description of the system being identified. As a result, the "best" order for any restricted class of model orders $q_0 \leq q \leq \bar{q}$ (where $\bar{q}$ is less than q_{best}) must necessarily correspond to the largest model in the class, $\bar{q}$.

Since $q_0 \leq \bar{q} < q_{best}$, Assumption 5.1 and Result 5.3 are valid for all q in the range $q_0 \leq q \leq \bar{q}$, and $AIC_q^{(2)}$ (eqn 5.20) can be used to identify the "best" model within this restricted class. But, the best model is $\bar{q}$. So by Result 5.4, $AIC_q^{(2)}$ will be a minimum at $\bar{q}$ for all models in this class. Now, the proof of Result 5.5 can be used to demonstrate that $T_{\bar{q}}$ will be less than T_q for all $q < \bar{q}$.

....QED

It is important to note that Result 6.3 is essentially a restatement of Result 5.5 where knowledge of q_{best} has been used to define a more restricted class of weighting sequence models that still satisfy Assumption 5.1. As such, the set of results derived from Result 5.5 for the model class Θ_{WS} can now be extended to the restricted model class defined by $q_0 \leq q \leq \bar{q}$ for any given $\bar{q}$ in the range $q_0 \leq \bar{q} < q_{best}$. More specifically, Result 5.6 can be extended to establish the quantity $\hat{B}^2_{max}(\bar{q})$ as a valid upper bound for $B^2_{\bar{q}-1}$. Results 5.8 and 5.9 can be extended to establish $\hat{B}^2_{FR_{max}}(\bar{q})$ as a valid upper bound for the frequency response bias associated with the model of order $\bar{q}$ over all frequencies $0 \leq \omega T \leq \pi$. And the frequency-dependent modifications of Results 5.10 and 5.11 can be extended to establish $\hat{B}^2_{FR_{max}}(z;\bar{q})$ as a valid upper bound for the frequency response

bias associated with the model of order $\bar{q}$ at $z = \exp(j\omega T)$. Hence, the truncation algorithm proposed in Chapter 5 can also be used to identify valid bias bounds for more severe truncations than q_{best} simply by restricting the identification of minimum T_q to the smaller classes of models defined by $q_0 \leq q \leq \bar{q}$ (where $\bar{q}$ is less than q_{best}).

With this additional bias information now available, an optimal frequency-dependent truncation can be identified in the following manner:

Criterion 6.1: For any specified frequency $\omega_1 T$, the optimal truncation corresponds to the model order $q_{opt}(\omega_1 T)$ in the range $q_0 \leq q \leq q_{best}$ which minimizes

$$\Delta g_{max}(\omega_1 T) = \hat{B}_{FR_{max}}(z_1;q) + \sqrt{[Q_{\alpha,q}\ \lambda_{max}\{H_q^T(\omega_1 T)\ V_q\ H_q(\omega_1 T)\}]} \quad ....(6.4)$$

where $\hat{B}_{FR_{max}}(z_1;q)$ represents a valid upper bound on the frequency response bias at $\omega_1 T$ for the model of order q, V_q represents the parameter estimate covariance matrix for the model of order q (eqn 3.4b), and $H_q^T(\omega_1 T)$ and $Q_{\alpha,q}$ are defined in Sections 3.1.2 and 3.2.1 respectively.

Comment: For any given q, the maximum distance between $g[\exp(j\omega_1 T)]$ and $\hat{g}_T[\exp(j\omega_1 T);q]$ is bounded by:

$$|\Delta g[\exp(j\omega_1 T)]| = |g - \hat{g}_T| = |g_T - \hat{g}_T + g_E| \leq |g_T - \hat{g}_T| + |g_E|$$

But as shown in Chapter 3, $|g_T - \hat{g}_T| \leq \sqrt{[Q_{\alpha,q}\ \lambda_{max}\{H_q^T(\omega_1 T)\ V_q\ H_q(\omega_1 T)\}]}$. Furthermore, $|g_E| \leq \hat{B}_{FR_{max}}(z_1;q)$, and $\hat{B}_{FR_{max}}(z_1;q)$ is known for all q in the range $q_0 \leq q \leq q_{best}$. Hence, $\Delta g_{max}(\omega_1 T)$ (eqn 6.4) can be generated for each given model order and establishes a valid upper bound for $|\Delta g[\exp(j\omega_1 T)]|$. The optimal truncation, therefore, clearly corresponds to the model which minimizes $\Delta g_{max}(\omega_1 T)$ over all models q in the range $q_0 \leq q \leq q_{best}$.

Criterion 6.1 produces a truncation which minimizes the frequency response uncertainty bound at a specified frequency. Furthermore, once this new truncation is specified, the frequency response extensions of Result 6.3 (highlighted above) can be used to generate a complete set of frequency-dependent bias bounds, $\hat{B}_{FR_{max}}(z;q_{opt})$. Hence, a new set of (modified) uncertainty bounds can be developed using Result 6.2. It should, however, be noted that boundary reductions achieved using Criterion 6.1 will generally be restricted to specific frequency ranges. Indeed, the new truncation may actually produce larger uncertainty bounds at other frequencies. For this reason, it is important to select the frequency to be used in Criterion 6.1 based on the general frequency response characteristics of the test system. When this is done, reductions in boundary size can be obtained over the range of critical frequencies while restricting boundary increases to frequencies where an accurate knowledge of system frequency response is less important.

6.1.3 Optimal, System-Specific Frequency Response Uncertainty Bounds

As suggested above, the techniques of the previous chapters can be used in a variety of ways to modify and improve the ultimate description of frequency response uncertainty. In fact, these techniques establish a useful means of tailoring this description to the specific system under investigation. Although an optimal description of frequency response uncertainty for any given system obviously depends on the unique characteristics of that system and the particular applications being considered, the steps required to produce this description may be summarized as shown in the following procedure.

Procedure 6.1:

1. For any given set of test data, use the truncation criterion of Results 5.5 and 5.6 to identify the model order q_{best}.

2. For this specified truncation, implement the algorithm implied by Results 5.8 and 5.9 to identify $\hat{B}_{FR_{max}}(q_{best})$. Incorporate this bias bound into the statistical description of uncertainty associated with the given model as shown in Result 6.1. Identify the critical frequencies of the system using this initial uncertainty description.
3. Implement the algorithm implied by Results 5.10 and 5.11 to establish improved bias bounds at preselected individual frequencies. Combine these frequency-dependent bias bounds with the confidence regions for the given model as shown in Result 6.2 to obtain a complete description of frequency response uncertainty for the system.
4. If refinements are required over the range of critical frequencies, use Criterion 6.1 to select the truncation level, q_{opt}, which minimizes the maximum uncertainty bound at the desired frequency. For q_{opt}, identify frequency-dependent bias bounds for all frequencies, $0 \leq \omega T \leq \pi$, using the frequency-domain extensions of Result 6.3. Combine these new bias bounds with the confidence regions for the new model as shown in Result 6.2 to obtain an optimal system-specific description of frequency response uncertainty.

Procedure 6.1 provides the general framework for establishing a description of frequency response uncertainty that is tailored to the system under investigation. This description, in turn, provides the information required to assess the effects of uncertainty on closed-loop stability and performance. An example which highlights the development of this uncertainty description is provided in Section 6.3.1.

6.2 Extending the Uncertainty Description to MIMO Systems

6.2.1 Joint Uncertainty Bounds for the Elements of G(z)

Since each element of an [m x m] system transfer function matrix G(z) can be modelled as a scalar weighting sequence, SISO results from the

previous section can be adapted directly to the multivariable problem. To accomplish this task however, uncertainty information on the individual elements of G(z) must be combined appropriately. Clearly, a specified level of confidence on the complete set of parameters associated with a given multivariable transfer function matrix implies that the parameters of all elements of the matrix must lie within their individual confidence regions simultaneously. For the case where inputs are applied separately and outputs are measured independently, the element-by-element parameter estimates are independent and the probability associated with the complete set of confidence regions is simply the product of the individual probabilities. Thus, an α x 100% confidence bound for the parameters of the multivariable system can be established, for example, by generating α^{1/m^2} x 100% confidence bounds on each of the individual elements. When this is done, the multivariable uncertainty problem can be completely analyzed in terms of the uncertainties associated with the scalar elements of G(z).

It should be noted that the independence of the parameter estimates introduces additional flexibility in defining the desired uncertainty information. For instance, different confidence levels can be selected for the various elements of G(z) (and hence, the size of the confidence bounds associated with these elements can be adjusted) provided the product of the probabilities remains fixed. This relationship can, in fact, be used to improve the analysis of perturbed system behaviour even further as will be described in Section 6.2.3. In addition, the existence of independent parameter estimates implies that the truncation criteria developed in Chapter 5 can be directly applied to derive the bias bound estimates required to finalize the desired description of uncertainty for each element of G(z). Thus, a complete element-by-element uncertainty characterization can be produced and, as shown in the following section, this characterization can be transformed into an appropriate frequency response description of the perturbed multivariable system.

6.2.2 E-Contour Bounds for the Characteristic Loci

Having defined an appropriate statistical limit on the parameters of any given element of G(z), a frequency response confidence bound (eqn 3.19) can be established at any specified frequency ωT. Once this statistical bound is combined with the corresponding bias bound, the maximum distance from the nominal (estimated) frequency response to the boundary of the uncertainty region can be calculated using eqn 6.4. Hence, the difference between the true frequency response of element i,j (g^c_{ij}) and its nominal value ($\hat{g}_{ij}$) is bounded by:

$$|g^o_{ij}[\exp(j\omega T)] - \hat{g}_{ij}[\exp(j\omega T);q]| \leq \Delta g_{ij_{max}}(\omega T) \qquad ....(6.5)$$

where $\Delta g_{ij_{max}}(\omega T)$ is defined by eqn 6.4. Using the additive perturbation characterization discussed in Section 2.2, $\Delta g_{ij_{max}}(\omega T)$ becomes an element of the structured perturbation matrix P at the selected frequency. The procedure above can be repeated for each frequency and each element of G(z) to produce a complete description of multivariable uncertainty in terms of the set of structured perturbation matrices, $\{P[\exp(j\omega T)];\ 0 \leq \omega T \leq \pi\}$. Because the frequency response confidence bounds are elliptical, the maximum distance bounds used to generate P at any given frequency may produce a conservative assessment of uncertainty. This conservatism can, however, be eliminated by generating circular bounds at desired frequencies. Two particularly useful techniques to achieve this goal (input selection and parameter weighting) have already been presented and discussed in Chapter 3.

Given the structured uncertainty characterization defined above, structured E-contour bounds on the characteristic loci of the perturbed system can be constructed as proposed by Kouvaritakis and Latchman [KOU4], [KOU6]. It is important to note that this E-contour procedure produces necessary and sufficient bounds for the characteristic loci of the perturbed multivariable system (i.e. the established bounds are attainable maximum bounds for the characteristic loci based on the specified perturbation

matrix). This does not, however, imply that the characteristic loci of systems with perturbations outside the specified class lie outside these bounds. As a result, the α x 100% confidence established at the parameter space level forms a lower bound on the confidence associated with these characteristic loci bounds. However within the framework of the given problem, these bounds provide the best possible description of system uncertainty and, because they do contain the perturbed characteristic loci, these bounds can be used in a generalized-Nyquist analysis to assess robust stability and performance.

6.2.3 Final Adjustments to Improve the Uncertainty Description

In any stability assessment or gain/phase margin determination, the frequencies of primary interest are those where the characteristic locus bounds are closest to the critical point in the complex plane ([-1,0] for unity feedback systems). Hence, techniques which tailor the description of system uncertainty to produce tighter characteristic locus bounds at the critical frequencies will ultimately produce a more effective analysis of system behaviour. As mentioned previously, test input selection and parameter weighting (both described in Section 3.4) as well as the identification of frequency-dependent bias bounds (described in Section 5.3.2) can be used for this purpose. An additional technique is suggested by the availability of independent parameter estimates for each of the elements of G(z).

The E-contour procedure for element-by-element bounded perturbations relies on an 'optimal cross-condition number' argument to develop appropriate characteristic locus bounds. As the optimal cross-condition number is obtained using scaling matrices (L and R in eqn 2.23), it may be possible to adjust P at any given frequency (by altering the individual confidence bounds) such that the resulting cross-condition number is reduced. In this case, the corresponding E-contours would also be reduced. Because of nonlinearities in the relationships between the cross-condition

number and the elements of P as well as between specified confidence levels and their corresponding confidence limits, it is not possible to produce an analytic solution for the appropriate adjustments in P. However, characteristic locus boundary improvements may be obtained by adjusting the individual frequency response bounds according to the following procedure:

Procedure 6.2:

1. Generate E-contour bounds assuming equal confidence levels on all elements of G(z).
2. At the desired frequency, alter each element of P individually and generate new E-contours to quantify the sensitivity of the E-contours to changes in the individual elements of P.
3. Using this sensitivity assessment, decrease the confidence limits on the elements of G(z) which display high sensitivity and increase the limits on those which display low sensitivity (using the desired multivariable confidence level as the guide to allowable changes) to achieve reductions in the E-contours.

Reductions in the E-contour bounds obtained from this procedure will necessarily depend on the nature of the elements of $G\{\exp(j\omega T)\}$. In many cases, it may not be possible to obtain significant improvements due to limitations on the allowable reductions in individual confidence bounds imposed by the specified overall confidence level. For these situations, the equal confidence bounds described in Section 6.2.1 should be used.

6.3 Simulation Examples and Discussion

6.3.1 Results for SISO Systems

To demonstrate the development of frequency response uncertainty bounds using the techniques summarized in Procedure 6.1, simulation data was generated based on the following discrete-time system transfer function:

$$g(z) = \frac{.29(z^3 - .105z^2 - .658z - .003)}{z^4 - 2.0707z^3 + 1.3508z^2 - .2665z} = \frac{.29\ (z+.0046)(z+.758)(z-.867)}{z\ (z-.368)\ (z-.827)(z-.875)}$$

Pseudo-random zero-mean normally-distributed input (u) and measurement noise (ε) sequences with an input-signal-to-noise ratio ($\sigma_u^2/\sigma_\varepsilon^2$) of 16 were used to drive the difference equation model defined by g(z), and 1000 input/output data samples were collected. This simulation data was then input to a parameter-recursive least-squares algorithm to estimate the weighting sequence parameters for models of order 5 to 49, and the resulting estimate information was used to generate frequency response uncertainty information as described below.

First, the refinement procedure described in Appendix 5.1 was implemented to identify the following set of candidates for q_{best}:

$$Q = \{37, 36, 28, 27, 26, \cdots, 5\}$$

Next, the truncation algorithm described in Appendix 5.2 was used to establish the point of optimal truncation (defined by Results 5.5 and 5.6) as $q_{best} = 24$. In contrast, the model order identified using minimum $\hat{AIC}$ was $q_{\hat{AIC}} = 37$, while the model order identified using the AIC_α criterion proposed by Bhansali and Downham [BHA1] was $q_{AIC_\alpha} = 26$. For $q_{best} = 24$, the estimated upper bounds for "parameter" bias, $\hat{B}_{max}(q_{best})$, and frequency response bias, $\hat{B}_{FR_{max}}(q_{best})$, obtained as byproducts of the truncation process were found to be 0.053 and 0.185 respectively (compared to the true "parameter" bias of 0.028 and the true DC frequency response bias of 0.100). The estimated noise variance obtained from the residuals of the least-squares fit for $q_{best} = 24$ was then used to identify the parameter estimate covariance matrix, V_{24}, and V_{24} was used to generate the frequency response confidence bounds described in Chapter 3 for a confidence level of 95%. These confidence bounds were combined with the frequency response bias estimate above (as suggested by Result 6.1) to produce the uncertainty bounds displayed in Figure 6.1.

In addition to the uncertainty information generated above, bias bounds

at several preselected individual frequencies were calculated for $q_{best} = 24$ using the criterion described by Results 5.10 and 5.11. The resulting bias bounds, $\hat{B}_{FR_{max}}(z;24)$, and maximum uncertainty bounds, Δg_{max}, for this frequency-dependent refinement are displayed in Table 6.1, and the improvements over the bounds based on a single frequency response bias bound, $\hat{B}_{FR_{max}}(24)$, are noted. The frequency-dependent bias bounds established by this procedure were also used to alter the frequency response uncertainty regions for this system, and these regions are shown in Figure 6.2.

A closer examination of these uncertainty regions indicated that the bounds closest to the [-1,0] point correspond to frequencies in the range $\omega T = 50^o$ to $\omega T = 90^o$. Criterion 6.1 was, therefore, used to identify the truncation level which minimized the maximum uncertainty bound at $\omega T = 60^o$. The data used to establish this new truncation level is presented in Table 6.2. This data clearly demonstrates that, although the frequency response bias increases for more severe truncations, the combined effects of bias and variability decrease for a limited number of more severe truncations. Indeed for this example, Δg_{max} is minimized at $q_{opt} = 18$. Using this new truncation, frequency response bias bounds were identified (using the frequency response extensions of Result 6.3) for all frequencies shown in Table 6.1, and these new bias bounds were used to produce the modified uncertainty regions displayed in Figure 6.3. A further comparison of the frequency-dependent bias and maximum uncertainty bounds for models of order $q_{best} = 24$ and $q_{opt} = 18$ is provided in Table 6.3.

The frequency response uncertainty bounds displayed in Figures 6.1, 6.2, and 6.3 are all valid bounds for the true frequency response of the specified system. A comparison of these three descriptions, however, clearly highlights the improvements in the description of frequency response uncertainty that can be obtained using the refinements proposed in Section 6.1. For this system, the introduction of frequency-dependent bias bounds and the implementation of a frequency-dependent truncation criterion

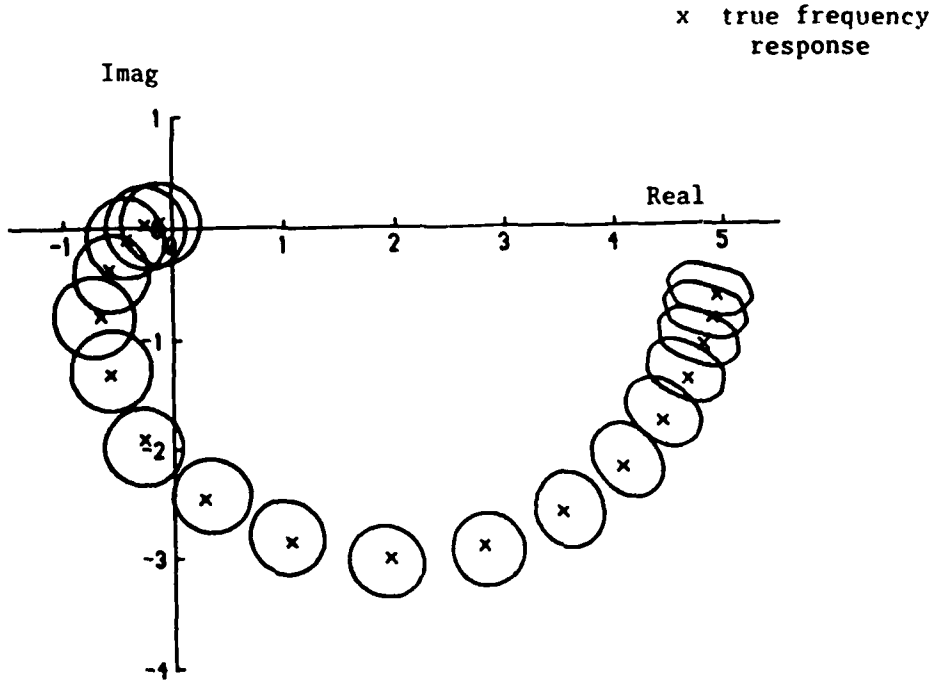

Figure 6.1: Frequency Response Uncertainty Bounds
(Model Order q_{best} = 24; Single Bias Bound)

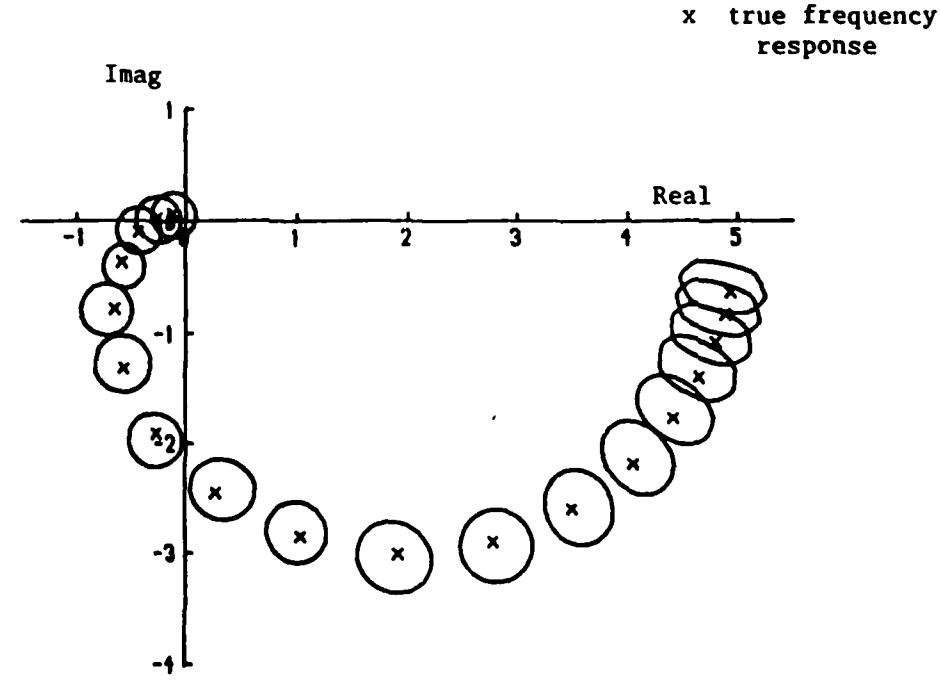

Figure 6.2: Frequency Response Uncertainty Bounds
(Model Order q_{best} = 24; Frequency-Dependent Bias Bounds)

ωT (deg)	$\hat{B}_{FR_{max}}(24)$	$\hat{B}_{FR_{max}}(z;24)$	percent reduction	Δg_{max} (single)	Δg_{max} (multiple)	percent reduction
10	.1849	.1245	32.7	.3449	.2845	17.5
20	.1849	.0750	59.4	.3579	.2480	30.7
30	.1849	.0538	70.9	.3683	.2372	33.7
40	.1849	.0428	76.9	.3672	.2251	38.7
50	.1849	.0356	80.7	.3476	.1982	43.0
60	.1849	.0305	83.5	.3532	.1988	43.7
70	.1849	.0268	85.5	.3610	.2029	43.8
80	.1849	.0241	87.0	.3602	.1994	44.6
90	.1849	.0219	88.2	.3681	.2050	44.3

Table 6.1: Frequency-Dependent Bounds for Model Order $q_{best} = 24$

q_{max}	$\hat{B}_{FR_{max}}(z;q)$	$\sqrt{[Q_{\alpha,q}\ \lambda_{max}(H^T V H)]}$	Δg_{max}
24	.0305	.1683	.1988
23	.0305	.1631	.1936
22	.0372	.1577	.1949
21	.0409	.1485	.1894
20	.0409	.1436	.1845
19	.0467	.1383	.1850
18	.0547	.1291	.1838
17	.0692	.1242	.1934
16	.0873	.1189	.2062
15	.1008	.1091	.2099

Table 6.2: Maximum Uncertainty Bounds at $\omega T = 60^o$

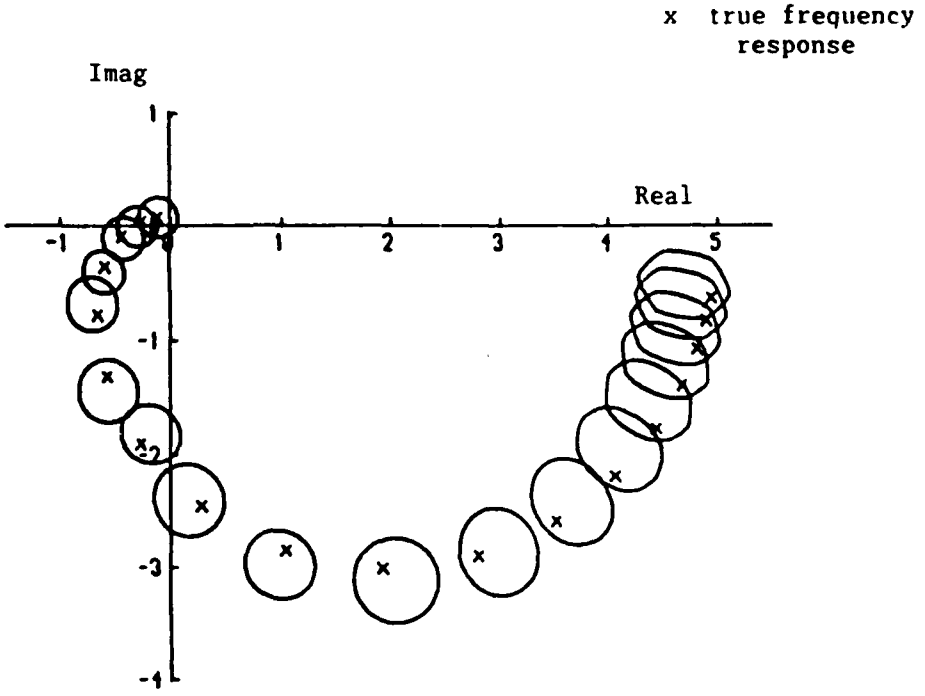

Figure 6.3: Frequency Response Uncertainty Bounds
(Model Order q_{opt} = 18; Frequency-Dependent Bias Bounds)

ωT (deg)	$\hat{B}_{FR_{max}}(z;24)$	$\hat{B}_{FR_{max}}(z;18)$	percent change	Δg_{max} (q=24)	Δg_{max} (q=18)	percent change
0	.1849	.2675	+44.7	.3924	.4269	+ 8.8
10	.1245	.1977	+58.8	.2845	.3154	+10.9
20	.0750	.1340	+78.7	.2480	.2659	+ 7.2
30	.0538	.0988	+83.6	.2372	.2391	+ 0.8
40	.0428	.0776	+81.3	.2251	.2134	- 5.2
50	.0356	.0640	+79.8	.1982	.1890	- 4.6
60	.0305	.0547	+79.3	.1988	.1838	- 7.5
70	.0268	.0480	+79.1	.2029	.1805	-11.0
80	.0241	.0430	+78.4	.1994	.1777	-10.9
90	.0219	.0392	+79.0	.2052	.1774	-13.5

Table 6.3: Uncertainty Bound Comparison (q_{best} = 24 vs q_{opt} = 18)

combined to reduce the maximum uncertainty bounds by nearly 50% over the range of critical frequencies identified above. These results translate, for example, into an improvement in gain margin (GM) from GM = 1.27 (for q_{best} = 24 and a single bias bound) to GM = 1.65 (for q_{best} = 24 and frequency-dependent bias bounds) and, ultimately, to GM = 1.73 (for q_{opt} = 18 and frequency-dependent bias bounds). Furthermore, the improvements obtained for q_{opt} = 18 are generated at the expense of only moderate increases in the uncertainty bounds at (less important) low frequencies.

In general, it is not possible to compare the results above with those obtained using other model selection criteria (such as $\hat{AIC}$ and the Bhansali/Downham criterion) because these other parameter-space criteria fail to address the problem of truncation bias. It is however interesting to note the differences between the maximum uncertainty bounds (bias plus confidence bound) derived for q_{opt} = 18 using the procedures in this chapter and the confidence bounds (which do not include bias) established for q_{AIC_α} = 26 and $q_{\hat{AIC}}$ = 37. These differences are presented in Table 6.4, and they clearly demonstrate the improvements that can be obtained using the algorithms proposed here. Indeed, even though the comparison is not equitable because the bounds for q_{opt} = 18 include bias while the bounds for q_{AIC_α} = 26 and $q_{\hat{AIC}}$ = 37 do not, the use of q_{opt} = 18 leads to refinements in the overall description of frequency response uncertainty over nearly all frequencies when compared to $q_{\hat{AIC}}$ = 37 and over most of the critical frequencies when compare to q_{AIC_α} = 26. Thus, the uncertainty bounds developed using the procedures in this chapter not only include the effects of bias, but they also produce a more refined description of frequency response uncertainty than that available when other truncation criteria are used.

The set of results presented in this section clearly demonstrates the accuracy of the frequency response uncertainty description that can be obtained using the procedures described in Section 6.1. They also highlight the ability to tailor the uncertainty description to the frequency response

ωT (deg)	Maximum Uncertainty Bound (q = 18)	Maximum Confidence Bound (q = 26)	percent difference	Maximum Confidence Bound (q = 37)	percent difference
10	.3154	.1702	+46.0	.2179	+30.9
20	.2659	.1805	+32.1	.2609	+ 1.9
30	.2391	.2020	+15.5	.2683	-12.2
40	.2134	.1943	+ 9.0	.2629	-23.2
50	.1890	.1720	+ 9.0	.2427	-28.4
60	.1838	.1813	+ 1.4	.2666	-45.0
70	.1805	.1855	- 2.8	.2618	-45.0
80	.1777	.1882	- 5.9	.2579	-45.1
90	.1774	.1970	-11.0	.2705	-52.5

Table 6.4: Uncertainty Bound Comparisons for q = 18, q = 26, and q = 37

characteristics of the particular system under investigation. The implications of this optimal description of frequency response uncertainty for the analysis of closed-loop behaviour are apparent.

6.3.2 Results for MIMO Systems

This section presents the complete development of multivariable frequency response uncertainty bounds for a two-input/two-output system using the results of Section 6.2. The following system (taken from Ibrahim and Munro [IBR1]) was used in the example:

$$G(s) = \begin{bmatrix} \frac{14.97\ (s+1.7)}{(s+10)\ a(s)} & \frac{95150\ (s+1.898)}{(s+100)\ a(s)} \\ \frac{85.2\ (s+1.44)}{(s+10)\ a(s)} & \frac{124000\ (s+2.037)}{(s+100)\ a(s)} \end{bmatrix}$$

where $a(s) = s^2 + 3.225s + 2.525$. Initial investigations indicated a requirement for compensation to stabilize the closed-loop system. In general, the implementation of a forward-loop multivariable compensator will

combine the elements of the original open-loop transfer function matrix and mix the uncertainties associated with each element of the system. As a result, any new assessment of system stability or performance based on the original uncertainty characterization will be conservative. To eliminate this conservatism, significant alterations to the open-loop system should be introduced prior to implementing the identification and uncertainty characterization procedures discussed previously. Fine-tuning adjustments can then be made based on the results of the robustness analysis. For this problem, the following constant precompensator was added prior to conducting the identification tests:

$$K = \begin{bmatrix} -3.1985 & 1.8484 \\ 0.011 & -0.00045 \end{bmatrix}$$

For simulation purposes, the transfer function matrix obtained by combining G and K was transformed to the corresponding discrete-time representation (of plant plus zero-order-hold) using a sample interval of 0.1 seconds. Test data was generated separately for each input (based on the resulting discrete-time model) using independent zero-mean input and noise sequences with variances of 1.0 and 0.04 respectively. One thousand input/output samples were collected for each test. The uncertainty characterization procedure summarized in Procedure 6.1 was then implemented to identify proper truncations and to generate appropriate frequency response uncertainty bounds for each element of G(z). The step-by-step results of this procedure are summarized here:

1. Using the truncation criterion of Results 5.5 and 5.6, model orders (q_{best}) of 29, 17, 14, and 23 were identified for elements g_{11}, g_{12}, g_{21} and g_{22} respectively.
2. The corresponding single frequency response bias bound, $\hat{B}_{FR_{max}}(q_{best})$, associated with each of these truncations was obtained using Results 5.8 and 5.9. Bounds of 0.067, 0.373, 0.186, and 0.318 were identified for elements g_{11}, g_{12}, g_{21} and g_{22} respectively.

3. Using the maximum uncertainty bounds (bias plus confidence) implied by the truncation and bias from steps (1) and (2), the frequency-dependent structured perturbation matrix was constructed and E-contours were generated as described in Section 6.2. An examination of the resulting characteristic locus bounds indicated a range of critical frequencies from $\omega T = 40^{o}$ to $\omega T = 70^{o}$ for which the bounds were closest to [-1,0].
4. Next, frequency-dependent bias bounds were generated for the truncations specified in (1) (i.e. for $q = q_{best}$) as well as for several more severe truncations ($q < q_{best}$). Using Criterion 6.1, a new truncation level was selected for each element to minimize the total uncertainty bound associated with that element at a preselected frequency in the range $[40^{o}, 70^{o}]$ and, hence, to improve the element-by-element uncertainty description associated with the multivariable system. Optimal truncation levels of 23, 15, 14, and 21 were identified for elements g_{11}, g_{12}, g_{21} and g_{22} respectively, and the parameter estimates for these four weighting sequence models are superimposed on the true system parameters in Figure 6.4.

For the optimal truncations identified in (4) above, frequency response confidence bounds were developed using Theorem 3.3. A 90% confidence level was selected for the multivariable problem and, as the test and identification procedures generated independent parameter estimates for each element of G(z), this specification imposed a requirement for 97.4% ($.9^{1/4} = .974$) confidence bounds on each element. Using $\alpha = .974$, the Wilson-Hilferty approximation was used to define the following frequency response boundaries for each element:

$$\Delta g^{t} \, (H^{T} V H) \, \Delta g = 59.15$$

In addition, parameter weighting was applied as described in Section 3.4.2 at $\omega T = 65^{o}$ to generate further refinements in the element-by-element bounds over the range of critical frequencies of the system.

The resulting parameter-weighted confidence bounds were combined (as

shown in Result 6.2) with the frequency-dependent bias bounds associated with the optimal truncation to produce a complete description of frequency response uncertainty for each individual element. These uncertainty regions are displayed in Figure 6.5, and maximum element-by-element bounds at several representative frequencies are presented in Table 6.5. The maximum bounds in Table 6.5 as well as corresponding ones at other frequencies were then used to create the frequency-dependent structured perturbation matrix and to generate structured E-contours for the perturbed system. The resulting characteristic locus bounds are displayed in Figure 6.6. As discussed in Section 6.2.2, these bounds identify the location of the perturbed system characteristic loci based on the given frequency response uncertainty description. Since a 90% confidence level was used to develop this uncertainty description, the confidence associated with these bounds is at least 90%.

The E-contour results generated for this particular test system suggest that the frequency response uncertainty associated with the given nominal system will have a significant impact on the performance of the closed-loop system. Indeed, prior to the implementation of parameter weighting to refine the element-by-element description of uncertainty, the structured E-contour bounds for the system included the [-1,0] point, suggesting the possibility of robust stability problems. And even though the refined E-contours derived from the parameter-weighted results exclude the [-1,0] point (demonstrating that stability problems are unlikely), the close proximity of these bounds to the critical point clearly highlights the need for additional compensation to increase the stability margins of the perturbed system and, hence, to improve the robust performance characteristics of the corresponding closed-loop system. From these results, it is clear that accurate uncertainty information is a vital element in any analysis of multivariable systems. The procedures described in this chapter provide the necessary tools to include this information in the analysis.

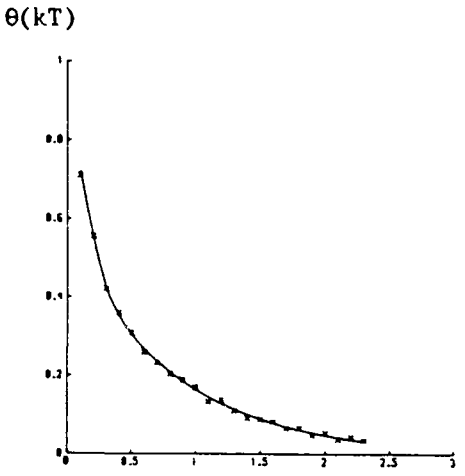

Figure 6.4a: Element g_{11}

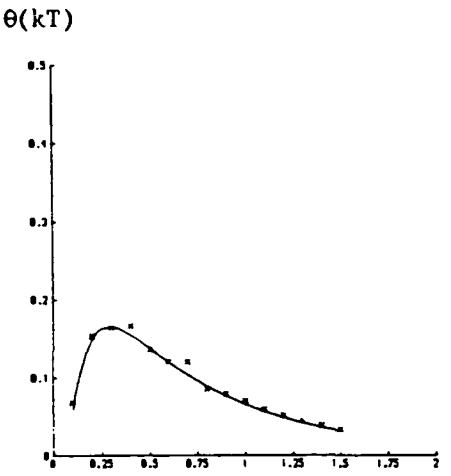

Figure 6.4b: Element g_{12}

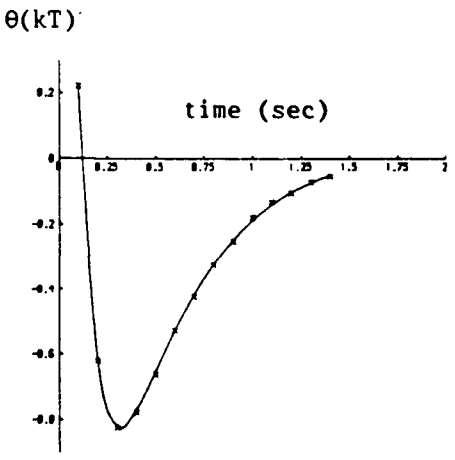

Figure 6.4c: Element g_{21}

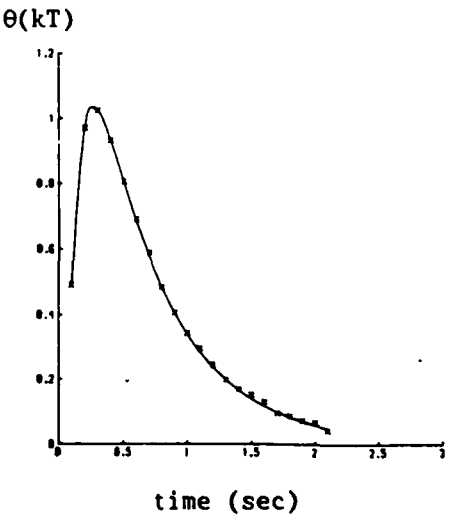

Figure 6.4d: Element g_{22}

Figure 6.4: Weighting Sequence Parameter Estimates

x true frequency response

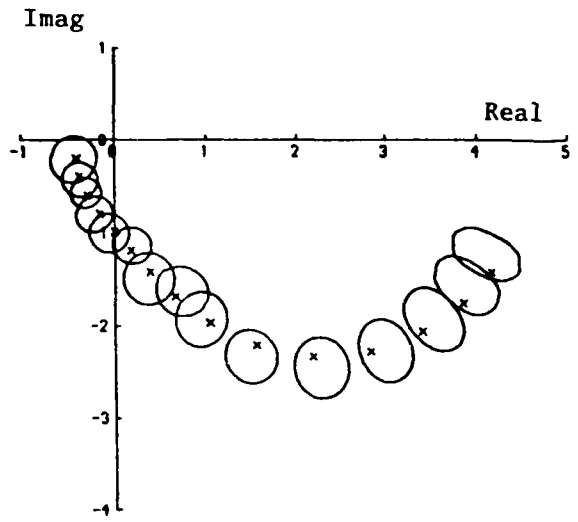

Figure 6.5a: Element g_{11}

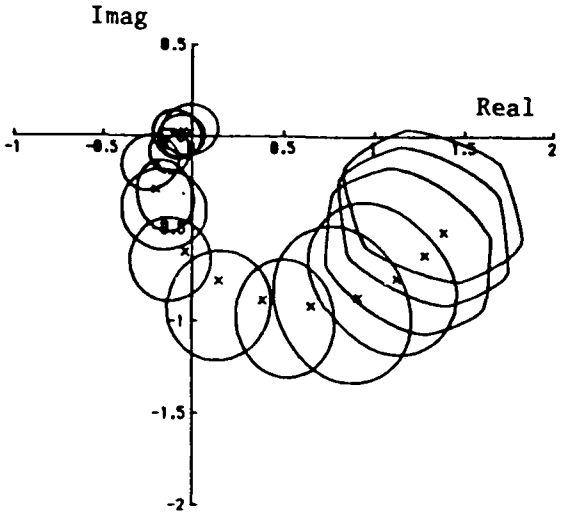

Figure 6.5b: Element g_{12}

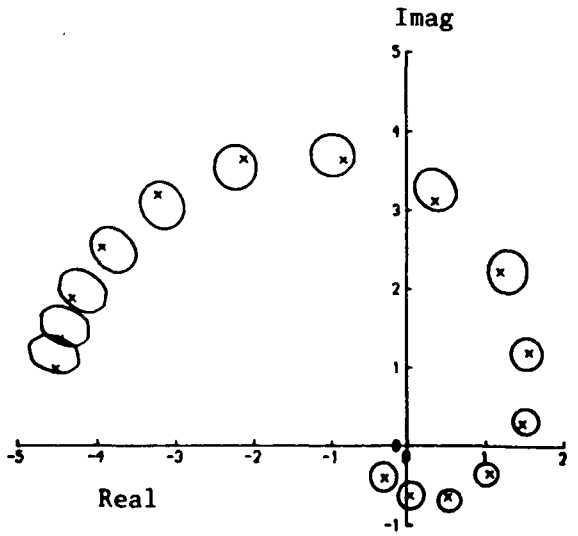

Figure 6.5c: Element g_{21}

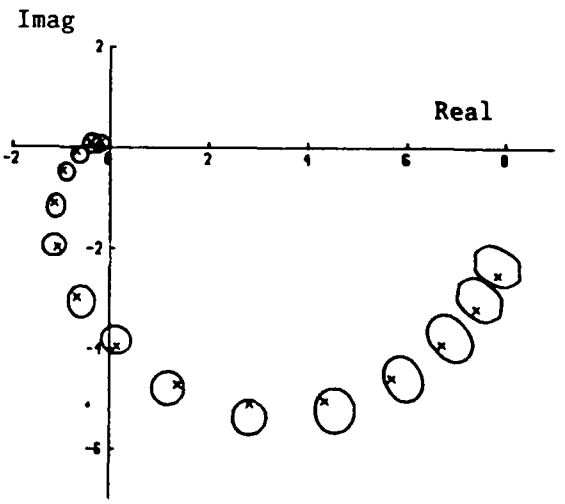

Figure 6.5d: Element g_{22}

Figure 6.5: Element-by-Element Frequency Response Uncertainty Bounds

Frequency, ωT (deg):		0	5	10	15	30	60	90	140
g_{11}	Confidence	0.176	0.149	0.143	0.141	0.138	0.134	0.147	0.150
	Bias	0.170	0.154	0.122	0.100	0.062	0.036	0.026	0.020
	Total	0.346	0.303	0.265	0.241	0.200	0.170	0.173	0.170
g_{12}	Confidence	0.127	0.119	0.100	0.106	0.096	0.100	0.096	0.097
	Bias	0.373	0.290	0.189	0.130	0.066	0.035	0.025	0.019
	Total	0.500	0.409	0.289	0.236	0.162	0.135	0.121	0.116
g_{21}	Confidence	0.116	0.110	0.093	0.099	0.095	0.089	0.094	0.101
	Bias	0.186	0.180	0.165	0.146	0.101	0.059	0.043	0.033
	Total	0.302	0.290	0.258	0.245	0.196	0.148	0.137	0.134
g_{22}	Confidence	0.163	0.144	0.143	0.142	0.129	0.136	0.128	0.125
	Bias	0.318	0.277	0.204	0.159	0.087	0.050	0.037	0.028
	Total	0.481	0.421	0.347	0.301	0.216	0.186	0.165	0.153

Table 6.5: Maximum Element-by-Element Bounds on G[exp(jωT)]

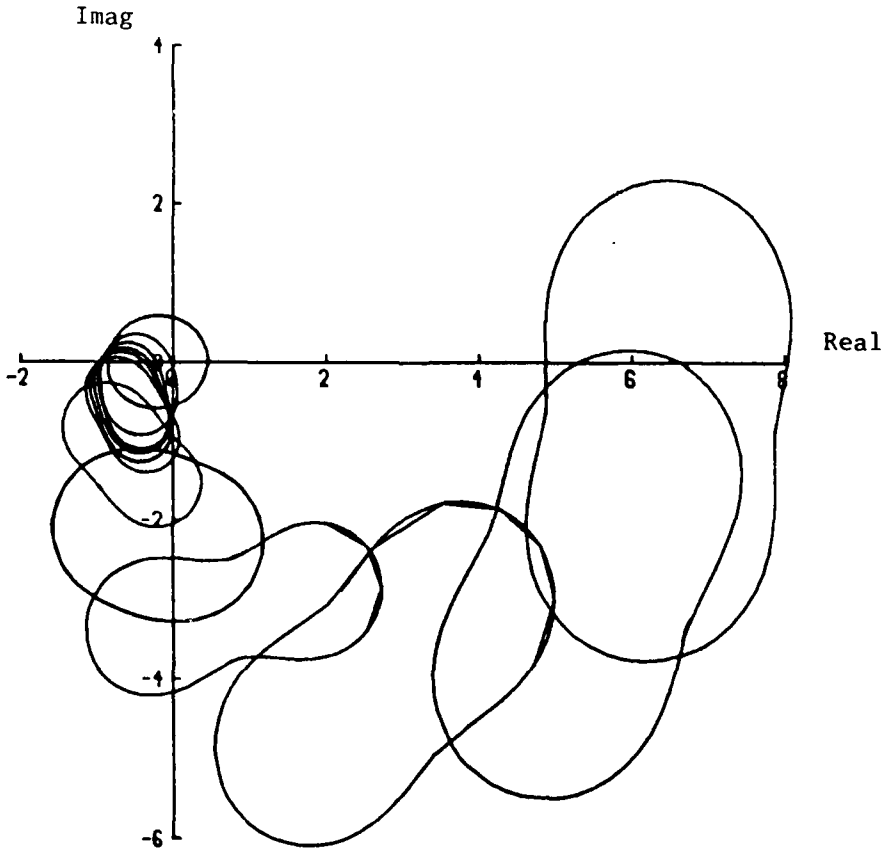

Figure 6.6: E-Contour Bounds for the Characteristic Loci of G(z)

CHAPTER SEVEN

A UNIFIED TIME DOMAIN/FREQUENCY DOMAIN APPROACH TO MULTIVARIABLE CONTROL

The frequency response description of uncertainty developed in the previous chapters quantifies the uncertainty introduced by the identification process. When combined with the structured uncertainty results summarized in Chapter 2, this description precisely defines the class of systems within which the true open-loop system exists and permits an analysis of the robustness properties of the corresponding closed-loop system. The remaining task is, of course, to design compensation which will produce adequate closed-loop response in the presence of this uncertainty.

One approach to the design of compensators for uncertain systems is the use of frequency-domain techniques based on the available uncertainty information. Currently existing H^{∞} design techniques, as discussed in Chapter 1, exemplify this approach. At the present time however, these methods are not capable of including a precise element-by-element description of frequency response uncertainty in the design since knowledge of system uncertainty is used only implicitly to generate weighting matrices for the specified optimization problem. Indeed, some current studies (e.g. [DOY3], [BIR1]) have begun to address the problem of incorporating this uncertainty information within an H^{∞} framework; though the results generated to date are tentative. An interesting and potentially useful frequency-domain alternative is suggested by the ability to construct E-contours from precise element-by-element frequency response uncertainty bounds. As suggested in [DAN2], manipulation of the characteristic locus uncertainty bands associated with a given system should provide an effective approach to robust compensator design; an approach that would be greatly enhanced by the much more accurate uncertainty information that is now available. Clearly however, additional research is required to incorporate frequency response uncertainty information explicitly in a frequency-domain methodology to produce robust control designs.

A second approach to control design in the presence of uncertainty (one which will be the focal point of developments in this chapter and the next) is the use of time-domain, self-tuning control techniques which combine on-line, computer-implemented control algorithms (to generate appropriate control signals) with on-line plant identification algorithms (to identify changes in the system). As highlighted in Chapter 1, a number of effective self-tuning control algorithms have been developed for SISO systems over the past decade. This success has prompted attempts by a number of researchers (including Borisson [BOR1], Goodwin et al [GOO2], Koivo [KOI1], and Dugard et al [DUG1]) to extend the concept of self-tuning control to multivariable systems. A majority of the proposed extensions have, however, relied on controller designs which attempt to decouple the dynamics of the open-loop plant so that SISO techniques can be applied directly. Using this approach, precise knowledge of the system transfer function matrix is required to eliminate the "undesireable" multivariable characteristics of the system. But this precise knowledge is not generally available when implementing adaptive algorithms and, as a result, these extensions have proven to be effective only under severely restricted conditions.

To overcome these problems, Mohtadi et al [MOH1] have proposed an algorithm which extends the concept of a finite-time-horizon quadratic cost function [CLA3] to the multivariable problem. This methodology reduces the requirement for system knowledge to an upper bound on the maximum delay term in the system delay matrix and has been shown, via simulation, to produce effective closed-loop control. However, the algorithm relies on the minimization of a single scalar function of the plant and controller outputs which implies that many of the special multivariable features of the system cannot be explicitly catered for. For example, the approach generally uses identical prediction and control horizons in each channel for simplicity and to avoid the problem of identifying "correct" input/output pairings. Depending on the relative complexity of the various channels, the effect of

this may well be unnecessarily complicated control activity in certain channels. In addition, the use of a single scalar cost function implies that control activity and loop-by-loop performance (i.e. the closed-loop response of the j^{th} output to the j^{th} input) can only be considered in an aggregate sense. Of course, individual weights on different inputs and outputs can be used to control the performance of individual loops, but the correct choice of these weights to achieve an acceptable compromise between performance and control activity is by no means obvious. As such, this method handles the inherent problems of multivariable interaction only in an indirect fashion.

From past experience in generalizing SISO frequency response techniques to the standard multivariable control problem, it would seem reasonable to anticipate that appropriate multivariable self-tuners could be realized by embedding SISO algorithms within a characteristic locus framework. This approach has, however, been rejected in the past for a number of reasons. For example, a link between the frequency-domain characteristics of the characteristic locus method and the time-domain representations required for self-tuning implementations is not readily apparent. Furthermore, control designs based on frequency response considerations tend to rely, to a large extent, on engineering insights that cannot be conveniently summarized in implementable computer algorithms for on-line applications. When multivariable weighting sequence models are considered however, it becomes possible to establish an interesting and particularly useful connection between time-domain and frequency-domain characteristics. Indeed, this connection suggests a methodology for generalizing existing SISO self tuning control algorithms to multivariable systems in much the same way that the characteristic locus method generalizes classical SISO frequency response techniques. Hence, weighting sequence descriptions may be used not only in the analysis of uncertain multivariable systems but also in the design of appropriate compensation via on-line self-tuning control algorithms.

The development of an appropriate multivariable self-tuning algorithm begins in this chapter with an investigation of the time-domain/frequency-domain relationships that can be developed for multivariable systems. Starting from the "characteristic sequences" methodology proposed by Kouvaritakis and Kleftouris [KOU2], characteristic subsystem models based on rational finite-dimensional z-domain functions are derived to establish a bridge between the frequency domain and the time domain. The properties of this z-domain description are investigated in detail and are shown to be particularly amenable to implementation via convolution. Thus, the resulting description may be used in conjunction with emerging computer capabilities (such as Very Large Scale Integration (VLSI) technology and parallel processing algorithms) to achieve feasible on-line control algorithms. Indeed, as shown at the end of this chapter, the proposed methodology offers a practical and potentially much more accurate alternative to standard multivariable frequency response control designs using the characteristic locus method. More importantly, it provides the required framework for incorporating SISO self-tuning concepts within a multivariable generalized-Nyquist design philosophy as will be discussed in Chapter 8.

7.1 Characteristic Sequences: A Time-Domain Alternative to the Characteristic Locus Description for Multivariable Systems

The characteristic locus method (CLM) described in Chapter 2 provides a frequency-domain approach to the analysis and design of multivariable control systems. However, implementation of any control algorithm must necessarily be accomplished in the time domain. This dichotomy has prompted some researchers to investigate alternatives to the CLM based solely on time-domain information. One particularly useful alternative is the characteristic sequences method (CSM) described below.

From Section 2.1, the defining equation for the eigenfunctions and characteristic directions of a multivariable system (written now in terms of z-transforms) is given by:

$$G(z)\, w_i(z) = g_i(z)\, w_i(z).$$

After transforming this relationship into the time domain using inverse z-transforms, the following convolution relationship can be established:

$$ {}^{s}G * {}^{s}w_i = {}^{s}g_i * {}^{s}w_i \qquad \ldots.(7.1)$$

where (i) ${}^{s}G = \{G(0), G(1), \cdots\}$ represents the weighting sequence of the multivariable plant;

(ii) ${}^{s}g_i = \{g_i(0), g_i(1), \cdots\}$ is the 'characteristic weighting sequence' (CWS) defined by the characteristic equation:

$$ \left| {}^{s}g_i * {}^{s}E - {}^{s}G \right| = {}^{s}0 \; ; \quad i=1, \cdots, m$$

with the determinant being taken in the convolutional sense and ${}^{s}E = \{I, 0, 0, \cdots\}$; and

(iii) ${}^{s}w_i = \{w_i(0), w_i(1), \cdots\}$ is the 'characteristic vector sequence' (CVS) corresponding to the appropriate CWS and defined by

$$ \{ {}^{s}g_i * {}^{s}E - {}^{s}G \} * {}^{s}w_i = {}^{s}0 \; ; \quad i=1, \cdots, m$$

This transcription of the CLM to the time domain was initially investigated by Thiga [THI1] and Gough et al [GOU1] who relied on convolution algebra and a Gaussian elimination-type algorithm to transform the multivariable weighting sequence, ${}^{s}G$, into the characteristic sequences identified above, thus producing a time-domain description of the eigenstructure of G(z). It was suggested that this eigenstructure information could be used to study system stability and performance and, ultimately, to design time-domain controllers to manipulate these characteristic sequences. However, the proposed algorithm for calculating these sequences has been found to be difficult to implement and, in general, does not admit a solution. Even when a solution does exist, the stability criterion suggested in [THI1] for use with the characteristic sequences will generally produce an invalid assessment of closed-loop stability.

To overcome these problems, Kouvaritakis and Kleftouris [KOU2] proposed an alternative approach. In particular, they developed an efficient, easy-to-implement "deconvolution" algorithm for calculating the CWS and CVS when

the eigenvalues of G(0) are distinct. [This standard algorithm is summarized in Appendix 7.1. A modified version for the much more unusual case of repeated eigenvalues has also been developed [CL04] and is described in Appendix 7.2.] Furthermore, they demonstrated that, if ${}^{S}W$ is defined as the matrix sequence whose columns are the individual CVS, then a dual eigenvector matrix sequence ${}^{S}V$ can be defined by

$$ {}^{S}V * {}^{S}W = {}^{S}W * {}^{S}V = {}^{S}E \qquad \ldots.(7.2) $$

and the dual CVS can also be calculated using a "deconvolution" algorithm. As a result, the weighting sequence description of the plant can be rewritten in terms of the characteristic sequences as:

$$ {}^{S}G = {}^{S}W * {}^{S}\Lambda * {}^{S}V \qquad \ldots.(7.3) $$

where the elements of the diagonal matrix sequence ${}^{S}\Lambda$ are the individual CWS and, more importantly, these characteristic sequences can be easily computed.

Kouvaritakis and Kleftouris also recognized that the CWS can be related to the characteristic loci via z-transforms. Indeed, provided the CWS decay to zero, they may be truncated and used to establish z-domain expressions which identify regions in the complex plane containing the characteristic loci of the system. Thus, closed-loop stability may be assessed via the generalized Nyquist criterion, and the only conservatism introduced in the resulting evaluation arises from the upper bounds used to account for the effects of truncation. For all practical purposes then, the CSM provides the same assessment of closed-loop stability as the CLM. A rudimentary design approach based on sequence manipulation was also proposed in [KOU2]. However, the relationships between the time domain and the frequency domain highlighted here suggest that a more useful multivariable design methodology can be obtained by combining the CLM and CSM in a more fundamental manner. The necessary relationships and the resulting design techniques are developed and discussed in the following sections.

7.2 Z-Domain Characteristic Subsystem Descriptions for MIMO Systems

7.2.1 Z-transform Relationships and Power Series Representations

The characteristic locus theory summarized for continuous-time systems in Chapter 2 also applies, as mentioned previously, to discrete-time systems using z-transforms in place of Laplace transforms. Within this discrete-time context, the eigenfunctions and corresponding characteristic directions of the multivariable plant can be directly related to the characteristic sequences described above. To establish these relationships, consider the z-transform of the multivariable weighting sequence defined by:

$$\hat{G}(z) = \sum_{i=0}^{\infty} G_i \, z^{-i} \qquad \ldots.(7.4)$$

[Note: Throughout the remainder of this chapter and the next, it will be necessary to distinguish z-domain functions from the coefficients of their corresponding weighting sequence representations. For this purpose, the notation $\hat{\cdot}$ will be used to denote z-domain functions as shown above.] Using this relationship in conjunction with the convolution property of the z-transform, eqn 7.3 may be rewritten in terms of z-transforms as:

$$\hat{G}(z) = \hat{W}(z)\,\hat{\Lambda}(z)\,\hat{V}(z) = \sum_{i=1}^{m} \hat{g}_i(z)\,\hat{w}_i(z)\,\hat{v}_i^t(z) \qquad \ldots.(7.5)$$

where $\hat{g}_i(z)$, $\hat{w}_i(z)$, and $\hat{v}_i^t(z)$ are described by the following power series:

$$\hat{g}_i(z) = \sum_{j=0}^{\infty} g_i(j) \, z^{-j} \qquad \ldots.(7.6a)$$

$$\hat{w}_i(z) = \sum_{j=0}^{\infty} w_i(j) \, z^{-j} \qquad \hat{v}_i^t(z) = \sum_{j=0}^{\infty} v_i^t(j) \, z^{-j} \qquad \ldots.(7.6b,c)$$

Eqn 7.5 describes the same relationship between the transfer function matrix $\hat{G}(z)$ and its eigenfunctions and characteristic directions as that identified by the CLM (e.g. eqn 2.3 with s replaced by z). This result implies that the CWS and CVS simply define the coefficients associated with the z-domain weighting sequence representations for the eigenfunctions and corresponding characteristic directions of $\hat{G}(z)$.

The utility of these z-domain descriptions depends entirely on the nature of the CWS and CVS. As suggested by Kouvaritakis and Kleftouris, the

CWS can be used to assess closed-loop stability via the generalized Nyquist criterion provided the CWS decay to zero (i.e. $\lim_{j\to\infty} g_i(j) = 0$) [KOU2]. It is just as important to recognize that, when the CVS and dual CVS possess this same decay property, truncated versions of these sequences can be used to accurately approximate the characteristic directions of the plant. Under these circumstances, the CLM and CSM may be combined to achieve acceptable control designs via convolution implementations as will be discussed later in this chapter. Clearly though, the key to using the CWS and CVS in multivariable control designs is the asymptotic decay of these sequences. For this reason, it is particularly important to investigate the convergence properties of these sequences and to develop techniques which will ensure that the resulting convergence conditions are satisfied.

7.2.2 Convergence Conditions for the CWS

As discussed above, the CWS and CVS are directly related to the eigenfunctions and characteristic directions of $\hat{G}(z)$. It therefore seems reasonable to expect that the theory of algebraic functions can be used to establish conditions which guarantee the convergence of the power series representations in eqn 7.6 and, more importantly, the decay of the CWS and CVS. In fact, specific properties of the algebraic function $\hat{g}(z)$ can be translated directly into the desired convergence conditions. Before starting this investigation however, it is important to recognize that, since the characteristic gain is defined by the characteristic equation $\Delta(z,\hat{g}) = 0$ (see eqn 2.2 with s replaced by z), the properties of $\hat{g}$ depend on the characteristics of $\Delta(z,\hat{g})$. Furthermore, $\Delta(z,\hat{g})$ can be categorized in one of the following three ways:

Case 1: $\Delta(z,\hat{g})$ is irreducible over the field of rational functions in z.

Case 2: $\Delta(z,\hat{g})$ is reducible to nonlinear (and possibly some linear) factors in z as suggested be eqn 2.1 (with s replaced by z).

Case 3: $\Delta(z,\hat{g})$ is completely reducible to linear factors in z, (i.e.

$\Delta(z,\hat{g}) = \prod_{i=1}^{m} [\hat{g}(z) - \hat{g}_i(z)]$ where each $\hat{g}_i(z)$ is a rational function of z).

Since the characteristics of $\Delta(z,\hat{g})$ for Case 2 are completely defined by the characteristics for Cases 1 and 3, an investigation of the properties of $\hat{g}$ need only examine situations when $\Delta(z,\hat{g})$ is irreducible or reducible to linear factors. Furthermore, transfer function matrices arising from practical situations will, in general, lead to characteristic equations which are irreducible. For this reason, attention will be focused on Case 1 throughout the remainder of the discussion, although relevant points related to Case 3 will be highlighted when appropriate.

When $\Delta(z,\hat{g})$ is irreducible, several important properties of the functions, $\hat{g}_i(z)$, which describe the branches of $\hat{g}(z)$ can be identified. One such property, which is useful for our purposes, is the following:

Lemma 7.1: Let C_0 denote the region of the complex z-plane defined by $|z| \geq r_0$. Let $\Delta(z,\hat{g}) = \det\{\hat{g}I - \hat{G}(z)\}$ be irreducible and of degree m in $\hat{g}(z)$, and suppose that $\hat{g}(z)$ has no poles or branch points in C_0. Then, there are m (distinct) analytic functions $\hat{g}_1(z), \ldots, \hat{g}_m(z)$ defined in C_0 which satisfy the equation $\Delta(z,\hat{g}) = 0$.

Proof: See Lemma 23.1 in [SMI1].

The conditions established above for the analyticity of the $\hat{g}_i(z)$ can also be used to produce conditions for the decay of the CWS as shown in the following theorem:

Theorem 7.1: Let C_1 denote the region of the complex z-plane defined by $|z| \geq 1$. Let $\Delta(z,\hat{g})$ be irreducible and of degree m in $\hat{g}(z)$, and suppose that $\hat{g}(z)$ has no poles or branch points in C_1. Then, the elements of each CWS must decay to zero (i.e. $\lim_{j\to\infty} g_i(j) = 0$; $i=1, \cdots, m$).

Proof: If $\hat{g}(z)$ has no poles or branch points in C_1, Lemma 7.1 indicates that the branches of $\hat{g}(z)$ are analytic for all $|z| \geq 1$. By Taylor's

theorem, each $\hat{g}_i(z)$ can be expanded in a power series of the form:

$$\hat{g}_i(z) = \sum_{j=0}^{\infty} g_i(j)\, z^{-j} \qquad \ldots.(7.7)$$

and this series must converge for all $|z| \geq 1$. In particular, it must converge for $z = 1$. Thus, the infinite sum $\hat{g}_i(1) = \sum_{j=0}^{\infty} g_i(j)$ must converge, but this can only happen if $\lim_{j\to\infty} g_i(j) = 0$.

....QED

The asymptotic decay implied by Theorem 7.1 guarantees that the CWS can be truncated to produce sufficiently accurate z-domain representations for the branches of the characteristic gain, $\hat{g}(z)$. Furthermore, these power series representations can be examined to assess the effects of using finite-term approximations. For instance, eqn 7.6a can be written as:

$$\hat{g}_i(z) = \sum_{j=0}^{q-1} g_i(j)\, z^{-j} + \hat{\delta g}(z);$$

and, if r_0 denotes the largest distance from the origin to a pole or branch point of $\hat{g}(z)$, it can be shown (using standard relationships, e.g. [CHU1]) that the error in the characteristic locus generated by truncating the CWS at q elements is bounded by:

$$|\delta g(e^{j\omega T})| \leq \inf_{r} \sup_{\omega T} \left\{ \frac{|g(re^{j\omega T})|}{(1 - r)}\, r^q \right\} \qquad \ldots.(7.8)$$

for r in the range $r_0 \leq r < 1$ and ωT in the range $0 \leq \omega T \leq \pi$. In essence, this result provides a means of translating desired characteristic locus accuracy into appropriate CWS truncation levels.

7.2.3 Convergence Conditions for the CVS

Theorem 7.1 establishes appropriate conditions for the decay of the CWS. These same conditions will also guarantee the decay of the CVS and dual CVS. The first results which must be produced to verify this observation are given by Lemma 7.2 and Theorem 7.2 which identify special properties of the repeated zeros of $\Delta(z,\hat{g})$ and the branch points of $\hat{g}(z)$, respectively. These results are then combined with standard power series

relationships to establish the desired conditions for CVS convergence.

To begin, the following property of the repeated zeros of $\Delta(z,\hat{g})$ can be identified:

Lemma 7.2: Let $\Delta(z,\hat{g})$ be irreducible, and let z_0 represent a point in the complex plane which is not a pole of $\hat{g}(z)$ and for which $\hat{g}_0$ is a zero of $\Delta(z_0,\hat{g})$ with multiplicity k_g. Then, $d\hat{g}/dz|_{(z_0,\hat{g}_0)}$ is finite if, and only if, z_0 is a zero of $\Delta(z,\hat{g}_0)$ with multiplicity $k_z \geq k_g$.

Proof: When $\hat{g}_0$ is a zero of $\Delta(z_0,\hat{g})$ with multiplicity k_g, the following conditions will be satisfied for all $k < k_g$ and $1 \leq j \leq k$:

$$\frac{\partial^k \Delta}{\partial \hat{g}^k}\bigg|_{(z_0,\hat{g}_0)} = 0 \qquad \frac{\partial^k \Delta}{\partial z^{k-j}\,\partial \hat{g}^j}\bigg|_{(z_0,\hat{g}_0)} = 0 \qquad \ldots.(7.9a,b)$$

Similarly when z_0 is a zero of $\Delta(z,\hat{g}_0)$ with multiplicity k_z, the following conditions will be satisfied for all $k < k_z$ and $1 \leq j \leq k$:

$$\frac{\partial^k \Delta}{\partial z^k}\bigg|_{(z_0,\hat{g}_0)} = 0 \qquad \frac{\partial^k \Delta}{\partial z^{j}\,\partial \hat{g}^{k-j}}\bigg|_{(z_0,\hat{g}_0)} = 0 \qquad \ldots.(7.10a,b)$$

Using these relationships, the lemma can be proved in two parts as shown below.

Sufficiency: Consider the k^{th} total differential of $\Delta(z,\hat{g})$ defined by:

$$d^k(\Delta) = \left\{ \frac{\partial}{\partial z}\, dz + \frac{\partial}{\partial \hat{g}}\, d\hat{g} \right\}^k \Delta \qquad \ldots.(7.11)$$

Now, if eqns 7.9a,b and 7.10a,b are satisfied for all $k < k_g$ and $1 \leq j \leq k$, then $d^{k_g}(\Delta) \equiv 0$. So if $k_z \geq k_g$, the following condition must be satisfied:

$$\left\{ \frac{\partial^{k_g}\Delta}{\partial z^{k_g}} + k_g \frac{\partial^{k_g}\Delta}{\partial z^{k_g-1}\,\partial \hat{g}} \left[\frac{d\hat{g}}{dz}\right] + \cdots \right.$$

$$\left. + k_g \frac{\partial^{k_g}\Delta}{\partial z\,\partial \hat{g}^{k_g-1}} \left[\frac{d\hat{g}}{dz}\right]^{k_g-1} + \frac{\partial^{k_g}\Delta}{\partial \hat{g}^{k_g}} \left[\frac{d\hat{g}}{dz}\right]^{k_g} \right\} \Bigg|_{(z_0,\hat{g}_0)} = 0 \qquad \ldots.(7.12)$$

Since $\Delta(z,\hat{g})$ is a polynomial in z ang $\hat{g}$, all of the partial derivative terms in eqn 7.12 are either zero or finite. Furthermore, by assumption,

$\partial^{k_g}\Delta/\partial^{k_g}\hat{g}|_{(z_0,\hat{g}_0)} \neq 0$. Hence, eqn 7.12 can only be satisfied if $d\hat{g}/dz|_{(z_0,\hat{g}_0)}$ is finite.

Necessity: Assume that $d\hat{g}/dz|_{(z_0,\hat{g}_0)}$ is finite and $k_g > 1$. Since $\Delta(z,\hat{g}) = 0$, its first total differential must be zero. Thus,

$$\left\{ \frac{\partial \Delta}{\partial z} + \frac{\partial \Delta}{\partial \hat{g}} \frac{d\hat{g}}{dz} \right\}\Big|_{(z_0,\hat{g}_0)} = 0 \qquad \ldots.(7.13)$$

By assumption $\partial^k\Delta/\partial\hat{g}^k|_{(z_0,\hat{g}_0)} = 0$ for all $k < k_g$. So eqn 7.13 can only be satisfied if $\partial\Delta/\partial z|_{(z_0,\hat{g}_0)} = 0$. But this result implies that $d^2(\Delta) \equiv 0$; and, if $k_g > 2$, this condition can only be satisfied (under the given assumptions) if $\partial^2\Delta/\partial z^2|_{(z_0,\hat{g}_0)} = 0$. But, this implies that $d^3(\Delta) \equiv 0$. The same arguments hold for all $k < k_g$ and, hence, $\partial^k\Delta/\partial z^k|_{(z_0,\hat{g}_0)} = 0$ for all $k < k_g$. Thus, z_0 must be a zero of $\Delta(z,\hat{g}_0)$ with multiplicity $k_z \geq k_g$.

....QED

With Lemma 7.2 in place, the following special property of the branch points of $\hat{g}(z)$ can now be identified:

Theorem 7.2: Let $\Delta(z,\hat{g})$ be irreducible, and let z_0 represent a point in the complex plane which is not a pole of $\hat{g}(z)$ and for which $\hat{g}_0$ is a repeated zero of $\Delta(z_0,\hat{g})$ with multiplicity k_g. Then z_0 is a branch point if, and only if, $\hat{g}_0$ is a repeated eigenvalue of $\hat{G}(z_0)$ associated with a nonsimple Jordan form.

Proof: Since z_0 is not a pole of $\hat{g}(z)$, the transfer function matrix $\hat{G}(z)$ may be rewritten in Taylor series form as:

$$\hat{G}(z) = \hat{G}(z_0) + \sum_{i=1}^{\infty} G_0(i)\,(z - z_0)^i \qquad \ldots.(7.14)$$

(where $G_0(i)$ denotes the i^{th} coefficient of the Taylor series expansion about the point z_0) and this series must converge for all z in a neighborhood of z_0. The proof of the theorem may now be separated into two parts.

Necessity: Assume first that z_0 is a branch point of $\hat{g}(z)$. Also assume, for the moment, that the eigenvalue/eigenvector decomposition of $\hat{G}(z_0)$ can be written in simple Jordan form (i.e.

$$\hat{G}(z_0) = \hat{W}(z_0)\,\hat{\Lambda}(z_0)\,\hat{V}(z_0) = [\hat{W}_k \mid \hat{W}_{m-k}] \left[\begin{array}{c|c} \hat{\Lambda}_k & 0 \\ \hline 0 & \hat{\Lambda}_{m-k} \end{array}\right] \left[\begin{array}{c} \hat{V}_k^T \\ \hline \hat{V}_{m-k}^T \end{array}\right] \quad \ldots.(7.15)$$

where $\hat{\Lambda}_k = \text{diag}\,[\hat{g}_0, \cdots, \hat{g}_0]$; $\hat{\Lambda}_{m-k} = \text{diag}\,\{\hat{g}_{k+1}, \cdots, \hat{g}_m\}$; and $\hat{W}_k$, $\hat{W}_{m-k}$, $\hat{V}_k^T$, and $\hat{V}_{m-k}^T$ are matrices of appropriate dimensions containing the corresponding eigenvectors and dual eigenvectors of $\hat{G}(z_0)$ respectively). Using this decomposition, eqn 7.14 can be rewritten as:

$$\hat{G}(z) = \hat{W}(z_0) \left\{\hat{\Lambda}(z_0) + \sum_{i=1}^{\infty} \{\hat{V}(z_0)\, G_0(i)\, \hat{W}(z_0)\}\,(z - z_0)^i\right\} \hat{V}(z_0) \quad \ldots.(7.16)$$

and the characteristic equation ($\det[\hat{g}I - \hat{G}] = 0$ at $\hat{g} = \hat{g}_0$) becomes:

$$\Delta(z,\hat{g}_0) = |\hat{W}(z_0)|\;|\hat{M}(z)|\;|\hat{V}(z_0)| = 0 \quad \ldots.(7.17)$$

where $$\hat{M}(z) = \hat{\Lambda}^*(z_0) - \sum_{i=1}^{\infty} \{\hat{V}(z_0)\, G_0(i)\, \hat{W}(z_0)\}\,(z - z_0)^i$$

and $$\hat{\Lambda}^*(z_0) = \left[\begin{array}{c|c} 0 & 0 \\ \hline 0 & \hat{g}_0 I - \hat{\Lambda}_{m-k} \end{array}\right] \quad \ldots.(7.18)$$

Alternatively, $\hat{M}(z)$ can be rewritten in the following form:

$$\hat{M}(z) = \left[\begin{array}{c|c} -\sum_{i=1}^{\infty} \hat{V}_k^T G_0(i) \hat{W}_k (z-z_0)^i & -\sum_{i=1}^{\infty} \hat{V}_k^T\, G_0(i)\, \hat{W}_{m-k}\,(z-z_0)^i \\ \hline -\sum_{i=1}^{\infty} \hat{V}_{m-k}^T G_0(i) \hat{W}_k (z-z_0)^i & (\hat{g}_0 I - \hat{\Lambda}_{m-k}) - \sum_{i=1}^{\infty} \hat{V}_{m-k}^T G_0(i) \hat{W}_{m-k} (z-z_0)^i \end{array}\right]$$

Since $|\hat{W}(z_0)|\;|\hat{V}(z_0)| = 1$, eqn 7.17 reduces to $\Delta(z,\hat{g}_0) = |\hat{M}(z)| = 0$. Now, Schur's formula for the determinant of partitioned matrices, given by

$$\det \left[\begin{array}{c|c} X & Y \\ \hline Z & W \end{array}\right] = \det X \;\det\{W - Z\, X^{-1} Y\}\,,$$

can be used to identify $|\hat{M}(z)|$. But, $(z - z_0)$ is a common factor in all of the elements of $X = -\sum_{i=1}^{\infty} \hat{V}_k^T G_0(i) \hat{W}_k (z-z_0)^i$. Hence, z_0 must necessarily be a zero of $\Delta(z,\hat{g}_0)$ with multiplicity at least equal to k_g. By Lemma

7.2, this implies that $d\hat{g}/dz|_{(z_0,\hat{g}_0)}$ is finite and, hence, that z_0 is not a branch point. This result, however, contradicts the initial assumption and, therefore, $\hat{g}_0$ must be a repeated eigenvalue of $\hat{G}(z_0)$ associated with a nonsimple Jordan form.

Sufficiency: Assume that $\hat{g}_0$ is a repeated eigenvalue of $\hat{G}(z_0)$ associated with a nonsimple Jordan form. Provided that the definition of $\hat{W}(z_0)$ is extended to include (wherever appropriate) pseudo-eigenvectors, eqn 7.17 can still be used to investigate the properties of $\Delta(z,\hat{g}_0)$. However now, the upper left block of $\hat{\Lambda}^*(z_0)$ (eqn 7.18) will no longer be zero because of the unity elements in the off-diagonal positions of the Jordan form representation for the eigenvalues of $\hat{G}(z_0)$. In this situation, $(z - z_0)$ is no longer a common factor in the upper left block of $\hat{M}(z)$ and, hence, z_0 cannot be a zero of $\Delta(z,\hat{g}_0)$ with multiplicity greater than or equal to k_g. By Lemma 7.2 then, $d\hat{g}/dz|_{(z_0,\hat{g}_0)}$ is unbounded and, hence, z_0 is a branch point of $\hat{g}(z)$. ....QED

Theorem 7.2 identifies an alternative definition for the branch points of the algebraic function $\hat{g}(z)$. More importantly, when combined with Theorem 7.1, it provides a means of establishing the convergence properties of the CVS and dual CVS. The appropriate result can be developed in three stages as shown here:

Definition 7.1: [CHU1] The Cauchy product of the two infinite power series

$$\hat{f}(z^{-1}) = \sum_{k=1}^{\infty} a_k z^{-k} \qquad \text{and} \qquad \hat{g}(z^{-1}) = \sum_{k=1}^{\infty} b_k z^{-k}$$

is given by: $$\hat{h}(z^{-1}) = \sum_{k=0}^{\infty} c_k z^{-k}$$

where the coefficients, c_k, are defined by:

$$c_k = \sum_{i=0}^{k} a_i b_{k-i}$$

Lemma 7.3: The Cauchy product of two convergent power series converges to the product of these series at all points interior to their circles of convergence.

Proof: See p 164 in [CHU1].

Theorem 7.3: If $\hat{G}(z)$ is stable, $\Delta(z,\hat{g})$ is irreducible and of degree m in $\hat{g}(z)$, and $\hat{g}(z)$ has no branch points in C_1, then each of the m CVS and m dual CVS must decay to zero.

Proof: By assumption, $\hat{g}(z)$ has no poles or branch points in C_1. Hence by Theorem 7.1, each eigenfunction, $\hat{g}_i(z)$, can be written as a power series in z^{-1} which converges for all z in C_1. Furthermore, by Theorem 7.2, $\hat{W}(z)$ is full rank at each and every point in C_1. As a result, there exists a complete set of characteristic directions, $\{\hat{w}_i(z);\ i = 1,\cdots,m\}$, each of which can be defined (for all z in C_1) by a relationship of the form:

$$\{\hat{g}_i(z)I - \hat{G}(z)\}\ \hat{w}_i(z) = 0$$

where $\hat{g}_i(z)$ is the corresponding eigenfunction of $\hat{G}(z)$.

The result above implies that each one of the m characteristic directions can be generated completely in terms of products, sums, and/or differences of the corresponding eigenfunction and the various elements, $\hat{g}_{ij}(z)$, of $\hat{G}(z)$. But from above, each $\hat{g}_i(z)$ can be written as a power series in z^{-1} which converges for all z in C_1 and, since $\hat{G}(z)$ is stable, the same is true for each $\hat{g}_{ij}(z)$. Hence, $\hat{w}_i(z)$ can be written entirely in terms of Cauchy products and/or sums of power series. Lemma 7.3 and other standard power series results can, therefore, be used to demonstrate that the power series representation for $\hat{w}_i(z)$ must converge for all z in C_1. As a result, $\hat{w}_i(z)$ can be written as a power series in z^{-1} which converges for all $|z| \geq 1$ and, in particular, for $z = 1$. But, this can only happen if $\lim_{j\to\infty} w_i(j) = 0$. Hence the elements of each of the m individual CVS must decay to zero.

Identical arguments can be used to prove the same result for each of the m dual CVS since the dual characteristic directions are defined by:

$$\hat{v}_i^t(z)\ \{\hat{g}_i(z)I - \hat{G}(z)\} = 0 \qquad \ldots\ldots\text{QED}$$

The fact that $w_i(j)$ and $v_i^t(j)$ decay to zero guarantees that the CVS and dual CVS can be truncated to produce sufficiently accurate descriptions of the characteristic directions of $\hat{G}(z)$. However because $\hat{w}_i(z)$ and $\hat{v}_i^t(z)$ are not unique, appropriate truncation levels cannot be identified in the same manner as that shown previously for the CWS. Instead, the number of terms in ^{S}W and ^{S}V needed to achieve an appropriate level of accuracy may be estimated by relating $\hat{W}(z)$, $\hat{\Lambda}(z)$ and $\hat{V}(z)$ to $\hat{G}(z)$. In particular, using the following representations:

$$\hat{G}(z) = \sum_{j=0}^{N-1} G(j)\, z^{-j} + \delta\hat{G} = \hat{G}_T + \delta\hat{G} \qquad \hat{W}(z) = \sum_{j=1}^{q-1} W(j)\, z^{-j} + \delta\hat{W} = \hat{W}_T + \delta\hat{W}$$

$$\hat{\Lambda}(z) = \sum_{j=0}^{n-1} \Lambda(j)\, z^{-j} + \delta\hat{\Lambda} = \hat{\Lambda}_T + \delta\hat{\Lambda} \qquad \hat{V}(z) = \sum_{j=1}^{q-1} V(j)\, z^{-j} + \delta\hat{V} = \hat{V}_T + \delta\hat{V}$$

(where n, N, and q are selected so that $|\delta\hat{G}|$, $|\delta\hat{\Lambda}|$, $|\delta\hat{W}|$, and $|\delta\hat{V}|$ are $O(\varepsilon)$ in size for all $|z| = 1$), $\hat{G}(z)$ can be rewritten as:

$$\hat{G} = \hat{G}_T + \delta\hat{G} = \hat{W}_T\,\hat{\Lambda}_T\,\hat{V}_T + \delta\hat{W}\,\hat{\Lambda}_T\,\hat{V}_T + \hat{W}_T\,\delta\hat{\Lambda}\,\hat{V}_T + \hat{W}_T\,\hat{\Lambda}_T\,\delta\hat{V} + O(\varepsilon^2)$$

By eliminating all terms of $O(\varepsilon^2)$, this relationship reduces to:

$$\hat{W}_T\,\hat{\Lambda}_T\,\hat{V}_T = \hat{G}_T - \{\delta\hat{W}\,\hat{\Lambda}_T\,\hat{V}_T + \hat{W}_T\,\delta\hat{\Lambda}\,\hat{V}_T + \hat{W}_T\,\hat{\Lambda}_T\,\delta\hat{V}\} \qquad \ldots\ldots(7.19)$$

Furthermore, for systems where $\hat{G}(z)$ is not poorly conditioned (i.e. the eigenfunctions of $\hat{G}$ are not widely disparate and the eigenvectors of $\hat{G}$ are not excessively skew), the three perturbation terms in eqn 7.19 will be $O(\varepsilon)$ in size and can be neglected when compared to $\hat{G}_T$. In this case, the number of terms in the series representation of $\hat{W}_T\,\hat{\Lambda}_T\,\hat{V}_T$ must equal the number of terms in the series representation of $\hat{G}_T$ and, under the assumption that the lengths of $\hat{W}_T$ and $\hat{V}_T$ are equal, this implies that $n+2q-2 = N$. So, $\hat{W}_T$ and $\hat{V}_T$ must each contain $q = (N-n)/2 + 1$ terms. [Notice that, when the plant is perfectly conditioned (i.e. $\hat{G}(z) = \hat{g}(z)I$), N equals n and the above analysis

implies that $q = 1$ which agrees with the fact that $\hat{W}(z) = \hat{V}(z) = I$.] If, however, $\hat{G}(z)$ is poorly conditioned, the perturbation terms in eqn 7.19 will generate an additional Q significant terms. Hence, $\hat{W}_T$ and $\hat{V}_T$ must now contain $q = (N-n+Q)/2 + 1$ terms each. Although it is not possible to obtain a general expression for Q, the number of extra sequence elements generated by these error terms will tend to be small for all but the most poorly conditioned plants. Thus, the truncation levels for ${}^s w_i$ and ${}^s v_i^t$ can be expected to be significantly smaller than either N or n, and this conclusion agrees with observations for a large number of systems.

7.2.4 Extensions for Special Situations

The results established in Sections 7.2.2 and 7.2.3 suggest that, for the generic case when $\Delta(z,g)$ is irreducible, the CWS, CVS and dual CVS can be used to generate accurate finite-series representations for $\hat{g}_i(z)$, $\hat{w}_i(z)$, and $\hat{v}_i^t(z)$ provided the open-loop system is stable and $\hat{g}(z)$ has no unstable branch points. In fact, these results may be extended to unstable systems by pulling out the unstable poles of $\hat{G}(z)$ as common factors to produce:

$$\hat{G}(z) = \frac{1}{\hat{d}_u(z)} \hat{S}(z) \qquad \ldots.(7.20)$$

where $\hat{S}(z)$ is a stable transfer function matrix and $\hat{d}_u(z)$ is a scalar function containing the unstable poles of $\hat{G}(z)$. The convergence conditions of Theorems 7.1 and 7.3 can now be applied to $\hat{S}(z)$ and, since this transfer function matrix is stable, its CWS and CVS will decay provided $\hat{S}(z)$ has no unstable branch points. Hence, the eigenfunctions and characteristic directions of $\hat{S}(z)$ can be accurately described by finite-dimensional z-domain representations as discussed previously. But from eqn 7.20, the characteristic directions of $\hat{S}(z)$ and $\hat{G}(z)$ are the same. Furthermore, the respective eigenfunctions, $\hat{s}_i(z)$ and $\hat{g}_i(z)$, are related by:

$$\hat{g}_i(z) = \frac{\hat{s}_i(z)}{\hat{d}_u(z)}$$

As a result, accurate finite-dimensional z-domain representations for the eigenfunctions and characteristic directions of unstable systems can also be generated provided no unstable branch points exist.

The results of the previous sections can also be extended to the much more unusual case when $\Delta(z,g)$ is reducible to linear factors. In this situation, there are no branch points. Hence, the CWS must necessarily decay. At first glance, this observation also seems to imply that the CVS and dual CVS will also decay. However unlike the previous situation where repeated eigenvalues associated with a nonsimple Jordan form could only occur at branch points, it is now possible for a nonsimple Jordan form to exist at any point z_0 where $\hat{G}(z_0)$ has repeated eigenvalues. If this occurs, $\hat{W}(z)$ will lose rank as $z \to z_0$ and, in the limit, $\hat{V}(z) = \hat{W}^{-1}(z)$ will be unbounded. For $|z_0| \geq 1$, this suggests that $\hat{V}(z)$ cannot be written as a power series in z^{-1} with decaying coefficients. Hence, the resulting CSM representation of the system will be unsuitable for control design purposes.

For this problem however, the CSM algorithm may be modified to produce decaying sequences. Preliminary attempts by Li and Cameron [LI1] have produced modifications for the extremely unlikely situation when $\Delta(z,g)$ has repeated linear factors associated with a nonsimple Jordan form at all points in the complex plane, a situation which implies that $\hat{G}(z)$ is identically similar to $\hat{J}(z)$ (i.e. $\hat{G}(z) \equiv \hat{W}(z)\,\hat{J}(z)\,\hat{V}(z)$ for all z, where $\hat{J}(z)$ denotes the appropriate Jordan form). But, they have not addressed the less unlikely situation where $\hat{G}(z) = \hat{W}(z)\,\hat{J}(z)\,\hat{V}(z)$ at isolated values of z. Modifications to handle this situation are developed in Appendix 7.2.

Again, it must be stressed that $\Delta(z,g)$ will, generically, be irreducible. Hence, the developments for the case when $\Delta(z,g)$ is reducible to linear factors are presented primarily for completeness. More importantly, the fact that $\Delta(z,g)$ is irreducible suggests that, for all practical control problems, the convergence conditions of Theorems 7.1 and 7.3 must be satisfied to obtain suitable finite dimensional characteristic

subsystem descriptions. Unstable branch points must, therefore, be avoided to permit the use of these subsystem descriptions in control designs. The problems of recognizing and eliminating unstable branch points are examined in greater detail in the following section.

7.3 An Investigation of Unstable Branch Points

7.3.1 Recognizing Unstable Branch Points

Closer examination of the CSM algorithm indicates that the initial element of the plant weighting sequence, G(0), is a key component in the calculation of the CWS and CVS. Indeed once the eigenvalues and eigenvectors of G(0) are identified, the remaining sequence elements can be readily computed using simple algebraic operations. Thus, the eigenvalues and eigenvectors of G(0) have a particularly significant effect on all elements of the CWS and CVS, and one should therefore anticipate that these quantities can be directly related to the convergence characteristics of the CWS and CVS. In fact, several conditions based on the eigenvalues of G(0) can be established to identify the existence of unstable branch points as shown below.

It is known [SMI1] that the branch points of $\hat{g}(z)$ are a subset of the zeros of the discriminant polynomial, $\hat{D}_g(z)$, associated with $\Delta(z,\hat{g}) = 0$. [Note: For a 2 x 2 system, the characteristic equation is

$$\Delta(z,\hat{g}) = \hat{a}(z)\,\hat{g}^2 + \hat{b}(z)\,\hat{g} + \hat{c}(z) = 0$$

and $\hat{D}_g(z) = \hat{b}^2(z) - 4\,\hat{a}(z)\,\hat{c}(z)$. A precise definition of $\hat{D}_g$ for the general case can be found, for example, in [BLI1].] A detailed investigation of $\hat{D}_g$ should, therefore, provide insight into the specified problem. To begin, $\hat{G}(z)$ can be written in power series form as shown in eqn 7.4 and the coefficients G_i will decay to zero. [Note: For all of the following developments, $\hat{G}(z)$ will be assumed to be stable. If the open-loop system is unstable, the following results will hold for $\hat{S}(z)$ (defined by eqn 7.20) and, hence, they can also be extended to unstable systems.] Using this

power series representation, $\Delta(z,\hat{g})$ can be rewritten as:

$$\Delta(z,\hat{g}) = \left| \hat{g}(z)\, I - \sum_{i=0}^{\infty} G(i)\, z^{-i} \right| = 0 \; ; \qquad \ldots.(7.21)$$

and so, the largest power of z in the discriminant polynomial, $\hat{D}_g(z)$, must necessarily be z^0. Furthermore, the coefficient of the z^0-term can be identified simply by setting $z^{-1} = 0$. When this is done, eqn 7.21 reduces to the characteristic equation defining the eigenvalues of G(0) (i.e. $|gI - G(0)| = 0$). Hence, the coefficient of the z^0-term in $\hat{D}_g$ is equal to the discriminant, D_0, of the polynomial defined by $|gI - G(0)| = 0$. With this in mind, the following result can be developed:

Lemma 7.4: Let $\Delta(z,\hat{g})$ be irreducible and of degree m in $\hat{g}(z)$. Assume G(0) has distinct eigenvalues, and let p_0, p_1, and p_{-1} denote the number of pairs of complex conjugate eigenvalues of G(0), $\hat{G}(1)$, and $\hat{G}(-1)$ respectively. Then if p_0 is odd (even) and p_1 is even (odd), there is at least one zero of $\hat{D}_g$ in C_1. Similarly if p_0 is odd (even) and p_{-1} is even (odd), there is at least one zero of $\hat{D}_g$ in C_1.

Proof: Since D_0 is the coefficient of z^0 in $\hat{D}_g$, $\hat{D}_g$ can be written as:

$$\hat{D}_g(z) = z^{-k} \left\{ D_0\, z^k + \sum_{i=0}^{k-1} \gamma_i\, z^i \right\} \qquad \ldots.(7.22)$$

where k is always even and γ_i are appropriately-determined coefficients. Furthermore, $D_0 \neq 0$ since G(0) has distinct eigenvalues. So the existence of zeros of $\hat{D}_g$ in C_1 will be a function of the sign of D_0.

Consider first the case where p_0 is even. Since D_0 is the discriminant of the polynomial defined by $|gI - G(0)| = 0$, D_0 is positive if p_0 is even [BAR1]. Hence, by Jury's stability criterion [SAU1], $\hat{D}_g$ will have a zero in C_1 if $\hat{D}_g(1)$ is negative. But $\hat{D}_g(1)$ is negative if, and only if, p_1 is odd [BAR1]. Alternatively when p_0 is odd, D_0 is negative and Jury's criterion implies that $\hat{D}_g$ has a zero in C_1 if $-\hat{D}_g(1)$ is negative (i.e. $\hat{D}_g(1) > 0$). But $\hat{D}_g(1)$ is positive if, and only if, p_1 is even.

Since k (in eqn 7.22) is always even, similar arguments can be used

to construct the stated conditions for $\hat{G}(-1)$. ....QED

The conditions presented in Lemma 7.4 can be used to identify the existence of repeated values of $\hat{g}(z)$ for some z in C_1. Although branch points of $\hat{g}$ are (by Lemma 7.2 and Theorem 7.2) only a subset of the repeated values of $\hat{g}$, for all practical situations the two will be the same. As such, Lemma 7.4 highlights conditions which guarantee the existence of unstable branch points. [Note: Although this observation appears to diminish the importance of Lemma 7.2 and Theorem 7.2, it will be shown in the next section that these two earlier results can be used to predict situations in which the existence of unstable branch points is irrelevant.] Furthermore, the conditions of Lemma 7.4 can be refined as follows:

Theorem 7.4: Let $\Delta(z,\hat{g})$ be irreducible and of degree m in $\hat{g}(z)$, and let p_0, p_1, and p_{-1} denote the number of pairs of complex conjugate eigenvalues of G(0), $\hat{G}(1)$, and $\hat{G}(-1)$ respectively. Furthermore, assume that the real eigenvalues of $\hat{G}(1)$ and $\hat{G}(-1)$ are all distinct. Then, if $p_0 \neq p_1$ or $p_0 \neq p_{-1}$, unstable branch points must exist.

Proof: For the moment, assume that $\hat{g}$ has no branch points in C_1. Then by Theorem 7.1, the elements of each CWS must decay, and these elements can be related to $\hat{g}_i(z)$ by eqn 7.6a. Since $\hat{g}_i(z)$ is a branch of the characteristic gain function, $\hat{g}_i(1)$ is an eigenvalue of $\hat{G}(1)$. As a result, each eigenvalue of $\hat{G}(1)$ can be rewritten in the following way:

$$\hat{g}_i(1) = \sum_{j=0}^{\infty} g_i(j) \qquad \ldots.(7.23)$$

First, consider the case $p_0 < p_1$. This condition implies that there are more complex eigenvalues of $\hat{G}(1)$ than there are complex eigenvalues of G(0). But a review of the standard CSM algorithm in Appendix 7.1 suggests that the number of complex eigenvalues of G(0) is precisely the same as the number of complex CWS. As a result, the relationship imposed by the condition $p_0 < p_1$ suggests that a complex number (one of the eigenvalues

of $\hat{G}(1)$) is identically equal to an infinite sum of real numbers. Clearly this cannot be the case. So, the initial assumption that $\hat{g}(z)$ has no unstable branch points cannot be valid.

Next consider the case $p_0 > p_1$ (i.e. more complex CWS than complex eigenvalues of $\hat{G}(1)$). In this case, eqn 7.23 can only be satisfied if $\sum_{j=0}^{\infty} \text{Imag}\{g_i(j)\} = 0$ for some i. But, the standard CSM algorithm also suggests that complex CWS can only exist in complex conjugate pairs. So, $\sum_{j=0}^{\infty} \text{Imag}\{g_i(j)\} = 0$ necessarily implies that $\hat{G}(1)$ will have repeated real eigenvalues. But this result violates the assumption that the eigenvalues of $\hat{G}(1)$ are distinct. Thus the initial assumption that $\hat{g}(z)$ has no unstable branch points cannot be valid. Hence, unstable branch points must exist when $p_0 \neq p_1$.

Similar arguments will produce a corresponding result for $z = -1$ since

$$\hat{g}_i(-1) = \sum_{j=0}^{\infty} g_i(j)\,(-1)^j \qquad \text{....QED}$$

It must be pointed out that the conditions established by Theorem 7.4 are only sufficient. If $p_0 = p_1 = p_{-1}$, unstable branch points may still exist. However if either of the conditions, $p_0 \neq p_1$ or $p_0 \neq p_{-1}$, is satisfied, unstable branch points must exist. As a result, a quick assessment of potential convergence problems can be made prior to implementing the CSM algorithm.

One further condition for the existence of unstable branch points may be established by recognizing that the eigenvalues of $G(0)$ are the eigenvalues of $G(z)$ evaluated at $z^{-1} = 0$. This leads to the following result:

Theorem 7.5: For the case when $\Delta(z,g)$ is irreducible, $z^{-1} = 0$ will be a branch point of $g(z)$ if and only if $G(0)$ has repeated eigenvalues associated with a nonsimple Jordan form.

Proof: Since the eigenvalues of G(0) are also the eigenvalues of $\hat{G}(z)$ for $z^{-1} = 0$, this result follows immediately from Theorem 7.2.

....QED

7.3.2 Coping with Unstable Branch Points

Theorems 7.4 and 7.5 provide a means of recognizing many situations when the sequences generated by the standard CSM algorithm will not decay. For these cases, it may not be possible to obtain accurate, finite-dimensional z-domain representations for $\hat{g}_i$, $\hat{w}_i$, and $\hat{v}_i^t$ via truncation of the CWS and CVS. However, the requirement for stable branch points is not as restrictive as it may first appear. Indeed in many instances, appropriate finite-sequence representations may still be obtained in a straightforward manner. The procedures required to accomplish this task can be divided into three categories, each of which will be addressed separately in the following discussion.

Case 1: Latent ("Pseudo") Branch Points

As demonstrated by Lemma 7.2 and Theorem 7.2, repeated zeros, $\hat{g}_0$, of $\Delta(z_0,\hat{g})$ for $|z_0| \geq 1$ may not correspond to unstable branch points. Indeed, if z_0 is a repeated zero of $\Delta(z,\hat{g}_0)$ with the appropriate multiplicity, then z_0 is not a branch point. So, the convergence characteristics of the CWS and CVS will not be affected by its presence. This key characteristi also suggests that, under certain conditions, accurate sequence representations can still be obtained directly from the CSM algorithm despite the presence of unstable branch points.

In particular, the required conditions correspond to the situation when two unstable branch points, z_0 and z_1, lie sufficiently close to each other. This situation gives rise to branch points which are, in reality, only latent (or "pseudo") branch points in the sense that the effects of z_0 are nearly cancelled by those of z_1 (a phenomenon similar to that associated with pole/zero cancellations). The existence of these latent branch points can be identified by evaluating the discriminant polynomial of $\Delta(z,\hat{g}) = 0$

(defined for contant $\hat{g}$), $D_z(\hat{g})$, with $\hat{g}$ set equal to $\hat{g}_0$. If $D_z(\hat{g}_0)$ is sufficiently small, there must exist a point z_1 near z_0 which is also a zero of $\Delta(z,\hat{g})$. For this situation, there will be significant delays in the divergent effects of z_0 and z_1 on the elements of the CWS and CVS. As a result, the CSM algorithm will produce sequences which decay initially and which can be truncated to establish the desired finite-sequence representations. Of course, an upper limit on the length of the truncation is now dependent on the point at which the effects of the unstable branch points become apparent. However for z_0 and z_1 sufficiently close, extremely accurate representations will already have been obtained. Indeed, the example in Section 7.5.2 demonstrates the degree of accuracy which can be achieved in these situations.

Case 2: Discrete Fourier Transform (DFT) approximations

When the unstable branch points of $\hat{g}(z)$ are isolated however, their effects on the CWS and CVS will be immediate and significant. In these situations, the CSM algorithm cannot be used to obtain the desired sequence representations, but useful finite sequences can be obtained using a frequency-response-matching (or Discrete Fourier Transform, DFT) approach. For control design purposes, the desired sequences, ${}^{s}g_i$, ${}^{s}w_i$, ${}^{s}v_i^t$, must accurately describe the frequency response behaviour of the eigenvalues and eigenvectors of $\hat{G}(z)$. Viewed from this perspective, a realization of the appropriate sequence representations can be achieved using an inverse DFT approach as discussed in many digital signal processing texts (e.g. [BEL1]). A key element in the procedure proposed here is the use of the inverse DFT on the frequency-dependent eigenvalues and eigenvectors of $\hat{G}(z)$. An algorithm for calculating ${}^{s}g_i$ based on the eigenvalues of $\hat{G}(z)$ becomes:

Procedure 7.1:

(1) Select the number of sequence elements, N, appropriately large.

(2) Identify the eigenvalues of $\hat{G}(z)$, $\hat{g}_1(z)$, $\cdots$, $\hat{g}_m(z)$, at the N

values of z given by $z_i = \exp\{j(2\pi i/N)\}$, $i = 0, \cdots, N-1$.

(3) Form the matrix F and vectors $\{\hat{g}_i(z), i = 1, \cdots, m\}$ as shown here:

$$F = \begin{bmatrix} z_0^{-1} & \cdots & z_0^{-N} \\ z_1^{-1} & \cdots & z_1^{-N} \\ \cdot & & \cdot \\ \cdot & & \cdot \\ \cdot & & \cdot \\ z_{N-1}^{-1} & \cdots & z_{N-1}^{-N} \end{bmatrix} \qquad \hat{g}_i(z) = \begin{bmatrix} \hat{g}_i(z_0) \\ \hat{g}_i(z_1) \\ \vdots \\ \hat{g}_i(z_{N-1}) \end{bmatrix}$$

(4) Calculate the vectors $\{g_i, i = 1, \cdots, m\}$ containing the elements of ${}^{s}g_i$ using the relationship:

$$g_i = 1/N \; F^* \; \hat{g}_i(z) \qquad \ldots.(7.24)$$

where F^* is the complex conjugate transpose of F.

(5) Truncate the elements of each vector g_i appropriately to obtain the desired sequence representations.

Physical arguments associated with the frequency response characteristics of the quantities involved in Procedure 7.1 suggest that the sequences, ${}^{s}g_i$, calculated using this procedure can be truncated. In particular, when the vector g_i is calculated as shown in eqn 7.24, the phase characteristics of $\hat{g}_i(z)$ and the structural properties of the matrix F will combine to produce a sequence of elements which will, in general, decay. Indeed, observations of several examples indicate that, for systems with widely-separated unstable branch points, the sequences calculated using Procedure 7.1 do decay except for a small increasing "tail" over the last few elements. Hence for N sufficiently large, accurate truncations can be identified. As a result, although the elements of the true CWS cannot be truncated, the truncated sequences obtained from Procedure 7.1 will generally produce finite-series representations which accurately describe $\hat{g}_i(z)$.

The same technique can also be applied to obtain sequence representations for the characteristic and dual characteristic directions of $\hat{G}(z)$. It should be noted, though, that the eigenvectors, $\hat{w}_i(z)$, of $\hat{G}(z)$ are only unique to a scalar function of z; in other words, $\hat{w}_i(z) = \hat{f}(z)\,\hat{w}_i^*(z)$ where

$\hat{f}(z)$ is an arbitrary scalar function. Hence when the frequency-dependent eigenvectors of $\hat{G}(z)$ are evaluated, care must be taken to ensure that the same scaling is used at each value of z. (In practice, this simply requires normalizing the same element of each eigenvector to unity over all frequencies.) Once this is done, the frequency-dependent dual eigenvectors can be calculated using the relationship $\hat{V}(z) = \hat{W}^{-1}(z)$, and Procedure 7.1 can be implemented to identify appropriate sequence representations for $\hat{w}_i(z)$ and $\hat{v}_i^t(z)$. Indeed, an example is presented in Section 7.5.3 to demonstrate the accuracy of the representations that can be achieved using this approach.

Case 3: Constant Precompensation

The inverse DFT method outlined above will generally overcome the problem of unstable branch points to produce accurate finite sequence representations for the characteristic gains and directions. Of course, this solution relies on the time-consuming calculation of the eigenvalues and eigenvectors of $\hat{G}(z)$ at a large number of points on the unit circle and, hence, leads to a considerable increase in computational complexity when compared to the CSM algorithm. For this reason, the approach is much more appropriate for use in off-line design methodologies. In many situations however, the problem of unstable branch points can be solved without resorting to the inverse DFT method.

Consider for a moment, the multivariable control design problem from a practical perspective. An obvious goal of the design process is to produce a closed-loop system with acceptable transient and steady-state characteristics and low interaction. Hence, adequate compensation will, in general, attempt to produce a closed-loop system that is stable, near-diagonal, and minimum phase. When this is achieved, the z-domain characteristics of the eigenfunctions and diagonal elements of $\hat{R}(z)$ will tend to become the same, the only deviations arising from the small perturbations introduced by the off-diagonal elements of $\hat{R}(z)$.

Consequently, the closed-loop system will either have no unstable branch points or, at worst, unstable branch points (introduced by the off-diagonal perturbations) which are very close together. Since branch points of the open-loop and corresponding closed-loop system are identical, this suggests that adequate multivariable compensation will generally reposition unstable branch points to locations inside the unit circle (or, at worst, produce latent unstable branch points).

Based on these considerations, it seems reasonable to suggest that some simple form of precompensation can be used to reposition unstable branch points prior to implementing the CSM algorithm while, at the same time, taking a step toward achieving the closed-loop design objectives. Indeed, as demonstrated by example in Section 7.5.1, implementing constant alignment compensation to reduce high frequency interaction will, in many cases, accomplish this additional task. More sophisticated "branch-point placement" algorithms are also possible, although these have yet to be investigated in detail. Once appropriate precompensation has been introduced to eliminate unstable branch points, the CSM algorithm will produce CWS and CVS that can be used in multivariable control designs to meet desired stability margins and other performance objectives based on classical SISO design techniques. An appropriate methodology for implementing these compensators is discussed in the following section.

7.4 "Exactly" Commutative Control via Convolution

7.4.1 General Comments on Commutative Controllers

For discrete-time multivariable systems, the control design problem becomes one of selecting a (possibly dynamic) precompensator, $\hat{K}(z)$, so that the closed-loop system described by the transfer function matrix

$$\hat{R}(z) = \{I + \hat{G}(z)\,\hat{K}(z)\}^{-1}\,\hat{G}(z)\,\hat{K}(z) = \{I + \hat{Q}(z)\}^{-1}\,\hat{Q}(z) \quad \ldots.(7.25)$$

behaves in an appropriate manner. Returning to the frequency-domain approach implied by the characteristic locus method and discussed in Chapter

2, it can be seen that the properties of the closed-loop system above are directly related to the frequency-dependent eigenvalues and eigenvectors of the open-loop transfer function matrix, $\hat{Q}(z) = \hat{G}(z)\hat{K}(z)$. Thus, desired closed-loop response can be obtained by choosing $\hat{K}(z)$ to manipulate these quantities appropriately. In essence, the CLM reduces the multivariable design problem to a set of SISO problems without resorting to ad hoc attempts to diagonalize the plant. So, the ultimate design can, in fact, be based on classical frequency response techniques.

Unfortunately, the selection of $\hat{K}(z)$ is a rather challenging task because it is not generally possible to relate the eigenvalues and eigenvectors of $\hat{Q}$ to the individual eigenvalues and eigenvectors of $\hat{G}$ and $\hat{K}$ in a systematic manner. If, however, $\hat{G}$ and $\hat{K}$ share a common set of eigenvectors, the eigenvalues of $\hat{Q}$ are the products of the individual (corresponding) eigenvalues of $\hat{G}$ and $\hat{K}$ and direct compensation of each eigenvalue is possible. When $\hat{K}(z)$ is designed in this manner, $\hat{G}$ and $\hat{K}$ commute (i.e. $\hat{G}(z)\,\hat{K}(z) = \hat{K}(z)\,\hat{G}(z)$); so $\hat{K}(z)$ is often referred to as a commutative controller. But as implied by algebraic function theory, the functions $\hat{g}_i(z)$, $\hat{w}_i(z)$, and $\hat{v}_i^t(z)$ associated with $\hat{G}(z)$ are generally irrational functions of z and so it is not possible to construct a realizeable controller $\hat{K}(z)$ that commutes exactly with $\hat{G}(z)$ for all values of z. As a result, appropriate approximations for $\hat{W}(z)$ and $\hat{V}(z)$ must be generated to accomplish this design task.

In the past, the use of rational, s-domain (or z-domain) approximations for $\hat{W}$ and $\hat{V}$ has been rejected on the grounds that the increased complexity of the resulting controller produces unacceptable designs. So, past efforts have concentrated on producing constant approximations for $\hat{W}$ and $\hat{V}$ which are correct over limited frequency ranges [KOU1], [EDM1], [KOU3]. Clearly, the effectiveness of the resulting control designs depends on the accuracy of the approximation; but more importantly, the results obtained will only be valid over a narrow range of frequencies. As a result, the SISO design

methodology associated with the CLM becomes a more complex task requiring a combination of several frequency-dependent compensators. In addition, the specified modifications to the individual characteristic loci (required to achieve desired closed-loop characteristics) will only be accurately reproduced at frequencies where the constant approximation is accurate; a particularly significant restriction for systems with rapidly-changing frequency-dependent eigenvectors. As such, the use of constant approximations for $\hat{W}$ and $\hat{V}$ may significantly reduce the effectiveness of the resulting control design.

Until recently, concerns about design complexity have justified these constant approximations because the use of serial algorithms for compensator implementations translates complexity directly into excessive computation time. However with the rapid advances being made in Very Large Scale Integration (VLSI) technology and parallel processing algorithms (e.g. [KUN1] or [KUN2]), so-called increased complexity may no longer be a valid reason to resort to such simple approximations. Indeed, by discarding the standard perspective of implementing difference equation controllers and instead focusing on "convolution controller" implementations using the finite-series representations developed previously, the commutative controller problem can be reformulated as one that relies solely on parallel operations involving large-dimensioned matrices. Existing computer capabilities can then be used (at no extra computational expense) to produce nearly exact replicas of $\dot{W}$ and $\dot{V}$ over all frequencies. Under these circumstances, the control engineer will no longer be bound to eigenframe approximations at a single frequency or a limited set of frequencies and hence, modifications to the individual subsystems can be embedded within an "exactly" commutative controller design to establish a complete multivariable design methodology based solely on classical SISO frequency response methods. Two on line algorithms for implementing this controller are described below.

7.4.2 A Three-Stage Convolution Algorithm

Consider the standard closed-loop system shown in Figure 7.1. A three-term representation for a controller based on the CSM results described previously will consist of the following components: $\hat{W}_T(z)$, $\hat{V}_T(z)$, and $\hat{\Lambda}_K(z)$, where $\hat{W}_T(z)$ and $\hat{V}_T(z)$ are the truncated series representations of $\hat{W}$ and $\hat{V}$ (consisting of n_w and n_v terms respectively) and $\hat{\Lambda}_K(z)$ is a diagonal (difference equation) compensator designed to modify the individual characteristic loci based on classical frequency response considerations. For this situation, the compensated closed-loop system takes the form shown in Figure 7.2, and by examining the signals e, e_1, e_2, and u in more detail, an appropriate implementation algorithm can be established for this controller.

First, consider the transfer function $\hat{V}_T(z)$. By definition, $\hat{e}_1(z) = \hat{V}_T(z)\,\hat{e}(z)$, and the inverse z-transform of this relationship yields the convolution relationship ${}^s e_1 = {}^s V_T * {}^s e$. Hence, on-line calculation of the sequence ${}^s e_1$ simply requires:

(i) the (possibly parallel) implementation of a series of matrix-vector multiplications given by:

$$e_1(k) = \sum_{j=0}^{n_v-1} V_T(j)\, e(k-j) \qquad \ldots.(7.26)$$

(ii) storage of the n_v elements of ${}^s V_T$ and the last n_v elements of ${}^s e$.

Similar relationships hold for $\hat{W}_T(z)$ yielding the following relationship between the controller output, u, and e_2:

$$u(k) = \sum_{j=0}^{n_w-1} W_T(j)\, e_2(k-j) \qquad \ldots.(7.27)$$

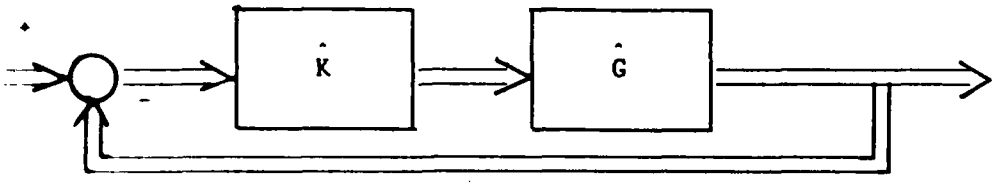

Figure 7.1: Standard Closed-Loop Configuration

Finally, the implementation of the diagonal controller can be accomplished via standard SISO difference equations. More specifically, if the i^{th} diagonal element of $\dot{\Lambda}_K(z)$ is given by:

$$\dot{\Lambda}_{K_{ii}}(z) = \frac{n_i(z)}{d_i(z)} = \frac{\sum_{j=0}^{p_i} n_i(j)\, z^{-j}}{\sum_{j=0}^{q_i} d_i(j)\, z^{-j}}$$

with $d_i(0) = 1$, then the time domain relationship between the i^{th} element of e_1 and the i^{th} element of e_2 is:

$$e_{2_i}(k) = \sum_{j=0}^{p_i-1} n_i(j)\, e_{1_i}(k-j) - \sum_{j=1}^{q_i} d_i(j)\, e_{2_i}(k-j) \qquad \ldots\ldots(7.28)$$

The control algorithm described above can clearly be performed in three distinct stages; the first and last involving n_v and n_v matrix vector multiplications respectively and the second involving only scalar multiplications. In addition, the calculations required at each stage can be performed using appropriate convolutions. Thus, parallel processing can be applied not only to each individual matrix-vector multiplication but also to the entire convolution summation. Using VLSI technology, the resulting algorithm should, therefore, yield a computationally-efficient parallel implementation. Furthermore, when n_u and n_v are small (as has been observed for a large number of systems), serial implementations will also yield adequate results. These observations suggest that the algorithm highlighted above can be applied on-line to a wide variety of multivariable systems.

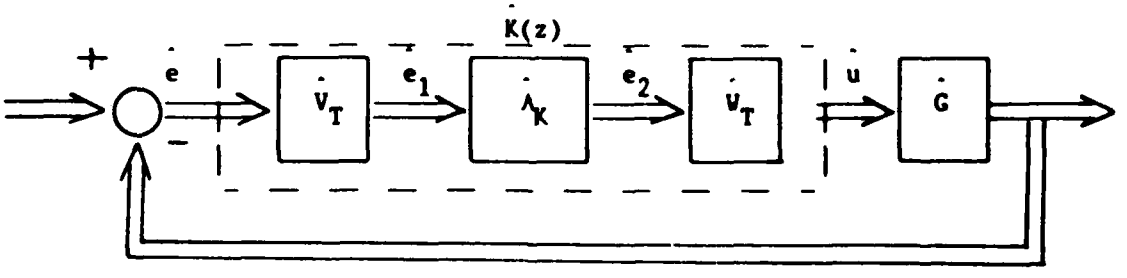

Figure 7.2: Closed-Loop Configuration for Three-Stage Convolution Control

7.4.3 A Single Stage Convolution Algorithm

Although many of the calculations in the three-stage algorithm can be performed simultaneously, the existence of three separate stages suggests that some amount of serial computation is still required, and this leads to an increase in the overall computation time associated with each controller output. If the diagonal controller $\Lambda_K(z)$ is viewed from a different perspective however, many of the remaining serial calculations can be eliminated and on line implementations can be speeded up still further.

To establish this alternative algorithm, consider the following. If $\Lambda_K(z)$ is stable, it too can be written as an infinite power series with decaying coefficients. In this case, the complete compensator $\dot{K}$ can be expressed in sequence form as:

$$^{S}K = {}^{S}W_T * {}^{S}\Lambda_K * {}^{S}V_T$$

Since all three sequences on the right hand side decay, the elements of ^{S}K must do the same. Thus, K(z) can be accurately approximated by a truncated power series (with n_k terms); and its output at sample k will be given by:

$$u(k) = \sum_{j=0}^{n_k - 1} K(j)\, e(k-j) \qquad \ldots.(7.29)$$

On line calculation of the control signal now involves only a single set of matrix vector multiplications instead of the three-stage calculation suggested previously.

Of course, a single stage implementation requires $^{S}\Lambda_K$ to be a decaying sequence which implies that $\Lambda_K(z)$ cannot include integral action. If integral action is desired, a diagonal compensator of the form

$$\dot{K}_I(z) = \dot{f}(z)\, I \quad \text{where} \quad \dot{f}(z) = \frac{z - z_1}{z - 1} \qquad \ldots.(7.30)$$

can be inserted into the forward loop without changing any of the other compensator terms, and the simple form of this additional compensator ensures that any increase in computation time is negligible. It should be noted that the use of scalar integral control as suggested by eqn 7.30 places absolutely no restrictions on the final design. Indeed, all other

characteristic locus modifications (such as gain balancing) can be achieved through the appropriate selection of $\dot{\Lambda}_K$. Furthermore, if integral control is not required in all loops, $\dot{\Lambda}_K$ can be adjusted to selectively eliminate the integral action in the loops which do not require it. Thus, the desired controller can be implemented as shown in Figure 7.3.

7.4.4 Additional Truncation Considerations

For the implementations suggested above, the truncation levels n_v, n_w, and/or n_k become design variables to be selected by the control engineer. Of course, the primary goal in the selection of n_v and n_w is to achieve accurate approximations for the eigenvector and dual eigenvector functions of the open-loop plant. But additional truncation level constraints will be imposed by the computation times required to generate the compensator output u (for serial implementations) or the hardware required to store the sequence parameters (for parallel implementations). As discussed in Section 7.2.3, accurate eigenframe representations can typically be achieved with truncations that are much smaller than those associated with ${}^{S}\Lambda$ or ${}^{S}G$. So in most cases, these additional constraints will not play a significant role in the selection or accuracy of the desired compensator.

It should, however, be noted that further reductions in n_v and n_w may be possible depending on the nature of the resulting closed-loop system. As is clearly evident in the single-stage algorithm above, $\dot{W}_T(z)$ and $\dot{V}_T(z)$ are primarily required to alter the transient response of the closed-loop system. As a result, the settling time achieved in the ultimate closed-loop

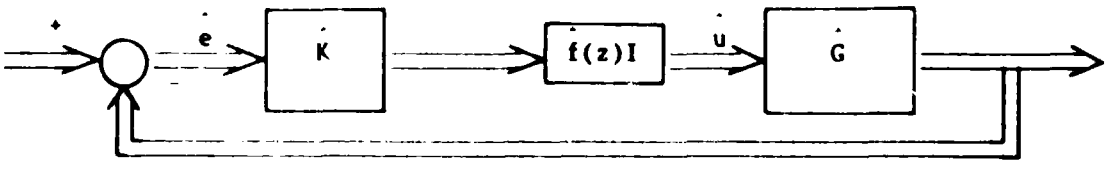

Figure 7.3: Closed-Loop Configuration for Single Stage Convolution Control

design may be used as a guide to reducing these truncation levels further. To see this more clearly, consider the situation where the desired settling time of the controlled plant is pT. It is easy to show that system response for $T \leq t \leq pT$ to a pulse at time zero is completely specified by the first p elements of the weighting sequences ${}^{S}V$, ${}^{S}W$, ${}^{S}\Lambda_K$, and ${}^{S}G$. Since all transient behaviour dies out by t = pT, the compensator sequence ${}^{S}K$ need not have more than p elements and, because ${}^{S}K = {}^{S}W * {}^{S}\Lambda * {}^{S}V$, this condition implies that the individual sequences themselves need not have more than p elements. Thus depending on the final closed-loop design, the computation time requirements (for serial implementations) or the storage requirements (for parallel implementations) may be reduced still further, based on these practical considerations, to guarantee timely on-line results.

7.5 Simulation Results and Discussion

7.5.1 Design Results using Characteristic Subsystem Descriptions

A two-input/two-output discrete-time system described by the transfer function matrix

$$\hat{G}(z) = \begin{bmatrix} \dfrac{.75(z^3+.27z^2-.39z-.08)}{z^4-1.33z^3+.11z^2+.29z-.03} & \dfrac{-.29(z^3-.40z^2-1.07z-.16)}{z^4-1.22z^3-.09z^2+.34z} \\ \dfrac{-.21(z^3+.07z^2-1.34z-.62)}{z^4-1.65z^3+.52z^2+.26z-.11} & \dfrac{.57(z^3+.78z^2-.26z-.23)}{z^4-1.14z^3-.30z^2+.57z-.09} \end{bmatrix} \quad \ldots\ldots(7.31)$$

was used to demonstrate the design methodology proposed in this chapter. An examination of the characteristic loci and the alignment between the characteristic directions and the standard basis vectors for this system indicated the existence of extremely poor stability margins and significant interaction effects, and these conditions are validated by the closed-loop step responses shown in Figure 7.4. These results clearly demonstrate the need for compensation to achieve adequate closed-loop response.

The design of an appropriate multivariable compensator for this system was accomplished in two steps. First, a constant precompensator, K_h, was

identified to align the characteristic directions to the standard basis vectors at high frequencies and, hence, to eliminate high frequency interaction. Using the ALIGN algorithm [KOU1], K_h was selected so that $G(z^*)\, K_h = I$ at $z^* = \exp(j\frac{\pi}{2})$ (i.e. $\omega T = 90^o$). The resulting precompensator is given by:

$$K_h \quad \begin{bmatrix} 2.305 & 1.068 \\ 1.382 & 2.559 \end{bmatrix}, \qquad \ldots\ldots(7.32)$$

and its implementation produced misalignment angles of less than 12^o over the frequency range $90^o \leq \omega T \leq 180^o$ as compared to misalignment angles of 15^o to 45^o for the original system. It should also be noted that the implementation of K_h not only achieved the desired alignment characteristics, but it also repositioned the two unstable branch points ($z = 1.31$ and $z = 1.308$) of $G(z)$. In fact, the magnitude of each of the 30 branch points of GK_h was less than 0.92. As a result, the CSM algorithm was implemented for the system $G(z)\, K_h$ to produce CVS and CVS whose elements decay. These sequences are displayed in Figs 7.5 through 7.7.

With series representations for $\bar{V}(z)$ and $\bar{V}(z)$ available, the second

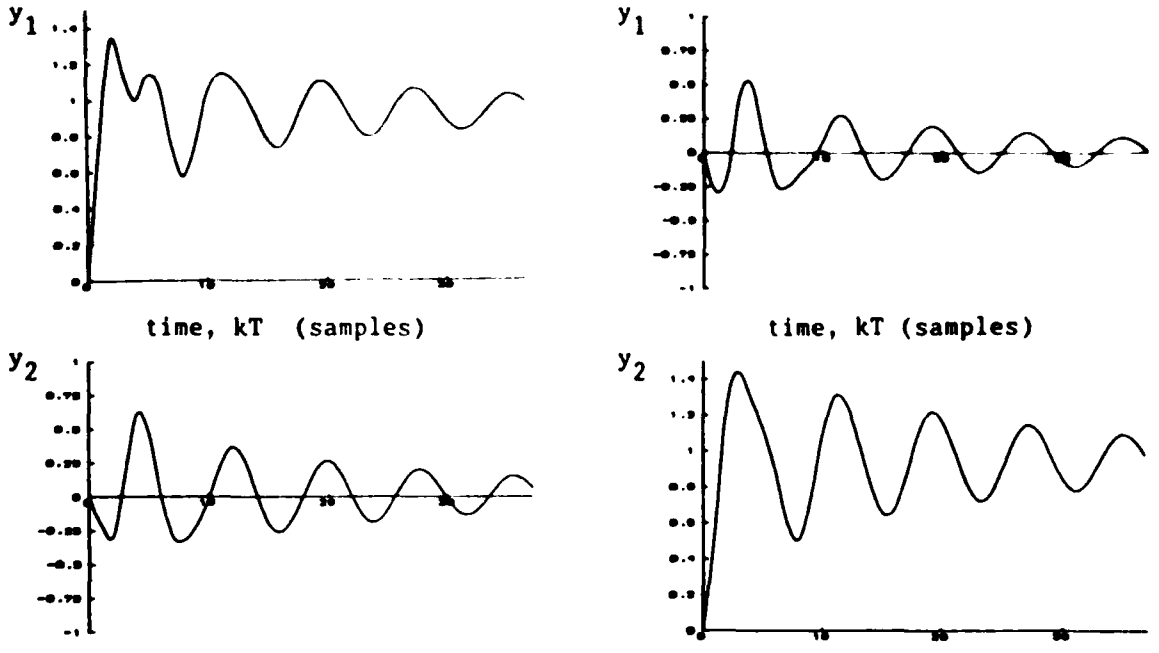

a) unit step; input 1 b) unit step; input 2

Figure 7.4: Time Response of the Uncompensated Closed-Loop System

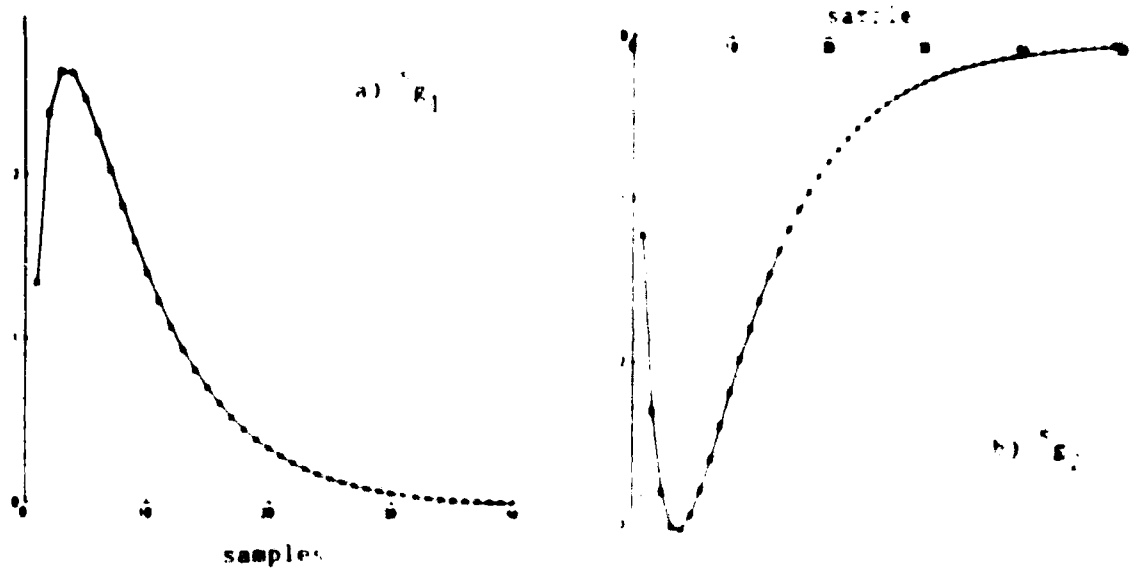

Figure 7.5: Open Loop Characteristic Weighting Sequences

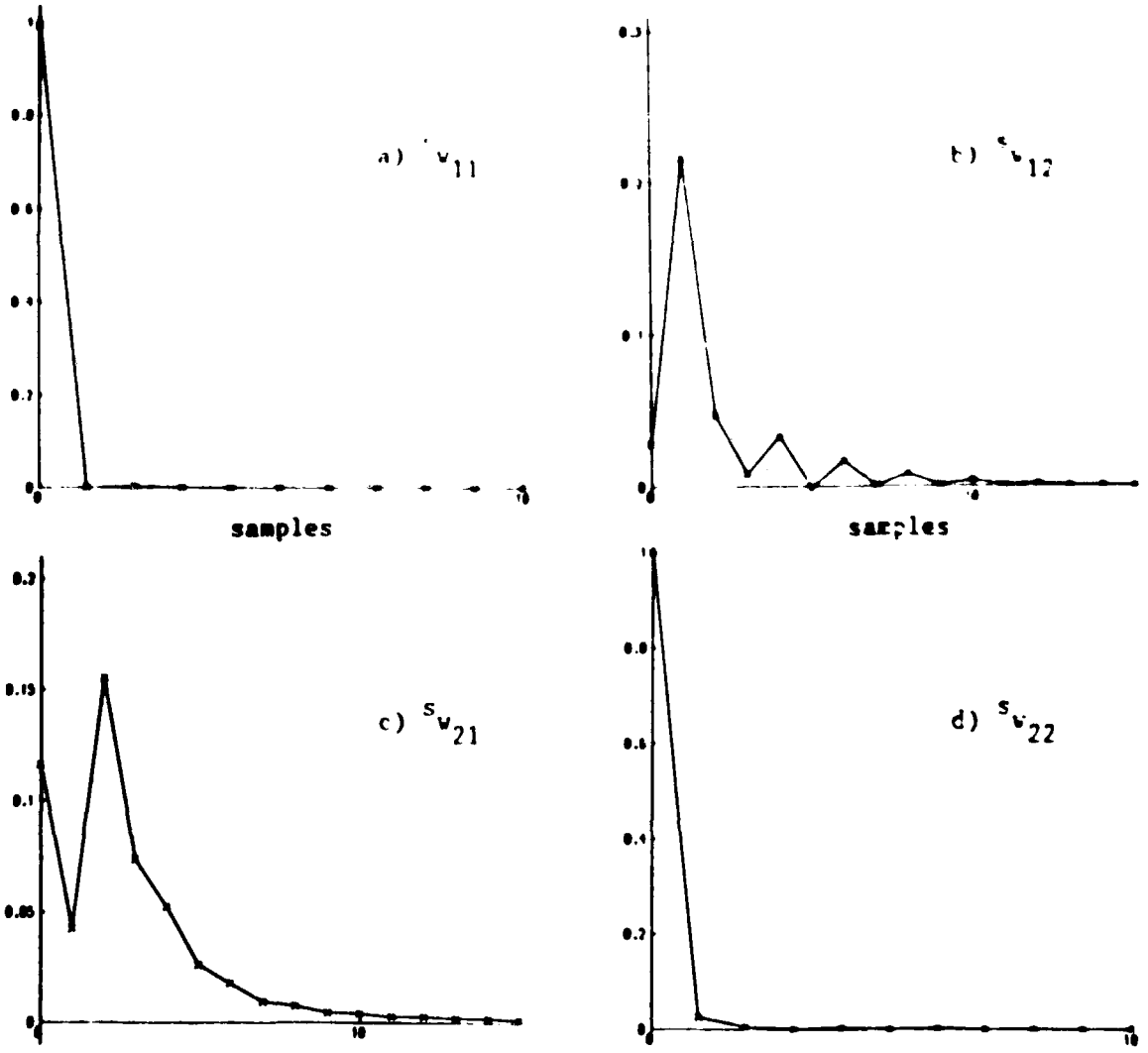

Figure 7.6: Open-Loop Characteristic Vector Sequences

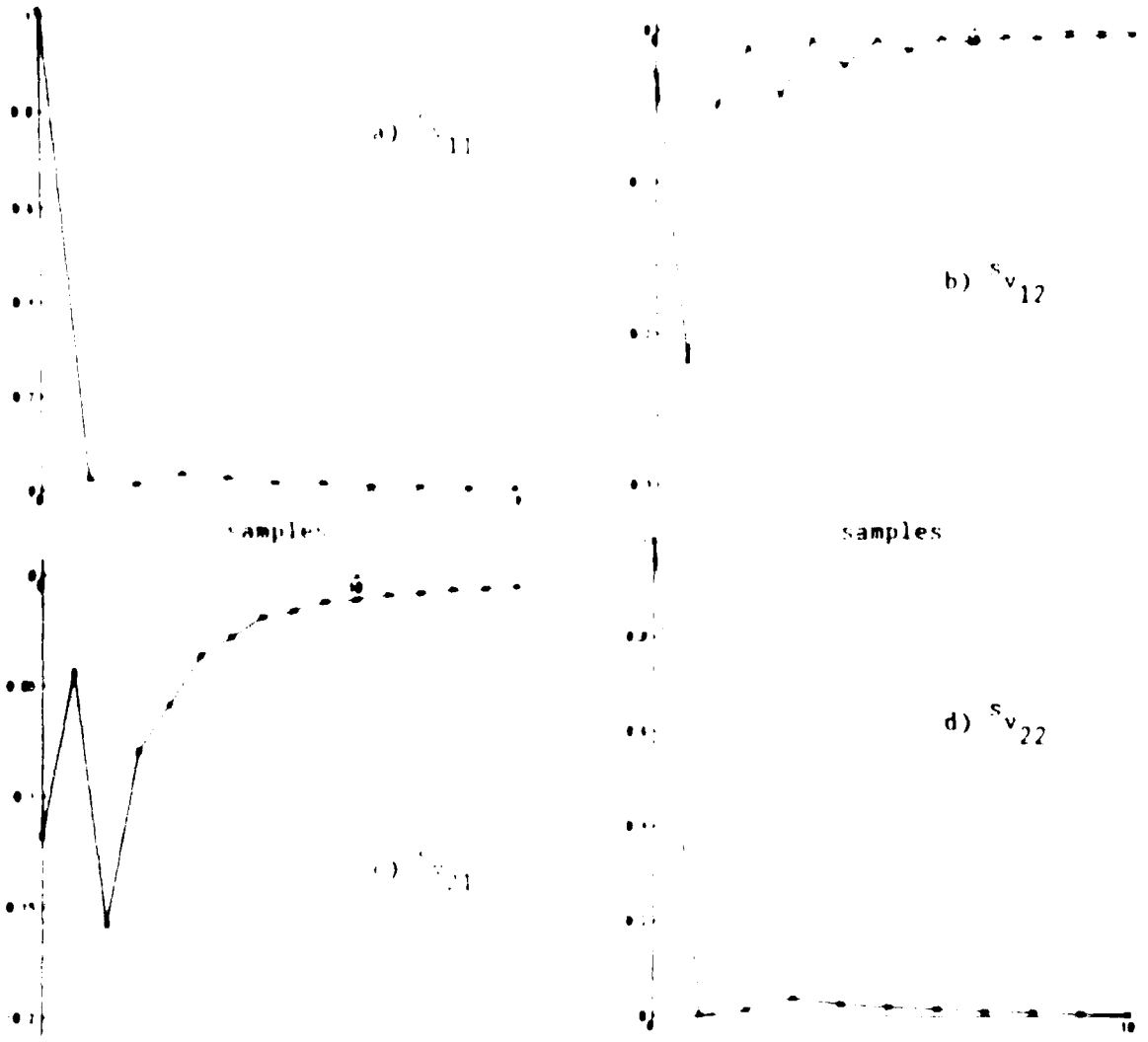

Figure 7.7: Open Loop Dual Characteristic Vector Sequences

step of the compensator design process focused strictly on modifying the two individual characteristic loci to obtain desired stability margins in each loop. This was accomplished using classical SISO frequency response methods, and the following diagonal compensator was identified:

$$\hat{\Lambda}_k(z) = \begin{bmatrix} .2 & 0 \\ 0 & \dfrac{.256\ (z - .686)}{(z - .364)} \end{bmatrix} \qquad ....(7.33)$$

where the negative gain in loop 2 was required simply to reorient the characteristic locus associated with this loop. $\hat{\Lambda}_k(z)$ was then combined with 5-term series representations for the characteristic and dual characteristic directions (obtained from the CVS and dual CVS) to establish the desired commutative controller, $\hat{K}(z) = \hat{W}_T(z)\ \hat{\Lambda}_k(z)\ \hat{V}_T(z)$. [The characteristic loci of the system before and after the introduction of $\hat{K}(z)$

are presented for comparison in Figure 7.8. [A more detailed comparison will be discussed shortly.] The complete dynamic compensator (defined by $\hat{K}(z)$) was then implemented using a three stage algorithm. In addition, a scalar integral compensator

$$\hat{K}_I(z) \qquad \frac{1.05\,(z \quad .01)}{(z \quad 1)}\, I$$

was added to the design to eliminate steady state errors. The resulting closed loop step responses are displayed in Figure 7.9 and, as desired, acceptable transient response has been obtained, steady-state error has been eliminated, and interaction is negligible.

To highlight the accuracy of the finite series implementation suggested here, the characteristic loci of the compensated system, $\{GK_h\}\{W_T \hat{\Lambda}_K V_T\}$, were compared to the desired characteristic loci (defined by the diagonal matrix $\{\Lambda_{GK_h} \quad \hat{\Lambda}_K\}$). The results of this comparison over the entire frequency range ($0 \leq \omega T \leq \pi$) are presented in Figure 7.10 as percentage differences between the actual and desired for three different truncation levels. As expected, the level of truncation selected has a significant effect on the accuracy of the approximation. However, reasonable truncations (in this case, 5 to 10 terms) do produce extremely accurate results over all frequencies. Figure 7.10 also presents results obtained by implementing $\hat{\Lambda}_K(z)$ using an an approximately commutative controller (ACC). For this study, the ACC was designed (using standard techniques [MAC3]) to achieve commutativity at the gain crossover frequency ($\omega T = 33^o$) and produced a controller of the form $\hat{K}(z) = W_A \hat{\Lambda}_k(z) V_A$, where W_A and V_A are the constant approximations obtained for $\hat{W}(z)$ and $\hat{V}(z)$ at $\omega T = 33^o$ and are given by:

$$W_A = \begin{bmatrix} 0.9879 & 0.1985 \\ 0.1173 & 1.0370 \end{bmatrix} \qquad V_A = \begin{bmatrix} 1.0360 & -0.1983 \\ -0.1172 & 0.9869 \end{bmatrix}$$

This additional information demonstrates that each of the three convolution controllers performed significantly better than the ACC over all frequencies including the frequency where the ACC was designed to perform best.

The conclusions that can be drawn from these simulation results are

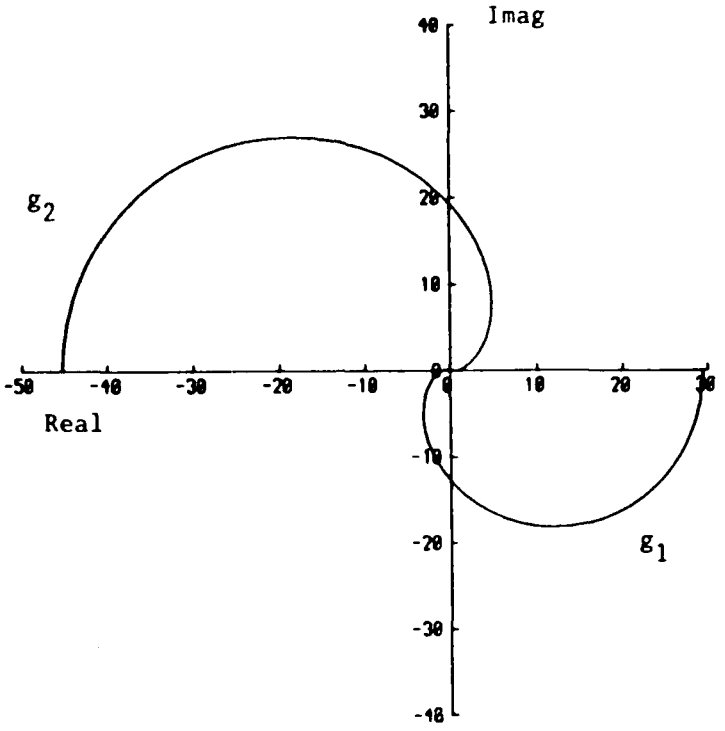

a) Characteristic Loci of $\dot{G}K_h$

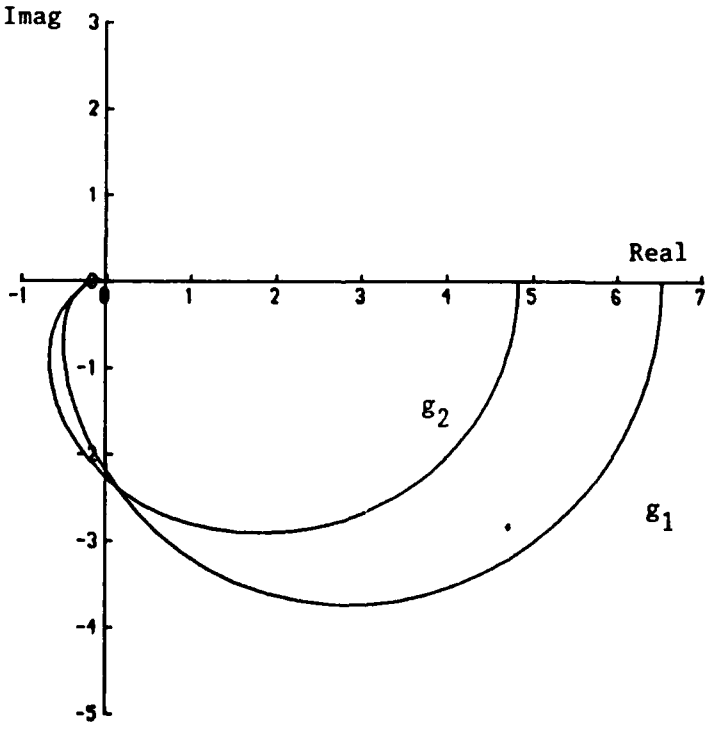

b) Characteristic Loci of $\dot{G}K_h\dot{K}$

Figure 7.8: Open-Loop Characteristic Loci

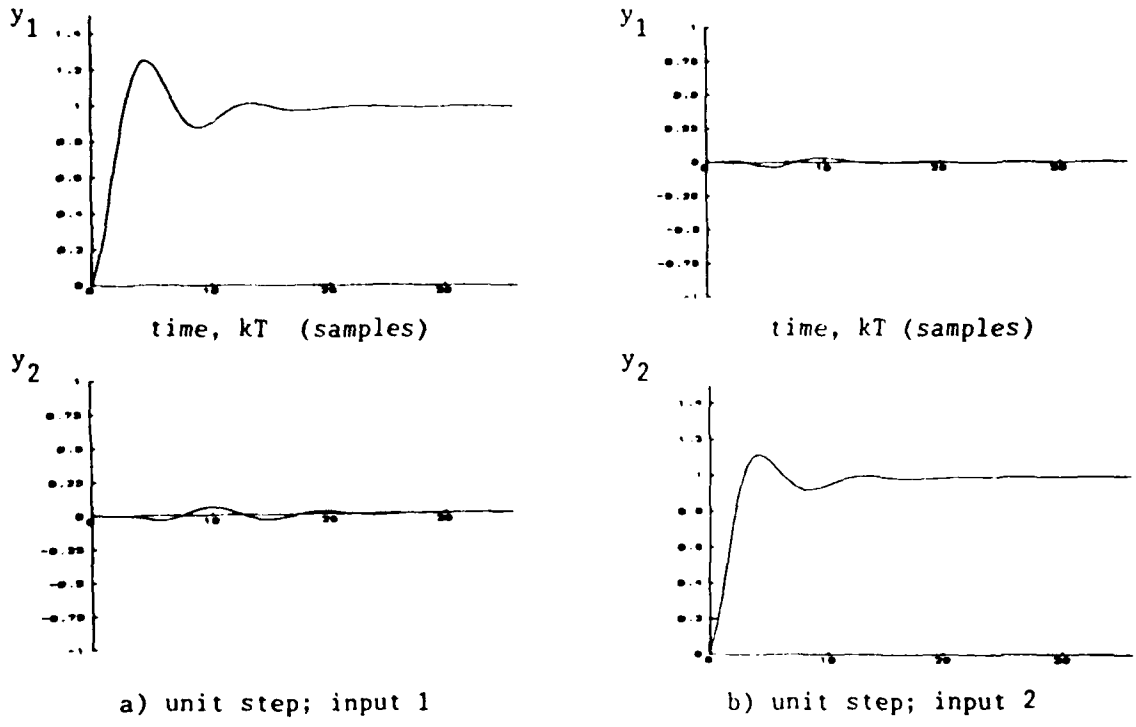

a) unit step; input 1 b) unit step; input 2

Figure 7.9: Time Response of Compensated Closed-Loop System

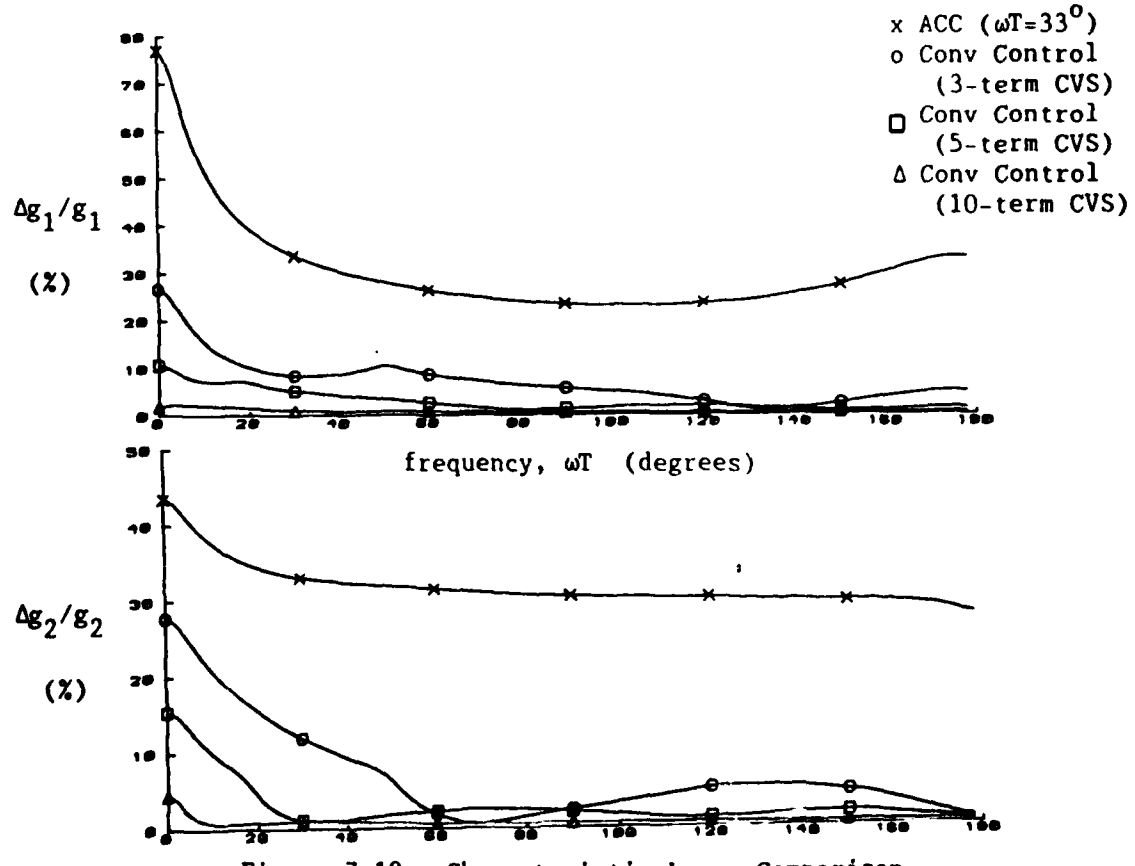

Figure 7.10: Characteristic Locus Comparison (Stable Branch Point Example)

clear. Reasonable truncations of the CVS and dual CVS produce extremely accurate approximations for the characteristic directions of the system. Indeed, as shown in Figure 7.10, the differences for 5- and 10 term truncations are negligible. As a result, "exactly" commutative controllers can be designed using the characteristic subsystem representations described in this chapter, and modifications to the characteristic loci of the system (as prescribed by a classical SISO analysis) can be achieved simultaneously over all frequencies using a single compensator design.

7.5.2 A Latent Branch Point Example

The case of latent unstable branch points described in Section 7.3.2 was also investigated via simulation. As mentioned above, $\dot{G}(z)$ (given by eqn 7.31) has branch points at $z = 1.31$ and $z = 1.308$. The proximity of these branch points to one another, however, suggests that their effects on the CWS and CVS will be significantly delayed, and so the CSM algorithm should produce sequences which decay initially. Indeed, for this example, the effects of these latent unstable branch points did not become noticeable until after the tenth terms in ${}^{S}W$ and ${}^{S}V$. In fact, an element-by-element comparison of the sixth terms is ${}^{S}W$ and ${}^{S}V$ to the first (and largest) terms in these sequences is presented in Table 7.1 and clearly demonstrates that accurate 5-term sequence representations for $\dot{W}$ and $\dot{V}$ were available.

A convolution controller was implemented using these 5-term sequence representations together with the following diagonal compensator:

$$\dot{\Lambda}_k(z) = \begin{bmatrix} .62 & 0 \\ 0 & \dfrac{1.93\ (z - .63)}{(z + .0855)} \end{bmatrix}$$

For purposes of comparison, an ACC was designed using the same diagonal compensator and the following constant precompensators:

$$W_A = \begin{bmatrix} 0.7499 & 0.6 \\ -0.6358 & 0.8547 \end{bmatrix} \qquad V_A = \begin{bmatrix} 0.8359 & -0.5869 \\ 0.6218 & 0.7334 \end{bmatrix}$$

(where W_A and V_A were selected to approximate $\dot{W}$ and $\dot{V}$ at the gain crossover frequency, $\omega T = 55^{\circ}$). Figure 7.11 presents the percentage error between the

Element	$\left\lvert \frac{w_{ij}(5)}{w_{ij}(0)} \right\rvert$	$\left\lvert \frac{v_{ij}(5)}{v_{ij}(0)} \right\rvert$
11	.003	.004
12	.002	.003
21	.007	.008
22	.001	.002

Table 7.1: A Comparison of the Elements of ^{5}W and ^{5}V

actual compensated characteristic loci and the desired characteristic loci for these implementations. Again, the results clearly demonstrate the effectiveness of convolution implementations to achieve "exactly" commutative control. Furthermore, they suggest that the CSM algorithm can, indeed, be implemented to produce useful finite-sequence representations in the presence of unstable, but latent, branch points.

It should be noted that the accuracy of any given finite-sequence

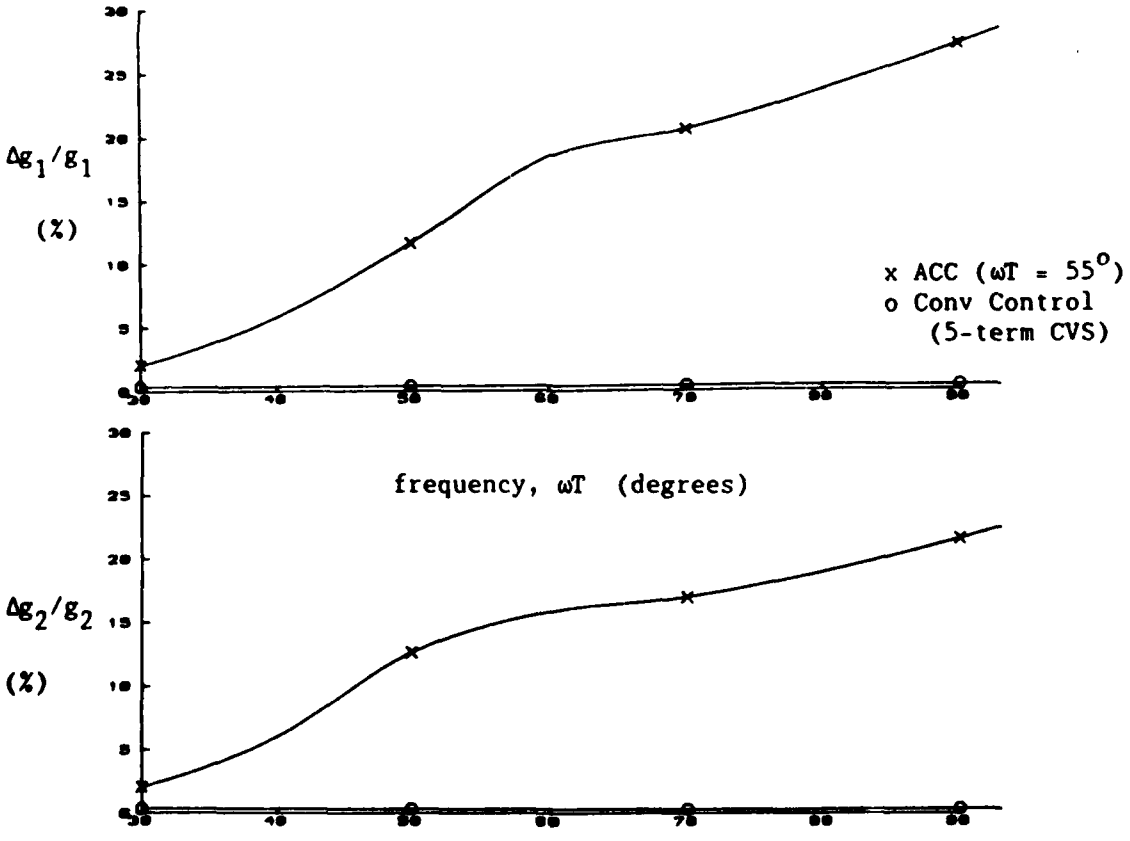

Figure 7.11: Characteristic Locus Comparison
(Latent Branch Point Example)

implementation is strongly influenced by the characteristics of the original system. As such, it is not generally possible to draw conclusions from a comparison of results for different systems. Thus, although the convolution controller designed for this latent branch point example appears to be more accurate than the controller for the example in Section 7.5.1, one must not conclude that the introduction of latent unstable branch points is a good thing to do. Indeed, in the absence of unstable branch points, the CVS and dual CVS will decay, and this guarantees that more accurate approximations can be obtained simply by increasing the number of terms in the truncated sequences, a procedure that cannot be used when latent unstable branch points exist.

7.5.3 Design Results using DFT Approximations

A final simulation was conducted to demonstrate the use of the finite sequences obtained using the inverse DFT approach described in Section 7.3.2. The system used for this study was obtained by combining $\hat{G}(z)$ (eqn 7.31) with the constant precompensator $S = \begin{bmatrix} 1.095 & .568 \\ .183 & 1.085 \end{bmatrix}$ (where S was selected solely to generate widely-separated unstable branch points). The new transfer function matrix, $\hat{G}_1 = \hat{G}\,S$, was found to have unstable branch points at $z = 10.4$ and $z = 1.8$ and, as expected, the CSM algorithm produced sequences which diverge immediately.

The inverse DFT algorithm was, therefore, implemented with N = 180 to generate appropriate sequence representations for the eigenvectors and dual eigenvectors of $\hat{G}_1$. As mentioned previously, appropriate scaling of the frequency-dependent eigenvectors must be accomplished prior to implementing the algorithm. So for this case, the diagonal elements of $\hat{W}(z)$ were normalized to unity at each frequency, and $\hat{V}(z) = \hat{W}^{-1}(z)$ was then computed. Using the resulting frequency-dependent information, sequence representations of the form:

AD-A186 086 A WEIGHTING SEQUENCE APPROACH TO THE ANALYSIS AND DESIGN OF MULTIVARIABLE CONTROL SYSTEMS(U) AIR FORCE INST OF TECH WRIGHT-PATTERSON AFB OH D J CLOUD 1987 3/3

UNCLASSIFIED AFIT/CI/NR-87-131D F/G 12/4 NL

END
DATE FILMED
1 88
DTIC

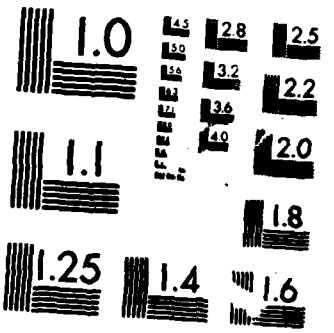

MICROCOPY RESOLUTION TEST CHART
NATIONAL BUREAU OF STANDARDS-1963-A

$$S_W = \begin{bmatrix} s_e & s_{w_{12}} \\ s_{w_{21}} & s_e \end{bmatrix} \qquad S_V = \begin{bmatrix} s_{v_{11}} & s_{v_{12}} \\ s_{v_{21}} & s_{v_{22}} \end{bmatrix}$$

were produced (as suggested by Procedure 7.1) where ${}^{s}e = \{1, 0, \cdots\}$ and the first six terms of the remaining sequences are listed in Table 7.2.

A convolution controller was then implemented using five-term approximations for $\hat{W}$ and $\hat{V}$ and the following diagonal compensator:

$$\hat{\Lambda}_k(z) = \begin{bmatrix} .81 & 0 \\ 0 & \dfrac{1.36\ (z - .63)}{(z + .0855)} \end{bmatrix}$$

For purposes of comparison, an ACC was designed using the same diagonal compensator and the following constant precompensators:

$$W_A = \begin{bmatrix} 1.0190 & 0.3117 \\ -0.6381 & 0.9096 \end{bmatrix} \qquad V_A = \begin{bmatrix} 0.8081 & -0.2769 \\ 0.5668 & 0.9051 \end{bmatrix}$$

(where W_A and V_A were selected to approximate $\hat{W}$ and $\hat{V}$ at the gain crossover frequency, $\omega T = 55^{o}$). Figure 7.12 presents the percentage difference between the actual compensated characteristic loci and the desired characteristic loci for these implementations. This comparison suggests that, although the improvements in accuracy are not as dramatic as seen previously, significant improvements may still be obtained over wide frequency ranges (including the frequency at which the ACC was designed to perform best) using the finite-sequence representations generated by the

k	${}^{s}w_{12}$	${}^{s}w_{21}$	${}^{s}v_{11}$	${}^{s}v_{12}$	${}^{s}v_{21}$	${}^{s}v_{22}$
0	0.2348	-.4128	0.8105	-.2041	0.2851	0.8105
1	-.1451	-.3725	-.0311	0.1141	0.2863	-.0311
2	-.0026	-.0020	0.0338	-.0056	0.0009	0.0338
3	0.0214	-.0304	-.0109	-.0153	0.0343	-.0109
4	-.0217	0.0159	0.0085	0.0171	-.0145	0.0085
5	0.0200	-.0053	-.0025	-.0192	0.0092	-.0025

Table 7.2: Elements of ${}^{s}W$ and ${}^{s}V$ obtained form Inverse DFT Algorithm

inverse DFT method. Hence in situations where unstable branch points cannot be avoided by precompensation, it is still possible to obtain accurate convolution controllers.

The design methodology described and demonstrated in this chapter offers the exciting potential to produce an entire range of multivariable algorithms which take advantage of the tremendous computing powers currently being developed. Indeed, using this methodology, it should be possible to extend the concept of SISO expert system design based on frequency response information (e.g. [JAM1]) to multivariable problems. In addition, the methodology offers the potential for implementing multivariable self-tuning algorithms in a true generalized-Nyquist setting by combining system identification with either on-line frequency response design methods or existing SISO self-tuning design algorithms. One such algorithm is developed in the next chapter.

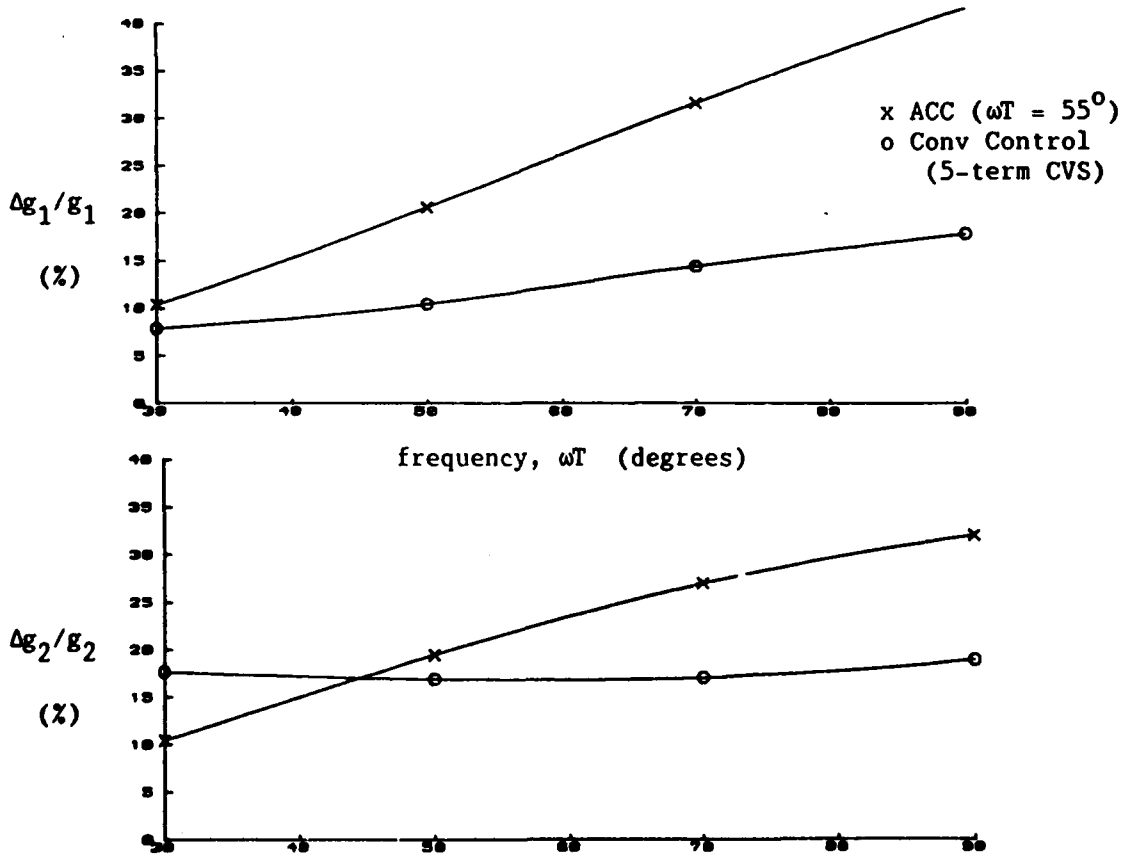

Figure 7.12 Characteristic Locus Comparison
(Unstable Branch Point Example)

Appendix 7.1: The Standard CSM Algorithm [KOU2]

Let $g_i(0)$ and $w_i(0)$ denote the i^{th} eigenvalue/eigenvector pair of G(0). To obtain the values of $g_i(k)$ and $w_i(k)$ for any $k > 0$, first form the matrix:

$$M(k) = G(k)\, W(0) + \sum_{j=1}^{k-1} [G(k-j)\, W(j) - W(j)\, \Lambda(k-j)] \quad ....(A7.1)$$

where $\Lambda(j) = \text{diag}\,[g_1(j), \cdots, g_m(j)]$, and

$W(j) = [\, w_1(j) \mid w_2(j) \mid \cdots \mid w_m(j)]$.

(Note: if k=1, the summation term in eqn A7.1 should be dropped.) Then, denoting the i^{th} column of M(k) by $m_i(k)$, calculate $g_i(k)$ and $w_i(k)$ using the relationships:

$$g_i(k) = v_i^t(0)\, m_i(k) \quad ....(A7.2a)$$

$$w_i(k) = T_i^{\dagger}(0)\, m_i(k) + \alpha_i(k)\, w_i(0) \quad ....(A7.2b)$$

where $\alpha_i(k)$ is an arbitrary constant (which, for convenience, may be set to zero) and $T_i^{\dagger}(0)$ is the commuting g_2-Penrose inverse of $[g_i(0)I - G(0)]$ given by:

$$T_i^{\dagger}(0) = \sum_{\substack{j=1 \\ j \neq i}}^{m} \frac{1}{g_i(0) - g_j(0)}\, w_j(0)\, v_j^t(0) \quad ....(A7.3)$$

Appendix 7.2: Modifications to the Standard CSM Algorithm

As suggested by the developments in Sections 7.1 and 7.2, situations do exist for which the standard CSM algorithm presented in Appendix 7.1 cannot be used to generate the CWS and CVS. In particular, the following three special situations may arise:

Case 1: G(0) (the first element of the plant weighting sequence) has repeated eigenvalues associated with a simple Jordan form;

Case 2: the characteristic polynomial $\Delta(z,\hat{g})$ is reducible to linear factors and $\hat{G}(z_0)$ has repeated eigenvalues associated with a nonsimple Jordan form for some $|z_0| \geq 1$ and $z_0^{-1} \neq 0$; and

Case 3: the characteristic polynomial $\Delta(z,\hat{g})$ is reducible to linear factors and G(0) (i.e. $\hat{G}(z_0^{-1}=0)$) has repeated eigenvalues associated with a nonsimple Jordan form.

In each instance, modifications to the standard CSM algorithm can be developed to generate appropriate sequence representations for $\hat{g}_i(z)$, $\hat{w}_i(z)$, and $\hat{v}_i^t(z)$. These modifications are derived below. It must, however, be stressed that the cases above rarely occur in practice and so the developments here are presented primarily for completeness.

Case 1: Simple, Repeated Eigenvalues of G(0)

When $\Delta(z,\hat{g})$ is irreducible and G(0) has repeated eigenvalues associated with a simple Jordan form, the standard CSM algorithm cannot be used to generate all of the CWS and CVS. Yet in the absence of unstable branch points, decaying sequences do exist (as suggested in Sections 7.2.2 and 7.2.3). So, an alternative algorithm must be developed to handle this special problem. Ray has examined a similar problem [RAY1]; however, his proposed modifications handle only the situation when $\Delta(z,\hat{g})$ is reducible to linear factors. For the more general case, the following modifications are required.

Since G(0) has simple, repeated eigenvalues, it can be written in the following form:

$$G(0) = W(0)\ \Lambda(0)\ V(0) \qquad \ldots.(A7.4)$$

where $\Lambda(0) = \text{diag}\ \{\lambda_1(0), \cdots, \lambda_1(0), \lambda_{p+1}(0), \cdots, \lambda_m(0)\}$; $p > 1$

$$W(0) = [\ W_p(0) \mid w_{p+1}(0) \mid \cdots \mid w_m(0)]$$

$$V(0) = [\ V_p(0) \mid v_{p+1}(0) \mid \cdots \mid v_m(0)]^T$$

and $W_p(0)$ and $V_p(0)$ are both dimensioned [m x p] and satisfy the equations:

$$\{\lambda_1(0)I - G(0)\}\ W_p(0) = 0 \qquad V_p^T(0)\ \{\lambda_1(0)I - G(0)\} = 0 \quad \ldots.(A7.5a,b)$$

$$V_p^T(0)\ W_p(0) = I \qquad \ldots.(A7.5c)$$

with rank $\{W_p(0)\}$ = rank $\{V_p(0)\}$ = p. The CWS and CVS associated with the

nonrepeated eigenvalues of G(0) can still be calculated using the standard CSM algorithm. However, modifications are required to calculate the CWS and CVS associated with the repeated eigenvalues. To begin, any vector of the form

$$w(0) = W_p(0)\, u(0) \qquad \ldots.(A7.6)$$

(where u(0) is an arbitrary vector of dimension p) satisfies eqn A7.5a. Now consider the CWS and CVS associated with one of the repeated eigenvalues, $\lambda_1(0)$. Let $w_i(0)$ denote the first element of this CVS and $\lambda_i(1)$ denote the second element of this CWS. Then from eqn A7.6, $w_i(0)$ can be written as:

$$w_i(0) = W_p(0)\, u_i(0) \qquad \ldots.(A7.7)$$

Substituting eqn A7.7 into the convolution equations defined by eqn 7.1 produces the following result at the second stage of the convolution:

$$G(1)\, W_p(0)\, u_i(0) + G(0)\, w_i(1) = \lambda_i(1)\, W_p(0)\, u_i(0) + \lambda_1(0)\, w_i(1) \qquad \ldots.(A7.8)$$

Multiplying by $V_p^T(0)$ then produces:

$$V_p^T(0)\, G(1)\, W_p(0)\, u_i(0) = \lambda_i(1)\, u_i(0) + V_p^T(0)\{\lambda_1(0)I - G(0)\}w_i(1) \qquad \ldots.(A7.9)$$

But $V_p^T(0)\, [\lambda_1(0)I - G(0)] = 0$, so eqn A7.9 reduces to:

$$\{V_p(0)\, G(1)\, W_p(0)\}\, u_i(0) = \lambda_i(1)\, u_i(0) \qquad \ldots.(A7.10)$$

Thus, $u_i(0)$ and $\lambda_i(1)$ are the eigenvectors and eigenvalues of $V_p^T(0)\, G(1)\, W_p(0)$, and $w_i(0)$ is uniquely determined by eqn A7.7. Once $w_i(0)$ is known for all i=1, $\cdots$,p, the standard CSM algorithm can be implemented without further changes to calculate the remaining terms in each of the p CWS and CVS provided the commuting g_2-Penrose inverse of $[\lambda_i(0)I - G(0)]$ for i=1, $\cdots$,p is calculated as:

$$[\lambda_i(0)I - G(0)]^{\#} = \sum_{j=p+1}^{m} \frac{w_j(0)\, v_j(0)}{\lambda_j(0) - \lambda_1(0)} \qquad \ldots.(A7.11)$$

Clearly if some of the eigenvalues of $V_p^T(0)\, G(1)\, W_p(0)$ are repeated and associated with a simple Jordan form, the above procedure can be reapplied at the next stage of the convolution to establish the desired unique representations for $w_i(0)$. It should be noted that this algorithm also applies when all of the eigenvalues of G(0) are repeated. In this situation

however, it can be simplified considerably since $W_p = V_p = I$. Hence, $w_i(0)$, $i=1, \cdots, m$ are simply the eigenvectors of $G(1)$.

Case 2: Nonsimple, Repeated Eigenvalues of $\hat{G}(z_0)$ $[z_0^{-1} \neq 0]$

A second situation for which the standard CSM algorithm cannot be applied is when $\Delta(z,\hat{g})$ is reducible to linear factors and $\hat{G}(z_0)$ has repeated eigenvalues associated with a nonsimple Jordan form for some $|z_0| \geq 1$. As discussed in Section 7.2.4, this situation implies that $\hat{W}(z)$ loses rank at z_0 and hence $\hat{V}(z)$ cannot be expanded in a power series with decaying coefficients. To overcome this problem, modified versions of the CWS can be used to obtain the desired sequence representations for ${}^{s}g_i$, ${}^{s}w_i$, and ${}^{s}v_i^t$.

For simplicity, the case where $\hat{G}(z_0)$ has a single repeated eigenvalue with multiplicity two will be considered. In this situation, the eigenvalue/eigenvector decomposition of $\hat{G}(z_0)$ is given by:

$$\hat{G}(z_0) = \hat{W}^*(z_0)\, \hat{J}(z_0)\, \hat{V}^*(z_0) \qquad \ldots.(A7.12)$$

where $\hat{W}^*(z_0)$ contains an appropriate pseudo-eigenvector so that $\hat{W}^*(z_0)$ and $\hat{V}^*(z_0)$ are full rank,

$$\hat{J}(z_0) = \begin{bmatrix} \hat{g}_1(z_0) & 1 & | & \\ 0 & \hat{g}_1(z_0) & | & 0 \\ - & - & - & - \\ & 0 & | & \hat{\Lambda}_{m-2}(z_0) \end{bmatrix}$$

and $$\hat{\Lambda}_{m-2}(z_0) = \text{diag}\,\{\hat{g}_3(z_0), \cdots, \hat{g}_m(z_0)\}.$$

From eqn A7.12, it is clear that the problem of $\hat{W}(z)$ losing rank at z_0 may be avoided simply by redefining the CWS to ensure that the resulting power series representation derived from the CWS contains a nonzero element in the appropriate off-diagonal position.

When $z_0^{-1} \neq 0$, $G(0)$ will, by assumption, have a simple Jordan form, and the desired modifications can be achieved by defining the CWS in the following way:

$${}^{s}\tilde{\Lambda} = \{\, \Lambda(0), J(1), \Lambda(2), \cdots, \Lambda(k), \cdots \} \qquad \ldots.(A7.13)$$

where $$\Lambda(k) = \text{diag}\,\{g_1(k), \cdots, g_m(k)\}$$

and $$J(1) = \Lambda(1) + \begin{bmatrix} 0 & 1 & | & 0 \\ 0 & 0 & | & \\ & & | & \\ 0 & & | & 0 \end{bmatrix}$$

With the modified CWS defined in this manner, $\hat{J}(z)$ can be written in power series form as:

$$\hat{J}(z) = \Lambda(0) + J(1)\, z^{-1} + \sum_{i=2}^{\infty} \Lambda(i)\, z^{-i} \qquad \ldots.(A7.14)$$

Hence, the diagonal elements of $\hat{J}(z)$ still represent the power series representations for the characteristic gains of $\hat{G}(z)$, while the nonzero off-diagonal term in $J(1)$ ensures that $\hat{J}(z_0)$ has a nonzero term in the appropriate off-diagonal position. As a result, $\hat{W}^*(z)$ will be full rank at z_0, and decaying sequence representations for both $\hat{W}^*$ and $\hat{V}^*$ can be obtained.

Since $\Lambda(0)$ in eqn A7.13 is identical to that used by the standard CSM algorithm, the initialization procedure for this modified algorithm will be exactly the same as that given in Appendix 7.1. Furthermore, the algorithm defined by eqns A7.1 and A7.2 can still be used to calculate $g_i(k)$ and $w_i^*(k)$ provided the following adjustment is made to the second column of the matrix M(k):

$$m_2'(k) = m_2(k) - w_1^*(k-1) \qquad \ldots.(A7.15)$$

This adjustment is required to ensure that the convolution relationship defined by eqn 7.1 remains valid for the modified CWS. Of course, the above results can also be extended to the problem of a repeated nonsimple eigenvalue of $\hat{G}(z_0)$ with multiplicity q. For this situation, the only required modifications to the standard algorithm are given by:

$$m_i'(k) = m_i(k) - w_{i-1}^*(k-1) \qquad \ldots.(A7.16)$$

The modifications identified above are not, however, adequate when $z_0^{-1} = 0$ (i.e. when G(0) has repeated, nonsimple eigenvalues) because the modified CWS defined by eqn A7.13 cannot account for the nonsimple Jordan structure of G(0). For this special situation, more complex modifications are required as described below.

Case 3: Nonsimple, Repeated Eigenvalues of G(0)

When $\Delta(z,\hat{g})$ is reducible to linear factors and G(0) has repeated eigenvalues associated with a nonsimple Jordan form, another modified version of the CSM algorithm can be established to produce the desired results by redefining the CWS in the following way:

$$^{s}\tilde{\Lambda} = \{ J(0), \Lambda(1), \Lambda(2), \cdots, \Lambda(k), \cdots \} \qquad \ldots.(A7.17)$$

where $\Lambda(k) = \text{diag}\,\{g_1(k), \cdots, g_m(k)\}$;

$$J(0) = \begin{bmatrix} g_1(0) & 1 & & \\ 0 & g_1(0) & & 0 \\ - & - & - & - \\ & 0 & & \Lambda_{m-2} \end{bmatrix};$$

and $\Lambda_{m-2}(0) = \text{diag}\,\{g_3(0), \cdots, g_m(0)\}$.

[Note: For simplicity, the problem of a single repeated eigenvalue with multiplicity two will again be highlighted, although the results can be extended to other situations.] Unfortunately, this new definition of the CWS suggests that the initialization procedures associated with the algorithm will be affected by the modifications. Therefore, a modified procedure must ensure not only that appropriate calculations are made at each step but also that an appropriate initialization procedure is defined.

For the CWS defined by eqn A7.17, G(0) can be rewritten as:

$$G(0) = W^{*}(0)\, J(0)\, V^{*}(0)$$

where $w_2^{*}(0)$ and $v_1^{*t}(0)$ are defined by:

$$G(0)\, w_2^{*}(0) = g_1(0)\, w_2^{*}(0) + w_1^{*}(0)$$

$$v_1^{*t}(0)\, G(0) = g_1(0)\, v_1^{*t}(0) + v_2^{*t}(0)$$

so that $W^{*}(0)$ and $V^{*}(0)$ are full rank, and the following convolution relationships can be established:

$$\sum_{i=0}^{k} G(k-i)\, W^{*}(i) = \sum_{i=0}^{k-1} W^{*}(i)\, \Lambda(k-i) + W^{*}(k)\, J(0) \qquad \ldots.(A7.18)$$

Thus, the standard CSM algorithm may still be used to calculate $^{s}g_i$ and $^{s}w_i^{*}$ for $i = 3, \cdots, m$, provided the appropriate generalized inverse (described

in [LI1]) is used. However, further modifications are required when computing ${}^{s}g_i$ and ${}^{s}w_i^*$ for i = 1, 2.

For further ease of presentation in the developments to follow, only the case where m = 2 will be considered. The set of equations defined by A7.18 then reduces to:

$$\sum_{i=0}^{k} G(k-i)\, w_1^*(k) = \sum_{i=0}^{k} g_1(k-i)\, w_1^*(k) \quad ; \quad k \geq 0 \qquad \ldots.(A7.19a)$$

$$\sum_{i=0}^{k} G(k-i) w_2^*(i) = \sum_{i=1}^{k} g_2(k-i) w_2^*(i) + g_1(0) w_2^*(k) + w_1^*(k); \; k \geq 0 \quad \ldots.(A7.19b)$$

Now, $g_1(0)$, $w_1^*(0)$, and $w_2^*(0)$ can be calculated using standard techniques on G(0). The problem of computing $g_1(1)$, $g_2(1)$, $w_1^*(1)$ and $w_2^*(1)$ can then be addressed by examining eqns A7.19a,b when k=1. In particular, multiplying through by $v_1^{*t}(0)$ and $v_2^{*t}(0)$, respectively, yields:

$$v_1^{*t}(0)\, G(1)\, w_1^*(0) + v_2^{*t}(0)\, w_1^*(1) = g_1(1) \qquad \ldots.(A7.20a)$$

$$v_1^{*t}(0)\, G(1)\, w_2^*(0) + v_2^{*t}(0)\, w_2^*(1) = v_2^{*t}(0)\, w_1^*(1) \qquad \ldots.(A7.20b)$$

$$v_2^{*t}(0)\, G(1)\, w_1^*(0) = 0 \qquad \ldots.(A7.20c)$$

$$v_2^{*t}(0)\, G(1)\, w_2^*(0) = g_2(1) + v_2^{*t}(0)\, w_1^*(1) \qquad \ldots.(A7.20d)$$

But these four equations generate only 3 constraints on the 4 desired unknowns. Eqn A7.20c simply implies that $w_1^*(0)$ is also an eigenvector of G(1). The necessary fourth constraint can, however, be obtained by proceeding to k = 2 and multiplying through eqn A7.19a by $v_2^{*t}(0)$ to produce:

$$v_2^{*t}(0)\, G(2)\, w_1^*(0) + v_2^{*t}(0)\, G(1)\, w_1^*(1) = g_1(1)\, \{v_2^{*t}(0)\, w_1^*(1)\} \qquad \ldots.(A7.21)$$

$g_1(1)$ and $w_1^*(1)$ can now be identified in the following manner. Since $w_1^*(0)$ and $w_2^*(0)$ span the two-dimensional space, $w_1^*(1)$ can be written as a linear combination of these vectors:

$$w_1^*(1) = \alpha_1(1)\, w_1^*(0) + \beta_1(1)\, w_2^*(0) \qquad \ldots.(A7.22)$$

Substituting this expression in eqns A7.20a and A7.21 generates the following equation for $\beta_1(1)$:

$$\beta_1^2(1) + \{v_1^{*t}(0)G(1)w_1^*(0) - v_2^{*t}(0)G(1)w_2^*(0)\}\beta_1(1) - v_2^{*t}(0)G(2)w_1^*(0) = 0 \quad \ldots (A7.23)$$

Once $\beta_1(1)$ has been computed, the remaining unknowns can be identified using eqns A7.20a,b,d. Notice that the value for $\alpha_1(1)$ in eqn A7.22 will not affect any of the other unknown quantities, and hence, can be arbitrarily specified (or, for convenience, set to zero). It is also important to note that both solutions for $\beta_1(1)$ identified by eqn A7.23 are valid. Since $g_2(0) = g_1(0)$, the selection of either solution will simply identify the two distinct sequences, ${}^s g_1$ and ${}^s g_2$.

Once $w_i(1)$ and $g_i(1)$ are known, the calculation of $w_i(k)$ and $g_i(k)$ for $i = 1, 2$ can be accomplished using the following procedures:

(1) Form $m_i(k)$ as defined by eqn A7.1.

(2) Form $\tilde{m}_i(k+1) = G(k+1)\, w_i^*(0) + G(k)\, w_i^*(1) + \sum_{j=2}^{k-1} G(k-j+1)\, w_i^*(j)$.

(3) Let $w_1^*(k) = \alpha_1(k)\, w_1^*(0) + \beta_1(k)\, w_2^*(0)$ where $\alpha_1(k)$ is arbitrary, $\beta_1(k)$ is defined by:

$$\beta_1(k) = \frac{1}{\{g_1(1)+\beta_1(1)-\lambda_2(1)\}} \{v_2^{*t}(0)\, \tilde{m}_1(k+1) - \beta_1(1)\, v_1^{*t}(0)\, m_1(k)\},$$

and $\lambda_2(1) = v_2^{*t}(0)\, G(1)\, w_2^*(0)$.

(4) Calculate $g_1(k)$, $g_2(k)$ and $w_2^*(k)$ using the following relationships:

$$g_1(k) = v_1^{*t}(0)\, m_1(k) + \beta_1(k)$$

$$g_2(k) = v_2^{*t}(0)\, m_2(k) - \beta_1(k)$$

$$w_2^*(k) = -w_2^*(0)\, v_1^{*t}(0)\, \{m_2(k) - w_1^*(k)\} + \alpha_2(k)\, w_1^*(0)$$

where $\alpha_2(k)$ is an arbitrary constant (which may, for convenience, be set to zero).

Although the above procedure highlights the development when $m = 2$, it can also be extended to higher dimensions. The details of these additional developments will not, however, be presented here.

CHAPTER EIGHT

A MULTIVARIABLE GENERALIZATION OF PREDICTIVE SELF-TUNING CONTROL

The characteristic subsystem decomposition developed and investigated in the previous chapter establishes an important link between the frequency-domain design of multivariable control systems and the time-domain implementation of the resulting design. As demonstrated in Sections 7.4 and 7.5, the subsystem representations can be used to simplify the off-line design of multivariable compensators significantly by completely reducing the multivariable control problem to a set of independent SISO problems. They also hold the key to the development of on-line, computer-implemented control algorithms which account for the multivariable nature of the system within a true generalized-Nyquist framework.

As highlighted in Chapter 1, a number of successful SISO control algorithms have been developed for use in on-line self-tuning applications where the resulting control law is combined with on-line identification of the model parameters of the plant. Each of these SISO algorithms relies on a system description that can be embedded in an on-line computer procedure to generate appropriate controller outputs. For SISO systems, such descriptions are readily available. However when MIMO systems are considered, the additional complexities introduced by the multivariable characteristics of the problem make the development of an appropriate description much more challenging. Indeed, past efforts have resorted to methods which either attempt to eliminate these multivariable characteristics completely by decoupling the dynamics of the open-loop system or, alternatively, consolidate the available multivariable information into a single scalar measure thereby addressing the fundamental problem of multivariable interaction in only an indirect manner. But now, with the characteristic subsystem descriptions developed previously, the multivariable problem can be decomposed into a set of independent SISO problems within a time-domain, rather than the more conventional frequency-domain,

setting. The result is a complete multivariable system description which can be used in conjunction with existing on-line SISO control algorithms to yield effective multivariable generalizations of these algorithms.

A particularly convenient SISO algorithm for this application is the Generalized Predictive Control (GPC) algorithm proposed by Clarke et al [CLA3], [CLA4]. Though based on a difference equation model of the plant, this algorithm relies on explicit knowledge of the first several elements of the corresponding weighting sequence to establish an optimal, on-line control law. This particular characteristic of SISO GPC provides an immediate and important link to the CWS that can be exploited when developing an implementable algorithm for multivariable systems.

The goal of this chapter is to integrate the SISO GPC approach into the characteristic subsystem framework and to demonstrate the utility of the resulting algorithm for self-tuning applications involving multivariable systems. The development begins by reformulating the GPC control law in terms of the characteristic subsystem descriptions developed in Chapter 7. The result is a predictive control law based on the identification of independent controls for each subsystem. Next, the self-tuning requirement for on-line identification of appropriate model parameters is addressed. It is suggested that standard identification algorithms can be combined with the standard CSM algorithm (Appendix 7.1) to obtain the required subsystem descriptions. However, more computationally-efficient algorithms for the direct identification of the subsystems are also proposed. Finally, a brief summary of the computational requirements of the algorithm is presented, and the chapter concludes with simulation results which demonstrate the effectiveness and flexibility of the proposed algorithm.

8.1 Long-Range Predictive Control Using Subsystem Descriptions

In this section, a multivariable generalization of SISO GPC will be developed using the characteristic subsystem descriptions developed

previously. Although a weighting sequence description of the plant is used in the initial development of the subsystem control laws (producing results with obvious connections to Dynamic Matrix Control [CUT1]), the results will also be extended to systems described by difference equation models. For this reason, attempts will be made (as far as possible throughout the development) to keep the notation consistent with that of the SISO GPC algorithm presented in [CLA3].

8.1.1 Plant Models and Output Prediction

Consider the multivariable system described by the input-output relationship

$$y(t) = \mathbf{G}\, u(t) + (1/\Delta)\, \xi(t) \qquad \ldots.(8.1)$$

where y, u, and ξ are [m x 1] output, input, and noise vectors respectively defined at time t, the elements of ξ are assumed to be uncorrelated with zero mean, **G** is a polynomial matrix in powers of z^{-1}, and $\Delta = 1 - z^{-1}$ is a scalar. [From this point forward, bold print will be used to denote operators on time-domain information.] As suggested in the previous chapter, **G** may be written in eigenvalue/eigenvector form as:

$$\mathbf{G} = \mathbf{W}\, \mathbf{\Lambda}\, \mathbf{V} \qquad \ldots.(8.2)$$

and since $\mathbf{V} = \mathbf{W}^{-1}$, premultiplication of eqn 8.1 by $\mathbf{V}\,\mathbf{\Delta}$ yields the modified input/output relationship:

$$\mathbf{\Delta}\, \tilde{y}(t) = \mathbf{\Lambda}\, \mathbf{\Delta}\, \tilde{u}(t) + \tilde{\xi}(t) \qquad \ldots.(8.3)$$

where $\tilde{y}(t) = \mathbf{V}\, y(t)$; $\tilde{u}(t) = \mathbf{V}\, u(t)$; $\tilde{\xi}(t) = \mathbf{V}\, \xi(t)$ ....(8.4)

In effect, this transformation constitutes a projection (in a "convolutional" sense) onto the eigenvector frame and reduces the multivariable description of the system to a set of m scalar models each described by a relationship of the form:

$$\mathbf{\Delta}\, \tilde{y}_i(t) = g_i\, \mathbf{\Delta}\, \tilde{u}_i(t) + \tilde{\xi}_i(t) \qquad \ldots.(8.5)$$

This set of subsystem descriptions provides the foundation for generalizing the SISO GPC algorithm to multivariable systems.

To establish the appropriate controls, consider first the problem of

predicting future system outputs. From eqn 8.3, the system outputs, referred to the eigenvector frame, at a time k samples in the future are given by:

$$\tilde{y}(t+k) = \tilde{y}(t+k-1) + \Lambda \Delta \tilde{u}(t+k) + V \xi(t+k) \quad \ldots.(8.6)$$

Now using similar relationships for $\tilde{y}(t+k-1)$, $\tilde{y}(t+k-2)$, $\cdots$, $\tilde{y}(t+1)$, eqn 8.6 can be rewritten as:

$$\tilde{y}(t+k) = \tilde{y}(t) + \left\{ \sum_{j=0}^{k-1} z^{-j} \right\} \Lambda \Delta \tilde{u}(t+k) + \left\{ \sum_{j=0}^{k-1} z^{-j} \right\} V \xi(t+k) \quad \ldots.(8.7)$$

By defining $\tilde{E}_k$ and $\tilde{N}_k$ as matrix series in powers of z^{-1} such that

$$\tilde{E}_k = \sum_{j=0}^{k-1} \tilde{E}_k(j)\, z^{-j} \quad \text{and} \quad \left\{ \sum_{j=0}^{k-1} z^{-j} \right\} V = \tilde{E}_k + z^{-k} \tilde{N}_k \quad \ldots.(8.8)$$

the portion of $\tilde{y}(t+k)$ due entirely to future values of noise can be isolated. The best available estimate of $\tilde{y}(t+k)$ at time t is, therefore, given by:

$$\tilde{y}(t+k|t) = \tilde{y}(t) + \left\{ \sum_{j=0}^{k-1} z^{-j} \right\} \Lambda \Delta \tilde{u}(t+k) + \tilde{N}_k \xi(t) \quad \ldots.(8.9)$$

Furthermore from eqn 8.1,

$$\xi(t) = \Delta y(t) - G \Delta u(t) = W \Delta \tilde{y}(t) + W \Lambda \Delta \tilde{u}(t) \quad \ldots.(8.10)$$

and this relationship can be introduced into eqn 8.9 to produce:

$$\tilde{y}(t+k|t) = \{I + \tilde{N}_k W \Delta\} \tilde{y}(t) + \left[\left\{ \sum_{j=0}^{k-1} z^{-j} \right\} V - z^{-k} \tilde{N}_k \right] W \Lambda \Delta \tilde{u}(t+k)$$

or, following the notation in [CLA3],

$$\tilde{y}(t+k|t) = \tilde{F}_k W \tilde{y}(t) + \tilde{G}_k' \Delta \tilde{u}(t+k) = \tilde{F}_k y(t) + \tilde{G}_k \Delta u(t+k) \quad \ldots.(8.11)$$

where $\tilde{F}_k = (V + \tilde{N}_k \Delta)$, $\tilde{G}_k' = \tilde{E}_k W \Lambda$, $\tilde{G}_k = \tilde{E}_k G$ $\quad \ldots.(8.12)$

Finally, eliminating $\tilde{N}_k$ from eqns 8.8 and 8.12 yields the Diophantine identity:

$$V = \tilde{E}_k \Delta + z^{-k} \tilde{F}_k \quad \ldots.(8.13)$$

from which $\tilde{F}_k$ and $\tilde{E}_k$ can be identified. For this eigenvector weighting sequence formulation of the problem, the solution of eqn 8.13 is given by:

$$\tilde{E}_k(j) = \sum_{i=0}^{j} V(i); \quad j = 0, \cdots, k-1$$

$$\tilde{F}_k(0) = \sum_{i=0}^{k} V(i) \qquad \tilde{F}_k(j) = V(j+k); \quad j > 0$$

Using the results above, it is easy to demonstrate that the first k elements of $\tilde{G}'_k$ are given by:

$$\tilde{G}'_k(j) = \sum_{i=1}^{j} \Lambda(i); \quad j = 1, \cdots, k \qquad \ldots.(8.14)$$

where $\Lambda(i)$ denotes the i^{th} element of ${}^{s}\Lambda$ (defined in Chapter 7). Since each term in eqn 8.14 is diagonal, eqn 8.11 indicates that each predicted subsystem output, $\{\tilde{y}_i(t+k|t);\ k > 0\}$, is directly related only to known quantities and to the unknown scalar inputs, $\{\tilde{u}_i(t+j);\ 0 \leq j < k\}$, associated with the same subsystem. Furthermore, the first k terms of $\Delta \tilde{G}'_k$ are given by:

$$\Delta\tilde{G}'_k(j) = \Lambda(j); \quad j = 1, \cdots, k \qquad \ldots.(8.15)$$

So, the relationship between $\tilde{y}_i(t+k|t)$ and $\{\tilde{u}_i(t+j);\ 0 \leq j < k\}$, is completely defined by the first k elements of the appropriate CWS. On this basis, the multivariable self-tuning control problem can be reduced to a set of scalar problems as shown in Figure 8.1, and a predictive control law for each scalar subsystem can be generated using the appropriate CWS. The result is a multivariable generalization of SISO predictive self-tuning control in a true, generalized-Nyquist framework.

Before proceeding to this control law development, it must be noted that the output predictions and Diophantine identity defined by eqns 8.11 and 8.13 were developed using a weighting sequence description of the system transfer function matrix. If instead, a difference equation model of the form:

$$\mathbf{A}\,\Delta\, y(t) = \mathbf{B}\,\Delta\, u(t) + \xi(t) \qquad \ldots.(8.16)$$

was assumed, the predicted outputs in the eigenvector frame would still satisfy the relationships defined by eqn 8.11 provided $\tilde{G}'_k = \tilde{E}_k \mathbf{A}\, \mathbf{V}\, \Lambda$, $\tilde{G}_k = \tilde{E}_k \mathbf{B}$ and $\tilde{E}_k$ and $\tilde{F}_k$ are defined by the modified Diophantine identity:

$$\mathbf{V} = \tilde{E}_k\, \mathbf{A}\, \Delta + z^{-k}\, \tilde{F}_k \qquad \ldots.(8.17)$$

Furthermore, $\tilde{y}_i(t+k|t)$ would still be directly related only to known quantities and to the unknown scalar inputs $\{\tilde{u}_i(t+j);\ 0 \leq j < k\}$. So, the multivariable control problem could still be reduced to m scalar problems.

8.1.2 The Predictive Control Law

Assuming that a sequence of future set point or reference vectors $\{c(t+k);\ k > 0\}$ are available, these quantities may be projected onto the eigenvector frame using the relationship

$$\tilde{c}(t+k) = V\, c(t+k) \qquad \ldots.(8.18)$$

to establish the scalar subsystem set point sequences, $\{\tilde{c}_i(t+k),\ k > 0\}$. Appropriate controls can then be identified separately for each individual subsystem using the basic GPC algorithm presented in [CLA3]. In particular, the future controls for the i^{th} subsystem can be chosen to minimize the cost function

$$J_i = E\{ \sum_{j=N_1}^{N_2} [\tilde{y}_i(t+j) - \tilde{c}_i(t+j)]^2 + \sum_{j=0}^{N_2-1} \rho_i(j)\, \Delta\tilde{u}_i^2(t+j)] \qquad \ldots.(8.19)$$

where N_1 is the minimum prediction horizon, N_2 is the maximum prediction horizon, $\rho_i(j)$ is a sequence of control weights (for simplicity in the

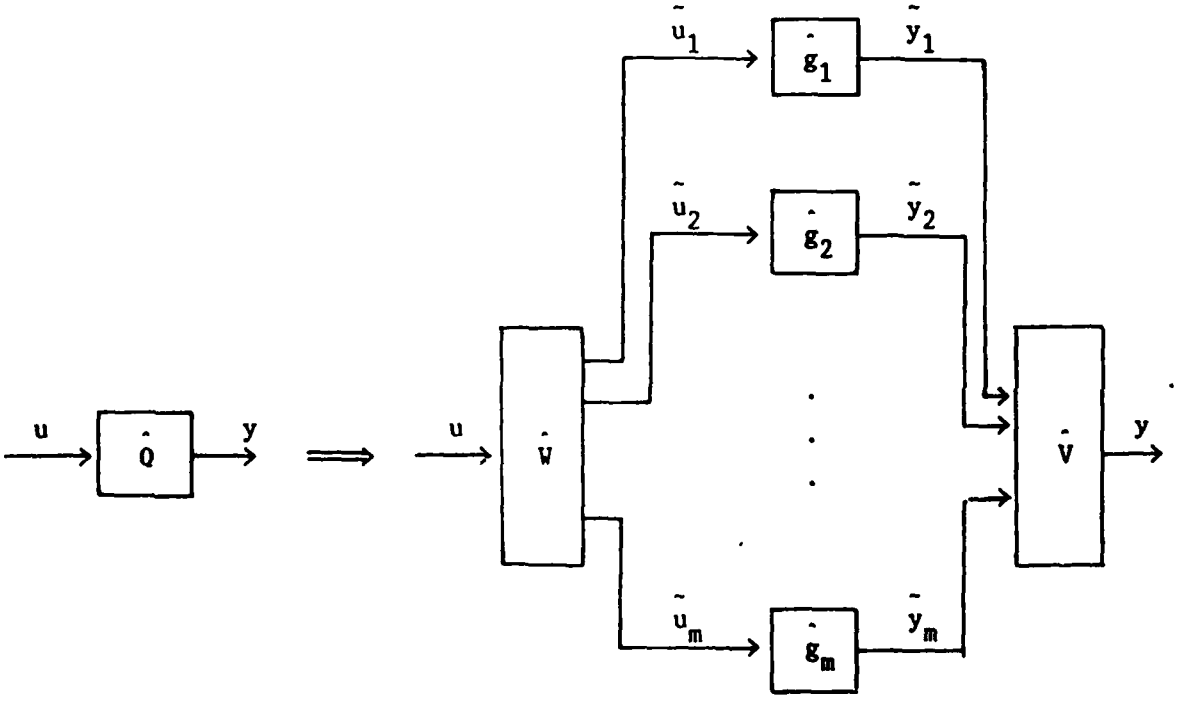

Figure 8.1: Characteristic Subsystem Description of a Multivariable Plant

following development, $\rho_i(j)$ will be assumed to be constant over all j and will be set equal to ρ_i), and the expectation in eqn 8.19 is conditioned on data up to time t assuming no future measurements are available. Using eqn 8.11, $\tilde{y}_i(t+k|t)$ can be written in terms of future inputs and known data as:

$$\tilde{y}_i(t+k|t) = \sum_{j=0}^{k-1} \bar{g}_i(k-j)\, \tilde{\Delta u}_i(t+j) + \tilde{r}_i(k) \qquad \ldots.(8.20)$$

where $$\bar{g}_i(k) = \sum_{j=1}^{k} g_i(j), \qquad \ldots.(8.21a)$$

$$\tilde{r}_i(k) = \tilde{f}_i^{k\,t}\, y(t) + \tilde{g}_i^{k\,t}\, \Delta u(t+k) - z^{k-1} \left\{ \left\{ \sum_{j=0}^{k-1} \bar{g}_i(j+1)\, z^{-j} \right\} \tilde{\Delta u}_i(t) \right\} \ldots.(8.21b)$$

and $\tilde{f}_i^{k\,t}$, $\tilde{g}_i^{k\,t}$ are the i^{th} row vectors of $\tilde{F}_k$ and $\tilde{G}_k$ respectively. [Note: The fact that the first k elements of $\tilde{G}_k'$ are diagonal has been used implicitly to establish the expressions for $\tilde{y}_i(t+k|t)$ and $\tilde{r}_i(k)$ given by eqns 8.20 and 8.21b, respectively.] From eqn 8.20, the predicted outputs $\tilde{y}_i(t+j|t)$ for $j = N_1, \cdots, N_2$ can now be written in vector form (with a slight abuse of notation) as:

$$\tilde{y}_i(N_1,N_2) = \bar{G}_i\, \tilde{\Delta u}_i + \tilde{r}_i \qquad \ldots.(8.22)$$

where $$\tilde{y}_i(N_1,N_2) = [\, \tilde{y}_i(t+N_1|t) \;\cdots\; \tilde{y}_i(t+N_2|t)\,]^t,$$

$$\tilde{\Delta u}_i = [\, \tilde{\Delta u}_i(t) \;\cdots\; \tilde{\Delta u}_i(t+N_2-1)\,]^t, \qquad \tilde{r}_i = [\, \tilde{r}_i(1) \;\cdots\; \tilde{r}_i(N_2)\,]^t$$

and $\bar{G}_i$ is a matrix of dimension $[(N_2 - N_1 + 1) \times N_2]$ given by:

$$\bar{G}_i = \begin{bmatrix} \bar{g}_i(N_1) & \cdots & \bar{g}_i(1) & & \\ \vdots & & & \ddots & 0 \\ \bar{g}_i(N_2) & \cdots & & & \bar{g}_i(1) \end{bmatrix}$$

J_i (defined by eqn 8.19) can now be written as:

$$J_i = \{ (\bar{G}_i\, \tilde{\Delta u}_i + \tilde{r}_i - \tilde{c}_i)^t\, (\bar{G}_i\, \tilde{\Delta u}_i + \tilde{r}_i - \tilde{c}_i) \} + \rho_i\, \tilde{\Delta u}_i^t\, \tilde{\Delta u}_i$$

where $\tilde{c}_i = [\tilde{c}_i(t+N_1) \cdots \tilde{c}_i(t+N_2)]^t$ is the vector of future set points for the specified subsystem, and minimizing J_i with respect to the vector $\tilde{\Delta u}_i$ (assuming no constraints on the future controls) generates the desired incremental control law given by:

$$\tilde{\Delta u}_i = \{ \bar{G}_i^T \bar{G}_i + \rho_i I \}^{-1} \bar{G}_i^T (\tilde{c}_i - \tilde{r}_i) \qquad \ldots.(8.23)$$

The current control increment for subsystem i ($\tilde{\Delta u}_i(t)$) is, then, the first element of the vector $\tilde{\Delta u}_i$.

8.1.3 Implementing the Control Law

An implementation diagram for the predictive control algorithm developed in the previous sections is displayed in Figure 8.2. As suggested by this diagram, the implementation can be conveniently separated into three distinct tasks:

(1) prediction of future subsystem outputs over the specified prediction horizons,

(2) identification of incremental controls for each subsystem, and

(3) transformation of the identified subsystem controls to produce the actual system controls (which are to be applied to the plant).

Assuming that **V**, **W**, and the CWS are available, each of these tasks can be summarized as follows:

Task 1: Subsystem Output Prediction

From eqn 8.23, it is clear that the first step in calculating the appropriate incremental controls is the identification of $\tilde{r}$, the vector of future output predictions based on past known input/output data. One method of generating this information is suggested by the previous discussion. In particular, the appropriate Diophantine identity (eqn 8.13 or 8.17) can be used to solve for $\tilde{E}_k$ and $\tilde{F}_k$. If a weighting sequence model is used, the solution (as mentioned previously) is obvious. If a difference equation model is used, a recursive algorithm based on a simple matrix extension of the scalar algorithm proposed in [CLA3] can be used to accomplish the task. Using $\tilde{E}_k$, $\tilde{F}_k$, and **G** (or **A**,**B**), the prediction of future subsystem outputs due to past available information can then be computed as shown in eqn 8.21b.

For presentation purposes, the use of Diophantine identities provides a convenient means of describing the relationship between future outputs and

past, present, and future information. In practice however, it is possible to predict the future outputs using an alternative and computationally more efficient procedure. Indeed, simulation techniques are typically used in the SISO GPC algorithm to generate this information, and the same approach can be extended to the multivariable problem. In the absence of information on the future noise, $\xi(t+k)$ can be assumed to be zero and system output at time t+k is described by:

$$y(t+k) = y(t+k-1) + G\,\Delta u(t+k) \qquad \ldots.(8.24a)$$

or

$$y(t+k) = y(t+k-1) + (I - A)\,\Delta y(t+k-1) + B\,\Delta u(t+k) \qquad \ldots.(8.24b)$$

Eqn 8.24 defines input/output relationships which can be used in a simulation algorithm (using available input/output information) to establish the desired output predictions in the plant frame. The corresponding eigenframe predictions can then be generated by transforming these plant-

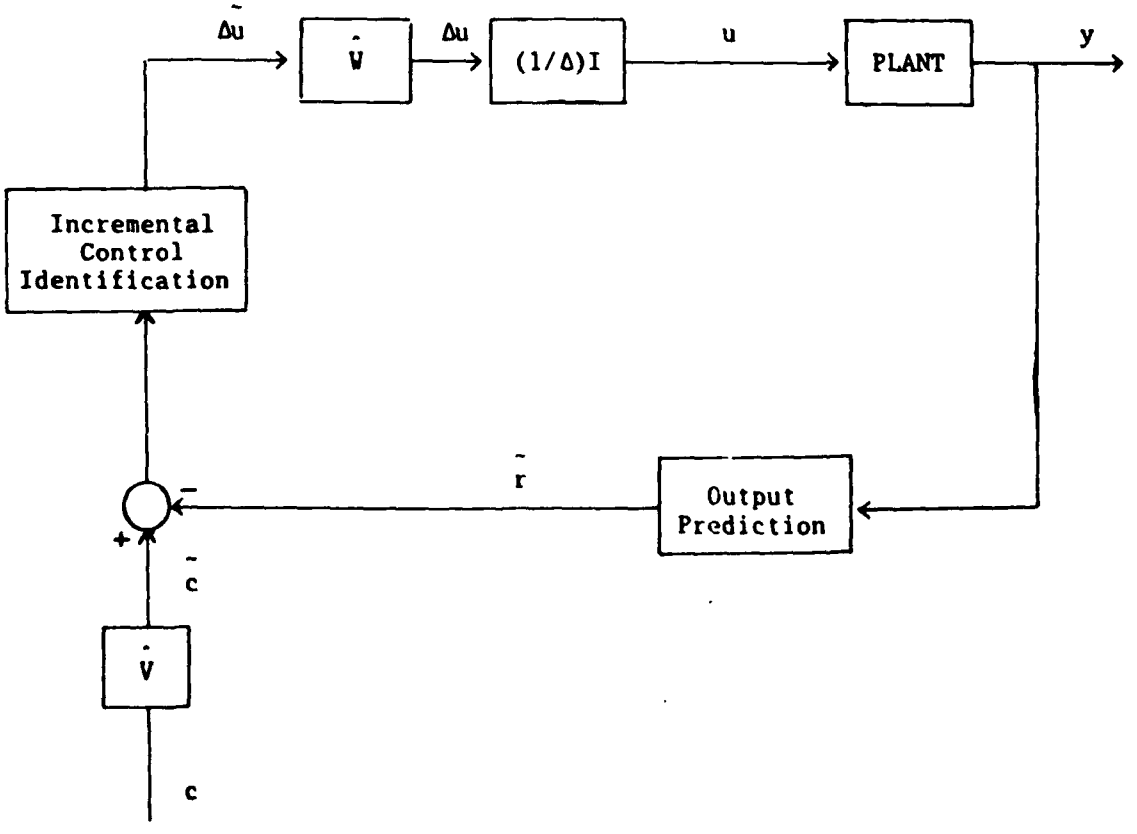

Figure 8.2: Implementation of the Multivariable Predictive Control Algorithm

frame predictions in a manner analogous to that for the set point information (eqn 8.18).

One further point concerning the computation of $\tilde{r}$ using simulation techniques (as suggested above) must also be highlighted. Since the proposed control law (eqn 8.23) is defined in the eigenvector frame, it must be assumed that future control increments in the eigenvector frame are zero. This does not imply that the corresponding future plant-frame control increments (used in eqn 8.21b or eqn 8.24) are zero. In fact, future plant-frame controls are defined by:

$$\Delta u(t+k) = W \tilde{\Delta u}(t+k) \; ; \; k \geq 0$$

and may be non-zero depending on the length of W and the value of k. These non-zero future control increments must be included in the calculation of $\tilde{r}$ (when using plant frame information) to obtain the proper results.

Task 2: Incremental Subsystem Control Identification

Using specified plant-frame reference signals, corresponding subsystem reference vectors, $\tilde{c}$, can be obtained by transforming the plant-frame signals as shown in eqn 8.18. The appropriate incremental control can then be calculated using $\tilde{c}$, $\tilde{r}$, and the control law described by eqn 8.23.

Task 3: Control Transformation and Application

The incremental subsystem controls generated by Task 2 at time t, $\{\tilde{\Delta u}_i(t); \; i=1, \cdots, m\}$, can be transformed into the plant frame using the vector relationship:

$$\Delta u(t) = W \tilde{\Delta u}(t) \qquad \ldots.(8.25)$$

where $\Delta u(t) = [\Delta u_1(t) \cdots \Delta u_m(t)]^t$ and $\tilde{\Delta u}(t) = [\tilde{\Delta u}_1(t) \cdots \tilde{\Delta u}_m(t)]^t$ denote the vectors of incremental controls in the plant and eigenvector frames respectively at time t. The control vector to be applied to the plant is, therefore, given by:

$$u(t) = u(t-1) + \Delta u(t) \qquad \ldots.(8.26)$$

As in the scalar case, the applied control includes integral action. It should also be noted that, for this implementation, the integral action is

brought specifically to a point past $\hat{W}$ to keep the length of the truncated sequences to a minimum.

The fundamental characteristic of the multivariable predictive control algorithm proposed above is that it provides independent control over each scalar characteristic subsystem of the plant. Indeed, the incremental control law for each subsystem (eqn 8.23) is identical to the scalar control law associated with SISO GPC. As a result, the user has precisely the same flexibility in the selection of control parameters for each subsystem as that available in the standard SISO GPC control algorithm. More specifically, minimum and maximum prediction horizons (N_1, N_2) and control horizons (N_u) can be selected independently for each subsystem using considerations similar to those presented in [CLA3] for the choice of these parameters. In addition, the refinements to SISO GPC identified in [CLA4] can also be applied independently to each subsystem. An important implication of the characteristic decomposition results presented in this chapter is, therefore, that the user can now implement direct control over each individual subsystem. In effect, the proposed algorithm establishes appropriate controls for each of the m loops of the multivariable system directly without regard to "correct" input/output pairings.

An assumption implicit throughout the development above is that effective loop-by-loop control of multivariable systems can be achieved via control of the characteristic subsystems. The validity of this assumption can be substantiated by returning to the characteristic locus framework from which the proposed algorithm was derived. Two points, in particular, must be highlighted. First, the analyticity of the $\hat{g}_i(z)$ implies a one-to-one correspondence between the closed-loop poles of the system and the proximity of the characteristic loci to the critical point (-1,0) in the complex plane. As a result, good subsystem performance (as defined by $\hat{g}_i$) implies and is implied by good loop performance.

Second, the difference between individual loop performance and corresponding subsystem performance may be quantified in terms of bounds that depend on the frequency-dependent eigenfunctions of the open-loop system and the angular misalignment between the frequency-dependent eigenvectors and the standard basis vectors [MAC1],[KOU8]. Furthermore, it can be shown that these bounds become negligible (and hence, the deviations between loop and subsystem performance become insignificant) as the closed-loop eigenfunctions become equal and/or the misalignment angles become small over the entire range of frequencies from 0 to π/T. At low frequencies, integral action ensures high open-loop gains in all loops, so that existing differences between the closed-loop eigenfunctions are necessarily small. Hence, the relative deviation between loop and subsystem performance for low frequency inputs is guaranteed to be small.

At high frequencies however, it is not generally possible to generate high gains because of stability considerations. At these frequencies therefore, alternative methods must be used to maintain small deviations between loop and subsystem performance. A useful solution to this problem is the introduction of precompensation which aligns the high-frequency eigenvectors of the closed-loop system to the standard basis vectors. Since the eigenvectors of the open- and closed-loop systems are the same, this task can be achieved using a constant real precompensator which accurately approximates the column structure of $\hat{G}^{-1}\{e^{j\omega T}\}$ at appropriately high frequencies. Indeed for discrete systems, a compensator of the form:

$$K_h = \hat{G}^{-1}\{e^{j\pi}\} = \hat{G}^{-1}(-1)$$

is a simple candidate since $\hat{G}(-1)$ will, in general, be invertible. In instances when $\hat{G}(-1)$ is rank deficient, application of the ALIGN algorithm [KOU1] at a slightly lower frequency will produce a suitable precompensator. Using this compensation, the angular misalignment between the high frequency eigenvectors and the standard basis vectors can be reduced significantly and, hence, the relative deviation between loop and subsystem performance

during fast transients will also be small. Furthermore, unless the system is characterized by rapidly changing eigenvectors (as might occur in systems where resonant phenomena are associated with individual inputs and/or outputs), the high and low frequency behaviour described above will carry over to intermediate frequencies ensuring small deviations over this range of frequencies as well. Thus for most practical problems, the deviation of loop performance from subsystem performance is guaranteed to be small for all inputs. This result, combined with the analyticity argument above, suggests that adequate loop-by-loop performance can indeed be successfully achieved via independent control of the individual characteristic subsystems.

Yet another argument that substantiates the close correlation between loop and subsystem performance is the following: uniform control design objectives (described by eqn 8.19) for the individual characteristic subsystems will produce subsystem controls (eqn 8.23) which tend to balance the eigenfunctions of the open-loop system and, hence, to match the closed-loop eigenfunctions. But matching the closed-loop eigenfunctions, as explained above, reduces the bound on the relative deviation between loop and subsystem performance. In many instances then, the desired correlation between loop and subsystem performance may be achieved simply by implementing the predictive control law of Section 8.1.2 without resorting to high frequency alignment compensation. Indeed, the simulation results presented in Section 8.6 demonstrate that low interaction can be achieved using the proposed algorithm without high frequency alignment compensation.

8.2 Indirect Identification of the CWS and CVS

As suggested above, the predictive control law defined by eqn 8.23 can be implemented in a nonadaptive manner using prior knowledge of the system transfer function matrix and, hence, the CWS, CVS, and dual CVS. However when on-line system identification is required for adaptive applications,

appropriate identification techniques must now include the ability to generate the required CWS and CVS information. As shown in this section and the next, there are two ways to accomplish this task.

The first alternative is to use existing recursive estimators to identify the open-loop system model and, then, to use the standard CSM algorithm described in Chapter 7 to generate the necessary elements of the CWS and CVS. It is important to note that the implementation of the standard CSM algorithm relies on the convolution relationship

$$s_G * s_{w_i} = s_{g_i} * s_{w_i}$$

Hence, a weighting sequence description of the open-loop plant must be available when using this algorithm. The elements of the desired weighting sequences can, in fact, be established in one of two ways.

First, $\hat{G}(z)$ may be parameterized as a finite weighting sequence of the form:

$$\hat{G}(z) = \sum_{i=1}^{N_G} G(i)\, z^{-i}$$

and standard recursive algorithms can be used to identify the elements directly. Alternatively, $\hat{G}(z)$ may be formulated in difference equation form as:

$$\hat{G}(z) = \hat{A}(z)^{-1}\, \hat{B}(z)$$

and, again, standard recursive estimators can be used to identify the polynomial matrices $\hat{A}$ and $\hat{B}$. When the difference equation formulation is used with the standard CSM algorithm, the required weighting sequence elements can be generated by simulating the system response for the model $\mathbf{A}\, y(t) = \mathbf{B}\, u(t)$ starting from zero initial conditions and applying an impulse to each of the inputs in turn. However, it should also be noted that, for difference equation models, a potentially more efficient algorithm for computing the CWS and CVS directly from $\hat{A}$ and $\hat{B}$ can be developed via an extension of the standard CSM algorithm. The fundamentals of this extension are highlighted in Appendix 8.1.

The selection of an appropriate multivariable model to accomplish the

tasks described above depends on a number of factors. Among the most important is the number of parameters to be estimated as this requirement directly affects the computation time associated with the identification algorithm. For multivariable systems, the number of model parameters required is a function of the number of poles associated with each individual element of $\hat{G}(z)$, the location of these poles, and the dimension of the system. So unlike the standard SISO problem, the lengths of $\hat{A}$ and $\hat{B}$ may, in certain cases, be comparable to the length of ${}^{s}G$. Furthermore, the overall computational complexity of the self-tuning control algorithm also depends on the computation time associated with the particular control implementation selected, a quantity which can vary considerably depending on the model selected. For these reasons, the problem of multivariable model selection to achieve efficient computational implementations is not as well-defined as in the scalar case and, indeed in some situations, the selection of a weighting sequence model may produce computational advantages. Further computational considerations are examined in more detail in Section 8.5.

8.3 Direct Identification of the CWS and CVS

The intermediate task of identifying $\hat{G}(z)$ prior to generating the CWS and CVS can be eliminated provided a method exists to estimate the CWS and CVS directly from the available input/output information. Returning to eqn 8.3 and assuming a noise-free environment, the relationship between $\tilde{y}_i$ and $\tilde{u}_i$ is:

$$\mathbf{v}_i^t \, y(t) = g_i \, \mathbf{v}_i^t \, u(t) \qquad \ldots.(8.27)$$

where $\mathbf{v}_i^t$ denotes the i^{th} row of $\mathbf{V}$. In convolutional terms, eqn 8.27 can be written as:

$$ {}^{s}v_i^t * {}^{s}y = {}^{s}g_i * {}^{s}v_i^t * {}^{s}u \qquad \ldots.(8.28)$$

and this relationship can be expanded into matrix form (with a slight abuse of notation) to produce:

$$V_i \, y = G_i \, V_i \, u \qquad \ldots.(8.29)$$

where $y = [\, y^t(1) \cdots y^t(N) \,]^t \qquad u = [\, u^t(0) \cdots u^t(N-1) \,]^t$

$$V_i = \begin{bmatrix} v_i^t(0) & & \\ v_i^t(1) & v_i^t(0) & 0 \\ \vdots & \ddots & \ddots \end{bmatrix} \qquad G_i = \begin{bmatrix} g_i(1) & & \\ g_i(2) & g_i(1) & 0 \\ \vdots & \ddots & \ddots \end{bmatrix}$$

and N is the number of input/output measurements available. Under the assumption that ${}^{s}v_i^t$ and ${}^{s}g_i$ can be accurately truncated after N_v^i and N_g^i terms respectively (i.e.

$${}^{s}v_i^t = \{v_i^t(0), \cdots, v_i^t(N_v^i-1)\} \qquad {}^{s}g_i = \{g_i(1), \cdots, g_i(N_g^i))\},$$

eqn 8.29 can be reformulated as

$$Y\,x = U\,M\,x \qquad \ldots.(8.30)$$

where x is an $[mN_v^i \times 1]$ vector and Y, U and M are matrices of dimension $[N \times mN_v^i]$, $[N \times m(N_g^i+N_v^i-1)]$ and $[m(N_g^i+N_v^i-1) \times mN_v^i]$ respectively, defined by:

$$x = [\, v_i^t(0) \mid \cdots \mid v_i^t(N_v^i-1) \,]^t$$

$$Y = \begin{bmatrix} y^t(1) & & & \\ \cdot & \cdot & & 0 \\ \cdot & & \cdot & \\ \cdot & & & \ddots \\ y^t(N) & \cdot & \cdot \cdot & y^t(N-N_v^i+1) \end{bmatrix} \qquad U = \begin{bmatrix} u^t(0) & & & \\ \cdot & \cdot & & 0 \\ \cdot & & \cdot & \\ \cdot & & & \ddots \\ u^t(N-1) & \cdot & \cdot \cdot & u^t(N-N_g^i-N_v^i+1) \end{bmatrix}$$

$$M = \begin{bmatrix} g_i(1)\, I_m & & & \\ & \ddots & & 0 \\ & & \ddots & \\ & & & g_i(1)\, I_m \\ g_i(N_g^i)\, I_m & & & \\ & \ddots & & \\ & & \ddots & \\ 0 & & & g_i(N_g^i)\, I_m \end{bmatrix}$$

From eqn 8.30, each CWS/dual CVS pair must satisfy the relationship $(Y - UM)\,x = 0$. Hence, direct identification of these quantities may be posed as a constrained minimization problem: select x and the corresponding M so that $||(Y - UM)\,x||^2$ is minimized subject to the constraint that the vector x is normalized (i.e. $x^t x = 1$). This formulation yields a cost

function of the form:

$$J = || (Y - UM) x ||^2 + \lambda (1 - x^t x) \quad ....(8.31)$$

where λ is a Lagrange multiplier introduced to include the constraint, and the solutions to this problem are given by the parameter sets, $\{{}^s g_i, {}^s v_i^t\}$. which simultaneously satisfy the conditions:

$$\partial J/\partial x = 0 \qquad \partial J/\partial g_i(j) = 0 \; ; \; j = 1, \cdots, N_g^i \quad ....(8.32a,b)$$

Closer examination of eqn 8.32a yields the relationship

$$(Y - UM)^T (Y - UM) x - \lambda x = 0 \quad ....(8.33)$$

This result not only establishes a necessary condition on x for J to be a minimum, but it also suggests a procedure for computing x given M. In particular, eqn 8.33 can be rewritten as:

$$(Y - UM)^T (Y - UM) x = \lambda x \quad ....(8.34)$$

But, this result defines an eigenvalue/eigenvector relationship between x and λ (or J). Hence, the x which minimizes J is simply the eigenvector associated with the smallest eigenvalue of $(Y - UM)^T (Y - UM)$.

Additional conditions for the solution of this minimization problem are imposed by eqn 8.32b which yields a set of linear equations in the elements of ${}^s g_i$. In particular,

$$\partial J/\partial g_i(j) = -2 \{x^t [\partial M/\partial g_i(j)]^T U^T (Y - UM) x\} = 0 \quad ....(8.35)$$

Defining the $[N_g^i \times 1]$ vector g and the $[m(N_g^i + N_v^i - 1) \times N_g^i]$ matrix X as:

$$g = [\, g_i(1) \; \cdots \; g_i(N_g^i) \,]^t$$

$$X = \begin{bmatrix} v_i(0) & & & \\ & \ddots & & 0 \\ & & \ddots & \\ & & & v_i(0) \\ v_i(N_v^i - 1) & & & \\ & \ddots & & \\ & & \ddots & \\ 0 & & & v_i(N_v^i - 1) \end{bmatrix}$$

the following relationships may also be established:

$$M\,x = X\,g \qquad \ldots.(8.36a)$$

$$\begin{bmatrix} x^t\ [\partial M/\partial g_i(1)]^t \\ \vdots \\ x^t\ [\partial M/\partial g_i(N_g)]^t \end{bmatrix} = X^T \qquad \ldots.(8.36b)$$

Upon substitution of these expressions into the set of equations 8.35, the following result is obtained:

$$g = \{X^T\,U^T\,U\,X\}^{-1}\,X^T\,U^T\,Y\ x \qquad \ldots.(8.37)$$

Hence, the elements of ${}^{s}g_i$ are simply functions of the known system inputs and outputs and the vector x.

Eqn 8.37 can be used in conjunction with eqn 8.34 to produce the following iterative algorithm for the direct identification of $\{{}^{s}g_i,\ {}^{s}v_i^t;\ i = 1, \cdots, m\}$.

Algorithm 8.1: Direct Identification of $\{{}^{s}g_i,\ {}^{s}v_i^t\}$

For each i (i = 1, $\cdots$,m),

(1) Initialize x to x_0.

(2) Solve for g_0 using x_0 and eqn 8.37.

(3) Identify x_1 as the eigenvector associated with the smallest eigenvalue of $(Y\text{-}UM_0)^T(Y\text{-}UM_0)$ where M_0 is defined (as shown previously) using the elements of g_0.

(4) Repeat steps 2 and 3 until the solution converges.

Algorithm 8.1 can be used to identify the sequences ${}^{s}\Lambda$ and ${}^{s}V$ required to implement the control law defined in Section 8.1.2. Of course, ${}^{s}W$ must also be generated to perform the necessary transformations back to the original plant frame. With ${}^{s}V$ known, this can be achieved using a "deconvolution" algorithm based on eqn 7.2.

There are two important characteristics of this algorithm that should also be highlighted here. First, the solution for g defined by eqn 8.37 takes the form of a standard least-squares solution. Second, the eigenvector update in step 3 of the algorithm relies only on the minimum

eigenvalue of $(Y - UM)^T(Y - UM)$ and its associated eigenvector. From a computational point of view, this relationship implies that an iterative algorithm such as the 'power method' may yield a more efficient solution for x than standard eigenvalue/eigenvector decomposition algorithms. Together, these characteristics suggest that it may be possible to implement a recursive version of the algorithm. This development will be discussed in more detail in Section 8.3.2.

8.3.1 Convergence of the Algorithm

To ensure that Algorithm 8.1 identifies the correct solutions, its convergence characteristics must be investigated in detail. One way to accomplish this task is to demonstrate that, for an initial value of x (x_0) sufficiently close to the true x (x_o), the algorithm converges to the desired solution. As shown in Appendix 8.2, a perturbation analysis of the algorithm in the vicinity of the solutions $\{{}^{s}g_i, {}^{s}v_i^t\}$ which set J to zero clearly establishes this characteristic. As noted in the appendix, the algorithm may jump from one solution to another under certain circumstances. However, these special conditions correspond to pathological situations when two or more eigenvectors, $\hat{v}(z)$, are nearly parallel for all z and when the corresponding eigenfunctions, $\hat{g}(z)$, are nearly equal for all z. Since the likelihood of this situation arising in practice is negligible, initializing the algorithm with accurate seeds will ensure that the proper solutions are obtained. The requirement for an accurate initial seed can, in fact, be satisfied using the standard CSM algorithm in conjunction with estimates of the plant weighting sequence obtained from a standard identification algorithm. From this perspective, implementation of an appropriate identification algorithm would require a run of the standard identification algorithm (discussed in Section 8.2) for just as long as necessary to generate the seed and a subsequent switch to Algorithm 8.1.

Further investigations of the general convergence characteristics of the algorithm, however, suggest that the requirement for an accurate initial

seed may be unnecessary. To verify this observation, consider first the problem of identifying the eigenvalues and left eigenvectors of an [m x m] matrix A using an iterative algorithm similar to the one proposed above. The cost function for this problem becomes:

$$J_A = || v^t (A - \mu I) ||^2 + \lambda (1 - v^t v) \quad ....(8.38)$$

where μ is the desired eigenvalue and v^t is the corresponding left eigenvector. The stationarity conditions can then be written as:

$$(A - \mu I) (A - \mu I)^T v = \lambda v \quad ....(8.39a)$$

$$\mu = \{v^t (A^T + A) v\} / 2 v^t v \quad ....(8.39b)$$

Upon substituting the above expression for μ into eqn 8.38, J_A becomes solely a function of v, and it is possible to establish the Hessian of J_A (d^2J/dv^2) as:

$$1/2 \frac{d^2J}{dv^2} = (A - \mu I)(A - \mu I)^T - \frac{d\mu}{dv} \left[\frac{d\mu}{dv} \right]^t - \lambda I \quad ....(8.40)$$

where $$\frac{d\mu}{dv} = \frac{1}{v^t v} \{(A - \mu I) + (A - \mu I)^T\} v$$

The characteristics of J_A at its stationary points can now be investigated in more detail. Let $\{\mu_o, v_o^t\}$ define a stationary point of J_A. Then under the normalizing constraint $v_o^t v_o = 1$, eqns 8.39a,b imply:

$$v_o^t (A - \mu_o I) (A - \mu_o I)^T v_o = \lambda \quad \text{and} \quad v_o^t A v_o = \mu_o$$

which, together with eqn 8.40, give

$$1/2 \, v_o^t \frac{d^2J}{dv^2} v_o = v_o^t (A - \mu_o I)(A - \mu_o I)^T v_o - \lambda - 2 \{v_o^t A v_o - \mu_o\} = 0$$

Hence, d^2J/dv^2 must be rank deficient at every stationary point of J_A. More information can, however, be established by recognizing that $(A - \mu I)$ can be written in terms of its singular value decomposition as:

$$A - \mu I = R_1 \Sigma R_2^T \quad ....(8.41)$$

where $\Sigma = \text{diag}\{\underline{\sigma}, \sigma_2, \cdots, \sigma_{m-1}, \bar{\sigma}\}$. Substituting eqn 8.41 into eqn 8.40 yields:

$$1/2 \frac{d^2J}{dv^2} = R_1 \Sigma^2 R_1^T - \lambda I - \{R_1 \Sigma R_2^T + R_2 \Sigma R_1^T\} v v^t \{R_1 \Sigma R_2^T + R_2 \Sigma R_1^T\} \quad ....(8.42)$$

Special characteristics of the stationary points can now be reintroduced. In particular, eqn 8.39a must be satisfied at the stationary point. But since the stationary point was reached by selecting the v which corresponds to the minimum λ, λ must be exactly equal to $\underline{\sigma}^2$ and v_o^t must identify the first row of R_1^T. Using these relationships, the following result can be derived from eqn 8.42:

$$1/2\ v_o^t \frac{d^2J}{dv^2} v_o = (\underline{\sigma}^2 - \lambda) - 4\ \underline{\sigma}^2 (v_o^t w_o)^2 = -4\ \underline{\sigma}^2 (v_o^t w_o)^2 \quad \ldots.(8.43)$$

where w_o identifies the first column of R_2 at the specified stationary point. As shown previously, $v_o^t \frac{d^2J}{dv^2} v_o = 0$. But from eqn 8.43, it is now evident that this can be achieved in two different ways: either $\underline{\sigma}^2 = 0$ or $v_o^t w_o = 0$. Thus, the only stationary points of J_A which do not correspond to the correct solutions of the problem are those for which the minor input and output principal directions of $(A - \mu_o I)$ are orthogonal (i.e. $v_o^t w_o = 0$) and $\underline{\sigma}^2 \neq 0$. In these special cases, eqn 8.43 clearly demonstrates that, for small perturbations ($\tilde{v} = v_o + \delta v$) away from v_o, $\tilde{v}^t \frac{\partial^2 J}{\partial v^2} \tilde{v}$ will always be negative. In essence then, each of these special stationary points is a local maximum and the algorithm will only stop at one of these points if the initial value for v is exactly equal to v_o. Thus, the only stable solutions identified by the algorithm will correspond to the true eigenvalues and eigenvectors of A.

A rigorous investigation of the general convergence characteristics of the original problem requires the identification and analysis of the Hessian of J (where J is defined by eqn 8.31) in a manner analogous to that shown above. Although it is possible to generate an appropriate expression for this quantity, the result obtained does not exist in a form that can be readily investigated to identify the characteristics of J at its stationary points. It is, however, possible to extend the discussion and results above to this original problem by recognizing that the solutions $\{{}^s g_i, {}^s v_i^t\}$ for which J = 0 also define the functions $\hat{g}_i(z)$ and $\hat{v}_i^t(z)$ which satisfy the

relationship $\hat{v}_i^t \{\hat{G} - \hat{g}_i I\} = 0$. The format of the original problem is, therefore, identical to that examined above, and the conclusions reached should extend directly. This observation suggests the following result:

Conjecture: The only stable solutions $\{{}^s g_i, {}^s v_i^t\}$ generated by Algorithm 8.1 will be those for which J (defined by eqn 8.31) is identically zero (i.e. the correct solutions).

This result implies that Algorithm 8.1 may be used independently to identify the m solutions $\{{}^s g_i, {}^s v_i^t\}$ required to implement the control law of Section 8.1.2.

8.3.2 A Recursive Implementation of the Algorithm

Although Algorithm 8.1 will, in general, identify the desired solutions, the iterative nature of the algorithm makes it difficult to implement when on-line identification is required. It is interesting to note, however, that the solution for g_i defined by eqn 8.37 is also the solution to a scalar model identification problem of the form:

$$\tilde{y}_i(k) = \sum_{j=1}^{N_g^i} \tilde{u}_i(k-j)\, g_i(j)$$

where $\tilde{y}_i$ and $\tilde{u}_i$ are the appropriate elements of $\tilde{y}$ and $\tilde{u}$ (defined in eqn 8.4) and, hence, represent the inputs and outputs of the system filtered by the appropriate function $\hat{v}_i^t(z)$. Viewing the problem from this perspective, it seems reasonable to anticipate that a two-stage recursive algorithm can be used to generate the desired parameter estimates. One such algorithm is proposed below:

Algorithm 8.2: Recursive Algorithm for the Identification of $\{{}^s g_i, {}^s v_i^t\}$

(1) At time t, let

$$\tilde{y}_i(t) = v_i^t\, y(t) \qquad \tilde{u}_i(t-1) = v_i^t\, u(t-1)$$

$$\tilde{d}_i^t(t) = [\, \tilde{u}_i(t-1) \;\; \tilde{u}_i(t-2) \;\; \cdots \;\; \tilde{u}_i(t-N_g^i) \,]$$

Then,

$$\hat{g}_i(t) = \hat{g}_i(t-1) + K(t) \{ \tilde{y}_i(t) - \tilde{d}_i^t(t) \hat{g}_i(t-1) \}$$

$$K(t) = P(t-1) \tilde{d}_i(t) / \{ 1 + \tilde{d}_i^t(t) P(t-1) \tilde{d}_i(t) \}$$

$$P(t) = \{ I - K(t) \tilde{d}_i^t(t) \} P(t-1)$$

(2) Using the elements of $\hat{g}_i(t)$, $\{\hat{g}_i(k), k = 1, \cdots, N_g^i\}$, define

$$\alpha^t(j) = y^t(t-j) - \sum_{k=1}^{N_g^i} \hat{g}_i(k) u^t(t-j-k) ; \quad j = 0, \cdots, N_v^i-1$$

$$\gamma^t = [\alpha^t(0) \cdots \alpha^t(N_v^i-1)]$$

Then,

$$\Gamma(t) = \Gamma(t-1) + \gamma \gamma^t$$

$$z(t) = \{ \Gamma(t) - kI \} x(t-1)$$

(where k is chosen so that $|\underline{\sigma} - k| > |\sigma_i - k|$ for all i)

$$x(t) = \begin{bmatrix} v_i(0) \\ \cdot \\ \cdot \\ \cdot \\ v_i(N_v^i-1) \end{bmatrix} = z(t) / \sqrt{\{z^t(t) z(t)\}}$$

Part 1 of Algorithm 8.2 is simply a recursive least-squares algorithm applied to appropriately filtered input/output data. Part 2 uses the current estimates of $\hat{g}_i(t)$ to update $(Y - UM)^T(Y - UM)$ and implements an "inverse power method" algorithm (assuming that only small changes in x are introduced by the additional data) to update x. It is interesting to note that the need to specify the constant k which ensures that $|\underline{\sigma}(\Gamma) - k| > |\sigma_i(\Gamma) - k|$ can be eliminated by focusing attention on Γ^{-1} instead of Γ [MOH2]. In particular, Γ^{-1} can be updated recursively using the 'matrix inversion lemma', which states that:

$$\Gamma^{-1}(t) = [\Gamma(t-1) + \gamma\gamma^t]^{-1} = \Gamma^{-1}(t-1) - \frac{\Gamma^{-1}(t-1) \gamma\gamma^t \Gamma^{-1}(t-1)}{1 + \gamma^t \Gamma^{-1}(t-1) \gamma} ;$$

and since $\bar{\sigma}(\Gamma^{-1}) = 1 / \underline{\sigma}(\Gamma)$, the eigenvector associated with $\underline{\sigma}(\Gamma)$ is identical to the one associated with $\bar{\sigma}(\Gamma^{-1})$. Thus, a "power method" algorithm can be applied directly to Γ^{-1} in a manner similar to that shown

in step 2 of Algorithm 8.2 to compute x(t).

8.4 A Scalar Difference Equation Formulation of the Problem

For situations when a large number of elements are required in each CWS to produce an accurate system description, the direct identification algorithm of the previous section and the use of the resulting estimates to predict future subsystem outputs may create a significant computational burden. In these cases, both the identification and prediction problems may be reformulated in terms of scalar difference equations to reduce the computational complexity of the self-tuning algorithm. The desired results are derived below.

8.4.1 Direct Identification of Subsystem Difference Equation Models

For systems with no unstable branch points, $\hat{g}_i(z)$ can be described exactly by a rational infinite-length polynomial in powers of z^{-1} (whose coefficients decay to zero) as shown in Chapter 7. Under these conditions, it is also possible to identify two finite-length polynomials,

$$\hat{a}_i(z) = 1 + a_i(1)\, z^{-1} + \cdots + a_i(N_a^i)\, z^{-N_a^i}$$

and

$$\hat{b}_i(z) = b_i(1)\, z^{-1} + \cdots + b_i(N_b^i)\, z^{-N_b^i}$$

such that the function $\hat{b}_i / \hat{a}_i$ describes $\hat{g}_i$ to a specified level of accuracy. As a result, $\hat{g}_i$ may be replaced by $\hat{b}_i / \hat{a}_i$ and the identification algorithm of the previous section can be extended directly to this new formulation.

In particular, eqn 8.27 can be rewritten as:

$$\mathbf{a}_i\, \mathbf{v}_i^t\, y(t) = \mathbf{b}_i\, \mathbf{v}_i^t\, u(t) \qquad \ldots.(8.44)$$

or, in convolutional terms, as:

$$s_{a_i} * s_{v_i^t} * s_y = s_{b_i} * s_{v_i^t} * s_u$$

Expanding this relationship into matrix form produces:

$$A_i\, V_i\, y = B_i\, V_i\, u \qquad \ldots.(8.45)$$

where y, u, and V_i are defined as shown in Section 8.3, while A_i and B_i are

given by:

$$A_i = \begin{bmatrix} 1 & & & 0 \\ a_i(1) & 1 & & \\ & a_i(1) & \ddots & \\ & & \ddots & 1 \\ a_i(N_a^i) & & & a_i(1) \\ & \ddots & & \\ 0 & & & \end{bmatrix} \qquad B_i = \begin{bmatrix} b_i(1) & & & 0 \\ & b_i(1) & & \\ & & \ddots & \\ & & & b_i(1) \\ b_i(N_b^i) & & & \\ & \ddots & & \\ 0 & & & \end{bmatrix}$$

As before, eqn 8.45 can be rearranged to produce

$$Y\ L\ x = U\ M\ x \qquad \ldots.(8.46)$$

where x is defined as shown previously; Y and U are now matrices of dimension $[N \times m(N_a^i+N_v^i)]$ and $[N \times m(N_b^i+N_v^i-1)]$ respectively, defined in a manner analogous to that shown in Section 8.3; and L and M are matrices of dimension $[m(N_a^i+N_v^i) \times mN_v^i]$ and $[m(N_b^i+N_v^i-1) \times mN_v^i]$ respectively, defined by:

$$L = \begin{bmatrix} I_m & & & 0 \\ a_i(1)\ I_m & \ddots & & \\ & \ddots & & I_m \\ & & \ddots & a_i(1)\ I_m \\ a_i(N_a^i)\ I_m & & & \\ & \ddots & & \\ 0 & & & a_i(N_a^i)\ I_m \end{bmatrix}$$

$$M = \begin{bmatrix} b_i(1)\ I_m & & & 0 \\ & \ddots & & \\ & & \ddots & b_i(1)\ I_m \\ & & & \\ b_i(N_b^i)\ I_m & & & \\ & \ddots & & \\ 0 & & & b_i(N_b^i)\ I_m \end{bmatrix}$$

Parameter identification for the polynomials $\hat{a}_i$, $\hat{b}_i$, and $\hat{v}_i^t$ can now be formulated as a constrained minimization problem with the following cost function:

$$J = || (YL - UM) x ||^2 + \lambda (1 - x^t x) \quad ....(8.47)$$

In a manner analogous to that of Section 8.3, the following relationships can be established:

$$L x = x_t + \begin{bmatrix} 0^t \\ - - - \\ X_a \end{bmatrix} a \qquad M x = X_b b \quad ....(8.48a,b)$$

where $x_t = [\, x^t \mid 0^t \,]^t$

$a = [a_i(1) \cdots a_i(N_a^i)]^t$ $\qquad$ $b = [b_i(1) \cdots b_i(N_b^i)]^t$

and X_a and X_b are defined in the same manner as shown previously, but with different dimensions; namely, X_a and X_b are dimensioned $[m(N_a^i+N_v^i-1) \times N_a^i]$ and $[m(N_b^i+N_v^i-1) \times N_b^i]$ respectively . Furthermore, if Y is partitioned as:

$$Y = [\, y_k \mid Y_{k-1} \,]$$

where y_k contains the first m columns of Y and Y_{k-1} is a matrix of dimension $[N \times m(N_a^i + N_v^i - 1)]$, then

$$(YL - UM) x = Y x_t + [\, Y_{k-1} X_a \mid - U X_b \,] \theta \quad ....(8.49)$$

with $\theta = [\, a^t \mid b^t \,]^t$

Using the relationships above, the conditions which identify a stationary point of J become:

$$(YL - UM)^T (YL - UM) x = \lambda x \quad ....(8.50a)$$

$$\theta = \{ \tilde{D}^T \tilde{D} \}^{-1} \tilde{D}^T Y x_t \quad ....(8.50b)$$

where $\tilde{D} = [\, - Y_{k-1} X_a \mid U X_b \,]$

The form of these results is identical to that described in Section 8.3 for the weighting sequence problem. As such, Algorithms 8.1 and 8.2 can be used for this new problem formulation simply by making the substitutions implied by eqn 8.50. Furthermore, the convergence characteristics of the modified algorithms will be exactly the same as those given earlier. When using this difference equation formulation for the characteristic subsystems

however, it also becomes necessary to modify the output prediction relationships associated with the predictive control law which were developed in Section 8.1.1. The required modifications are discussed below.

8.4.2 Output Prediction

With parameter estimates for $\hat{a}_i$, $\hat{b}_i$, and $\hat{v}_i^t$ available, the plant transfer function matrix can be written in the following form:

$$\hat{G}(z) = \hat{W}\ \hat{\Lambda}_a^{-1}\ \hat{\Lambda}_b\ \hat{V} = \{\hat{W}\ \hat{\Lambda}_a^{-1}\ \hat{V}\}\ \{\hat{W}\ \hat{\Lambda}_b\ \hat{V}\} = (\hat{A}')^{-1}\ \hat{B}' \qquad ....(8.51)$$

where $\hat{\Lambda}_a = \text{diag}\ \{\hat{a}_1, \cdots, \hat{a}_m\}$ and $\hat{\Lambda}_b = \text{diag}\ \{\hat{b}_1, \cdots, \hat{b}_m\}$. Output prediction can now be formulated in a manner analogous to that for the standard difference equation formulation discussed at the end of Section 8.1.1. However, it should be noted that output prediction will now be performed entirely in the eigenvector frame. With this in mind, it can be shown that the best available estimates of $\tilde{y}(t+k)$ at time t are given by:

$$\tilde{y}(t+k|t) = \tilde{F}_k\ \tilde{y}(t) + \tilde{E}_k\ W\ \Lambda_b\ \tilde{\Delta u}(t+k) \qquad ....(8.52)$$

where $\tilde{E}_K$ and $\tilde{F}_k$ are defined by the modified Diophantine identity:

$$\tilde{E}_k\ W\ \Lambda_a\ \Delta + z^{-k}\ \tilde{F}_k = I \qquad ....(8.53)$$

Furthermore, if $\tilde{G}_k'$ and $\tilde{G}_k$ are redefined as

$$\tilde{G}_k' = \tilde{E}_k\ W\ \Lambda_b \qquad\qquad \tilde{G}_k = \tilde{E}_k\ W\ \Lambda_b\ V$$

the relationship between $\tilde{y}_i(t+k|t)$, $\{\tilde{\Delta u}_i(t+j);\ j=1,\cdots,k-1\}$, and $\tilde{r}_i(k)$ is precisely the same as that shown in eqns 8.20 and 8.21. Hence, the predictive control law for this alternate subsystem description is identical to that defined by eqn 8.23.

As before, the Diophantine relationships provide a convenient means of describing the relationship between future outputs and past, present, and future information. It should, however, be noted that, in practice, the desired eigenframe output predictions may be generated in a manner which is computationally more efficient than that suggested by eqn 8.52. Using an approach analogous to that discussed in Section 8.1.3, each subsystem output can be described by the scalar relationship:

$$\tilde{y}_i(t+k) = \tilde{y}_i(t+k-1) + a_i\,\Delta\tilde{y}_i(t+k-1) + b_i\,\Delta\tilde{u}(t+k-1) \quad \ldots.(8.54)$$

and this result can be used to simulate the desired output predictions provided $\tilde{y}(t)$ is generated by transforming the known plant outputs into the eigenframe using **V**.

8.5 Computational Considerations for Implementation

As with any control algorithm, the feasibility (practicability) of implementations involving the multivariable self-tuning algorithm proposed in this chapter depends upon the computational complexity of the algorithm. This is a particularly pressing issue for multivariable systems since the degree of complexity increases rapidly with the dimension of the system. Thus, it is not sufficient to address only the theoretical foundations of the control algorithm; one must also consider its computational requirements. The following discussion addresses these concerns.

A useful measure of the computational complexity of on-line control algorithms is the number of scalar multiplication-additions required to implement the algorithm. Under the assumption that all algorithm operations must be performed using a serial implementation (as is currently done in practice), this quantity can be identified by recognizing that a [j x k]-matrix by [k x n]-matrix multiplication requires (jkn) scalar operations and that $(n^3\sqrt{n})$ is a readily available upper bound on the number of operations required to perform [n x n] matrix inversions and eigenvalue/eigenvector decompositions. In addition, several other variables which directly affect the computational complexity of the algorithm can be defined as follows:

m = plant dimension

N_G = number of matrix elements in ${}^sG$ $\qquad$ N_g^i = number of elements in ${}^sg_i$

N_{AB} = number of matrix elements in **A**,**B** $\qquad$ N_{ab}^i = number of elements in a_i,b_i

N_v^i = number of elements in ${}^sv_i^t$ $\qquad$ N_w^i = number of elements in ${}^sw_i$

N_u^i = control horizon for subsystem i

N_1^i = minimum prediction horizon for subsystem i

$N_2^i = N_y^i$ = maximum prediction horizon for subsystem i

For simplicity, it will be assumed that A is diagonal and that $N_g^i = N_g$, $N_{ab}^i = N_{ab}$, $N_v^i = N_v$, $N_w^i = N_w$, $N_u^i = N_u$, $N_1^i = 1$, and $N_2^i = N_y^i = N_y$ for all i. Using these definitions and assumptions, the per-cycle computations required for each portion of the proposed algorithm can be estimated. General expressions for these estimates are displayed in Table 8.1.

Clearly, quantifying the computational complexity of the general algorithm is a difficult task involving a large number of system-dependent variables. It is, however, instructive to identify the complexity associated with several representative situations. This has been accomplished for different algorithm configurations, and the results are summarized in Tables 8.2 and 8.3. For purposes of comparison, the computational complexity of the multivariable algorithm proposed by Mohtadi et al [MOH1] (and denoted here by MSC) has also been identified under the same assumptions. [Note: The algorithm structure identified in these tables has been coded in the following manner:

A -- Proposed algorithm with $\hat{G} = \hat{A}^{-1} \hat{B}$

B -- Proposed algorithm with $\hat{G} = \sum_{i=1}^{N_G} G(i)\, z^{-i}$

C -- Proposed algorithm with identification of $\{{}^{s}g_i, {}^{s}v_i^t\}$ using Algorithm 8.2

D -- Proposed algorithm with identification of $\{a_i, b_i, {}^{s}v_i^t\}$ using a modified version of Algorithm 8.2

E -- MSC algorithm with $\hat{G} = \hat{A}^{-1} \hat{B}$.]

Although the results presented in Tables 8.2 and 8.3 are significantly affected by the assumptions made, they highlight several important characteristics of the proposed self-tuning algorithm. First, in applications which do not require on-line identification, "control-only" versions of the proposed algorithm prove to be computationally more

Table 8.1: Serial Calculations Required to Implement Proposed Algorithm

Model Parameter Identification:	
$\hat{G}(z) = \hat{A}^{-1}\hat{B}$	$2m \{ [(m+1) N_{AB}]^2 + 2 (m+1) N_{AB} \}$
$\hat{G}(z) = \sum_{i=1}^{N_G} G(i) z^{-i}$	$2m \{ [m N_G]^2 + 2 m N_G \}$
s_Λ	$3 m^3 N_v^2 + m^2 N_v (2N_g + 5) + m (2N_g^2 + 4N_g)$
Λ_a, Λ_b	$3 m^3 N_v^2 + m^2 N_v (4N_{ab} + 5) + 8m (N_{ab}^2 + N_{ab})$
Identification of $^s\Lambda$, ^sW via CSM (required for $A^{-1}B$ and $\sum_{i=1}^{N_G} G(i) z^{-i}$):	
$\hat{G}(z) = \hat{A}^{-1}\hat{B}$	$m^4 + m^3/2 \{N_y^2 + N_y + 2\sqrt{m} - 2\}$ $+ m^2/2 \{N_y (N_y-1) + N_{AB} (2N_y - N_{AB} + 1)\} - m$
$\hat{G}(z) = \sum_{i=1}^{N_G} G(i) z^{-i}$.	$m^4 + m^3/2 \{N_y^2 + N_y + 2\sqrt{m} - 2\} + m^2 N_y/2 (N_y-1) - m$
Dual CVS Calculations:	$m^3/2 \{N_v^2 + N_v + 2\sqrt{m}\}$
Output Prediction:	
$\hat{G}(z) = \hat{A}^{-1}\hat{B}$	$N_y m \{ m (N_{AB} + N_w + N_v) + N_{AB}\}$
$\hat{G}(z) = \sum_{i=1}^{N_G} G(i) z^{-i}$	$N_y m^2 \{N_G + N_w + N_v\}$
s_Λ	$m N_y N_g + 2 m^2 N_v$
Λ_a, Λ_b	$2 m N_y N_{ab} + 2 m^2 N_v$
Control Law Calculation:	$m N_u \{N_y + N_u N_y + N_u^2 \sqrt{N_u} + 1\}$
Coordinate Transformation:	$m^2 N_v$

Table 8.2: Summary of Required Computations for 2-Dimensional Systems

Assumptions (where applicable):

$m = 2$ $N_G = 25$ $N_g = 25$ $N_v = 5$ $N_y = 10$

$N_{AB} = 6$ $N_{ab} = 6$ $N_w = 5$

	Algorithm Structure				
	A	B	C	D	E
$N_u = 1$					
Identification	2400	11170	4530	1980	1630
Control	825	1465	605	345	500
Total	3225	12635	5135	2325	2130
$N_u = 2$					
Identification	2400	11170	4530	1980	1630
Control	930	1570	710	450	900
Total	3330	12740	5240	2430	2530
$N_u = 3$					
Identification	2400	11170	4530	1980	1630
Control	1120	1760	900	640	1740
Total	3520	12930	5430	2620	3370

Table 8.3: Summary of Required Computations for 3-Dimensional Systems

Assumptions (where applicable):

$m = 3$ $N_G = 25$ $N_g = 25$ $N_v = 5$ $N_y = 10$

$N_{AB} = 6$ $N_{ab} = 6$ $N_w = 5$

	Algorithm Structure				
	A	B	C	D	E
$N_u = 1$					
Identification	6590	37090	9000	4790	4150
Control	1730	3260	905	555	1140
Total	8320	40350	9905	5345	5290
$N_u = 2$					
Identification	6590	37090	9000	4790	4150
Control	1885	3415	1060	710	2530
Total	8475	40505	10060	5500	6680
$N_u = 3$					
Identification	6590	37090	9000	4790	4150
Control	2175	3705	1350	1000	5630
Total	8765	40795	10350	5790	9780

efficient than currently available algorithms such as the MSC algorithm. Indeed, for the simplest control problem (i.e. $m = 2$, $N_u = 1$), the use of algorithm structure C or D yields an algorithm with complexity comparable to that of the MSC algorithm. For more difficult control problems (i.e. $N_u > 1$ or $m > 2$), the proposed algorithm (using structure A, C, or D) becomes much less complex than the MSC algorithm. This latter result can be attributed directly to the fact that all control law calculations in the proposed algorithm involve only scalar operations for each subsystem, so increases in N_u or m do not affect this algorithm as dramatically as they affect the MSC algorithm. From the observations above, it is clear that, when off-line identification is used to identify the appropriate controller parameters, "control-only" versions of the proposed algorithm become practical for a wide range of systems using current serial capabilities.

A second characteristic highlighted by the results in Tables 8.2 and 8.3 is the dramatic impact of the identification task on the computational complexity of any multivariable algorithm. Indeed, in most instances, the computations required for on-line identification are significantly larger than those required for the control calculations. Again however, a comparison between the self-tuning algorithm proposed here and the MSC algorithm is instructive. Since the plant identification algorithm used with structure A is identical to that used in the MSC algorithm, one should expect the self-tuning algorithm proposed here (implemented using structure A) to yield a more complex procedure than that associated with the MSC algorithm because structure A requires the additional computation of the CWS and CVS. This is exactly the case for $N_u = 1$. However, as the difficulty of the control problem increases (requiring larger values of N_u), the more efficient control law of the proposed self-tuning algorithm offsets this initial disadvantage. As a result, this algorithm (implemented using standard recursive identification techniques) becomes comparable in complexity to the MSC algorithm for values of N_u greater than 1. Another

much more important observation is that, when direct subsystem identification is used (structure D), the proposed self-tuning algorithm becomes comparable in complexity to the MSC algorithm for $N_u = 1$ and much more efficient than the MSC algorithm for $N_u > 1$.

It is clear however that, when on-line identification is required, the complexity of the algorithm proposed here (and indeed any other multivariable algorithm) effectively precludes its implementation on all but small-dimensioned systems sampled at sufficiently slow rates when using serial computations. This must not be construed as a reason to ignore the algorithm. By its very nature, the general multivariable control problem is particularly well-suited to the computational savings offered by the advent of VLSI technology for parallel processing. For example, as suggested in [WHI1], the computational complexity of matrix operations can be reduced from $O(n^3)$ to $O(n)$ using parallel implementations, and this advance alone produces a significant reduction in the complexity of the algorithm as shown in Table 8.4. Furthermore, the characteristic subsystem approach offers even further computational savings due to the fact that each subsystem can be handled independently. Hence, the m subsystem control law algorithms can be performed simultaneously using parallel implementations. An indication of the additional savings that can be achieved using this approach is given in Table 8.5. These results clearly suggest that, using emerging parallel processing capabilities, the computational complexity of the proposed multivariable algorithm can be reduced to the same order as that associated with currently existing SISO self-tuning algorithms.

8.6 Simulation Results

Computer simulations were used to demonstrate the multivariable self-tuning control algorithm described in this chapter. The open-loop system used for these simulations was identical to that described in Section 7.5 with the system transfer function matrix given by eqn 7.31. As mentioned in

Table 8.4: Required Computations using Parallel Matrix Operations

Assumptions (where applicable):

$N_G = 25$ $N_g = 25$ $N_v = 5$ $N_y = 10$

$N_{AB} = 6$ $N_{ab} = 6$ $N_w = 5$ $N_u = 1$

		Algorithm Structure				
		A	B	C	D	E
m = 2:						
	Serial Operations	3225	12635	5135	2325	2130
	Parallel Matrix Operations	925	1435	1375	755	405
	Percent Reduction	71	89	73	68	81
m = 3:						
	Serial Operations	8320	40350	9905	5345	5290
	Parallel Matrix Operations	1500	2525	2365	1300	645
	Percent Reduction	82	94	76	76	88

TABLE 8.5: Required Computations using Parallel Subsystem Configurations

Assumptions (where applicable):

$N_G = 25$ $N_g = 25$ $N_v = 5$ $N_y = 10$

$N_{AB} = 6$ $N_{ab} = 6$ $N_w = 5$ $N_u = 1$

		Algorithm Structure				
		A	B	C	D	E
m = 2:						
	Parallel Matrix Operations	925	1435	1375	755	405
	Parallel Loop Calculations	815	1195	980	540	330
	Percent Reduction	12	17	29	28	19
m = 3:						
	Parallel Matrix Operations	1500	2525	2365	1300	645
	Parallel Loop Calculations	1225	1840	1285	715	450
	Percent Reduction	18	27	46	45	30

Section 7.5, there are two unstable branch points associated with this transfer function matrix. However, because of the proximity of these branch points to one another, their effects on the CWS and CVS are not significant initially. Indeed, the results presented in Section 7.5.2 clearly demonstrate the accuracy that can be achieved using 5-term sequences. Therefore, the control algorithm of Section 8.1 was implemented on this system using 5-term operators, **W** and **V**, to perform the necessary transformations.

For demonstration purposes, the simulations were generated by initially applying a positive unit step input to loop 1 followed by the application of a negative unit step input to loop 2 at sample 25. The closed-loop response of the plant and the outputs from the controller were observed for 50 samples. As on-line identification was not used in the simulations, the specification of subsystem control laws and the prediction of future subsystem outputs were accomplished using fixed parameters defined by the transfer function matrix in eqn 7.31. The minimum and maximum prediction horizons (N_1^i and N_2^i) were set to 1 and 10 respectively for both subsystems throughout the simulations, while the control horizons (N_u^i) and weighting factors (ρ_i) were varied.

Initial simulation runs examined the effects of changing N_u (assuming equal values for both subsystems) with ρ_i set to zero. The results for $N_u = 1$ and $N_u = 3$ are presented in Figures 8.3 and 8.4. Additional information (i.e. the settling time of system response, peak control activity, and maximum interaction as a percent of the commanded input) for these runs is presented in Table 8.6. In general, the closed-loop responses for these tests were stable and nonoscillatory. For $N_u = 1$, the response was sluggish and a moderate amount of interaction was present, but the control activity required to produce this response was particularly low. As N_u was increased to larger values, the system responded much more rapidly and interaction became negligible. However, the price for these improvements was unacceptably large control activity in both channels.

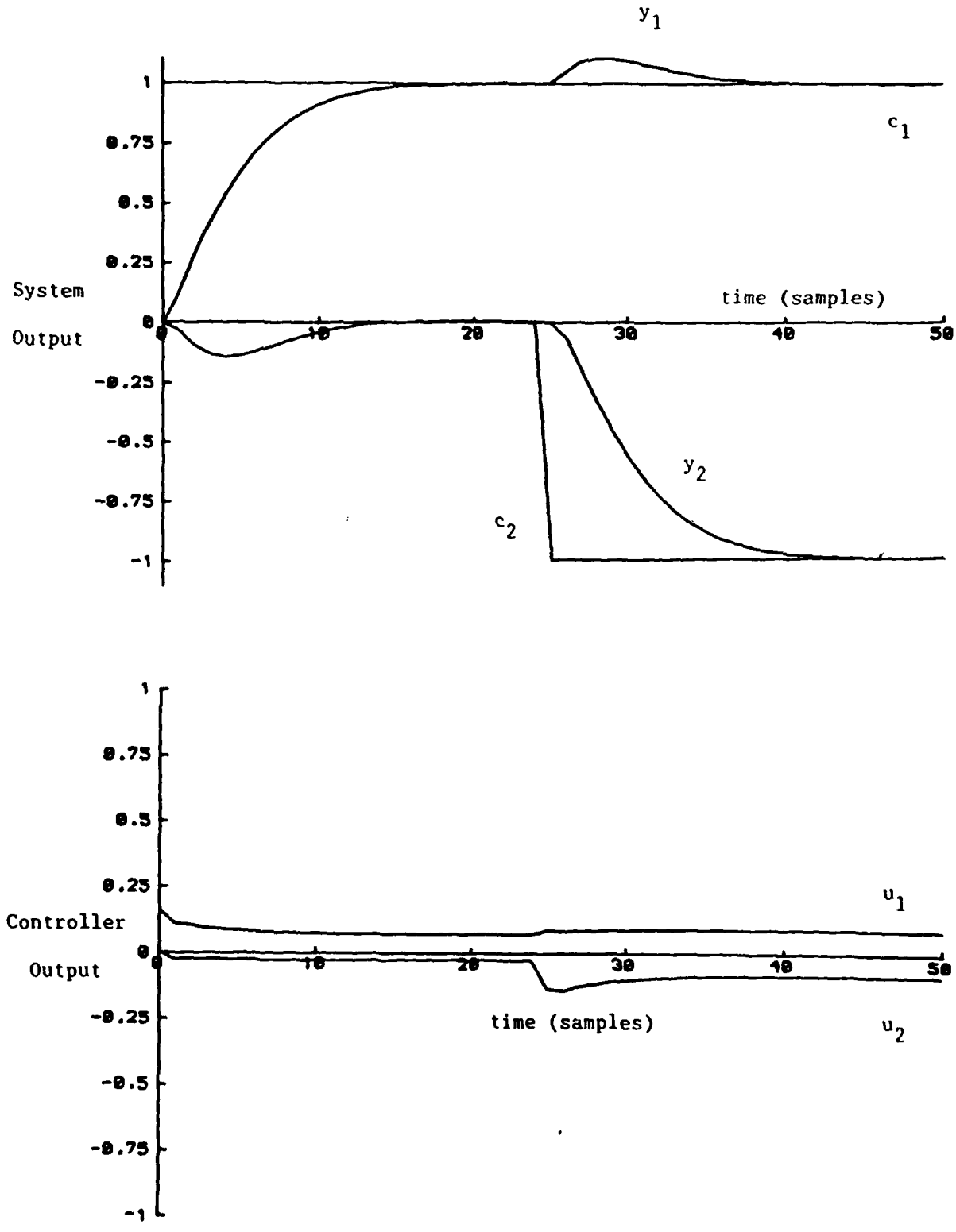

Figure 8.3: Simulation Results Without High Frequency Alignment Compensation
($N_u^1 = N_u^2 = 1$; $\rho_1 = \rho_2 = 0$)

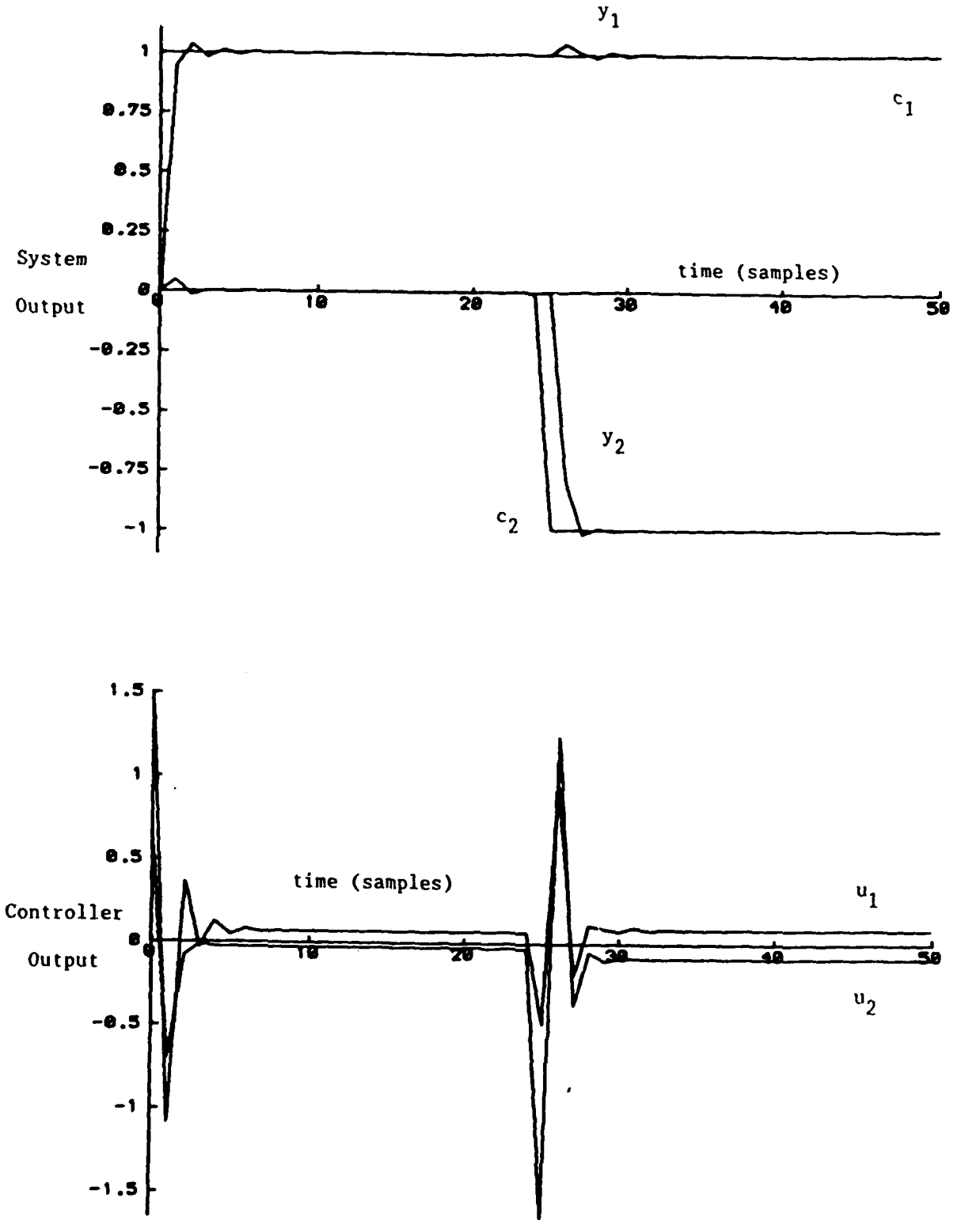

Figure 8.4 Simulation Results Without High Frequency Alignment Compensation

$(N_u^1 = N_u^2 = 3 \; ; \; \rho_1 = \rho_2 = 0)$

To maintain rapid response while reducing the level of control activity, non-zero control weights were included in the control law for values of N_u greater than 1. In particular, ρ_i was set to 1 for each subsystem, and the observed closed-loop response characteristics from the resulting simulations are included in Table 8.6. These results clearly demonstrate that rapid response was maintained with a more reasonable level of control activity, but the maximum level of interaction was significantly larger. To overcome the increased interaction, the additional flexibility associated with the ability to change the subsystem control horizons independently was used to improve the results. For $N_u^1 = 3$, $N_u^2 = 2$, and $\rho_1 = \rho_2 = 1$, acceptably rapid response was obtained using reasonable control activity while minimizing the peak level of interaction. The simulation results for this configuration are displayed in Figure 8.5.

All of the simulation results presented thus far were obtained without the aid of high frequency alignment compensation, and they clearly show that acceptable levels of interaction can be achieved without this additional compensation. It is, however, interesting to compare these results with those obtained by including appropriate high-frequency alignment compensation. The compensator used for this purpose was identical to that used in Section 7.5 (eqn 7.32). Again, 5-term operators, **W** and **V**, were used to perform the necessary transformations, and the control algorithm of Section 8.1 was implemented. In general, the use of this precompensator left the desired system responses and the corresponding levels of control activity relatively unaffected, but it did reduce interaction (as shown in Table 8.6). A representative example ($N_u^1 = N_u^2 = 3$; $\rho_1 = \rho_2 = 1$) of the compensated system response for this modified system is presented in Figure 8.6.

The simulations presented here demonstrate clearly that appropriate control of the characteristic subsystems translates directly into effective loop-by-loop control of the multivariable system. Moreover, it is possible

to use the additional flexibility associated with the independent control of each individual subsystem to fine tune system performance; a facility not explicitly available when a single scalar cost function is applied. The result is the achievement of good system response with moderate control activity and acceptably low levels of interaction.

Table 8.6: Performance Comparison of Simulation Results

N_u^1	N_u^2	ρ	Settling Time (samples)		Peak Control Activity		Maximum Interaction (%)	
			Loop 1	Loop 2	Loop 1	Loop 2	Loop 1	Loop 2
Without High Frequency Alignment Compensation:								
1	1	0	15	16	.16	.14	10.4	14.5
2	2	0	5	5	.88	.73	15.2	16.5
3	3	0	3	2	1.50	1.65	4.8	4.8
4	4	0	1	2	1.53	2.04	1.6	1.8
2	2	1	4	5	.62	.50	16.1	16.0
3	3	1	4	4	.53	.44	16.1	15.4
4	4	1	6	7	.51	.43	16.2	15.6
3	2	1	4	4	.57	.49	13.9	12.1
With High Frequency Alignment Compensation:								
1	1	0	15	17	.13	.15	8.7	9.6
3	3	1	5	5	.68	.81	7.8	5.8
3	2	1	5	6	.65	.84	7.7	6.1

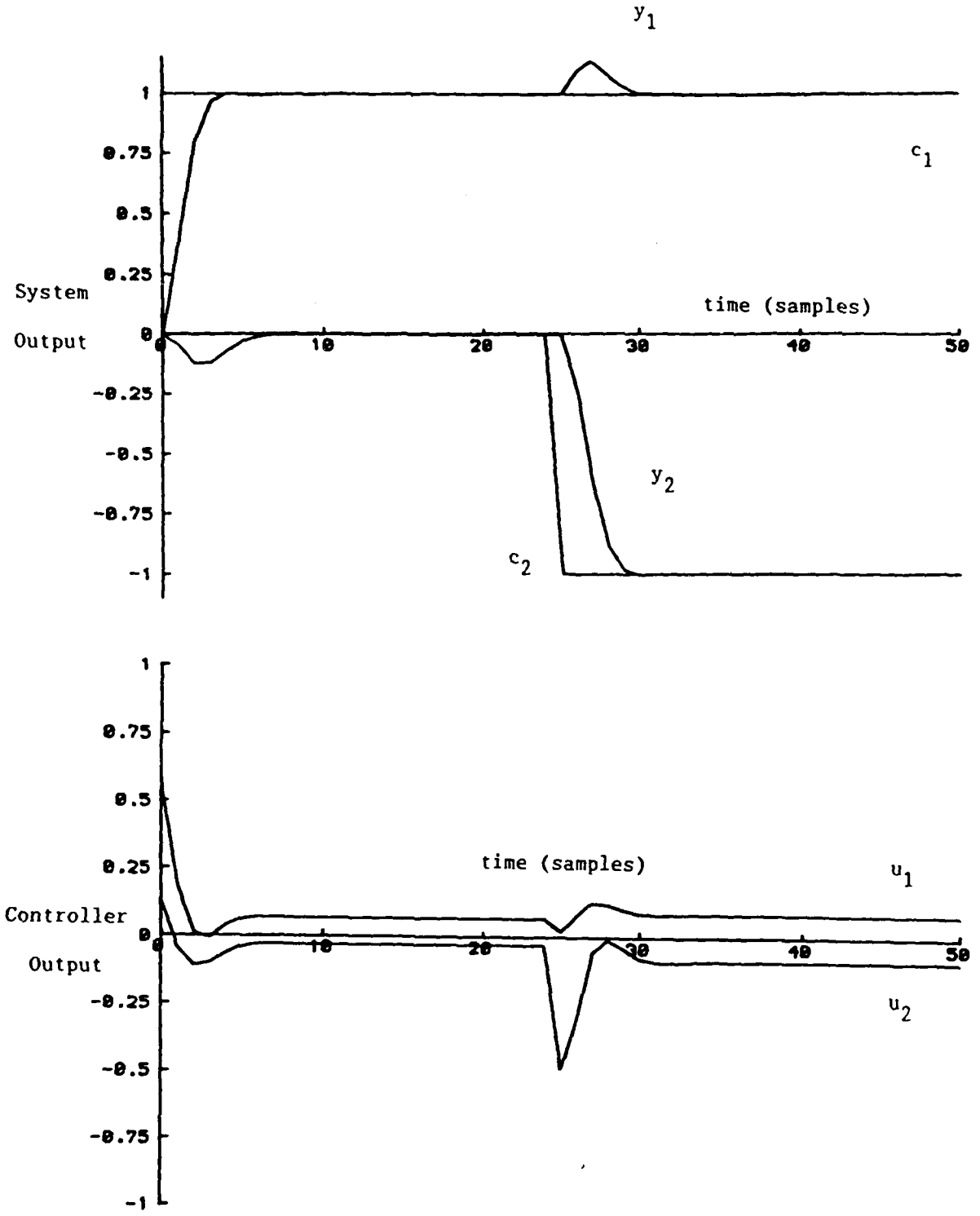

Figure 8.5: Simulation Results Without High Frequency Alignment Compensation

$(N_u^1 = 3 \; ; \; N_u^2 = 2 \; ; \; \rho_1 = \rho_2 = 1)$

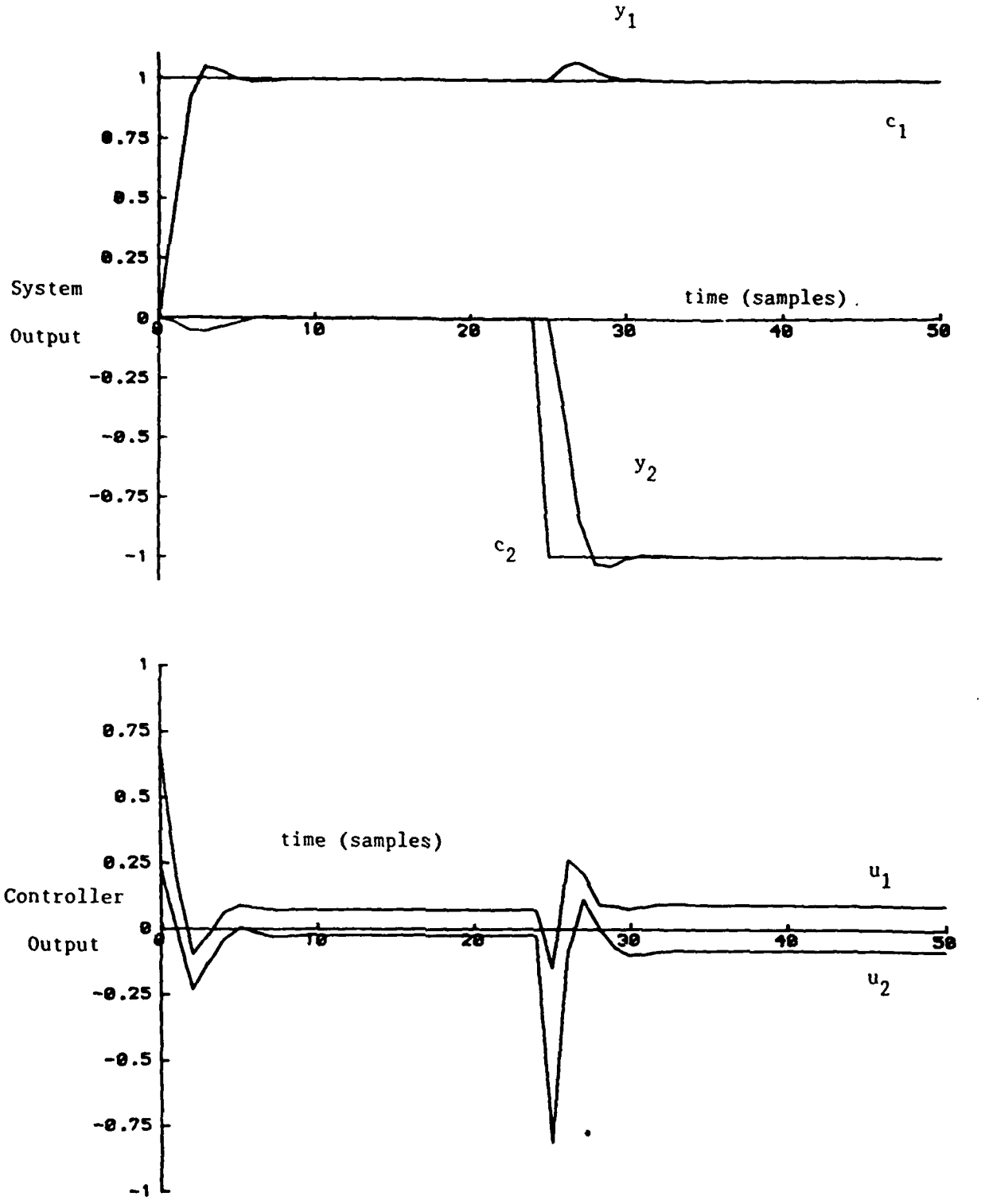

Figure 8.6: Simulation Results With High Frequency Alignment Compensation

$(N_u^1 = N_u^2 = 3 \; ; \; \rho_1 = \rho_2 = 1)$

Appendix 8.1 A Difference Equation Formulation of the CSM Algorithm

Consider the system described by the transfer function matrix

$$\hat{G}(z) = \hat{A}^{-1}(z)\,\hat{B}(z) \qquad \ldots.(A8.1)$$

where $\hat{B}(z) = \sum_{i=0}^{k} B(i)\, z^{-i}$ and $\hat{A}(z) = I + \sum_{i=1}^{k} A(i)\, z^{-i}$

The defining equation for the eigenfunctions and characteristic directions of this system is, therefore, given by $\hat{A}^{-1}\,\hat{B}\,\hat{w}_i = \hat{g}_i\,\hat{w}_i$; or alternatively,

$$\hat{B}\,\hat{w}_i = \hat{g}_i\,\hat{A}\,\hat{w}_i \qquad \ldots.(A8.2)$$

After transforming this relationship into the time domain using the inverse z-transform, the following convolution relationship can be established:

$$^{s}B * {}^{s}w_i = {}^{s}g_i * {}^{s}A * {}^{s}w_i \qquad \ldots.(A8.3)$$

where ${}^{s}g_i$ and ${}^{s}w_i$ *are the* i^{th} *CWS and CVS of the system* and ${}^{s}B$ and ${}^{s}A$ are given by ${}^{s}B = [B(0), \cdots, B(k)]$ and ${}^{s}A = [I, A(1), \cdots, A(k)]$.

Using eqn A8.3, the desired algorithm can be generated in much the same way as the standard CSM algorithm. In particular, at the initial stage of the convolution, eqn A8.3 indicates that $B(0)\, w_i(0) = g_i(0)\, w_i(0)$. Hence, $g_i(0)$ and $w_i(0)$ are the i^{th} eigenvalue/eigenvector pair of $B(0)$. For $j = 1$ (the next stage of the convolution), eqn A8.3 indicates that:

$$B(1)w_i(0) + B(0)w_i(1) = g_i(0)w_i(1) + g_i(0)A(1)w_i(0) + g_i(1)w_i(0) \qquad \ldots.(A8.4)$$

Premultiplying eqn A8.4 by $v_i^t(0)$ (i.e. the i^{th} dual eigenvector of $B(0)$) yields the following expression for $g_i(1)$:

$$g_i(1) = v_i^t(0)\,\{B(1) - g_i(0)\,A(1)\}\,w_i(0) \qquad \ldots.(A8.5a)$$

Furthermore, eqn A8.4 can be rewritten in the following form:

$$\{g_i(0)I - B(0)\}\,w_i(1) = \{B(1) - g_i(0)\,A(1) + g_i(1)I\}\,w_i(0)$$

Hence, $w_i(1)$ is given by:

$$w_i(1) = T_i^{\ddagger}(0)\,\{B(1) - g_i(0)\,A(1)\} + \alpha\, w_i(0) \qquad \ldots.(A8.5b)$$

where $T_i^{\ddagger}(0)$ is the commuting g_2-Penrose inverse of $\{g_i(0)I - B(0)\}$ (see eqn A7.3) and α is an arbitrary constant (which may be set to zero).

Similar results can be derived for each additional stage of the convolution defined by eqn A8.3 to produce a general algorithm, but the details of this development will not be presented here.

Appendix 8.2 A Perturbation Analysis of Algorithm 8.1

Given that x_o, g_o defines a stationary point of J (eqn 8.31) for which $J = \lambda = 0$, the following matrices (with their singular value decompositions) are given by:

$$R_o = Y - U M_o = S_1 \Sigma S_2^T \qquad A_o = R_o^T R_o = S_2 \Sigma^2 S_2^T$$

$$D_o = U X_o = T_1 \Gamma T_2^T$$

where M_o and X_o are defined as shown in Section 8.3 using the elements of x_o and g_o, $\Sigma = \text{diag} \{ 0, \sigma_2, \cdots, \sigma_{mN_v^i - 1}, \bar{\sigma} \}$ with $\sigma_2 \leq \sigma_3 \leq \cdots \leq \bar{\sigma}$, $\Gamma = \text{diag} \{\gamma_1, \cdots, \gamma_{N_q^i}\}$, and S_i and T_i are orthogonal matrices with $S_i^T S_i = T_i^T T_i = I$ for $i = 1,2$.

Assuming the initial value for x in Algorithm 8.1 is given by $x_0 = x_o + \delta x_0$, eqn 8.37 can be used to develop the initial estimate for g as:

$$\hat{g} = \{ (D_o + \delta D_0)^T (D_o + \delta D_0) \}^{-1} (D_o + \delta D_0)^T Y (x_o + \delta x_0)$$

$$\simeq \{I - (D_o^T D_o)^{-1} [\delta D_0^T D_o + D_o^T \delta D_0]\} \{g_o + (D_o^T D_o)^{-1} [\delta D_0^T Y x_o + D^T{}_o Y \delta x_0]\}$$

$$\simeq g_o + (D_o^T D_o)^{-1} \delta D_0^T (Y x_o - D_o g_o) + (D_o^T D_o)^{-1} D_o^T (Y \delta x_o - \delta D_o g_0)$$

But $Yx_o - D_o g_o = R_o x_o = 0$ (since x_o is a stationary point for which $J = 0$) and $Y \delta x_o - \delta D_o g_o = R_o \delta x_o$. Thus, the difference between $\hat{g}$ and g_o is:

$$\delta g_0 \simeq (D_o^T D_o)^{-1} D_o^T R_o \delta x_0 \qquad \ldots.(A8.6)$$

This result can now be used with eqn 8.34 to identify the error in the next estimate of x ($x_o + \delta x_1$) as shown here:

$$(A_o + \delta A_0)(x_o + \delta x_1) = \delta\lambda_0 (x_o + \delta x_1)$$

$$A_o \delta x_1 \simeq (\delta\lambda_0 I - \delta A_0) x_o$$

$$\delta x_1 \simeq A_o^{\dagger} (\delta\lambda_0 I - \delta A_0) x_o \qquad \ldots.(A8.7)$$

where $A_o^{\dagger} = S_2 \tilde{\Sigma}^2 S_2^T$ and $\tilde{\Sigma} = \text{diag} \{ 0, 1/\sigma_2, \cdots, 1/\bar{\sigma} \}$. By definition, $A_o^{\dagger} x_o = 0$ and so eqn A8.7 can be rewritten as:

$$\delta x_1 \simeq - A_o^{\dagger} \delta A_0 x_o \qquad \ldots.(A8.8)$$

Furthermore, δA_0 can be identified using the relationship

$$A_o + \delta A_0 = (Y - U M_o - U \delta M_0)^T (Y - U M_o - U \delta M_0)$$

which implies that $\delta A_0 \simeq - \delta M_0^T U^T R_o - R_o^T U \delta M_0$.

Remembering that $R_o x_o = 0$ and noting that $\delta M_0 x_o = X_o \delta g_0$ (where δg_0 is defined by eqn A8.6), δx_1 can now be written in terms of δx_0 as:

$$\delta x_1 \simeq A_o^{\ddagger} R_o^T D_o (D_o^T D_o)^{-1} D_o^T R_o \delta x_0 \quad \ldots.(A8.9)$$

Using the singular value decompositions defined above, δx_1 can also be written as:

$$\delta x_1 \simeq S_2 \tilde{\Sigma} S_1^T T_1 T_1^T S_1 \Sigma S_2^T \delta x_0 \quad \ldots.(A8.10)$$

This result can be extended to relate the error at the k^{th} iteration to the initial error as:

$$\delta x_k \simeq S_2 \tilde{\Sigma} (S_1^T T_1 T_1^T S_1)^k \Sigma S_2^T \delta x_0 \quad \ldots.(A8.11)$$

Thus, the magnitude of δx_k can be bounded (using singular value inequalities) by:

$$|| \delta x_k || \leq \frac{\bar{\sigma}}{\sigma_2} \{\bar{\sigma}[S_1^T T_1 T_1^T S_1]\}^k || \delta x_0 || \quad \ldots.(A8.12)$$

But $$\bar{\sigma}[S_1^T T_1 T_1^T S_1] \leq \bar{\sigma}[S_1^T] \bar{\sigma}[T_1] \bar{\sigma}[T_1^T] \bar{\sigma}[S_1] = 1 \quad \ldots.(A8.13)$$

and by the Major Principal Direction Alignment principle [KOU5], the equality in eqn A8.13 holds only if the major input and output principle directions of S_1 and T_1 are aligned. Thus in general, $\{\bar{\sigma}[S_1^T T_1 T_1^T S_1]\}^k \to 0$ as $k \to \infty$ and so $||\delta x_k|| \to 0$ as $k \to \infty$.

It should, however, be noted that the actual size of δx_k at any given step in the iteration is a function of $\bar{\sigma}$, σ_2, and the orientation of δx_0 as implied by conditions A8.11 and A8.12. In some instances, $||\delta x_k||$ may actually be larger then $||\delta x_0||$ during the first few iterations of the algorithm. For problems where two or more solutions are sufficiently close together, the orientation of δx_k combined with this amplification in size during the initial iterations may cause the algorithm to jump from the assumed solution, x_o, to another. Under these special circumstances, the algorithm will still converge to a correct solution, but it may not be the one originally assumed.

CHAPTER NINE

CONCLUSION

Research in the area of robust control system design during the past decade has produced a number of results which strive to incorporate information on system uncertainty into the analysis and design of feedback control systems in a systematic manner. The primary objective of this thesis was to advance towards this goal by establishing additional techniques for use in the analysis and design of multivariable control systems in the presence of uncertainty. This aim has largely been fulfilled by the developments presented in earlier chapters. In this chapter, the main results of the thesis are summarized and potential topics for further research are highlighted.

9.1 Summary

After the introduction in Chapter 1, a summary of the predominant multivariable frequency-domain analysis tools for both "certain" and "uncertain" systems was presented in Chapter 2 to provide the foundation and motivation for subsequent developments. The problem of generating an accurate description of frequency response uncertainty for use in these analysis techniques was addressed in Chapters 3 through 6. A method was derived in Chapter 3 to quantify the variability of the frequency response estimates obtained from an estimated parametric model. Finite weighting sequence models were found to be particularly useful for this purpose, but these models introduce the need to identify an appropriate level of truncation and, simultaneously, introduce a second element of uncertainty (i.e. the bias associated with the specified truncation). For these reasons, the problem of weighting sequence truncation was considered next, and two new truncation criteria were proposed. The first criterion (presented in Chapter 4) was derived using a geometric interpretation of the standard "parameter space" problem to address the bias/variability trade-off

by selecting the truncation which minimizes the expected distance between the true and estimated frequency response at a prespecified individual frequency. The second criterion (presented in Chapter 5) was derived using Akaike's criterion [AKA1] as a starting point and exploiting special properties of weighting sequence models to establish an implementable (rather than theoretical) procedure for optimal truncation. The implementation of this criterion was shown to produce not only a statistically optimal level of truncation, but also explicit upper bounds on the frequency response bias associated with this truncation. These bias bounds were combined with the variability information derived in Chapter 3 to establish a complete and quantitative description of frequency response uncertainty using results presented in Chapter 6. In addition, techniques to refine and tailor this uncertainty description to the frequency response characteristics of given systems were proposed. The results were also extended to multivariable systems to yield the desired frequency response uncertainty description in terms of element-by-element bounded perturbations, and it was shown that this description can be used to establish eigenvalue inclusion regions for use in the assessment of robust stability and performance.

In Chapter 7, attention shifted to the multivariable control design problem and, more specifically, to the development of a multivariable control design methodology that can be applied using on-line, computer-implemented algorithms. A z-domain "characteristic subsystem" decomposition was developed for multivariable systems to establish the necessary link between the conventional frequency-domain design philosophy of the generalized-Nyquist/characteristic-locus approach and the corresponding discrete-time computer implementations of these designs. Indeed, it was shown that this "characteristic subsystem" approach yields a much more accurate implementation for conventional frequency-domain designs than that available using currently-existing techniques. More importantly, this approach provided the foundation for extending SISO self-tuning control

algorithms to the multivariable problem in precisely the same manner as the characteristic locus design method generalizes classical frequency response design techniques. The derivation of one such multivariable self-tuner was presented in Chapter 8 using the SISO GPC algorithm as the basis for the development. The problem of on-line identification was also examined and two algorithms were proposed to generate the required subsystem descriptions directly from input/output data. These algorithms offer the potential for a significant reduction in the computational complexity of the overall self-tuning algorithm, and thus should make it possible to apply the proposed multivariable self-tuning algorithm to a large class of systems using existing computer capabilities.

9.2 Future Research

The developments in this thesis, as with any research effort, highlight several additional and potentially important topics for further study. From a frequency-domain point of view, the element-by-element bounds on system frequency response uncertainty developed in Chapters 3 through 6 establish a precise description of system uncertainty. This information should make it possible to enhance the development of frequency-domain control design techniques to handle system uncertainty.

For currently-existing approaches (which handle system uncertainty implicitly via specified performance indices), this uncertainty information, when incorporated into the performance index specifications for the given methodology, should produce control designs which are tailored to the known uncertainty characteristics of the system. Furthermore, this information should also make it possible to focus on new design methodologies to handle system uncertainty in a direct and explicit manner. As pointed out earlier, tentative steps have already been taken towards accomplishing this task within an H^{∞} framework ([DOY3], [BIR1]), and the ability to generate system-specific frequency response uncertainty information (as described in this thesis) should provide new impetus to the development of these techniques.

Alternatively, the results derived here offer the potential for the development of a robust design methodology based on a "characteristic-locus-type" approach. As demonstrated in Chapter 6, the precise element-by-element uncertainty bounds developed here can be combined with earlier structured E-contour results ([KOU4], [KOU6]) to produce accurate gain and phase information on the characteristic loci of the perturbed system. As such, it should be possible to produce closed-loop designs which achieve desired performance goals (while simultaneously accounting for the sensitivity of the characteristic loci to the specified uncertainty) by manipulating the eigenvalue inclusion bands rather than the nominal characteristic loci alone. The key to accomplishing these modifications is, of course, the ability to develop a controller structure which can be used to manipulate the characteristic locus bands. As yet, this task has not received a great deal of attention. But now that a precise characteristic locus uncertainty description can be generated, it seems reasonable to anticipate that investigations in this area will produce viable techniques for the design of robust control systems; thereby extending classical frequency response techniques to the problem of controlling "uncertain" multivariable systems.

Provided a characteristic locus approach to robust control design can be developed, the ability to produce tighter characteristic locus inclusion regions may also prove beneficial. The currently-proposed algorithm for generating these regions relies on a transformation from input/output data to element-by-element uncertainty bounds and, ultimately, to E-contour bounds for the characteristic loci. But as mentioned previously, this approach introduces an element of conservatism in the uncertainty description due to the fact that the specified confidence associated with the parameter uncertainty ellipsoids translates into a lower bound on the confidence associated with the corresponding E-contours. The development of algorithms which estimate "characteristic subsystem" descriptions directly from input/output data (as proposed in Chapter 8), however, suggests that it

may be possible to by-pass the intermediate steps in this process to produce confidence bounds directly on each individual characteristic locus using SISO results similar to those developed in this thesis. Though the steps in the development of this uncertainty description are not immediately obvious, investigations in this area could produce a more refined description of characteristic locus uncertainty while simultaneously eliminating the time-consuming intermediate steps associated with the current approach.

The time-domain and self-tuning control concepts derived in Chapters 7 and 8 also highlight several areas for future work. For example, additional research in the areas of branch point placement, on-line high frequency alignment compensation and direct subsystem identification are needed to produce a completely general multivariable self-tuning algorithm within the proposed characteristic subsystem framework. As highlighted previously, the location of branch points can be altered using constant precompensation. It seems reasonable, therefore, to anticipate that straightforward algorithms can be derived to generate simple precompensators which reposition branch points to desired locations in the z-plane. Such algorithms would not only ensure the general applicability of the characteristic subsystem framework for self-tuning applications by eliminating unstable branch points, but they could also be used to reposition stable branch points so as to increase the decay rates of the CVS and dual CVS. Hence, the number of terms needed to generate an accurate eigenvector approximation (and, as a result, the computational complexity of the control algorithm) could be reduced. Furthermore, since constant precompensation can also be used to achieve high frequency alignment, it may be possible to develop algorithms which simultaneously address the problem of reducing high frequency interaction; thereby improving system response still further at no extra computational expense. Initial efforts in this area [NIC1] have produced some encouraging results. However, a great deal of research is still required. As for direct subsystem identification, preliminary studies of the iterative

algorithms presented in Chapter 8 have also yielded promising results. However, the proposed algorithms must be investigated in much greater detail to establish their convergence characteristics (under stochastic conditions) and to validate the proposed on-line implementations. Once these tasks are accomplished, the resulting algorithms should provide a useful new technique for the multivariable system identification and a computationally-efficient means of incorporating identification into the self-tuning design.

In addition to these tasks, it must be stressed that the characteristic subsystem decomposition for multivariable systems established in Chapter 7 provides a general means of transforming the multivariable control problem into a set of independent SISO problems that are compatible with on-line computer implementations. As such, the development of real-time multivariable algorithms need not be restricted to the set of long-range predictive control algorithms such as SISO GPC. Indeed, studies to incorporate other SISO algorithms into this characteristic subsystem framework can be undertaken and should ultimately lead to a wide-range of multivariable self-tuning algorithms which account for the multivariable characteristics of the system in a true generalized-Nyquist sense. Furthermore, the eigenvalue decomposition used to generate the characteristic subsystems here suggests the possibility of establishing an alternative subsystem description based on singular value decompositions. As singular values are known to be less sensitive to perturbations, a singular-value-based subsystem description could be used to improve the sensitivity characteristics of the resulting control algorithms and, perhaps, to bridge the gap between self-tuning and H^{∞} control designs.

The final effort, the practical application of the proposed self-tuning control algorithm, goes without saying. It is hoped that future efforts will transform the theoretical developments presented here into a practical computer implementation for the control of real-life multivariable systems.

REFERENCES

[AKA1] Akaike, H.; "A new look at the statistical model identification"; IEEE Trans Aut Cont, Vol AC-19(6), pp 716-723; 1974.

[AST1] Astrom, K.J. and Wittenmark, B.; "On self-tuning regulators"; Automatica, Vol 9(2), pp 185-199; 1973.

[AST2] Astrom K.J. and Wittenmark, B.; "Self-tuning controllers based on pole-zero placement"; Proc IEE, Pt D, Vol 127(3), pp 120-130; 1980.

[BAR1] Barnett, S.; Matrices in Control Theory; London: Van Nostrand Reinhold; 1971.

[BEL1] Bellanger, M; Digital Processing of Signals; New York: John Wiley and Sons; 1984.

[BIR1] Bird, J.S. and Francis, B.A.; "On the robust disturbance attenuation problem"; Proc of the 25th IEEE CDC, Vol 3, pp 1804-1809; 1986.

[BHA1] Bhansali, R.J. and Downham, Y.K.; "Some properties of the order of an autoregressive model selected by a generalization of Akaike's FPE criterion"; Biometrika, Vol 64(3), pp 547-551; 1977.

[BLI1] Bliss, G.A.; Algebraic Functions; New York: Dover; 1966.

[BOR1] Borisson, U.; "Self-tuning regulators for a class of multivariable systems"; Automatica, Vol 15(2), pp 209-215; 1979.

[CAD1] Cadzow, J.A. and Martens, H.R.; Discrete-time and Computer Control Systems; Englewood Cliffs, NJ: Prentice-Hall; 1970.

[CHU1] Churchill, R.V., Brown, J.W., and Verhey, R.F.; Complex Variables and Applications; New York: McGraw-Hill; 1974.

[CLA1] Clarke, D.W. and Gawthrop, P.J.; "Self-tuning controller"; Proc IEE, Vol 122(9), pp 929-934; 1975.

[CLA2] Clarke, D.W. and Gawthrop, P.J.; "Self-tuning control"; Proc IEE, Vol 126(6), pp 633-640; 1979.

[CLA3] Clarke, D.W., Mohtadi, C., and Tuffs, P.S.; "Generalized Predictive Control, Part 1: the basic algorithm"; Automatica, Vol 23(2), pp 137-148; 1987.

[CLA4] Clarke, D.W., Mohtadi, C., and Tuffs, P.S.; "Generalized Predictive Control, Part 2: extensions and interpretation"; Automatica, Vol 23(2), pp 149-160; 1987.

[CLO1] Cloud, D.J. and Kouvaritakis, B.; "Statistical bounds on multivariable frequency response: an extension of the generalized Nyquist criterion"; Proc IEE, Pt D, Vol 133(3), pp 97-110; 1986.

[CLO2] Cloud, D.J. and Kouvaritakis, B.; "A frequency response-based model order selection criterion"; Proc of the 25th IEEE CDC, Vol 3, pp 1666-1667; 1986.

[CLO3] Cloud, D.J. and Kouvaritakis, B.; "Weighting sequence, optimal truncation and optimal frequency response uncertainty bounds"; Proc IEE, Pt D, Vol 134(3), pp 153-170; 1987.

[CL04] Cloud, D.J. and Kouvaritakis, B.; "Commutative controllers revisited: parallel computation, a new lease on life"; Int J Control, Vol 45(4), pp 1335-1370; 1987.

[CL05] Cloud, D.J. and Kouvaritakis, B.; "Characteristic decomposition and the multivariable generalization of predictive self-tuning control"; Proc IEE, Pt D, to be published; 1987.

[CUT1] Cutler, C.R. and Ramaker, B.L.; "Dynamic matrix control - a computer control algorithm"; Proc of the Joint Automatic Control Conference, Vol I, WP5-B; 1980.

[DAN1] Daniel, R.W. and Kouvaritakis, B.; "The choice and use of normal approximations to transfer function matrices of multivariable control systems"; Int J Control, Vol 37(5), pp 1121-1134; 1983.

[DAN2] Daniel, R.W. and Kouvaritakis, B.; "Analysis and design of linear multivariable feedback systems in the presence of additive perturbations"; Int J Control, Vol 39(3), pp 551-580; 1984.

[DAN3] Daniel, R.W. and Kouvaritakis, B.; "A new robust stability criterion for linear and nonlinear multivariable feedback systems"; Int J Control, Vol 41(6), pp 1349-1379; 1985.

[DAN4] Daniel, R.W., Kouvaritakis, B., and Latchman, H.; "Principal direction alignment: a geometric framework for the complete solution to the μ-problem"; Proc IEE, Pt D, Vol 133(2), pp 45-56; 1986.

[DAV1] Davis, M.H.A. and Vinter, R.B.; Stochastic Modelling and Control; London: Chapman-Hall; 1985.

[DEU1] Deutsch, R.; Estimation Theory; Englewood Cliffs, NJ: Prentice-Hall; 1965.

[DOY1] Doyle, J.C. and Stein, G.; "Multivariable feedback design: concepts for a classical/modern systhesis"; IEEE Trans Aut Cont, Vol AC-26(1), pp 4-16; 1981.

[DOY2] Doyle, J.C.; "Analysis of feedback systems with structured uncertainties"; Proc IEE, Part D, Vol 129(6), pp 242-250; 1982.

[DOY3] Doyle, J.C., Lenz, K. and Packard, A.; "Design examples using μ-synthesis: space shuttle lateral axis FCS during reentry"; Proc of the 25th IEEE CDC, Vol 3, pp 2218-2223; 1986.

[DUG1] Dugard, L., Goodwin, G.C., and Xianya, X.; "The role of the interactor matrix in multivariable stochastic adaptive control"; Automatica, Vol 20(5), pp 701-709; 1984.

[EDM1] Edmunds, J.M. and Kouvaritakis, B.; "Extensions of the frame alignment technique and their use in the characteristic locus design method"; Int Journal of Control, Vol 29(5), pp 787-796; 1979.

[EDM2] Edmunds, J.M.; "Confidence limits on identified frequency responses"; Control System Center, University of Manchester Institute of Science and Technology, Report No 607; 1984.

[EDM3] Edmunds, J.M.; "Model order determination for state-space control design methods"; Int Journal of Control, Vol 41(4), pp 941-946; 1985.

[EYK1] Eykhoff, P.; System Identification; London: Wiley Interscience; 1974.

[FRA1] Franklin, G.F. and Powell, J.D.; Digital Control of Dynamic Systems; Reading, MA: Addison-Wesley; 1980.

[FRE1] Freeman, T.G.; "Selecting the best linear transfer function model"; Automatica, Vol 21(4), pp 361-370; 1985.

[GAN1] Gantmacher, F.R.; The Theory of Matrices, Vol 1 & 2; New York: Chelsea; 1974.

[GIB1] Gibra, I.N.; Probability and Statistical Inference for Scientists and Engineers; Englewood Cliffs, NJ: Prentice-Hall; 1973.

[GOO1] Goodwin, G.C. and Payne, R.L.; Dynamic System Identification: Experiment Design and Data Analysis; New York: Academic Press; 1977.

[GOO2] Goodwin, G.C., Ramadge, P.J., and Caines, P.E.; "Discrete-time multivariable adaptive control"; IEEE Trans Aut Cont, Vol AC-25(3), pp 449-455; 1980.

[GOU1] Gough, N.E., Kleftouris, D., and Thiga, R.S.A.; "Computer-aided identification and multivariable control system design using convolution algebra"; Proceedings of the IFAC MVTS Symposium, Fredericton, Canada; 1977.

[HAN1] Hannan, E.J. and Quinn, B.G.; "The determination of the order of an autoregression"; J Royal Statist Soc, Vol B41, pp 190-195; 1979.

[HAR1] Harrison, R.F. and Kouvaritakis, B.; "Normality, scaling and eigenvalue inclusion regions"; Int J Control, Vol 41(6), pp 1317-1336; 1986.

[IBR1] Ibrahim, T.A.S. and Munro, N.; "Design of sampled data multivariable control systems"; Int J Control, Vol 22(3), pp 297-311; 1975.

[ILM1] SPECIAL ISSUE; "On Linear Multivariable Control Systems"; IEEE Trans Aut Cont, Vol AC-26(1); 1981.

[ISR1] SPECIAL ISSUE; "On Sensitivity and Robustness"; Proc IEE, Part D, Vol 129(6); 1982.

[JAM1] James, J.R., Frederick, D.K., and Taylor, J.H.; "The use of expert-systems programming for the design of lead-lag compensators"; Proc of the IEE Control '85 Conference, Vol 1, pp 180-185; 1985.

[JAN1] Janiszowski, K.; "Evaluation of the effects of identification errors on the dynamical properties of a process model"; Int J Control, Vol 41(2), pp 445-459; 1985.

[JEN1] Jensen, D.R. and Solomon, H.; "A Gaussian approximation to the distribution of a definite quadratic form"; J Am Stat Assoc, Vol 67, pp 898-902; 1982.

[JOH1] Johnson, N.L. and Kotz, S.; "Tables of distributions of quadratic forms in central normal variables, 1"; University of North Carolina, Chapel Hill: Institute of Statistics Mimeo Series 543; 1967.

[JOH2] Johnson, N.L. and Kotz, S.; "Tables of distributions of quadratic forms in central normal variables, II"; University of North Carolina, Chapel Hill: Institute of Statistics Mimeo Series 543; 1967.

[KAN1] Kantor, J.C. and Andres, R.P.; "Characterization of 'allowable perturbations' for robust stability"; IEEE Trans Aut Cont, Vol AC-28(1), pp 107-108; 1983.

[KEN1] Kendall, M. and Stuart, A.; The Advanced Theory of Statistics, Vol 1; London: Charles Griffin and Co; 1977.

[KOI1] Koivo, H.N.; "A multivariable self-tuning controller"; Automatica, Vol 16(4), pp 351-366; 1980.

[KOU1] Kouvaritakis, B.; "Characteristic locus methods for multivariable feedback system design"; PhD Thesis, University of Manchester; 1974.

[KOU2] Kouvaritakis, B. and Kleftouris, D.; "The characteristic sequences method for multivariable systems: a time domain approach to the characteristic locus method"; Int Journal of Control, Vol 31(1), pp 127-152; 1980.

[KOU3] Kouvaritakis, B.; "Complex align: a technique for the characteristic locus method of design"; Proc IEE, Part D, Vol 129(1), pp 1-5; 1982.

[KOU4] Kouvaritakis, B. and Latchman, H.; "Singular value and eigenvalue techniques in the analysis of systems with structured perturbations"; Int J Control, Vol 41(6), pp 1381-1412; 1985.

[KOU5] Kouvaritakis, B. and Latchman, H.; "Necessary and sufficient stability criterion for systems with structured uncertainties: the major principle direction alignment property"; Int J Control, Vol 42(3), pp 575-598; 1985.

[KOU6] Kouvaritakis, B. and Latchman, H.; "Block-structured perturbations, characteristic loci and root loci"; Proc of the IEE Control '85 Conference, Vol 1, pp 204-209; 1985.

[KOU7] Kouvaritakis, B. and Latchman, H.; "Necessary and sufficient stability conditions for the case of dependent additive perturbations"; Int J Control, Vol 43(6), pp 1615-1630; 1986.

[KOU8] Kouvaritakis, B. and Trimboli, M.S.; "Dynamic performance, interaction, and the characteristic locus method: a quantitative approach"; Dept of Engineering Science, University of Oxford, Report OUEL 1676/87; 1987.

[KUN1] Kung, H.T., Sproull, R.F., and Steele, G.L. (ed); VLSI Systems and Computations; Computer Science Dept, Carnegie-Mellon University; Rockville, MD: Computer Science Press; 1981.

[KUN2] Kung, S.Y., Whitehouse, H.J., and Kailath, T. (ed); VLSI and Modern Signal Processing; Englewood Cliffs, NJ: Prentice-Hall; 1985.

[LAT1] Latchman, H.A.; "Frequency response methods for uncertain multivariable systems"; D.Phil. Thesis, University of Oxford; 1986.

[LI1] Li, F. and Cameron, R.G.; "Extensions to the characteristic sequences method"; School of Control Engineering, University of Bradford, Research Report No. R378; 1985.

[LJU1] Ljung, L. and Yuan, Z.D.; "Asymptotic properties of black-box identification of transfer functions"; IEEE Trans Aut Cont, Vol AC-30(6), pp 514-530; 1985.

[LJU2] Ljung, L.; "Asymptotic variance expressions for identified black-box identification of transfer function models"; IEEE Trans Aut Cont, Vol AC-30(9), pp 834-844; 1985.

[LOH1] Loh, A.P., Correa, G.O., and Postlethwaite, I.; "Estimation of uncertainty bounds for robustness analysis"; Proc IEE, Pt D, Vol 134(1), pp 9-16; 1987.

[LUN1] Lunze, J.; "Robustness tests for feedback control systems using multidimensional uncertainty bounds"; System & Control Letters, Vol 4(2), pp 85-89; 1984.

[MAC1] MacFarlane, A.G.J. and Belletrutti, J.J.; "The characteristic locus design method"; Automatica, Vol 9(5), pp 575-588; 1973.

[MAC2] MacFarlane, A.G.J. and Postlethwaite, I.; "The generalized Nyquist criterion and multivariable root loci"; Int Journal of Control, Vol 25(1), pp 81-127; 1977.

[MAC3] MacFarlane, A.G.J. and Kouvaritakis, B.; "A design technique for linear multivariable feedback systems"; Int Journal of Control, Vol 25(6), pp 837-874; 1977.

[MEH1] Mehra, R.K.; "Choice of input signals" in Trends and Progress in System Identification, edited by P. Eykhoff; Oxford: Pergamon Press; 1981.

[MOH1] Mohtadi, C., Shah, S.L., and Clarke, D.W.; "Generalized predictive control of multivariable systems"; Dept of Engineering Science, University of Oxford, Report OUEL 1640/86; 1986.

[MOH2] Mohtadi, C.; personal communication.

[NIC1] Nicandrou, N.A. and Rossitor, J.A.; "A strategy for the design of constant and dynamic feedback multivariable precompensators"; Dept of Engineering Science, University of Oxford, Third Year Report; 1987.

[OWE1] Owens, D.H. and Chotai, A.; "Robust controller design for linear dynamic systems using approximate models"; Proc IEE, Part D, Vol 130(1), pp 45-56; 1984.

[PEI1] Peizer, D.B. and Pratt, J.W.; "A normal approximation for binomial, F, beta and other common, related tail probabilities"; J Am Stat Assoc, Vol 63, pp 1416-1456; 1968.

[POS1] Postlethwaite, I. and Foo, Y.K.; "Robustness with simultaneous pole and zero movement across the $j\omega$-axis"; Automatica, Vol 21(4), pp 433-443; 1985.

[RAY1] Ray, K.S. and Kouvaritakis, B.; "An extension of the characteristic sequences method to the case of repeated roots"; IEEE Trans Aut Cont, Vol AC-29(10), pp 933-935; 1984.

[ROS1] Rosenbrock, H.H.; "Design of multivariable control systems using the inverse Nyquist array"; Proc IEE, Vol 116(11), pp 1929-1936; 1969.

[SAF1] Safonov, M.G.; "Stability margins of diagonally perturbed multivariable feedback systems"; Proc IEE, Pt D, Vol 129(6), pp 251-256; 1982.

[SAU1] Saucedo, R. and Schiring, E.E.; Introduction to Continuous and Digital Control Systems; New York: Macmillan; 1968.

[SCH1] Schweppe, F.C.; Uncertain Dynamic Systems; Englewood Cliffs, NJ: Prentice-Hall; 1973.

[SCH2] Schwarz, G.; "Estimating the dimension of a model"; Ann. Statist., Vol 6, pp 461-464; 1978.

[SOL1] Solomon, H.; "Distribution of quadratic forms - tables and applications"; Applied Mathematics and Statistics Laboratories, Stanford University, Technical Report 45; 1960.

[SMI1] Smith, M.C.; "A generalized Nyquist/root locus theory for multi-loop systems"; PhD Thesis, Cambridge University; 1982.

[STR1] Strejc, V.; "Least squares and regression methods." in Trends and Progress in System Identification, edited by P. Eykhoff; Oxford: Pergamon Press, 1981.

[THI1] Thiga, R.S.A.; "Computer aided identification and design of discrete control systems"; PhD Thesis, University of Bradford; 1975.

[WEL1] Wellstead, P.E., Prager, D., and Zanker, P.; "Pole assignment self-tuning regulator"; Proc IEE, Vol 126(8), pp 781-787; 1979.

[WHI1] Whitehouse, H.J., Speiser, J.M., and Bromley, K.; "Signal processing applications of concurrent array processor technology"; in VLSI and Modern Signal Processing, edited by S.Y. Kung, H.J. Whitehouse, and T. Kailath; Englewood Cliffs, NJ: Prentice-Hall; 1985.

[WIL1] Wilkinson, J.H.; The Algebraic Eigenvalue Problem; Oxford: Oxford University Press; 1965.

[WIL2] Wilson, E.B. and Hilferty, N.M.; "The distribution of chi-square"; Proc. National Academy of Sciences, Vol 17, pp 684-688; 1931.

[YUA1] Yuan, Z.D. and Ljung, L.; "Unprejudiced optimal open loop input design for identification of transfer functions"; Automatica, Vol 21(6), pp 697-708; 1985.

[ZAM1] Zames, G.; "Feedback and optimal sensitivity: model reference transformations, multiplicative seminorms, and approximate inverses"; IEEE Trans Aut Cont, Vol AC-26(2), pp 301-320; 1981.

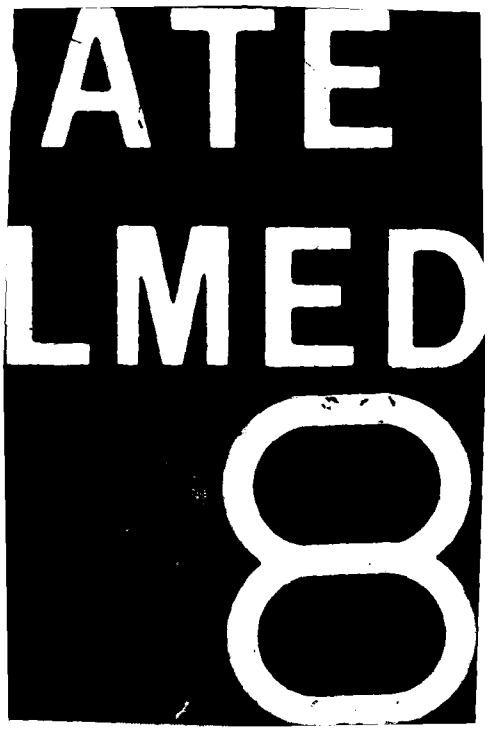
ATE
LMED
8